Effects of Genotoxin-Induced Stress by MNU and Etoposide on Cord Blood Hematopoietic Stem Cells and on Mesenchymal Stromal Cells from Cord Blood and Bone Marrow

Inaugural dissertation

for the attainment of the title of doctor
in the Faculty of Mathematics and Natural Sciences
at the Heinrich Heine University Düsseldorf

presented by
Meryem Ouzin
from Rabat, Morocco

Düsseldorf, Mai, 2025

From the Institute of Transplantation Diagnostics and Cell Therapeutics
At the Heinrich Heine University Düsseldorf

Published by permission of the
Faculty of Mathematics and Natural Sciences
At the Heinrich Heine University Düsseldorf

Supervisor: Prof. Dr. Gesine Kögler
Co-supervisor: Prof. Dr. Sebastian Wesselborg

Date of oral examination: 04.09.2025

Be curious. Read widely. Try new things.

What people call intelligence, just boils down to curiosity.

Aaron Swartz

Abstract

Genotoxic agents play a crucial role in the onset and development of hematological disorders and malignancies by inducing DNA damage thus disrupting cellular function and genomic integrity.

This thesis analyzed the genotoxic effects of the methylating agent N-methyl-N-nitrosourea (MNU) and the topoisomerase II chemotherapeutic agent etoposide on various cell types representing different developmental origins. The aim was to reflect the age-related considerations essential in toxicological assessments, including embryotoxicity, fetal toxicity, teratogenicity and age-specific sensitivity in children and adults, in vitro. To this end, induced pluripotent stem cells from $CD34^+$ HSCs (iPSCs), neonatal hematopoietic stem cells (HSCs) and mesenchymal stromal cells (MSCs) isolated from umbilical cord blood, as well as adult-derived MSCs isolated from bone marrow and induced MSCs from iPSCs (iMSCs) were used. The purpose was to assess the cellular responses following genotoxin-induced damage with a focus on DNA damage, cell viability and differentiation capacity of cells with different developmental ages.

Through a series of in vitro experiments, our experiments showed that iPSCs exhibited the highest sensitivity to genotoxic stress induced by MNU or etoposide. HSCs and MSCs demonstrated a more robust resistance to these agents likely due to their increased intrinsic DNA repair mechanisms.

A key focus of this thesis was the differential response of cycling and quiescent HSCs to genotoxic stress. Cycling HSCs exhibited a higher resistance to etoposide treatment. High MNU doses, however, resulted in the activation of apoptosis in cycling HSCs. Quiescent HSCs were not affected by etoposide, whereas MNU treatment resulted in a cell cycle stop and a dose-dependent increase of cell death.

Additionally, the study explored the impact of genotoxic exposure on stem cell differentiation by taking advantage of the multipotent differentiation potential of MSCs. Differentiation assays revealed that genotoxin-induced damage impaired lineage commitment since the osteogenic differentiation potential was significantly impaired mainly upon exposure to the genotoxin prior to the differentiation process. Treatment 7 days post differentiation start however, did not have an impact on osteogenic differentiation of MSCs from different developmental ages. The adipogenic and chondrogenic differentiation potentials of MSCs were less impacted upon genotoxic damage. These findings highlight the vulnerability of MSCs from different sources and donors and raise concerns regarding the long-term effects of environment toxins and chemotherapy-induced genotoxicity.

Furthermore, the iMSCs were characterized to evaluate their suitability as an alternative to primary MSCs and identified notable differences in their cytokine secretion profiles, which were more downregulated compared to BM-MSCs, HOX gene expression patterns, which were not expressed in contrast to BM-MSCs and a weak differentiation capacity into the osteogenic and adipogenic lineages.

This work provides valuable insights into the differential responses of stem and progenitor cells to genotoxic stress and underscores the need for targeted protective strategies in clinical settings. Understanding the mechanisms of genotoxic-induced

damage in stem cells is essential for developing improved therapeutic interventions for patients undergoing chemotherapy or exposed to environmental carcinogens. The in vitro experiments were conducted to develop methods in compliance with the 3R principle, aiming to reduce, refine and replace animal experiments in toxicological assessments.

Zusammenfassung

Genotoxine spielen eine entscheidende Rolle bei der Entstehung und Entwicklung von hämatologischen Erkrankungen und bösartigen Tumoren, da sie DNA-Schäden verursachen und so die Zellfunktion und die Genomintegrität beeinträchtigen.

In dieser Arbeit wurden die genotoxischen Auswirkungen von N-Nitroso-Methyl-Harnstoff (MNU) und dem Chemotherapeutikum und Topoisomerase II Inhibitor Etoposid auf verschiedene Zelltypen untersucht, die unterschiedliche Entwicklungsstadien repräsentieren, darunter induzierte pluripotente Stammzellen (iPSCs), hämatopoetische Stammzellen (HSCs), mesenchymale Stromazellen (MSCs) und induzierte mesenchymale Stromazellen (iMSCs). Ziel dieser Studie war es, die zellulären Reaktionen nach genotoxin-induzierten Schäden zu bewerten, wobei der Schwerpunkt auf die Bewertung der DNA-Schäden, Zelllebensfähigkeit und Differenzierungspotential von Zellen mit unterschiedlichen Entwicklunsgsstadien lag.

Durch eine Reihe von in vitro Experimenten konnten wir zeigen, dass iPSCs die höchste Empfindlichkeit gegenüber genotoxischem Stress aufweisen, der durch MNU oder Etoposid ausgelöst wurde. HSCs und MSCs zeigten eine robustere Resistenz gegenüber diesen Wirkstoffen, was wahrscheinlich auf ihre erhöhten intrinsischen DNA-Reparaturmechanismen zurückzuführen ist.

Ein Schwerpunkt dieser Arbeit war, die unterschiedliche Reaktion von zyklischen und ruhenden HSCs auf genotoxischen Stress zu erfassen. Zyklische HSCs wiesen eine höhere Resistenz gegenüber der Behandlung mit Etoposid auf. Hohe Konzentrationen an MNU führten jedoch zur Aktivierung der Apoptose in zyklischen HSCs. Ruhende HSCs wurden durch Etoposid nicht beeinträchtigt, während die Behandlung mit MNU zu einem Stopp des Zellzyklus und einem dosisabhängigen Anstieg der Apoptoserate führte.

Darüber hinaus wurden die Auswirkungen einer genotoxischen Exposition auf die Differenzierung von Stammzellen untersucht, indem das multipotente Differenzierungspotenzial von MSCs genutzt wurde. Differenzierungstests ergaben, dass genotoxin-induzierte Schäden die zelluläre Schicksalsentscheidung beeinträchtigten, da das osteogene Differenzierungspotenzial signifikant reduziert war, vor allem bei Exposition gegenüber dem Genotoxin vor dem Differenzierungsprozess. Die Behandlung 7 Tage nach Beginn der Differenzierung hatte jedoch keinen Einfluss auf die osteogene Differenzierung von MSCs aus verschiedenen Entwicklungsstadien. Das adipogene und chondrogene Differenzierungspotenzial von MSCs waren im Vergleich zum osteogenen Differenzierungspotenzial weniger stark beeinträchtigt. Diese Ergebnisse verdeutlichen die Anfälligkeit von MSCs aus unterschiedlichen Quellen und von verschiedenen Spendern und geben Anlass zur Sorge über die langfristigen Auswirkungen von Umweltgiften und chemotherapiebedingter Genotoxizität auch in Bezug auf das gesunde Gewebe.

Darüber hinaus wurden iMSCs charakterisiert, um ihre Eignung als Alternative zu primären MSCs zu untersuchen. Dabei wurden Unterschiede in ihren Zytokinsekretionsprofilen, die herunterreguliert waren im Vergleich zu BM-MSCs, HOX-Genexpressionsmustern, die nicht exprimiert sind im Vergleich zu BM-MSCs und

ihrem osteogenen und adipogenen Differenzierungspotenzial, welche deutlich schwächer sind, festgestellt.

Diese Forschungsarbeit liefert wertvolle Erkenntnisse über die unterschiedlichen Reaktionen von Stamm- und Vorläuferzellen auf genotoxischen Stress und unterstreicht die Notwendigkeit gezielter Schutzstrategien im klinischen Umfeld. Das Verständnis der Mechanismen von genotoxisch induzierten Schäden in Stammzellen ist für die Entwicklung verbesserter therapeutischer Maßnahmen für Patienten, die sich einer Chemotherapie unterziehen oder Umweltkarzinogenen ausgesetzt sind, von wesentlicher Bedeutung. Die in vitro Experimente wurden durchgeführt, um Methoden zu entwickeln, die dem 3R-Prinzip entsprechen und darauf abzielen, Tierversuche bei toxikologischen Bewertungen zu reduzieren, zu verfeinern und zu ersetzen.

Table of Contents

List of Abbreviations

MSC	Mesenchymal Stromal Cell
°C	Celsius
µg	Microgram
µL	Microliter
7-AAD	Aminoactinomycin D
APC	Allophycocyanin
BM	Bone marrow
bp	Base pair
CB	Cord blood
CD	Cluster of differentiation
cDNA	Complementary DNA
CFC	Colony forming cell
CFU	Colony forming unit
CPD	Cumulative population doubling
CT	Cycle threshold
d	Day
ddH_2O	Double distilled water
DDR	DNA damage repair / response
DMEM	Dulbecco´s modified Eagle´s medium
DMSO	Dimethyl sulfoxide
DNA	Deoxyribonucleic acid
dNTP	Deoxynucleotide
DSB	Double strand break
DTT	Dithiothreitol
FACS	Fluorescence activated cell sorting
FCS	Fetal calf serum

FITC	Fluorescein isothiocyanate
FSC	Forward scatter
GAPDH	Glyceraldehyde 3-phosphate dehydrogenase
h	Hour
H2AX	H2A histone family, member X
HSA	Human serum albumine
HSC	Hematopoietic stem cell
IL-3	Interleukin 3
IL-6	Interleukin 6
iPSC	Induced pluripotent stem cell
MACS	Magnetic activated cell sorting
MGMT	O^6-Methylguanine DNA Methyltransferase
min	Minutes
mm	Millimeter
MMR	Mismatch repair
MNC	Mononuclear cells
MNU	N-methyl-N-nitrosourea
nm	Nanometer
o.N.	Overnight
O^6-meG	O^6-methylguanine
PBS	Phosphate buffered saline
PBS-T	Phosphate buffered saline triton x-100
PD	Population doubling
PE	Phycoerythrin
PS	Penicilline, streptomycine
PSG	Penicilline, streptomycine and L-glutamine
rcf	Relative centrifugal force

rpm	Rounds per minute
RNA	Ribonucleic acid
RPL13a	Human ribosomal protein L13a
RT	Room temperature
RT-PCR	Reverse transcription-polymerase chain reaction
s	Seconds
SCF	Stem cell factor
SSC	Side scatter
TNC	Total nucleated cells
TP53	Tumor protein 53
TPO	Thrombopoietin
UCB	Umbilical cord blood
USSC	Unrestricted somatic stem cell

1. Introduction

1.1. Nitroso-Compounds: Mechanism of Action and Genotoxic Potential

The presence of nitroso-compounds such as N-nitrosodimethylamine (NDMA) and N-nitrosodiethylamine (NDEA) as impurities in widely used pharmaceutical drugs including sartans, antibiotics, antacids and antidiabetics triggered significant concerns among global regulatory agencies including the European Medicines Agency (EMA) and the U.S. Food and Drug Administration (FDA). These findings led to recalls and bans on affected batches, emphasizing the need for stricter monitoring and control of these compounds. Moreover, the detection of nitrosamines highlighted their highly genotoxic and carcinogenic potential, thus increasing the risk of cancer incidence and harming of human health. The International Council for Harmonization of Technical Requirements for Pharmaceuticals for Human Use (ICH) classified nitrosamine impurities as Class 1 according to the M7 guidelines. Around 300 nitroso-compounds are known, whereof more than 20 were classified by the International Agency for Research on Cancer (IARC) as carcinogenic to humans.

Nitrosamines are chemically stable compounds formed by the reaction of nitrites or nitrogen oxides with secondary or tertiary amines yielding in N-alkylnitrosamines and N-alkylnitrosamides [1]. This occurs during the manufacturing process of pharmaceuticals and personal care products but also during food processing and can be due to nitrite-containing starting raw materials, intermediates or re-used solvents, reactants and catalysts. Post-production factors such as moisture content, pH and storage temperature might also lead to nitrosamine impurity formation [2-4]. Additionally, nitrosamines can also be formed in the human body. Their precursors are ubiquitously present in processed meats, cheese, alcoholic beverages or cigarette smoke thus leading to the formation of nitrosamines under acidic pH in the mouth or stomach when the amino acids are converted to amines through bacterial decarboxylation followed by nitrosation [5].

Nitrosamines are pro-carcinogens in such that a metabolic activation by the cytochrome P450 isoenzymes is required for converting nitrosamines into reactive intermediates capable of DNA alkylation. The key enzyme hereby is CYP2E1, which is predominantly expressed in the liver but is also found in the colon and rectum [6]. It catalyses the α-hydroxylation step and results in the formation of diazomethane resulting in its spontaneous decomposition into nitrogen and a DNA reactive methyl carbocation that is able to attack the nitrogen ring and the oxygen atoms of DNA bases by S_N1-nucleophilic substitution at several positions depending on the given agent [7]. Beside N^7-methylguanine adducts, the formation of pre-mutagenic O^6-methylguanine is one of the main and most critical DNA lesions caused by alkylating nitrosamines. To a lower extent, also O^2-methylthymine and O^4-methylthymine adducts are formed. Opposite to nitrosamines, nitrosamides such as N-methyl-N-nitrosourea (MNU) do not require metabolic activation and decompose spontaneously in aqueous medium, forming diazonium ions and finally carbenium ions as alkylating species. N-nitrosoureas are the most relevant class among nitrosamides.

MNU was initially used as a first-generation anti-cancer drug, but was later on replaced by newly designed compounds such as procarbazine and dacarbazine, due to its instability [8]. These compounds, however, necessitate cytochrome P450 activation with the exception of temozolomide, which is nowadays preferentially used for treatment of malignant gliomas [9].

The DNA adducts resulting from MNU can be repaired by multiple DNA repair mechanisms. The first repair possibility is by the suicide enzyme O^6-methylguanine-DNA methyltransferase (MGMT). MGMT can remove methyl groups from O^6-methylguanine and O^4-methylthymine, with the repair of O^6-methylguanine being 10^5 to 10^3 times faster than that of O^4-methylthymine [10]. Kleihues and Margison studied the persistence of O^6-methylguanine adducts after intravenous injection of various rat tissues with MNU and showed that the neurotropic carcinogenicity of MNU depends on adduct removal [11]. Others have shown that overexpression of MGMT in transgenic mice skin leads to protection from tumor formation upon MNU exposure [12, 13]. Beside this, other groups have also shown that MGMT activity protects against different types of cancer including liver cancer, colon cancer and thymic lymphomas in various mouse models [14-17]. Mechanistically, MGMT acts by transferring the methyl group from guanine to the sulfur atom of the cysteine residue (C145) in its active site in a one-step reaction followed by its ubiquitination and degradation by the proteasome [18, 19].

Beside direct repair by MGMT, base excision repair (BER) is considered as one of the primary pathways involved in the removal of alkylation damage. This is accomplished in four sequential steps. The first step is catalyzed by DNA glycosylases that recognize and bind to the methylated base thus catalyzing cleavage of the glycosidic bond resulting in its release and in the formation of abasic apurinic or pyrimidinic sites (AP sites). In the second step, the emerged abasic sites are cleaved by apurinic endonucleases such as APEX1 thus generating 3´-OH and 5´-desoxyribose phosphate ends and DNA single-strand breaks (SSBs). In mammalian cells, AP sites and SSBs are recognized by the poly-ADP-ribose polymerase 1 (PARP1), which catalyzes the formation of ADP-ribose chains playing a role as a docking platform for the recruitment and assembly of the BER complex (XRCC1-POLβ-LIG3), when activated. The last BER step consists in the ligation of the nick by ligases after gap filling by DNA polymerases that use the undamaged strand as a template. The AP sites and SSBs formed during BER are highly toxic and mutagenic, hence the need of a tight process regulation and coordination to avoid intermediate accumulation.

If not repaired by MGMT or BER, persistent O^6-methylguanine adducts mispair with thymine instead of cytosine during replication resulting in G:C to A:T transition mutations. These mutations might play a pivotal role in the initiation of cytotoxicity, mutagenicity and carcinogenesis. In a repair attempt by the mismatch repair (MMR) machinery, O^6-methylguanine is recognized by MutSα, which interacts with MutLα to initiate the excision of the newly synthesized strand. This however does not lead to removal of the methylated base, which is in the template strand. Removal of the mispaired thymine by MMR results in futile and abortive repair cycles with eventual SSBs in turn resulting in replication fork collapse and giving rise to DNA double strand breaks (DSBs) after an additional replication cycle followed by chromosomal aberration or cell death. In MMR-deficient cells, the transition mutation persists leading therefore

to cell survival and increased mutagenesis [20]. Another model has been proposed for MMR as an actor in direct signaling in terms of DNA damage signal transduction beside its role in DNA damage repair (DDR). The MutSα complex acts as sensor for the activation of other DDR machineries upon recognition of the methylated adduct. This has been shown in mice experiments where missense mutations of *MSH2* and *MSH6* genes, leading to disruption of ATP processing ability of MutSα, thus preventing downstream steps of DDR despite normal affinity to the mismatch bases [21, 22]. Moreover, MutSα has been reported to bind to the mispaired bases O^6-methylguanine and thymine with a higher affinity compared to other mismatches and directly participates in ATR activation in an S-phase specific manner as measured by the phosphorylation of CHK1 and SMC1. This was not observed in MSH2-deficient HeLa cells [23].

DSBs represent the most damaging form of DNA lesions. The repair of DSBs arising because of MMR involves two major pathways: homologous recombination (HR) and non-homologous end-joining (NHEJ), each of which acts in different cell cycle phases, with HR mainly acting during replication and NHEJ throughout the interphase.

HR is a highly conserved and accurate DDR pathway as it uses the sister chromatid as a template to restore the DNA sequence at the break site. Its loss of functionality through defective *BRCA1* or *BRCA2* genes, leads to the preferential use of error-prone repair mechanisms thus elevating the risk of genomic alterations. Deleterious variants of other HR-related genes such as *ATM*, *RAD51* and *XRCC2* are associated with HR deficiency tumor phenotype, apoptosis and chromosomal aberrations [24].

In contrast, NHEJ operates without a template, directly ligating the broken DNA ends, thus being much faster but more error-prone than HR [25]. NHEJ begins with the recognition of DNA ends by the Ku70/Ku80 heterodimer for protection of further degradation and simultaneously acting as a scaffold for the assembly of NHEJ repair complex. DNA-dependent protein kinase catalytic subunit (DNA-PKcs) is recruited to the DNA-Ku complex thus forming the DNA-PK holoenzyme, which bridges and aligns the DNA ends. Following this, the DNA ligase IV/XRCC4 complex assisted by XRCC4-like factor (XLF) mediates the ligation of the DNA ends by sealing the phosphodiester bonds. The polymerases Pol μ or Pol λ fill the remaining gaps before ligation. After successful ligation, the NHEJ complex dissociates from the DNA. DNA-PKcs may undergo autophosphorylation to facilitate the release from DNA.

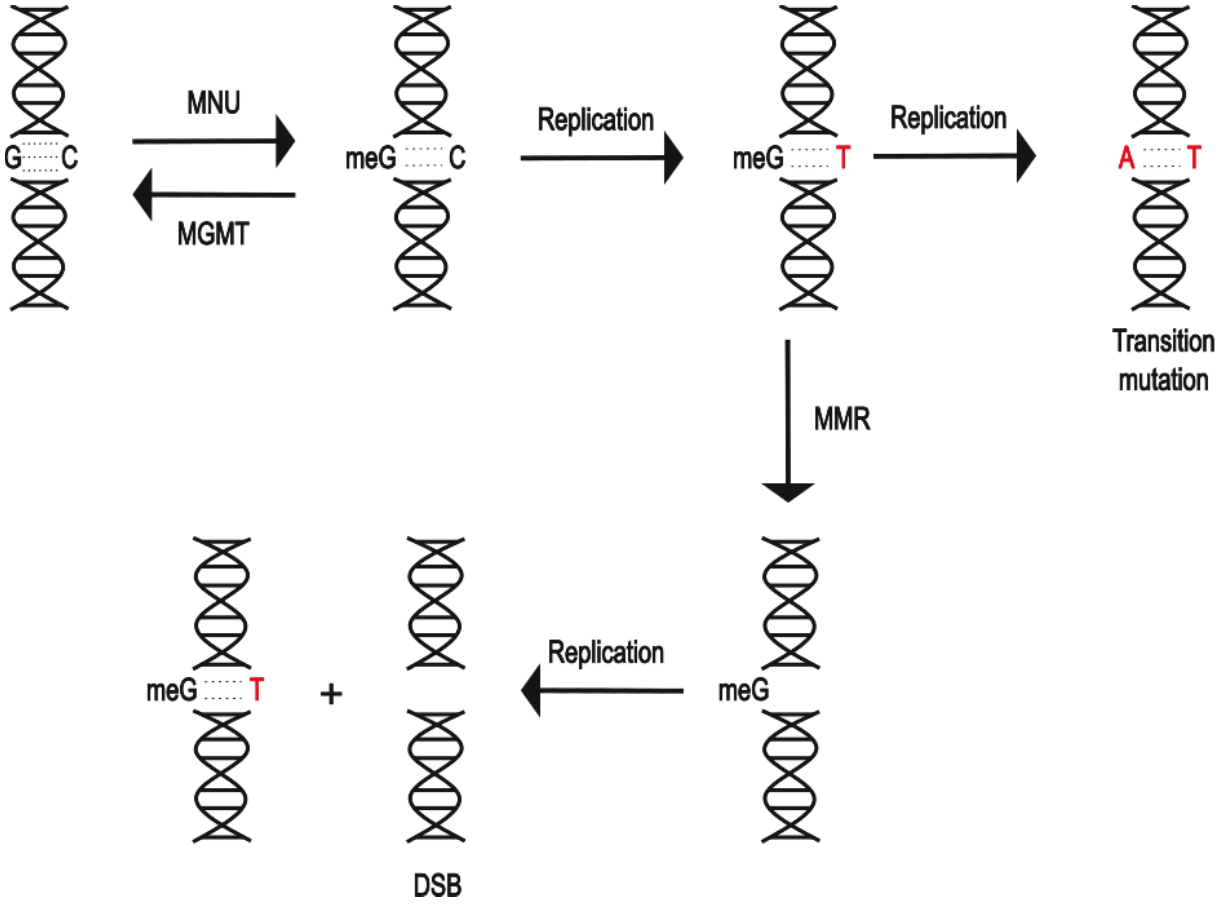

Figure 1: Schematic representation of the mechanism of action of MNU.

1.2. Etoposide: Mechanism of Action and Genotoxic Potential

Etoposide (VP-16) is a chemotherapeutic drug used for treating several types of cancers commonly lung cancer but also testicular cancer, ovarian, leukaemia, lymphoma and neuroblastoma [26-30]. Since its introduction in 1971, its mechanism of action and potent antineoplastic activity have been extensively studied. Due to its limited single-agent activity, it has been used as an essential part of combination therapies with cisplatin, carboplatin and cyclophosphamide [31-33]. While its primary target is rapidly dividing tumor cells, etoposide is not selective and can also impact healthy tissues and although it has been widely used, cases of therapy-related secondary leukaemia have been reported.

In humans, etoposide oxidation to etoposide catechol mainly involves cytochrome P450 3A family enzymes and/or peroxidases. Etoposide catechol is oxidized by myeloperoxidases (MPO) in the liver of bone marrow lysosomes [34]. Etoposide can also be directly metabolized to etoposide quinone by prostaglandin-endoperoxidases 1/2 (PGTS1/2) or by other peroxidases such as MPO. The oxidative metabolites of etoposide show a higher potency regarding the inhibition of DNA topoisomerase II than etoposide [35].

The mechanism of action of the semi-synthetic epipodophyllotoxin derivative etoposide is similar to the mechanism of action of its parent compound podophyllotoxin. Podophyllotoxin inhibits microtubule assembly by preventing tubulin polymerization and then destroying spindle fibres thus inhibiting the separation of sister chromatids

during mitosis [36]. This results in the arrest of cell division during mitosis with increased cell numbers in the metaphase. However, cells exposed to etoposide show a decreased metaphase ratio in contrast to podophyllotoxin [37]. Other studies have also shown that etoposide acts by a different mechanism compared to its parent compound since low doses of etoposide led to cell cycle perturbation in the late S- or early G_2-phase [38, 39]. Currently, it is well known that etoposide primarily acts by the inhibition of topoisomerase II (alpha and beta isoforms), an essential enzyme involved in DNA replication, transcription and chromosome segregation. Generally, topoisomerase II enzymes create a transient cleavage complex with the DNA through covalent binding of each subunit to the broken end of the 5´-phosphate group. The transient cleavage site is subsequently rapidly resealed. Topoisomerase II inhibitors act through interaction with the enzyme resulting in its trapping and collapse of the bifurcation resulting in DSBs. In turn, DSB accumulation impedes the progression of the replication fork thus triggering the activation of cell cycle checkpoints, apoptosis initiation and cell death [40]. For this reason, topoisomerase II inhibitors including etoposide play an integral role in cancer treatment.

NHEJ is commonly used for DSB repair. Hereby, the DNA ends are joined without the need for a homologous template. The trapped complex is first degraded by the proteasome and tyrosyl-DNA phosphodiesterase 2 releases the remaining end [41-43]. This process is efficient, however, inherently error-prone, often resulting in insertions, deletions or mismatch mutations at the repair site. Alternatively, the more accurate and precise HR, which uses the complementary DNA strand as a template, can be applied. Hereby, the MRE11-RAD50-NBS1 (MRN) complex recruits and activates ataxia-telangiectasia mutant kinase (ATM) dimers after damage recognition, that in turn, interact with checkpoint kinases leading to a G_2/M cell cycle arrest [44]. Following this, the nuclease activity of the MRN complex allows DNA cleavage prompting HR. However, HR is also associated with elevated mutagenesis, genetic instability and genomic rearrangements [45-47]. Faulty DSB repair can have varying consequences depending of mutation site and type, possibly resulting in protein loss or gain of function mutations thus increasing the risk of malignancies and neoplasms or structural alterations resulting in chromosomal rearrangements, which are strongly associated with secondary malignancies such as therapy-related acute myeloid leukaemia (t-AML). In addition to the increased risk of secondary malignancies, etoposide is well-known for its dose-limiting toxicity namely myelosuppression, which results from its cytotoxic effects on rapidly dividing hematopoietic cells in the bone marrow. This leads to increased infection risk, anaemia and bleeding.

In addition to DSBs, studies have shown that etoposide induces oxidative stress by reactive oxygen species (ROS) generation and accumulation in mitochondria additionally to ERK activation in human kidney proximal tubular cells thus leading to cytotoxicity, p53-mediated anti-apoptotic pathway and necrosis [48]. The reason for this is that etoposide undergoes redox cycling, which can result in the formation of semiquinone radicals that interact with molecular oxygen, producing ROS such as superoxide anions and hydrogen peroxide. Cells with efficient antioxidant systems, such as glutathione and catalase, may be able to counteract ROS generation.

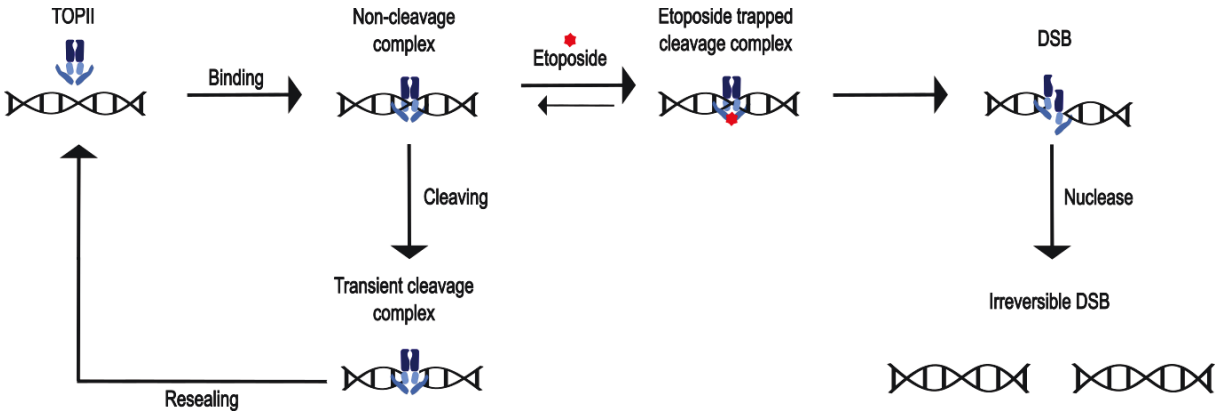

Figure 2: Schematic representation of the mechanism of action of etoposide. Modified from [49].

1.3. Testing of Genotoxic Effects during Drug Development and Risk Assessment in Compliance with the 3R Principle

Genotoxicity testing plays a crucial role in drug development and risk assessment to ensure the safety and efficacy of pharmaceutical compounds. Many regulatory frameworks and guidelines, such as those outlined by the ICH, require a series of in vivo tests assessing genotoxicity either per se or as follow-up to positive in vitro results. Traditional methods include assays like the Ames test, the mammalian bone marrow chromosomal aberration test (OECD TG 475) and the mammalian erythrocyte micronucleus assay (OECD TG 474). These assays have been instrumental for detecting mutagenic and clastogenic compounds. However, these approaches heavily rely on animal models, raising ethical concerns regarding animal welfare even though the identification of genotoxic effects is increasingly supported by an initial in silico screening phase.

To address these concerns, the 3R principle – replace, reduce, refine – has become a cornerstone of modern toxicological practices. This principle aims to minimize animal use and enhance the ethical standards of research while maintaining scientific rigor. Replacement focuses on the development and adoption of alternative methods such as advanced cell culture systems, computational models or high-throughput screening technologies. Reduction seeks to decrease the number of animals used for experiments by optimizing the design of the study and statistical analysis. Refinement involves improving the experimental procedures in order to minimize pain and stress in animal studies. In the field of genotoxicity testing, the 3R principle has led to significant advancements including the use of human-derived cell lines, organoids, 3D tissue models and induced pluripotent stem cells that provide more physiologically relevant data while reducing the alliance on animal models.

Cell culture models are highly valuable tools for toxicological testing in the 3R context, offering a highly accurate and reliable platform for assessing the safety of pharmaceutical compounds. Particularly models using human-derived cell lines closely mimic the biological processes and genetic responses of human tissues making them highly relevant for accurate predictions. Additionally, advanced techniques such as 3D cultures, co-culture systems, and organoids replicate the cellular architecture and microenvironment found in vivo, further enhancing their physiological accuracy. Cell culture models also allow for precise control over experimental conditions, including

exposure time, dose, and environmental factors, which can be challenging in animal studies. Furthermore, these models provide unique opportunities to evaluate the effects of genotoxic compounds on cell differentiation, developmental age and cell cycle status, offering insights that would be difficult to achieve through traditional methods.

In line with these advancements and in compliance with the 3R principle, this thesis explores the genotoxic effects of MNU and etoposide on various cell types representing different developmental stages. The objective was to reflect age-related considerations essential in toxicological assessments, including embryotoxicity, fetal toxicity, teratogenicity, and age-specific sensitivity in children and adults. To this end, induced pluripotent stem cells (iPSCs), neonatal hematopoietic stem cells (HSCs) and mesenchymal stromal cells (MSCs), as well as adult-derived MSCs and induced MSCs from iPSCs (iMSCs), were utilized.

1.4. The Importance of Developmental Age in Evaluating Genotoxic Effects

Aging is a universally conserved feature among eukaryotic organisms. It is characterized by a progressive decline of physiological integrity in molecules, cells, tissues and organisms. Biological and cellular age plays a pivotal role in understanding the impact of genotoxic agents as it reflects the cumulative physiological and cellular changes undergone by an organism, which can influence its susceptibility to DDR. Developmental age encompasses factors such as cellular senescence, oxidative stress and epigenetic modifications, which are critical determinants of a response to genotoxic stress.

When exposed to genotoxic agents like ionizing radiation, chemicals (e.g., etoposide or nitrosamines), or UV radiation, older cells tend to have a slower response time and often fail to initiate proper repair or apoptosis pathways. In contrast, younger cells can efficiently activate DNA damage checkpoints and initiate repair or cell cycle arrest.

Studies have shown that aged cells exhibit reduced DDR efficiency including HR and MMR leading to an increased accumulation of lesions and likelihood of mutations [50-52]. For instance, the repair of DSBs, one of the most severe forms of DNA damage, is slower and less accurate in aged cells compared to young cells [52]. The reduction in repair efficiency is thought to be associated with changes in the expression and activity of repair proteins such as DNA-PKcs, RAD51, and XRCC4, which are crucial for DSB repair. DNA-PKcs, which play a role in NHEJ, showed a higher expression in brains of neonatal mice compared to young adult mice, suggesting an age-dependent decrease in DSB repair efficiency [53]. RAD51 plays a role in HR and regulates cell cycle progression by preserving the G2/M transition. Its expression showed an age-dependent decrease in mouse oocytes and its depletion is accompanied by decreased ATP production and mitochondrial membrane potential and increased DNA degradation [54]. Li and colleagues showed that the expression of XRCC4 and LIG4 declined with increasing age in human fibroblasts and their restoration may suppress the stress-induced premature cellular senescence thus improving NHEJ efficiency and fidelity [55].

Moreover, one of the key factors in the diminished DDR in aging cells is the reduced activation of key signalling pathways, such as the ATM/ATR-mediated DNA damage response, which coordinates the activation of repair processes and cell cycle checkpoints. As a result, aged cells may undergo inappropriate cell cycle progression, or alternatively, enter a state of senescence or apoptosis, both of which can lead to genetic instability.

Furthermore, the decline in stem cell functionality and regenerative capacity with age can exacerbate the effects of genotoxic exposure, particularly in tissues reliant on high cellular turnover, such as the hematopoietic system. Incorporating developmental age into genotoxicity testing models ensures a more comprehensive risk assessment, capturing variations in susceptibility across different life stages and enhancing the relevance of preclinical findings to diverse populations.

1.5. Induced Pluripotent Stem Cells (iPSCs): A Novel Model for Genotoxicity Testing

In 2006, Takahashi and colleagues succeeded for the first time in generating iPSCs by retroviral transduction in a breakthrough experiment [56]. Four reprogramming transcription factors were selected as sufficient for the induction of pluripotency rendering mouse iPSCs resembling mouse embryonic stem cells (ESCs) in their biological potency, gene expression and epigenetic landscape: Oct4, Sox2, Klf4 and Myc [56]. In 2007, Yamanaka and Thomson independently demonstrated the possibility of generating iPSCs from human fibroblasts [57, 58]. Thomson and colleagues hereby used Nanog and Lin28 instead of Klf4 and Myc [58]. For this discovery, Shin´ya Yamanaka and Jon B. Gurdon were awarded the Nobel Prize for Medicine in 2012. The main motivation for their research was to overcome ethical concerns about the therapeutic use of ESCs and to provide better research approaches for understanding various diseases. The development of iPSCs has indeed opened vast opportunities for in vitro modelling of human biology, cell therapy applications and drug screening. Their usage is particularly attractive due to their similarity to embryonic stem cells but also given their human origin and the ability to derive patient-specific cells with a disease-relevant background. These factors may not be human-specific and not be manifested in animal models. Furthermore, iPSCs can be genetically modified and differentiated into other cell types that might otherwise be inaccessible thus holding a great promise for providing new approaches for next-generation cell therapies. The therapeutic use of iPSCs is, however, still very limited today due to their high self-renewal potential increasing the risk of tumor formation. Furthermore, the Sendai virus components of iPSCs pose a safety risk due to induced genetic instability [59]. Nowadays, various modifications to the original protocol have been developed for instance the usage of small-molecule assisted somatic cell reprogramming or fully chemical reprogramming.

IPSCs provide an unlimited source of patient-specific cells capable of differentiating into various tissue types, making them highly versatile for modeling human-specific genetic responses. Their ability to replicate the genetic and epigenetic landscape of human tissues enhances the accuracy of genotoxicity studies, particularly for assessing the impact of toxicants on cell differentiation and development. IPSCs offer a powerful tool for generating physiologically relevant data, which is essential for

understanding toxicological mechanisms and improving the translatability of preclinical findings to human biology.

1.6. The Hematopoietic Stem Cell Niche: Structure and Function

The blood system serves as a paradigm for the understanding of stem cell biology. Mature blood cells are predominantly short lived. Hematopoietic Stem Cells (HSCs) residing in specialized niches mainly the bone marrow are required to sustain continuous blood production throughout the life on an individual and replenish multipotent progenitors towards hematopoietic lineages e.g. red blood cells, myeloid cells, lymphocytes and megakaryocytes. The existence of microenvironments or niches that are specific for HSC maintenance was initially proposed by Schofield in 1978 [60]. This concept suggested that stem cells are in close association with other tissue-resident cells to determine their behaviour for instance by preventing their differentiation while ensuring their continuous proliferation. Based on this theory, advances in molecular biology and imaging techniques have resulted in a better understanding of the hematopoietic stem cell niche by determining the location of HSCs, thus revealing the molecular mechanisms underlying the stem cell niche. The bone marrow is a complex network between several cell types. Endothelial cells including arterioles, sinusoids and transition zone vessels. They regulate the trafficking and homing of hematopoietic stem cells and progenitors. Mesenchymal stromal cells are crucial elements of the bone marrow niche. They provide osteoblasts for bone tissue regeneration and control HSC fate both by direct interaction and through cytokine secretion.

1.7. Hematopoietic Stem Cells (HSCs)

HSCs sustain production of all blood cells throughout the life of an individual. Already in the 1960s, Till and McCulloch proposed the existence of self-renewing clonal precursor cells for all differentiated blood cells [61]. Weissmann and colleagues showed in 1989 that isolated mouse HSCs can reconstitute lethally irradiated mice upon transplantation, proving that HSCs are critical for sustaining lifelong hematopoiesis, enabling the continuous replenishment of blood cells and immune system components [62]. Further studies could identify different populations of hematopoietic stem and progenitor cells (HSPCs) and provided evidence for the hierarchical organization of hematopoiesis with long-term HSCs (LT-HSCs) at the top of the hierarchy, with their unique self-renewal and differentiation capacity in all types of blood cells. Moreover, LT-HSCs give rise to short-term HSC (ST-HSCs) and multipotent progenitors (MPPs), which possess a broad differentiation potential and proliferate rapidly but do not have the long-term self-renewal capacity. Further differentiation steps lead to increasingly lineage-specific progenitors until final production of mature cells.

Nowadays, HSCs are one of the most studied tissue-specific stem cells and the cornerstone of the hematopoietic niche, where they reside in a delicately balanced microenvironment, which plays a crucial role in maintaining their quiescence, supporting their self-renewal and regulating their differentiation into various blood lineages. Beyond their fundamental biological role, HSCs hold an immense clinical importance particularly in transplantation therapies and regenerative medicine since

their transplantation with the bone marrow or peripheral blood grafts result in long-term reconstitution of the hematopoietic system making them ideal candidates in clinical hematology for treatment if various malignancies and autoimmune blood diseases.

Fetal hematopoiesis begins around 2-3 weeks after fertilization in the yolk sac, where primitive hematopoietic cells emerge to meet the oxygenation needs of early embryonic tissues. This stage is characterized by the production of nucleated red blood cells and the absence of lymphoid differentiation. As development progresses, hematopoietic activity transitions to the fetal liver, which becomes the dominant site for definitive hematopoiesis. Unlike the yolk sac, the fetal liver supports the expansion of HSPCs capable of giving rise to a broader range of blood cell lineages. By mid-gestation, hematopoiesis gradually shifts to the bone marrow, a transition marked by the establishment of a more specialized and enduring hematopoietic niche. The coordinated movement between these sites ensures that the hematopoietic system can meet the dynamic physiological demands of growth and development.

While HSCs can be derived from various sources, including the bone marrow, peripheral blood and umbilical cord blood, the source significantly influences their biological characteristics and clinical utility. In particular, neonatal HSCs from cord blood and adult HSCs from the bone marrow exhibit distinct properties in terms of their proliferation, differentiation, and therapeutic applications. Understanding these differences is critical for optimizing their use in both research and clinical settings.

The umbilical cord consists of a vein allowing blood flow from the placenta to the embryo or foetus and two arteries carrying blood back to the placenta. Residual umbilical cord blood (UCB) can be collected in a non-invasive procedure after delivery by puncturing the umbilical cord vein without endangering the mother or the child. CB is rich in HSCs, which have been used since the first successful transplantation by Eliane Gluckman in 1988 for treatment of hematopoietic disorders as an alternative to the more invasive bone marrow transplantation [63]. Neonatal CB-HSCs from cord blood are considered more primitive and less mature compared to their counterparts for the adult bone marrow or from peripheral blood. They have various advantages including their high proliferation potential. Moreover, CB-HSCs exhibit lower immunogenicity, reducing the risk of graft-versus-host disease (GvHD) and making them an attractive option for unrelated allogeneic transplantation. After collection, CB units are stored in cord blood banks in order to immediately be available for allogeneic stem cell transplantations worldwide. However, due to the limited amount of umbilical CB and the resulting limited yield of HSCs, it has long primarily been used for treatment of children or by combination of two unrelated CB unit for treatment of adults [64]. Current research is focused on overcoming this limitation through ex vivo expansion technologies, which aim to increase the number of HSCs available for transplantation while preserving their functional integrity.

In addition to their therapeutic potential, neonatal CB-HSCs offer a valuable and rare platform for investigating genotoxic insults. Their high proliferative potential and primitive state allow to study DDR mechanisms at an early developmental stage, providing insights that cannot be readily obtained from adult cells, offering a unique perspective on how immature hematopoietic cells respond to environmental or pharmacological stressors. These properties make them indispensable for

toxicological assessments aimed at understanding the long-term consequences of genotoxic exposure during early life stages. Additionally, CB-HSCs can be obtained in a quiescent state, making them particularly interesting for testing genotoxic effects on quiescent cells, which are known to have distinct DDR mechanisms compared to cycling cells.

Adult HSCs from bone marrow have been extensively studied due to their critical role in maintaining lifelong hematopoiesis. Unlike neonatal CB-HSCs, adult bone marrow HSCs are typically more differentiated and have a lower proliferative potential, reflecting their function in maintaining the blood system over a longer period. Bone marrow HSCs are typically collected from healthy adult donors and serve as a gold standard for autologous and allogeneic stem cell transplants in clinical applications.

1.8. Mesenchymal Stromal Cells (MSCs)

Neonatal Cord Blood Unrestricted Somatic Stem Cells and Cord Blood Mesenchymal Stromal Cells (CB-USSCs and CB-MSCs)

In addition to HSCs, umbilical CB (UCB) also contains non-hematopoietic cell types and is considered one of the most abundant sources of neonatal stem cells. Multipotent mesenchymal stromal cells were first described in umbilical CB in 2000 by Erices and colleagues [65]. They can be collected in a non-invasive and less expensive method after the umbilical cord is discarded at the time of birth. Since there are no ethical concerns are associated with UCB, CB-MSCs attract special interest due to specific advantages of embryonic and adult stem cells. Moreover, it has been shown that CB-MSCs are less immunogenic thus not eliciting the proliferative response of allogeneic lymphocytes in vitro [66]. Additionally, CB-MSCs expanded in vitro retained low immunogenicity, immunomodulatory effects along with lower graft rejection and post-transplant infections in comparison to other sources in children with severe T-cell immune deficiency disorders [67].

In 2004, Kögler and colleagues characterized a population of cord blood unrestricted somatic stem cells (CB-USSCs), which were considered as more primitive than adult MSCs since they have a higher proliferative potential and longer telomeres [68]. Later on, MSCs have been also identified in cord blood (CB-MSCs). In contrast to CB-MSCs, CB-USSCs have been found to lack the adipogenic differentiation potential compared to CB-MSCs. This was shown to be due differentially expressed markers: CB-USSCs express the delta drosophila homolog-like 1 (DLK1) gene but not homeobox (HOX) genes, in contrast to CB-MSCs, which are negative for DLK1 but express all HOX genes [69, 70]. In addition to this, these cell populations also differ in their support of hematopoietic cells in vitro. $CD34^+$ HSCs cultured on a CB-USSC feeder layer showed higher proliferation rates compared to co-culture with CB-MSCs [71]. The potential of stromal cells from CB for bone formation has been demonstrated in pre-clinical models. Osteogenic pre-differentiated CB-USSCs induced heterotopic ossification on a collagen bone matrix after implantation into rats [72]. Uchida et al suggested that CB-MSCs contribute to fracture healing after bone marrow engraftment and their transplantation not only reconstructed the hematopoietic system but also the mesenchymal cell lineages in mice [73].

Adult Bone Marrow MSCs (BM-MSCs)

As described in 1.6 and 1.7, adult BM contains hematopoietic stem and progenitor cells but also non-hematopoietic cells, which are involved in forming the microenvironment and endosteal niche for the maintenance and support of HSCs. It is hypothesized that these cells function as in situ perivascular cells on the surface of sinusoids.

In 1966, Friedenstein and colleagues identified this non-hematopoeitic population with osteogenic potential in the bone marrow [74]. This cell type was later on called mesenchymal stromal cells (MSCs).

BM-MSCs exhibit a strong tendency to differentiate into osteoblasts followed by bone and cartilage when studied in vivo [75, 76]. This has been confirmed by Hochmann et al. and can be further influenced by culturing the cells under hypoxic conditions [77, 78]. In the context of treating tendinopathy, BM-MSCs are considered particularly suitable due to their increased expression of tenogenesis-related factors, such as collagen I, Scleraxis, and Tenomodulin [79].

BM-MSCs are also the most extensively researched cell type for cartilage regeneration, largely because of their superior chondrogenic potential. Studies have shown that cells isolated from the iliac crest and vertebral body demonstrate a higher capacity for chondrogenesis compared to those harvested from the femoral head [80]. Hochmann et al. further investigated the molecular basis of stromal differentiation and found that specific transcription factor binding sites in enhancer and promoter regions of ossification-related genes are accessible only in BM-MSCs [77]. This suggests that their differentiation potential is influenced by epigenetic mechanisms that are dependent on the tissue of origin [77].

Despite all their advantages, BM-MSCs have relatively slow proliferation rates, shorter culture periods and longer population doubling times compared to MSCs from other tissues [81]. These properties are exacerbated by the natural aging process during in vitro culture, which leads to gradual telomere shortening and increased vulnerability to oxidative stress [82]. A further limitation of BM-MSCs is that their differentiation potential declines with donor age, making them less effective when harvested from elderly patients [83].

MSCs derived from cord blood or bone marrow, are highly valuable for toxicological testing due to their immunomodulatory properties and ease of isolation. These cells provide a robust platform for assessing genotoxic effects in stromal and hematopoietic environments, closely mimicking in vivo conditions. MSCs are particularly useful for studying the interaction of toxic agents with stromal support cells and their role in maintaining tissue integrity, thereby offering critical insights into the broader impacts of genotoxic exposure.

1.9. Chondrogenic and Osteogenic Differentiation during Skeletal Development

The human skeleton is an essential part of the human body consisting of 206 bones forming the framework supporting the body and providing shelter for vital organs. During human embryogenesis, skeletal development begins in the fourth pregnancy week with the formation of vertebral bodies. Between the fifth and the seventh week,

the cartilage is formed, followed by bone formation in the ninth week. Bone largely consists of the structural protein collagen (COL), which is formed by calcium phosphate crystals in the form of hydroxyapatite to provide additional stability, tensile strength and stress resistance. The inorganic matrix composed of calcium and phosphorus salts contribute to bone hardness and rigidity. Non-collagenous proteins such as the bone sialoprotein (BSP), water, polysaccharides, cells and blood vessels are also involved. The different bone types can be classified microscopically, macroscopically or on the basis of their external shape.

Microscopical identification occurs by the determination of the arrangement of the collagen fibres. These appear disorganized in woven/fibrous bones with very rapid bone formation (more than 4 mm per day), a characteristic of foetal bone and callus formed during bone healing. In contrast, lamellar bone formation is slow (less than 1 µm per day) but the collagen fibres are organized in parallel layers, so-called lamellae, in order to provide mechanical stability and greater stiffness.

Macroscopically, bones are divided into cancellous/spongy/trabecular bones (roughly 20% of the skeletal system) and cortical/compact bones (approximately 90% of the skeletal system). Cortical bones can be distinguished from trabecular bones by their dense mineralization with a significantly more bone tissue per unit volume than trabecular bone that has high porosity (70-80%). Moreover, trabecular bone has a large surface exposed to bone marrow, fat and blood flow.

Finally, bones can also be distinguished on the basis of their external shape. The long bones such as the femur and the humerus are cylindrical in shape and function as levers to move muscles during contraction. The short bones such as hand and tarsal bones have a cubic-like shape and are formed by cancellous bone surrounded by a thin layer of cortical bone. Flat bones such as the sternum, the cranial bones and the scapulae have a similar structure to short bones. They are typically thin but curved, serve as points of attachment for muscles and protect organs. Irregular bones such as the vertebrae and the facial bones have more complex shape and consist of a thin layer of cortical bone. Sesamoid bones such as the patellae are small round bones that form in tendons for their protection since a great deal of pressure is generated in the joint.

Bone formation is a highly regulated and complex process that begins during embryonic development and continues into adulthood. It involves the differentiation of mesenchymal precursor cells into osteoblasts. Two primary ossification types occur during this process: intramembranous ossification and endochondral ossification.

Intramembranous ossification forms flat bones and begins during embryonic development when MSCs within the connective tissue membranes aggregate and differentiate into osteoblasts, which in turn secrete the osteoid matrix that mineralizes thus forming bone tissue. The osteoblasts become embedded within the matrix and mature into osteocytes. As the ossification process progresses, the woven bone is remodelled into lamellar bone and vascularization occurs supporting the formation of marrow cavities and ensuring nutrient supply. Intramembranous ossification is controlled by the runt-related transcription factor 2 (RUNX2), which is activated by bone morphogenetic proteins (BMPs). HOX genes also contribute to the regulation of intramembranous ossification.

Endochondral ossification is responsible for forming long bones and begins with a cartilage model acting as a template for bone development. The process starts by MSCs aggregating and differentiating into chondrocytes, which secrete the extracellular matrix (ECM) in form of COL2 and aggrecan (ACAN) to form hyaline cartilage. Proliferation and differentiation of non-hypertrophic chondrocytes is controlled by the SRY-Box 9 transcription factor (SOX9), the master regulator of chondrogenesis. SOX9 knockout in mice inhibits the expression of genes related to non-hypertrophic chondrocytes [84]. The formed cartilage undergoes apoptosis in the centre creating space for the invasion of blood vessels and osteogenic cells in such that cartilage is gradually replaced by bone and continues in both directions. Secondary ossification centres develop at one or both ends of the epiphysis, whereas a layer of cartilage cells remains to enable further bone growth.

Following the migration of MSCs to the skeletogenesis site, interactions between epithelial and mesenchymal tissue lead to the initiation of the condensation process. This is achieved at the cellular level by the increases cell density and at the molecular level by the expression of characteristic molecules of the ECM and cell adhesion such as COL1, N-cadherin and neural cell adhesion molecule (NCAM, CD56). This is initiated by the transforming growth factor (TGF-ß), which also acts as an inducer of chondrogenesis during in vitro differentiation.

BMPs including BMP2 and BMP4 were originally described as regulators of ossification but also play a role in mesenchymal condensation and in chondrogenesis. They support cell-cell contact formation through N-cadherin induction. Inhibition of BMP by noggin, preventing them from interaction with their receptors, blocked mesenchymal condensation in in vivo studies on chickens, resulting in complete inhibition of cartilage development [85].

In contrast to osteoblasts, osteoclasts are multinucleated cells derived from macrophages and thus from BM-HSCs and are responsible for the resorption of bone by dissolving hydroxyapatite and degrading the collagen-rich organic matrix. Osteoclasts enable continuous renewal and homeostasis of bone substance.

1.10. Adipogenic Differentiation during Adipose Tissue Formation

Adipose tissue is a dynamic organ that plays a role in energy storage and mobilization by adapting to physiological conditions with the goal of energetic balance in the organism. Moreover, the adipose tissue has emerged as the largest endocrine organ, secreting hormones and inflammatory molecules playing a role in adipogenesis, metabolism and inflammation. There are two different types of adipose tissue in mammals: white and brown adipose tissue. White adipose tissue is designed for energy storage in form of triglycerides whereas brown adipose tissue generates heat and dissipates energy. The adipose tissue consists of several types of cells such as adipocytes, pre-adipocytes, fibroblasts, stromal cells, T-cells, macrophages, monocytes and granulocytes. Identical to chondroblasts and osteoblasts, adipocytes develop from mesodermal progenitors. However, the embryogenesis of adipocytes remains to be clarified.

For adipogenic differentiation in vivo, MSCs receive cytokine signals from surrounding cells. However, in vitro, they lack these cues and thus require specific induction factors

to drive their commitment towards the adipogenic lineage. Dexamethasone, indomethacin and insulin are the three essential factors for the in vitro adipogenic differentiation of MSCs [86]. Dexamethasone, a synthetic glucocorticoid agonist, serves as a strong promoter of MSCs differentiation in general [87]. Indomethacin, a nonsteroidal anti-inflammatory drug, facilitates adipogenesis by activating PPARγ [88, 89]. Insulin plays a multifaceted role in adipogenesis, primarily through its interaction with insulin-like growth factor-1 (IGF-1) receptors, which are more abundant in pre-adipocytes than insulin receptors [90]. This binding initiates a signaling cascade involving the phosphorylation of the cAMP response element-binding protein (CREB), ultimately upregulating key adipogenic transcription factors such as C/EBPα and PPARγ [91]. Additionally, insulin promotes PPARγ activation by inhibiting necdin, a suppressor of CREB-induced PPARγ expression [92].

As MSCs commit to adipogenesis, transcriptional changes drive their transformation into pre-adipocytes. One of the earliest events is the phosphorylation of CREB, which subsequently activates C/EBPβ [93]. This activation triggers a cascade inducing the expression of adipocyte-specific genes, including PPARγ. PPARγ is indispensable not only for adipocyte differentiation but also for maintaining the mature adipocyte state[94] [95]. Once committed, MSCs transition into pre-adipocytes, which are flat, spindle-shaped cells resembling fibroblasts or smooth muscle cells. These pre-adipocytes express markers such as pre-adipocyte factor 1 (Pref-1) and GATA2, which are no longer detectable in fully differentiated adipocytes [96, 97].

Throughout the adipogenesis process, pre-adipocytes stop proliferating, start accumulating lipid droplets and acquire both the structural and biochemical traits of mature adipocytes including the activation of hormone-regulated lipogenesis and lipolysis pathways. Nakamura et al. analysed human MSCs at several days after the induction of adipogenesis and identified a set of genes modulated after differentiation [98]. Hereby, it was revealed that several genes from other lineages were downregulated such as the cytoskeleton and the ECM, whereas others were upregulated in early stages such as C/EBPβ or in a late stages such as C/EBPα, C/EBPβ, PPARγ and FABP4. Other clusters related to lipid metabolism and adipocyte differentiation were also identified. Various other gene expression profile analyses conducted during the adipogenic differentiation have identified numerous upregulated genes associated with metabolic processes such as gluconeogenesis and fatty acid synthesis, as well as secreted proteins like TGF-β, IGF1, and IGF2 [99]. Additionally, transcription factors including PPARγ and C/EBPα displayed a time-dependent increase in expression, on day 14 and day 21, respectively [99]. Mature adipocytes also exhibit characteristics such as growth arrest, insulin sensitivity, and the secretion of adipokines such as adiponectin [100]. These cells maintain high expression of PPARγ and C/EBPα, which play crucial roles in sustaining their differentiated state. These findings highlight the early transcriptional shifts in MSCs as they transition toward an adipocyte phenotype.

1.11. MSC Heterogeneity

MSCs are a diverse and highly heterogeneous population of cells and this inherent variability represents a huge challenge but also an opportunity in their therapeutic

applications. MSC heterogeneity originates from various intrinsic and extrinsic factors including donor characteristics, tissue source and culture conditions.

Donor-dependent variability is particularly pronounced and includes differences in age, gender and health status. For instance, MSCs derived from younger donors typically exhibit higher proliferative rates, reduced senescence, less apoptotic cells and enhanced differentiation capacity compared to cells from older donors [101]. Donor age has also been shown to negatively affect MSC differentiation into osteoblasts and to reduce the immunomodulatory effects and the cell response to oxidative stress. Moreover, Kanawa and colleagues showed a decreased expression of glycosaminoglycans (GAG), SOX9, collagen II and aggrecan in BM-MSCs harvested from older donors, which is associated with a decreased chondrogenic capacity [102]. These differences are crucial as age-related senescence can compromise the immunomodulatory effects and regenerative capacity of MSCs, which are necessary for clinical efficacy. A comparison of BM-MSCs isolated from 53 different donors showed differences in the phenotype with higher levels of $CD71^+$, $CD90^+$, $CD106^+$, $CD140b^+$, $CD146^+$, $CD166^+$, and $CD274^+$ subpopulations in samples from younger donors [83].

Gender also influences MSC properties, with studies showing that female-derived MSCs may exhibit superior anti-inflammatory and pro-angiogenic capacities compared to cell derived from male donors [103, 104]. However, they may also display reduced adipogenic differentiation potential with increasing age [104].

In addition to donor age and gender, donor health status and functional deficiencies and basic treatment such as corticoid intake can also have an impact on MSC characteristics and functionality. MSCs derived from osteoporosis patients revealed a similar morphology and surface markers as cells from healthy individual but showed lower proliferation rates in response to insulin-like growth factor-1 (IGF1) and an upregulated expression of the alkaline phosphatase and calcium phosphate deposition related to a deficient osteogenic potential [105]. Similarly, cells harvested from multiple sclerosis patients showed higher senescence, low secretion levels of anti-inflammatory cytokines and a decreased inhibition of T cell proliferation compared to cells from healthy individuals [106]. AT-MSCs derived from obese donors also showed an altered plasticity in terms of changed patterns of surface markers, decreased proliferation and differentiation potential compared to MSCs from lean donors [107].

MSC source further contributes significantly to their functional diversity and heterogeneity. BM-MSCs are considered the most studied type and are known for their high osteogenic differentiation potential making particularly suitable for bone and cartilage repair. However, they display slower proliferation rates and are prone to culture-induced aging, which can limit their clinical scalability. In contrast, adipose tissue-derived MSCs (AT-MSCs) offer higher initial cell yields, faster proliferation and lower senescence levels making them more preferable for certain application such as immune modulation and tissue repair [108]. MSCs isolated from perinatal tissues such as the umbilical cord or placenta have even greater proliferation rates and reduced senescence compared to adult-derived MSCs along with their unique immunomodulatory properties. These neonatal sources provide MSCs with broader

differentiation potential and low immunogenicity, which are attributes for their particular advantage in allogeneic therapies.

Culture conditions introduce another layer of variability, as MSC behaviour can be significantly influenced by environmental factors such as oxygen tension, medium composition and mechanical stimuli. For instance, MSCs cultured under hypoxic conditions better mimic their native niches such as bone marrow, leading to enhanced proliferation, reduced senescence and increased secretion of trophic factors that support angiogenesis and tissue repair [109, 110]. Similarly, the choice of culture medium for instance the presence of fetal bovine serum (FCS), chemically-defined media or xeno-free alternatives can affect cell morphology, genetic stability and thus therapeutic potential [111]. Repeated passaging during in vitro expansion can further amplify these differences, with higher passages often associated with reduced functionality and increased genetic instability [112].

The molecular and phenotypic diversity of MSCs, coupled with their variable differentiation potentials, complicates their standardization for clinical applications. For example, MSCs from different tissues may not only vary in their capacity to differentiate into osteogenic, chondrogenic or adipogenic lineages but may also differ in their paracrine effects including cytokines secretion and immunomodulation. Despite these challenges, recent efforts have been made to establish minimal criteria for MSC characterization, such as adherence to plastic, specific surface marker expression (e.g., CD44, CD73, CD90, CD105) and the ability to differentiate into specific lineages in vitro. However, these criteria fail to capture the functional and therapeutic nuances of MSC populations underscoring the need for more refined approaches to MSC standardization.

MSC heterogeneity also impacts the outcomes of clinical trials, where inconsistent results are often attributed to variations in MSC source, processing and donor characteristics. For example, BM-MSCs may perform better in orthopaedic applications while AT-MSCs might be preferred for immune-related conditions such as GvHD. Therefore, ongoing research is focused on understanding and mitigating the effects of MSC heterogeneity including exploring MSC derived from iPSCs (iMSCs) as a potential solution.

1.12. Induced Mesenchymal Stromal Cells (iMSCs)

The use of MSCs is fraught with ageing-related shortfalls such as limited expansion and early senescence. For this, iMSCs, MSCs derived from iPSCs, have emerged as a promising alternative to primary MSCs to circumvent these drawbacks in clinically relevant scenarios. They offer a renewable and standardized source of MSCs, overcoming issues of donor-dependent variability while retaining key regenerative properties. Additionally, they can be generated in a patient-specific manner reducing the risks of immune rejection in autologous therapies. However, it is still unclear if iMSCs possess the same characteristics as MSCs and despite their advantages, concerns remain regarding their genomic stability and long-term safety, highlighting the need for further research into their therapeutic potential and behavior under stress conditions.

One of the major challenges in the use of induced mesenchymal stem cells (iMSCs) is the development of robust and reproducible differentiation protocols that ensure their functional compatibility with specific therapeutic applications. The iMSCs require carefully optimized differentiation conditions to acquire the trilineage potential of primary MSCs. The variability in differentiation efficiency, potential epigenetic memory from the iPSC state and differences in functional characteristics compared to primary MSCs pose significant hurdles for their clinical translation. Establishing standardized protocols that consistently yield iMSCs with the appropriate phenotypic and functional attributes is therefore crucial to harnessing their full therapeutic potential in regenerative medicine and disease modeling.

2. Aim of this Work

This study aims to assess the genotoxic effects of MNU and etoposide in human cell types of varying developmental stages, including iPSCs, neonatal HSCs and MSCs, as well as adult MSCs and iMSCs in order to address developmental age-related sensitivities relevant for toxicological evaluations complying with the 3R principle.

Specifically, the effects of MNU and etoposide on these cell types will be analyzed taking into account not only the type of damage induced by these agents, which significantly vary in their mechanisms and outcomes, but also the importance of cell type and cellular status.

For HSCs, the study will investigate how quiescent and cycling cells respond differently to genotoxic damage induced by MNU or etoposide, as their DNA repair capacities and sensitivities to insults are closely tied to their cell cycle status.

MSCs, on the other hand, provide and essential platform for studying the impact of developmental age on genotoxic responses. Their ability to be isolated from donor of varying ages and their capacity of self-renewal and differentiation make them ideal for the examination of age-dependent differences in DDR.

Additionally, this study will assess the effects of DNA damage on the trilineage potential of MSCs in an agent-dependent manner but also the effect of MSC differentiation status on the outcome of the genotoxin-induced damage. This provides a unique opportunity to evaluate how DNA damage affects lineage commitment.

Moreover, cord blood-derived HSCs and MSCs offer an exceptional system for this investigation, as they represent cells from a very early developmental age, allowing comparison with cells from older sources such as the adult bone marrow.

This approach will enable a more comprehensive understanding of how both the differentiation status and developmental age influence cellular responses to genotoxic agents, shedding light on critical variables in toxicological and therapeutic contexts.

3. Material and Methods

3.1. Material

3.1.1. Consumables

Table 1: List of consumables.

Consumables	Manufacturer
15 mL / 50 mL tubes	Greiner bio-one (Frickenhausen)
24-well cell culture plate, tissue culture treated	Corning Costar (Kennebunk, USA)
6-well cell culture plate, tissue culture treated	Corning Costar (Kennebunk, USA)
96-well cell culture plate, flat bottom clear	Greiner bio-one (Frickenhausen)
Adhesive Clear PCR Seal	Biozym (Hessisch Oldendorf)
Blunt fill needle	BD (Fraga, Spain)
C-Chop Disposable hemocytometer	NanoEntek (Seoul, South Corea)
Cell culture flasks (T25, T75,T225)	Corning Costar (Kennebunk, USA)
Cell lifter 19 mm	Corning (NY, USA)
Cover slips	Thermo Fisher Scientific (Schwerte)
Cryotubes	Greiner bio-one (Frickenhausen)
Färbekasten ROTILABO®	Carl Roth (Karlsruhe)
MACS LS column	Miltenyi Biotec (Bergisch Gladbach)
MicroAmp™ optische 96-well plate	Thermo Fisher Scientific (Schwerte)
Millicell® EZ Slide 8-well glass	Merck (Darmstadt)
PCR tubes	Biozym Scientific (Oldendorf)
Pipette tips	Starlab (Hamburg)
Pipette tips OneTouch	Sorenson Bioscience (Salt Lake City, USA)
Pre-separation filters 30µm	Miltenyi Biotec (Bergisch Gladbach)
Pyrex cloning rings	Merck (Darmstadt)
Safe-lock tube 1.5 mL	Sardtedt (Nümbrecht)
Safe-lock tube 2 mL	Eppendorf (Hamburg)

Consumables	Manufacturer
Serological pipettes	Corning (NY, USA)
Sterile filters (0.45 µm)	Thermo Fisher Scientific (Waltham, MA, USA)
SuperfrostTMPlus Adhesion microscope slides	Epredia (Basel, Switzerland)
Syringe (1,3,5 mL)	Braun (Melsungen)
Transfer pipette	Sarstedt (Nümbrecht)
Tube 15 mL	Greiner bio-one (Frickenhausen)
X200 Filterkarten Weiss 200 Stück	Thermo Fisher Scientific (Waltham, MA, USA)

3.1.2. Chemicals

Table 2: List of chemicals.

Chemicals	Manufacturer
100 bp ladder	New England Biolabs (Ipswich, MA, USA)
5x First strand buffer	Invitrogen (Karlsruhe)
7-AAD viability dye	Beckman Coulter
ABsolute QPCR Mix, SYBR Green, low ROX	Thermo Fisher Scientific (Schwerte)
Accutase	Merck (Darmstadt)
Acetic Acid (glacial)	Merck (Darmstadt)
Agarose	Eurogenetic (Köln)
Alizarin Red S	Sigma-Aldrich (Steinheim)
Ammonium hydroxide	Sigma-Aldrich (Steinheim)
Annexin V-FITC Apoptosis Detection Kit	BD Pharmingen (Heidelberg)
Biolaminine 521 LN	BioLamina (Sundbyberg, Sweden)
Boric acid	Roth (Karlsruhe)
Chloroform	Merck (Darmstadt)
CliniMACS PBS/EDTA Buffer	Miltenyi Biotec (Bergisch Gladbach)
Cryosure DMSO	WAK-Chemie Medical (Steinbach)

Chemicals	Manufacturer
ddH_2O	Fresenius AG (Hilden)
Dexamethasone-soluble water, cell culture Tested	Sigma-Aldrich (Steinheim)
dNTP Mix (10 mM)	Invitrogen (Carlsbad, USA)
DTT (0.1 M)	Invitrogen (Carlsbad, USA)
E. coli RNase H (5 U/µL)	Thermo Fisher Scientific (Waltham, MA, USA)
Entellan	Merck (Darmstadt)
Ethanol (99.5%)	VWR International (Leuven, Belgium)
Ethanol ≥ 70% (v/v), TechniSolv®	VWR International (Leuven, Belgium)
Etoposide	TCI Europe N. V. (Zwijndrecht, Belgium)
FcR blocking reagent	Miltenyi Biotec (Bergisch Gladbach)
Fetal calf serum	Gibco (Paisley, Great-Britain)
Ficoll® (Biocoll Separating Solution)	Bio&SELL GmbH (Feucht)
Fluoromount-G™	Thermo Fisher Scientific (Schwerte)
Glycerol-2-phosphate	Sigma-Aldrich (Steinheim)
High glucose DMEM (4.5 g/L)	Sigma-Aldrich (Steinheim)
Hoechst 33342 Solution (20 mM)	Thermo Fisher Scientific (Schwerte)
IBMX	Sigma-Aldrich (Steinheim)
Indomethacine	Sigma-Aldrich (Steinheim)
Insulin	Gibco (Paisley, Great-Britain)
Insulin-Transferrin-Selenium	Thermo Fisher Scientific (Schwerte)
Iscove's Medium (without L-Glutamine)	Bio&SELL (Feucht)
Isopropanol	VWR International (Leuven, Belgium)
Low glucose DMEM (1 g/L)	Gibco (Paisley, Great-Britain)
Methanol	Merck (Darmstadt)
M-Freeze™ Cryoembedding media	Merck (Darmstadt)

Chemicals	Manufacturer
$MgCl_2$ (50 mM)	Invitrogen (Carlsbad, USA)
Midori Green	Biozym Scientific
MitoTracker™ Green FM	Thermo Fisher Scientific (Schwerte)
N-Methyl-N-Nitrosourea	Biozol (Eching)
Normal Goat Serum	Invitrogen (Karlsruhe)
Oil Red O	Waldeck
$Oligo(dT)_{20}$ (50 µM)	Invitrogen (Karlsruhe)
Oligonucleotides	Thermo Fisher Scientific (Schwerte)
Paraformaldehyde solution (PFA, 4% in PBS)	AppliChem GmbH (Darmstadt)
PBS pH 7.3	Sigma-Aldrich (Steinheim)
Penicillin-Streptomycin Mixture (PS)	Lonza (Basel, Switzerland)
ProLong Gold Antifade reagent with DAPI	Thermo Fisher Scientific (Schwerte)
Propidium iodide	Thermo Fisher Scientific (Schwerte)
Penicillin-Streptomycin-Glutamin Mixture (PSG)	Gibco (Paisley, Great-Britain)
Resazurin sodium salt	Sigma-Aldrich (Steinheim)
Rnase-free water	Sigma-Aldrich (Steinheim)
RNaseOUT (100 mM)	Thermo Fisher Scientific (Schwerte)
RNeasy Mini Kit	Qiagen (Hilden)
Sodium acetate	Sigma-Aldrich (Steinheim)
Sodium L-ascorbate	Sigma-Aldrich (Steinheim)
Sodium pyruvate	Sigma-Aldrich (Steinheim)
StemMACS ™ HSC-CFU lite with Epo	Miltenyi Biotec (Bergisch Gladbach)
SuperScript™ III Reverse Transcriptase	Thermo Fisher Scientific (Schwerte)
Tetramethylrhodamin, Methylester, Perchlorat (TMRM)	Thermo Fisher Scientific (Schwerte)
TRI Reagent	Sigma-Aldrich (Steinheim)
Triton X-100	Sigma-Aldrich (Steinheim)

Chemicals	Manufacturer
Trypan Blue Solution (0.4%)	Sigma-Aldrich (Steinheim)
TrypLE™ Express Enzyme (1X), no phenol red	Thermo Fisher Scientific (Schwerte)
Tween® 20	SERVA (Heidelberg)
Xylene	Merck (Darmstadt)
Y-2763215	Xylene	Merck (Darm
β-glycerophosphate disodium salt hydrate	Sigma-Aldrich (Steinheim)
β-mercaptoethanol	Sigma-Aldrich (Steinheim)

3.1.3. Buffers

Table 3: List of used buffers and their composition.

Buffer	Composition
10x TBE (gel electrophoresis)	Tris (108 g/L) EDTA (8 g/L) Boric acid (55 g/L) ddH_2O ad 1 L
Na_2EDTA (0.5 M, pH10)	Na_2EDTA (186 g) ddH_2O ad 1 L
NaOH (10 M)	NaOH (400 g) 900 mL ddH_2O
N-Lauroylsarcosine (10%)	N-Lauroylsarcosine (50 g) ddH_2O ad 500 mL (90 °C and shaking)
Lysis buffer (pH 10)	NaCl (2.5 M, 146.25 g) EDTA (100 mM) Tris (10 mM, 1.2 g) 400 mL ddH_2O N-Lauroylsarcosine (1%) ddH_2O ad 890 mL Directly before use: Triton X-100 (1 mL) DMSO (10 mL) Lysis buffer (89 mL)
Electrophoresis buffer (pH13)	NaOH (300 mM) Na_2EDTA (1 mM)
Neutralization buffer	Tris (400 mM) ddH_2O ad 900 mL Adjust to pH 7.5 ddH_2O ad 1 L
Low melting point agarose	LMP-agarose (0.5%) ddH_2O

Buffer	Composition
Propidium iodide staining solution	PI (50 µg/mL) ddH_2O

3.1.4. Technical Devices

Table 4: List of used technical devices.

Device	Manufacturer
AlphaImager MINI	Biozym Scientific (Oldendorf)
AVISO CellSelector robot control	Automated Lab Solutions (Jena)
Axiovert 25	Zeiss (Jena)
CELL-DYN Ruby	Abbott Diagnostics (Wiesbaden)
Centrifuge MIKRO 200R	Hettich (Tuttlingen)
Centrifuge ROTIXA 50RS	Hettich (Tuttlingen)
CO_2 Incubator	Binder (Gleisdorf, Austria)
CytoFlex	Beckman Coulter (Marseille, France)
Cytospin 3	Thermo Fisher Scientific (Schwerte)
Holten Laminair	Thermo Fisher Scientific (Schwerte)
Infinite® M Plex, multimode microplate reader, monochromator optics	Tecan (Männedorf, Switzerland)
Mastercycler EP gradient S PCR	Eppendorf (Hamburg)
Microplate reader	Tecan Trading AG (Männedorf, Switzerland)
Microscope camera CC12	Olympus Soft Imaging (Münster)
Microscope Olympus CKX41	Olympus (Münster)
NanoDrop ND-1000	Thermo Fisher Scientific (Schwerte)
Power supply PowerPac Basic	Bio-Rad Laboratories (Feldkirchen)
Quant Studio 3 qPCR cycler	Thermo Fisher Scientific (Schwerte)
Thermomixer comfort	Eppendorf (Hamburg)
Water bath Julabo SW 20	Julabo (Seelbach)

3.1.5. Media

Table 5: List of used media for cell culture and differentiation and their composition.

iPSC culture medium	**MSC and iMSC culture medium**
StemMACS iPS-Brew XF	DMEM low glucose
10 µM Y-2763215	30% FCS
MSC osteogenic medium	1% PS
DMEM low glucose	**MSC adipogenic culture medium**
10% FCS	DMEM high glucose
1% PS	10% FCS
10^{-7} M Dexamethasone	1% PSG
50 µg/mL Ascorbic acid	0.01 mg/mL Insulin
10 mM β-Glycerolphosphate	**MSC chondrogenic medium**
MSC adipogenic induction medium	DMEM high glucose
DMEM high glucose	1% PS
10% FCS	100 nM Dexamethasone
1% PSG	35 µg/mL Ascorbic acid 2-phosphate
0.1 mg/mL Insulin	1 mM Natrium pyruvate
1 mM IBMX	ITS (1:100 dilution)
10^{-6} M Dexamethasone	10 ng/mL TGF-β1
0.2 mM Indomethacine	
HSC culture medium	
SCGM	
25 ng/mL SCF	
25 ng/mL FLT3-L	
25 ng/mL TPO	
25 ng/mL IL-3	
25 ng/mL IL-6	

3.1.6. Cytokines

Table 6: List of used cytokines.

Cytokine	Manufacturer
Human FLT3-L	Miltenyi Biotec (Bergisch Gladbach)
Human IL-3	Miltenyi Biotec (Bergisch Gladbach)
Human IL-6	Miltenyi Biotec (Bergisch Gladbach)
Human SCF	Miltenyi Biotec (Bergisch Gladbach)
Human TGF-β1	Miltenyi Biotec (Bergisch Gladbach)
Human TPO	Miltenyi Biotec (Bergisch Gladbach)

3.1.7. Oligonucleotides

All used oligonucleotides were designed for this or for previous works by members of Prof. Dr. Kögler group in the ITZ and were synthesized and purified by HPLC by Thermo Fisher Scientific and diluted to a final concentration of 0.02 µM.

Table 7: List of used oligonucleotides, their sequences and expected product size of the amplicon.

Oligonucleotide	Forward sequence (5´-3´)	Reverse sequence (5´-3´)	Product size [bp]
Osteogenic Genes			
BMP2	CGCTCTTTCAATGGACGTGT	CAACGCTAGAAGACAGCGGG	98
BMP4	CCACCACGAAGAACATCTGG	ACGTCGTTCTCAGGGATGC	96
BSP	GGGCAGTAGTGACTCATCCG	AAGCTGGATTGCAGATAACCC	214
OCN (BGLAP)	CCTCACACTCCTCGCCCTATT	CCCTCCTGCTTGGACACAAA	117
ON	TAAACCCCTCCACATTCCCGCG	TTCTTGCTGAGGGGCTGCCAAG	159
OPN	GCCGAGGTGATAGTGTGGTT	AACGGGGATGGCCTTGTATG	149
OSX (SP7)	TGCTTGAGGAGGAAGTTCAC	CTGAAAGGTCACTGCCCAC	153
RUNX2	GAGTGGACGAGGCAAGAG	GGACACCTACTCTCATACTG	215
Adipogenic Genes			
ADIPOQ (APM1)	TCCGCAGTGTAGGCTTTACC	TACACTTGCTGGGGCATCTG	195
C/EBPα	GAGTCACACCAGAAAGCTAG	GATGGACTGATCGTGCTTC	184

C/EBPβ	TTTCGAAGTTGATGCAATCG	ACAGCAACAAGCCCGTAGG	130
FABP4	GCTTTGCCACCAGGAAAGTG	ATGACGCATTCCACCACCAG	280
PLIN1	CTCACCTTGCTGGATGGAGA	CGAGTGTTGGCAGCAAATTC	485
PPARγ	TCCATGCTGTTATGGGTGAA	TCAAAGGAGTGGGAGTGGTC	193
DDR Genes			
ATM	CCTTGTGCTAGTGGGCAGAA	ATGGGGAGCAAAGAACCCAG	150
BRCA1	CCACAGATCAACCTGGAATGG	GTAGAGTGCTACACTGCTCA	209
BRCA2	TTCTGAGGTGGACCTAATAGG	TGATTTGGATTCTGGTCGCC	193
MGMT	ACCGTTTGCGACTTGGTACT	GGGCTGGTGGAAATAGGCAT	246
NHEJ1	CCATTGTTGAAGGACGCTGC	CTAGCTCCCTCACTTGGCAC	217
P21 (CDKN1A)	TACATCTTCTGCCTTAGT	TCTTAGGAACCTCTCATT	162
P53	TTCCGAGAGCTGAATGAGGC	AATGTCAGTCTGAGTCAGGCC	166
RAD51	GCTGATGAGTTTGGTGTAGC	AACATAGCTTCAGCTTCAGG	215
XRCC4	CCTCTAGGAGAATCAGCTTCAAGA	AAAGAGGTCTTCTGGGCTGC	132
XRCC5	AGCATAGACTGCATCCGAGC	TCCCCATACATCCACGACCT	315
XRCC6	TGCGTGGATTGTCGTCTTCT	CTTCTTCATCGCCCTCGGTT	111
Housekeeping Genes			
GAPDH	GAGTCAACGGATTTGGTCGT	TTGATTTTGGAGGGATCTCG	238
RPL13a	GAGGTATGCTGCCCCACAAA	TTCAGACGCACGACCTTGAG	136

3.1.8. Antibodies

Table 8: List of used antibodies.

Antibodies	**Fluorophore**	**Clone**	**Manufacturer**
Phospho-Histone H2AX (Ser139), mouse	None	JBW301	Merck (Darmstadt)
53BP1, rabbit	None	Polyclonal	Cell Signalling Technology (Danvers, USA)
Anti-mouse, goat	Rhodamine Red-X	Polyclonal	Jackson ImmunoResearch (Ely, UK)

Anti-rabbit, goat	Alexa-Fluor 488	Polyclonal	Jackson ImmunoResearch (Ely, UK)
CD34, mouse	PE	8G12	BD Biosciences (San Jose, USA)
CD34, mouse	PE		Miltenyi Biotec (Bergisch Gladbach)
CD45, mouse	FITC	2D1	BD Biosciences (San Jose, USA)
CD38, mouse	APC	HIT2	BD Pharmingen (Heidelberg)
CD10, mouse	PE-Cy™7	HI10a	BD Pharmingen (Heidelberg)
CD45RA, mouse	APC-Alexa Fluor 750	2H4LDH11LDB9 (2H4)	Beckman Coulter (Marseille, France)
CD90, mouse	FITC	F15-42-1-5	Miltenyi Biotec (Bergisch Gladbach)

3.2. Methods

3.2.1. Cell Culture

All cell culture work described below was carried out under sterile conditions under a sterile workbench. All cells were cultivated at 37 °C with 21% O_2 and 5% CO_2.

All MSCs used in this work were generated or isolated by the group of Prof. Kögler at the Institute for Transplantation Diagnostics and Cell Therapeutics in the University Hospital Düsseldorf. Umbilical cord blood (UCB) units were donated to the José Carreras Cord Blood Bank by the respective mothers in accordance with the Declaration of Helsinki. The units used to isolate hematopoietic stem cells did not match the requirements for transplants and were used for research purposes with donator consent.

Table 9: Overview of the used cell lines.

Source	**Cell type**	**Cell line**	**Donor gender or age (if known or relevant)**
Neonatal Cord Blood	iPSC	R24	M
		R25	F
		R26	M
	Primary $CD34^+$ HSC	-	-
	CB-USSC	SA5/73	-

		SA8/25	-
		SA10/36	-
		USSC86b	-
	CB-MSC	SA6/51	-
		SA8/39	-
		USSC63	-
		USSC120a	-
	iMSC	R26	-
		R34	-
		R35	-
Adult Bone marrow	BM-MSC	KM9-14	23
		KM9-15	32
		KM114	43
		KM120	-
		KM8/06	52
		KM1/23	36
		KM2/23	31
		KM3/23	24

3.2.2. Generation and Culture of iPSCs

The iPSCs used in this work were generated by Catalent Düsseldorf GmbH by episomal reprogramming as described in Okita et. al. [113], from cord blood $CD34^+$ HSCs after their isolation and expansion. They were subsequently maintained in StemMACS iPS Brew XF medium on Biolaminine 521 LN matrix and were routinely replated twice per week in the presence of 10 µM Y-2763215 using Accutase. Y-2763215 (1:1000) was removed from the medium after 24 h.

3.2.3. Cryopreservation of iPSCs

IPSCs were frozen as vials of $1x10^6$ cells. For this, cells were centrifuged at 300 g for 3 min at RT. After discarding the supernatant, $1x10^6$ cells were resuspended in 900 µL culture medium with Y-2763215 (1:1000) before adding 100 µL DMSO. The tubes were inverted and frozen at -80 °C before transfer to liquid nitrogen.

3.2.4. Thawing of iPSCs

IPSCs were thawed in pre-warmed StemMACS iPS Brew XF medium, centrifuged at 300 g for 3 min at RT. After discarding the supernatant, the cells were resuspended in 2 mL medium containing Y-2763215 (1:1000) and plated as described in 3.2.2.

3.2.5. Generation of CB-MSCs and CB-USSCs

CB-MSCs and CB-USSCs were generated as described in [68].
Mononuclear cells (MNC) were separated by Ficoll gradient. The cells in the interphase were washed and the remaining erythrocytes were lysed using ammonium chloride. The obtained MNCs were diluted in culture medium containing $1x10^{-7}$ M/mL dexamethasone. The medium was exchanged one a week. As soon as new colonies become visible, culture medium without dexamethasone was used. CB-MSC or CB-USSC generation was only carried out if colonies were formed in the first 4 weeks. The single colonies were trypsinized using cloning rings for further expansion. To differentiate CB-MSC from CB-USSC colonies, DLK1 and HOX gene expression was analyzed. Additionally, the adipogenic differentiation potential was evaluated.
The units used to isolate CB-MSCs and CB-USSCs did not match the requirements for transplants and were used for research purposes with donator consent.

3.2.6. Generation of BM-MSCs

BM-MSCs were generated as described in [114].
Human bone marrow was obtained from healthy unrelated bone marrow donors. Mononuclear cells were isolated and cultured in 225 cm^2 flasks for 1 to 2 weeks at 37 °C in a humidified atmosphere and 5% CO2 using low-glucose DMEM with 30% pretested FCS, $1x10^{-6}$ M dexamethasone, penicillin (100 U/mL), streptomycin (0.1 mg/mL), and glutamine (2 mM). Adherent cells were transferred into 75 cm^2 flasks. After cells were confluent again, they were transferred into 225 cm^2 flasks, analyzed by flow cytometry to identify contaminating residual hematopoietic cells and used for the experiments. Hematopoietic cells were no longer detected from passage 3 on.

3.2.7. Generation of iMSCs

The iMSCs used in this work were generated by Catalent Düsseldorf GmbH as described in [115]. For this, iPSCs generated from $CD34^+$ HSCs were differentiated into iMSCs by adding 4 µM CHIR99021 into the iPSC culture medium for 6 days followed by a medium switch to RoosterNourish-MSC-XF. After thawing, iMSCs were cultivated in the MSC culture medium (Table 5).

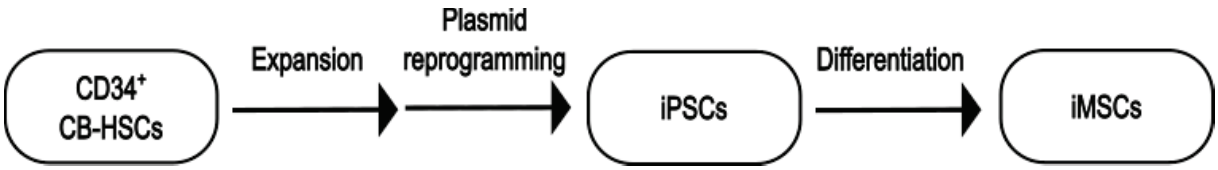

Figure 3: Experimental workflow followed for the generation of iMSCs.

3.2.8. Determination of Cell Numbers Using the Improved Neubauer Chamber

Manual determination of the cell count with the Improved Neubauer chambers was performed for cell counting. For this purpose, 10 µL of the cell suspension were mixed with 10 µL of 0.4% Trypan blue and added into the Improved Neubauer chamber. The Trypan blue dye is not able to penetrate the membrane by itself and hence is excluded from living cells, while it can pass the porous membrane of nonviable cells and stain their cytoplasm [116]. Under the light microscope, dead cells can therefore be distinguished from living cells due to their blue color.

To determine the cell numbers, cells on each of the four large squares were counted and offset against dilution, sample volume and chamber factor (Equation 1).

$$Total\ cell\ count = \frac{Counted\ cells * Volume * Dilution * Chamber\ factor}{Number\ of\ squares}$$

Equation 1: Formula for the calculation of cell numbers using an Improved Neubauer chamber.

3.2.9. Passaging of MSCs and iMSCs

MSCs were passaged twice a week after reaching a confluency of approximately 80%. For this, the cells were washed with PBS and incubated for 5 min at 37 °C with TrypLE (1x). The reaction was stopped with basal DMEM medium and the cells were centrifuged at 750 rcf for 7 min at 4 °C. After centrifugation, cells were resuspended in the appropriate medium and counted prior to usage for further experiments.

3.2.10. Cryopreservation of MSCs and iMSCs

For cryopreserved storage, 0.5-2x106 MSCs were harvested in 500 µL 80% FCS in DMEM medium mixed with 20% DMSO in DMEM and immediately transferred to -80 °C. The cryotubes were stored permanently after a few days in liquid nitrogen.

3.2.11. Thawing of MSCs and iMSCs

To thaw cryopreserved MSCs, the cell suspension in the cryotube was thawed in a water bath (37 °C) until only a small ice crystal remained. Subsequently, 2 mL 50% FCS in DMEM was quickly added to the cell suspension and transferred into a 15 mL tube and topped up with 15% FCS in basal DMEM. After a centrifugation step (7 min, 550 rcf, 4 °C), the supernatant was discarded and the cells were further transferred into culture medium.

3.2.12. Isolation of Mononuclear Cells from Cord Blood

In order to obtain HSCs from umbilical cord blood, mononuclear cells were isolated from cord blood units that were not suitable for transplantation. Since the numbers of $CD34^+$ HSCs are limited (0.1-1%), the mononuclear cells are pre-enriched to improve the recovery of the stem cells using Ficoll®-Paque [117]. Ficoll® consists of inert polysucrose of high density and is used to establish a density gradient [118]. Thus, the individual cell types of the blood are hereby separated due to their respective densities. Therefore, 35 mL of blood was carefully layered on 15 mL Ficoll® in a canonical 50mL tube. After centrifugation at 850 g at 20 °C for 20 min and without brakes, the mononuclear cells were enriched in the interphase between Ficoll® and plasma. The interphase was transferred into two 50 mL tubes, which were then filled up to 50 mL with PBS. After centrifugation at 750 g and 10 °C for 10 min, the supernatant was discarded and the resulting pellets were pooled in one tube using PBS and filled up to 50 mL. In order to further enhance purity and remove remaining platelets, an additional centrifugation step was conducted at 200 g and 20 °C for 15 min. The platelet containing supernatant was discarded and the pellet was resuspended in 50 mL of PBS/EDTA containing 0.5% HSA and filled up to 50 mL. After centrifugation at 550 g and 4 °C for 7 min, the supernatant was discarded and the pellet was resuspended in 50 mL of the HSA-containing PBS/EDTA and again centrifuged at 300 g and 4 °C for 5 min after determination of cell numbers using the CELL-DYN Ruby system. The resulting pellet was further used for isolation $CD34^+$ HSCs via Magnetic Activated Cell Sorting (MACS).

3.2.13. Determination of Cell Numbers using the CELL-DYN Ruby System

The CELL-DYN Ruby system is an automated multi-parameter hematology analyzer, which uses multiple angles of side scatter and hydrodynamic focusing to determine the nuclear optical cell count (NOC). This value can be used to calculate the total nuclear count (TNC) by multiplication with volume and dilution of the sample. Determination of the cell numbers with the CELL-DYN Ruby system was performed when suspensions with large amounts of cells were analyzed like whole blood samples or MNC fractions prior to MACS isolation. For this method, 300 µL of cell suspension in PBS or blood were used.

3.2.14. Magnetic Activated Cell Sorting (MACS)

After washing the MNC fraction, $CD34^+$ HSCs were further isolated using the MIDI-MACS system according to the manufacturer´s protocol. This method relies on antibodies labelled with magnetic nanoparticles targeting the surface marker CD34 expressed by the hematopoietic stem cells. After resuspension of the mononuclear cell pellet in 300 µL PBS/EDTA containing 0.5% HSA per $1x10^8$ cells, 100 µL of FcR Blocking Reagent and CD34 Microbeads were added to the same cell number. For magnetic labelling, cells were incubated at 4 °C for 30 min, washed with 10 mL buffer and centrifuged at 300 g and 4 °C for 10 min. After discarding the supernatant, the cells were again resuspended in an appropriate buffer volume.

Before application of the labelled cells, a MACS column was placed in the magnetic field of the MACS separator and equilibrated with 3 mL buffer. After the application of the whole cell suspension into the column, this was washed three times with 3 mL buffer each. To elute the purified $CD34^+$ HSCs, the column was transferred into a 15 mL tube, 5 mL buffer were added onto the column and the labelled cells were flushed out using a plunger. If required, the purity of the eluted cells was increased by repeating the magnetic separation using a second column.

3.2.15. Fluorescence Activated Cell Sorting (FACS)

FACS was used to reach higher purities (> 99%) of $CD34^+$ HSCs after MACS isolation. FACS allows the isolation of a certain cell type labelled with fluorescent antibody among a heterogeneous mixture. For this, the sample is injected into a narrow stream of sheath fluid with laminar flow in order to focus cells for analytics. Here, the cell characteristics are analyzed by the detector regarding the size (forward scatter), granularity (side scatter) or fluorescence signal of the cell. By breaking the stream into droplets containing only a single cell, a charge can be applied to each droplet depending on the cell characteristics. This way, a positive/negative charge can be applied to the desired cells and separate them from the remaining contaminants when passing a deflection system.

After MACS isolation and 30 min prior to FACS cell sorting, antibodies were added. Cells were sorted based upon their respective characteristics using MoFlo XDP. The instrument was used with standard optical configuration and samples were sorted using a 100 µm nozzle. First, live cells were selected based on FSC/SSC. Doublets were excluded by the SSC-width parameter and dead cells by staining with 7AAD-PE. CD34-PE and CD45-FITC antibodies were used to determine the HSCs. The HSC population was sorted via $CD34^+$ $CD45^{low}$.

3.2.16. Expansion of HSCs

After isolation, HSCs were cultured in SCGM medium containing SCF, TPO, FLT3-L, IL-6 and IL-3 to final concentrations of 25 ng/mL. $1x10^5$ to $1x10^6$ cells per well were added into a 24-well plate and cultured in 2 mL medium per well. The duration of the expansion depended on the experiment and the respective readout.

3.2.17. Colony Forming Unit Assay

The ability of HSCs to differentiate into all cells of the blood lineage was used as a functional readout regarding stem cell properties of isolated and expanded $CD34^+$ HSCs in culture. Every single $CD34^+$ HSC has the potential of differentiating into a colony-forming unit (CFU). It enables the identification of CFU-erythroid (CFU-E) and burst-forming unit erythroid (BFU-E), that lack self-renewal capacity and can only differentiate into cells of these hematopoietic lineages and CFU-granulocyte, erythroid, monocyte/macrophage, megakaryocyte (CFU-GEMM), that have multi-lineage differentiation potential and limited self-renewal.

Depending on the cell numbers and thus on the volume of the used $CD34^+$ HSCs, up to 160 µL Iscove´s medium was layered onto 840 µL of CFU medium. Next, 1000

CD34+ HSCs were added to the upper layer of Iscove´s medium. The phases were mixed using a 1 mL syringe and transferred into three wells of a 24-well plate each containing 250 µL. The neighboring cells were filled with ddH_2O to prevent dehydration. After 14 days of incubation, the readout was performed. For this, the colonies were counted and the total number colony forming cells (CFC) was calculated with respect to the total cell count in the sample with following equation:

$$\text{Total CFC} = \frac{\sum \text{Colonies in 1mL} * \text{Total cell count}}{\text{Cells used in assay}}$$

Equation 2: Formula for the calculation of the total number of colony forming cells.

3.2.18. Cell Fate Analysis of CD34+ HSCs

The subpopulations present in the CD34+ fraction were analyzed by flow cytometry using following monoclonal antibodies: CD34-PE, CD38-APC, CD10-PE-Cy™7, CD45Ra-APC-A750, CD90-FITC, propidium iodide. Cells were co-stained with all antibodies for 15 min and washed with PBS. The cells were subsequently analysed by flow cytometry.

3.2.19. MNU Treatment of iPSCs, MSCs and iMSCs

For MNU treatment, cells that were cultivated in culture medium medium were washed twice with PBS. The second PBS washing step was carried out at 37 °C for 5 min to remove any FCS remains, if included. MNU was diluted to the desired concentration in basal DMEM medium and added to the cells. After an incubation of 1 h at 37 °C, the treatment medium was removed and culture or differentiation medium was added to the cells.

3.2.20. MNU Treatment of HSCs

For MNU treatment, HSCs were washed once with PBS. MNU was diluted to the desired concentration in basal SCGM medium and added to the cells. After incubation for 1 h at 37 °C, the treatment medium was removed and culture SCGM medium was added to the cells.

3.2.21. Etoposide Treatment of iPSCs, MSCs and HSCs

For etoposide treatment, cells were washed once with PBS before incubation with etoposide diluted to the desired concentration in the appropriate culture medium. After 24 h, the treatment medium was removed, cells were washed with PBS and culture medium was added to the cells.

3.2.22. Growth Kinetics

To evaluate the cumulative population doublings (CPD), the following formula were applied.

$$PD = \frac{\log \frac{n_1}{n_0}}{log_2}$$

$$CPD = \Sigma PD$$

Equation 3: Formula for the calculation of the population doublings and cumulative populations doubling, where n_1 is the number of harvested cells, and n_0 is the number of plated cells.

3.2.23. Apoptosis Assay

Apoptosis detection and quantification was performed using Annexin V-FITC Apoptosis Detection Kit according to the manufacturer protocol. Flow cytometry analysis was performed using CytoFlex Flow Cytometer.

3.2.24. Alkaline Comet Assay

1-2x10^6 cells were washed with PBS, pelleted and stored on ice or at -20 °C. The cell number used for the assay is fixed upon all samples to be compared. 10 µL of the cell suspension was added to 120 µL LMP-Agarose (37 °C), placed on an object slide and covered with a coverslip, which was then cooled for 5 min at 4 °C. Next, the coverslip was carefully laterally removed and incubated for 1h in pre-cooled lysis buffer at 4 °C. The slides were removed from the lysis buffer, allowed to drain and placed into an electrophoresis chamber before over layering (2-3 mm) with pre-cooled electrophoresis buffer. After an incubation step of 25 min for alkaline denaturation of DNA at 4 °C, electrophoresis was carried out (25 min, 25 V and 300 mA) on ice. Subsequently, the slides were removed from the chamber, allowed to drain and three times over layered with neutralization buffer for 5min each. Next, the slides were immersed in ddH_2O followed by 5 min incubation in 80-100% ethanol. Next, the slides were diagonally tilted and dried o.N. For imaging, 50 µL PI solution was added onto the slide and covered with a coverslip. A minimum of 50 comets per condition were counted.

3.2.25. γH2AX/53BP1 Immunostaining

5x10^4 $CD34^+$ cells were harvested at different timepoints during treatment with MNU or etoposide. After resuspension in PBS/0.5% HSA, cells were transferred into a funnel of Cytospin3 inlets assembled with a microscope SuperFrost slide and a filter card. Cells were transferred onto the glass slide and centrifuged at 600g for 5min at RT. An 8 mm cloning ring was placed on the slide and cells were fixed with 4% formaldehyde-solution for 15 min, washed three times with PBS for 5 min, permeabilized with ice-cold methanol for 20 min at 0 °C and washed with PBS for 5 min. Non-specific antigen were incubated in 5% blocking buffer in PBS with triton X-100 for 1 h. Primary antibody co-staining with anti-γH2AX (Ser139) and anti-53BP1 rabbit polyclonal antibody was performed with 0.5 µg/mL each in blocking buffer overnight at 4 °C. Afterward, cells were washed twice with PBS for 5 min, once with PBS containing 0.4 M NaCL for 2 min and once with PBS-T (PBS/0.3%(v/v) triton X-100) for 5 min, before secondary antibody incubation with 0.5 µg/mL of Alexa Fluor 488 AffiniPure Goat Anti-rabbit IgG and Rhodamine Red™-X (RRX) AffiniPure Goat Anti-Mouse IgG each in blocking buffer for 1 h at RT and in the dark. After washing three times with PBS for 5 min and rinsing twice with PBS-T, cloning rings were removed, Fluoromount-G™ mounting medium was applied and the slides were covered with a coverslip. Cells were

examined using Axio Observer 7 and foci analysis was performed using ImageJ (Version 2.9.0).

3.2.26. Mitochondrial Staining of iPSCs

Mitotracker™ Green FM was used for membrane potential staining and Tetramethylrhodamin, Methylester, Perchlorat (TMRM) for staining of mitochondrial activity. Mitotracker was dissolved 1:20 in DMSO and a stock solution of TMRM at a concentration of 100 µM in DMSO was prepared. IPSCs were cultivated on thin slides for live imaging. Cell growth medium was removed. The staining solutions were added to the cells and incubated for 30 min at 37 °C before washing with PBS. A live imager for fluorescence was used for imaging and Image J for quantification.

3.2.27. Cell Cycle Analysis

For cell cycle analysis, propidium iodide (PI) was used for nuclear staining as described by Riccardi and Nicoletti [119]. 2.5×10^4 cells were washed twice with PBS for 7 min at 4 °C and 550 g. Cells were resuspended in 25 µL staining solution and incubated in the dark for 1 h at 4 °C prior to flow cytometry.

3.2.28. Osteogenic Differentiation of MSCs and iMSCs

For osteogenic differentiation, $0.1x10^6$ cells/well were seeded on a 6-well plate in culture medium. After 24 h or reaching a confluency of 50-70% cells, culture medium was exchanged by osteogenic differentiation medium to induced osteogenic differentiation. A medium exchange was carried out twice per week. Differentiation was carried out for 14 days.

3.2.29. Adipogenic Differentiation of MSCs and iMSCs

For adipogenic differentiation, adipogenic differentiation was induced by exchanging culture medium with induction medium after 24 h or reaching a confluency of 50-70% cells. The medium was exchanged twice a week, alternating between induction medium and adipogenic cultivation medium. Differentiation was carried out for 21 days.

3.2.30. Chondrogenic Differentiation of MSCs

Chondrogenic differentiation was conducted in 3D pellet culture and induced with TGF-β1. After cell passaging, $2x10^5$ cells were resuspended in 350 µL chondrogenic differentiation medium in a 15 mL tube and centrifuged for 7 min at 1500 rpm and 4 °C. For each cell line, a minimum of seven pellets per time point (d7, d14 and d21) were applied. A medium exchange was carried out twice per week. On d7, d14 and d21, the chondrogenic pellets were transferred to 96-well plate for measurement using the Aviso CellCelector to determine their area and diameter. A minimum of five chondrogenic pellets were used for RNA isolation and a minimum of one chondrogenic pellet was embedded for histology and Safranin O staining.

3.2.31. Alizarin Staining after Osteogenic Differentiation

To detect the presence of calcium deposits and thus for quantification of osteocyte and osteoblast mineralization, the Alizarin staining method was used. For this, differentiation cells were washed with PBS and fixed for 10 min with 70% Ethanol. Subsequently, the cells were washed with ddH_2O and stained for 10 min with 2% Alizarin-Red staining solution (pH 4.1-4.3) at RT. After staining, cells were washed five times with ddH_2O and in PBS was added for documentation using a microscope (4x magnification).

3.2.32. Oil Red O Staining after Adipogenic Differentiation

To detect the presence of lipids after adipogenic differentiation, cells were washed with PBS and fixed for 2 min at -20 °C with 4% formalin. Subsequently, cells were washed with 50% ethanol and stained for 20 min with the 0.2% Oil Red O working solution. For documentation, cells were washed with ethanol and ddH_2O and the morphology was documented using a microscope (4x magnification).

3.2.33. RNA Isolation

RNA isolation from undifferentiated cells was conducted using the RNeasy Mini Kit. For this, pellets with a minimum of $1x10^6$ cells were used following the manufacturer´s protocol.

RNA isolation from differentiated cells was performed using the phenol-chloroform extraction method. For this, cells were washed with PBS and 1 mL TRI Reagent® per 6-well was added. Subsequently, the cells were scraped off with the cell scraper and transferred into a 1.5 mL Eppendorf tube. 200 µL chloroform were added and the mixture was shaken until a pink milky mixture was obtained. After 3 min at RT, the mixture was centrifuged at 12000 g and 4 °C for 15 min. The upper aqueous phase was removed and transferred into a new tube. In the case of osteogenic samples, 3 M natrium acetate was added to a final concentration of 0.5 M. Next, 500 µL isopropanol was added and the samples were stored o.N. at -20 °C. Subsequently, the samples were centrifuged at 15000 rpm and 4 °C for 10 min before 1 mL 70% ethanol was added. After shortly vortexing, the samples were centrifuged for 5 min at 7500 g and 4 °C and the supernatant was carefully completely removed. The pellets were allowed to dry completely and 30 µL RNase-free water was added and resuspended.

Immediately after isolation, RNA concentration and purity were determined spectrophotometrically using the NanoDrop® ND-1000. RNA was either directly transcribed into cDNA or stored at -80 °C for later transcription.

3.2.34. Reverse Transcription

1 µg RNA was mixed with 1 µL of 10 mM dNTP-Mix and 50 µM OligodT primers and filled up to 10 µL with ddH_2O. This mix was incubated for 5 min at 65 °C and then at 4 °C for at least 1 min to increase polymerase accessibility to The RNA. Next, a mixture consisting of 4 µL 5x first strand buffer, 1 µL DTT (0.1 M), 1 µL SuperScript III polymerase and 1 µL RnaseOUT was prepared. The entire Mix 2 was added to Mix 1

and cDNA synthesis was carried out by incubation at 55 °C for 50 min. Following incubation at 70 °C for 15 min terminated the reaction. In a final step, remaining RNA was digested by adding 2 U of RNase H and incubating at 37 °C for 20 min. The resulting cDNA was stored at -20 °C.

3.2.35. Polymerase Chain Reaction (PCR)

PCR was used to amplify the synthesized cDNA. For each reaction, 25 ng cDNA (0.5 µL) was used as mixed as listed below. The chosen primers were designed with a melting temperature of 60 °C and the annealing temperature was set at 56 °C for amplification. Due to the short amplicon sizes (Table 7), the duration of the elongation phase was set to 30 s. An overview of the PCR conditions is shown on Table 11.

Table 10: Compounds and volumes of the PCR reaction mix.

Volume	Reagent
2.5 µL	10x PCR Buffer
0.5 µL	10 mM dNTP mix
0.75 µL	50 mM $MgCl_2$
2 µL	0.2 µM forward primer
2 µL	0.2 µM reverse primer
0.2 µL	Taq Polymerase
0.5 µL (25 ng)	cDNA template
16.55 µL	H_2O

Table 11: Used conditions for PCR.

Temperature	Duration	Cycles
96 °C	5 min	1
96 °C 56 °C 72 °C	30 s 30 s 30 s	35
72 °C	10 min	1

3.2.36. Quantitative Reverse Transcription PCR (qRT-PCR)

qRT-PCR analysis was carried out with intron-spanning primers specific for each gene. The respective primer sequences are given on Table 7. RPL13a was used as a reference gene for differentiated samples and GAPDH for undifferentiated samples.

50 ng of cDNA were applied for qRT-PCR in a total volume of 25 µL containing Sybr Green PCR Mastermix, 0.2 µM of primer (forward and reverse) and distilled water (10 min/95 °C – 15 s/95 °C – 1 min/60 °C for 40 cycles).

To analyze the comparative CT experiments, Step One Software (v.1.5.1) was used. Relative changes in gene expression were calculated by applying the comparative ΔΔCT method. Differential gene expression was calculated by the formula $2^{-\Delta\Delta CT}$ normalized to untreated cells. Fold changes <1 were transformed by the formula $-1/2^{-\Delta\Delta CT}$ in the case of downregulated genes and plotted together with positive fold changes and upregulated genes, respectively. Fold changes exceeding 10000 result from high CT values used and should be disregarded. They do not indicate a true upregulation.

3.2.37. Agarose Gel Electrophoresis

In agarose gel electrophoresis, the PCR products were analyzed regarding product size and band intensity. Therefore, a 2% agarose in TBE gel was substituted with 4 µL Midori Green per 100 mL was prepared. This allows a proper separation of the DNA fragments based on their length. A 100 bp DNA ladder was used for determination of product size. The DNA fragments were separated in gel electrophoresis by application of 175 V for 20 min and analysed under UV-light with a wavelength of 305 nm.

4. Results

In the following section, the results are presented in a structured manner, starting with the iPSCs, which represent the embryonic developmental stage (Chapter 4.1). This is followed by data on HSCs isolated from neonatal cord blood, representing the neonatal population (Chapters 4.2 and 4.3). Subsequently, results on MSCs of both neonatal and adult origin are presented (Chapters 4.4 and 4.5). The section concludes with findings on iMSCs, which are considered a promising alternative to primary MSCs for toxicological studies and clinical applications (Chapter 4.6).

4.1. DNA Damage Response of iPSCs after Treatment with MNU or Etoposide

To ensure the reliability of downstream analyses, it is crucial to first confirm the identity and quality of the iPSCs used in this study. Since they serve as a model for the embryonic developmental stage, verifying their pluripotency and undifferentiated state is essential for drawing meaningful conclusions. Therefore, prior to testing, the iPSCs were characterized to confirm their stem cell properties and ensure their suitability for genotoxicity assessment.

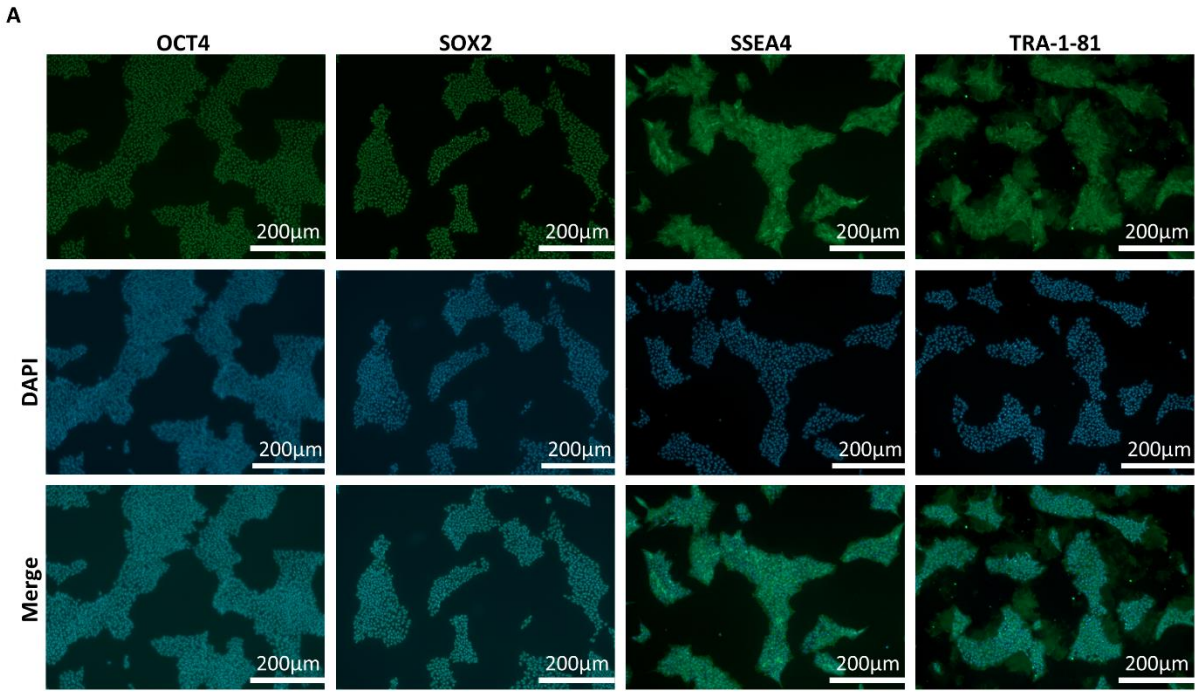

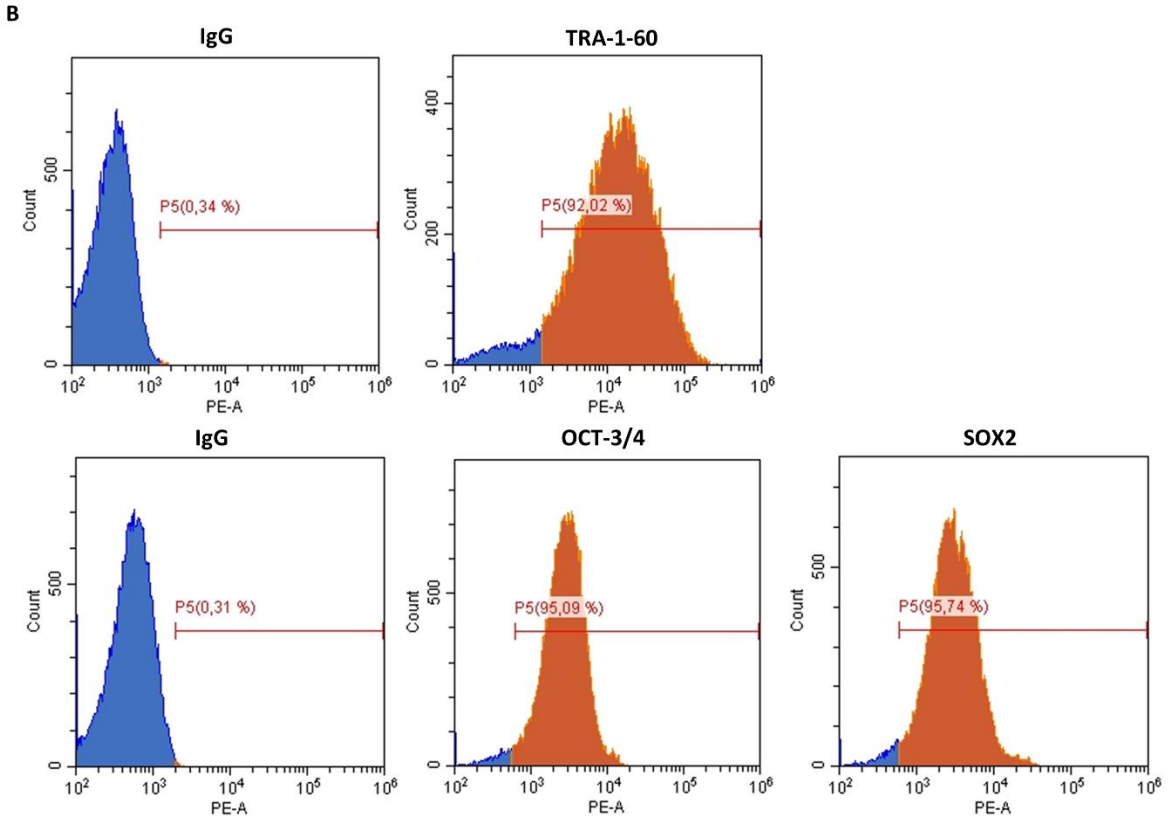

Figure 4: Characterization of iPSCs. A: Immunocytochemistry (IHC) staining of pluripotency markers (OCT4, SOX2, SSEA4 and TRA-1-81). Nuclei were stained with DAPI. Scale bars = 200 µm. B: Flow cytometry analysis showing negative IgG control and positive expression of pluripotency markers (TRA-1-60, OCT-3/4 and SOX2). Results were shown from a representative experiment of one cell line. Abbreviations: iPSCs, induced pluripotent stem cells; OCT, octamer-binding transcription factor; SOX2, SRY-box transcription factor 2; SSEA4, stage specific embryonic antigen 4; TRA, tumor-related antigen.

Figure 4 presents the characterization of iPSCs by immunofluorescence staining (A) and flow cytometry analysis (B). Panel A displays the expression of pluripotency markers OCT4a, SOX2, SSEA4 and TRA-1-81 of the R26 iPSC cell line, representatively for the other used iPSC cell lines. DAPI staining confirms nuclear localization and the merged images illustrate the co-localization of the nuclear markers with DAPI. The uniform distribution of these markers suggests successful maintenance of pluripotency. Panel B shows flow cytometry histograms of the TRA-1-60, OCT-3/4 and SOX2 expression with their corresponding isotope controls (IgG). These results indicate high expression levels of all tested pluripotency markers in the used iPSC cell lines with 92.02% cells positive for TRA-1-60, 95.09% for OCT-3/4 and 95.72% for SOX2.

A

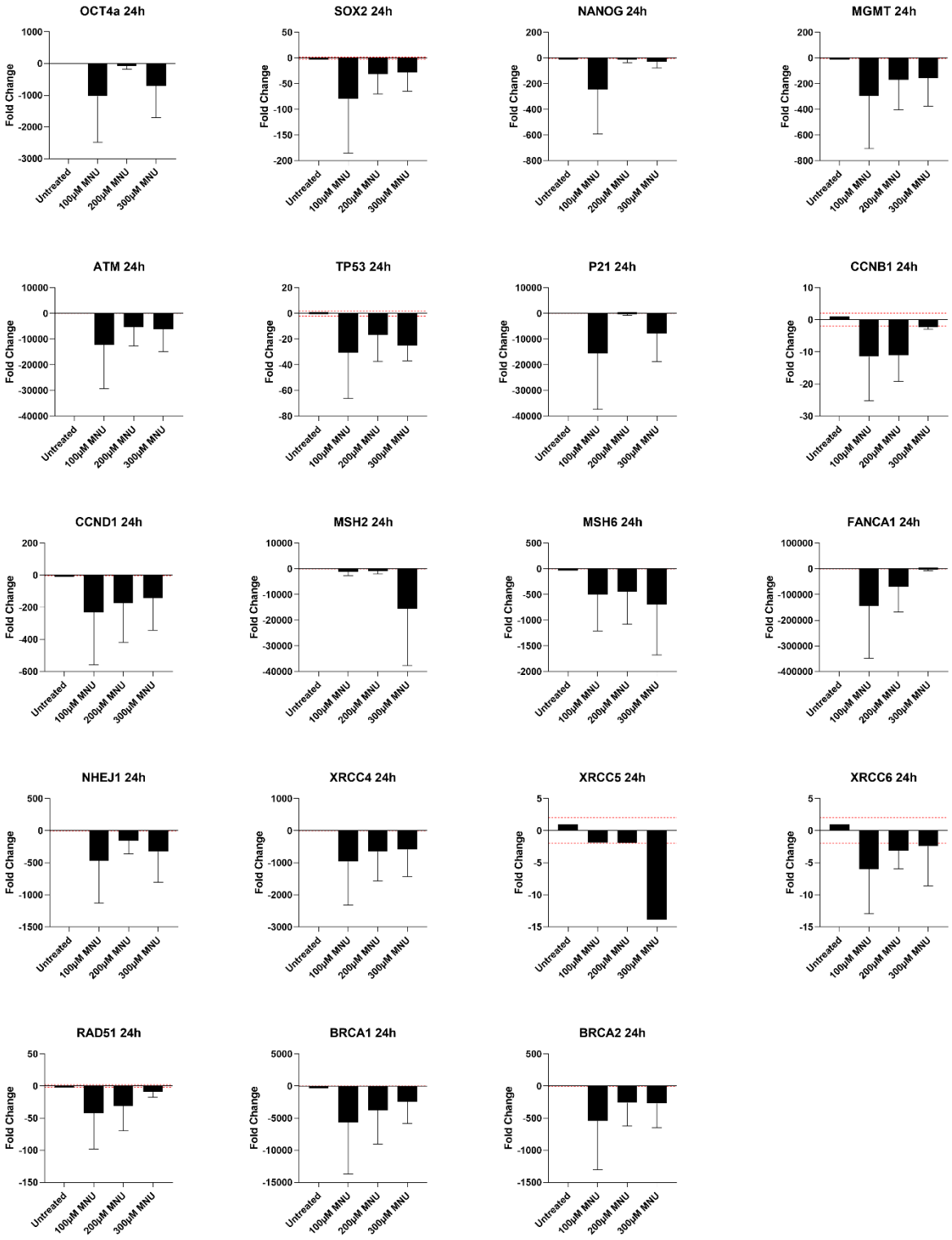
OCT4a 24h
SOX2 24h
NANOG 24h
MGMT 24h
ATM 24h
TP53 24h
P21 24h
CCNB1 24h
CCND1 24h
MSH2 24h
MSH6 24h
FANCA1 24h
NHEJ1 24h
XRCC4 24h
XRCC5 24h
XRCC6 24h
RAD51 24h
BRCA1 24h
BRCA2 24h
Fold Change
Untreated
100μM MNU
200μM MNU
300μM MNU

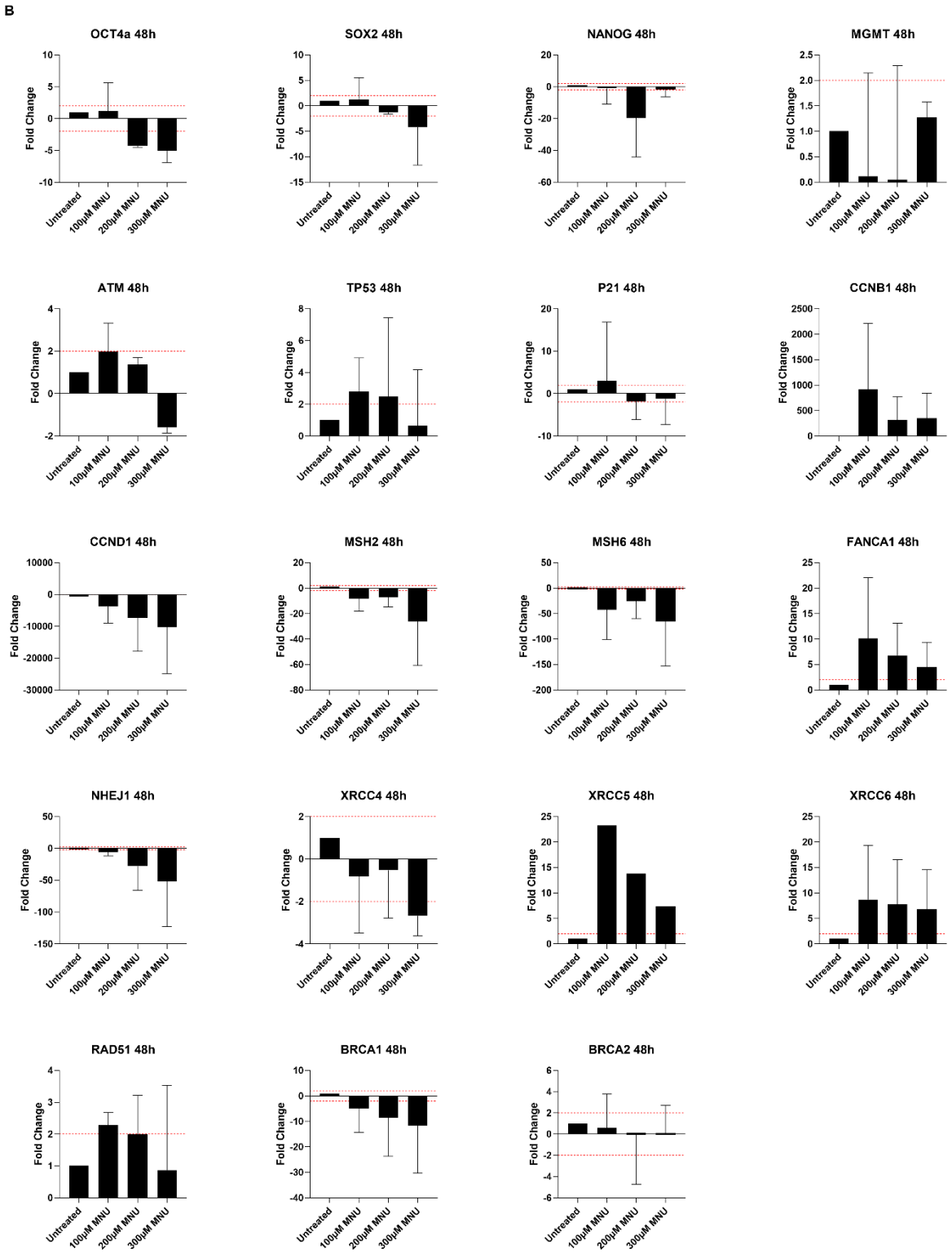

Figure 5: Analysis of DNA damage repair gene expression in iPSCs 24 h (A) and 48 h (B) after 1 h MNU treatment with varying concentrations (untreated, 100 µM, 200 µM and 300 µM). Data from two different cells lines (n = 2) was assessed by RT-qPCR. Fold changes are normalized to the untreated cells, represented as the baseline (Fold change = 1). Fold change was calculated using the $2^{-\Delta\Delta CT}$ method relative to the untreated control and normalized to the reference gene GAPDH. The red lines indicate the significance thresholds. 2 represents a two-fold increase and -2 represents a two-fold decrease. Abbreviations: ATM, ataxia telangiectasia-mutated kinase; BRCA1/2, breast cancer gene 1/2; CCNB1, cyclin B1; CCND1, cyclin D1; FANCA1, fanconi anemia complementation group A; MGMT, O^6-methyltransferase; MNU, N-methyl-N-nitrosourea; MSH2/6, mismatch repair proteins 2/6; NHEJ1, non-homologous end joining factor 1; OCT4a, octamer-binding transcription factor 4A; P21, cyclin-dependent kinase inhibitor 1; RAD51, RAD51 homolog; SOX2, sex determining region Y-box 2; TP53, tumor protein P53 ; XRCC4-6, X-ray cross complementing protein group 4-6;

The expression of several pluripotency and DDR genes in iPSCs 24 h (Figure 5A) and 48 h (Figure 5B) after MNU treatment was analyzed by RT-qPCR. In addition to a downregulation of OCT4a, SOX2 and Nanog expression 24 h after MNU treatment, the data also revealed a dose-dependent decrease in the RNA expression of DDR genes from various DDR pathways such as ATM, TP53 and MGMT. Cell cycle regulators including P21, CCNB1 and CCND1 were downregulated suggesting possible cell cycle arrest in response to MNU-induced damage. Additionally, HR and NHEJ genes including RAD51, BRCA1/2 and XRCC4/5/6 were downregulated. 48 h post MNU treatment, certain DDR genes including TP53, CCNB1, FANCA1, XRCC5, XRCC6 and RAD51 showed an increased expression compared to the 24 h time point. This was more pronounced in cells treated with lower doses of MNU and decreased with increasing genotoxin concentration.

This data suggests that MNU treatment affects iPSC pluripotency and induced the downregulation of DNA damage response in iPSCs thus influencing cell cycle regulation and DNA repair.

A

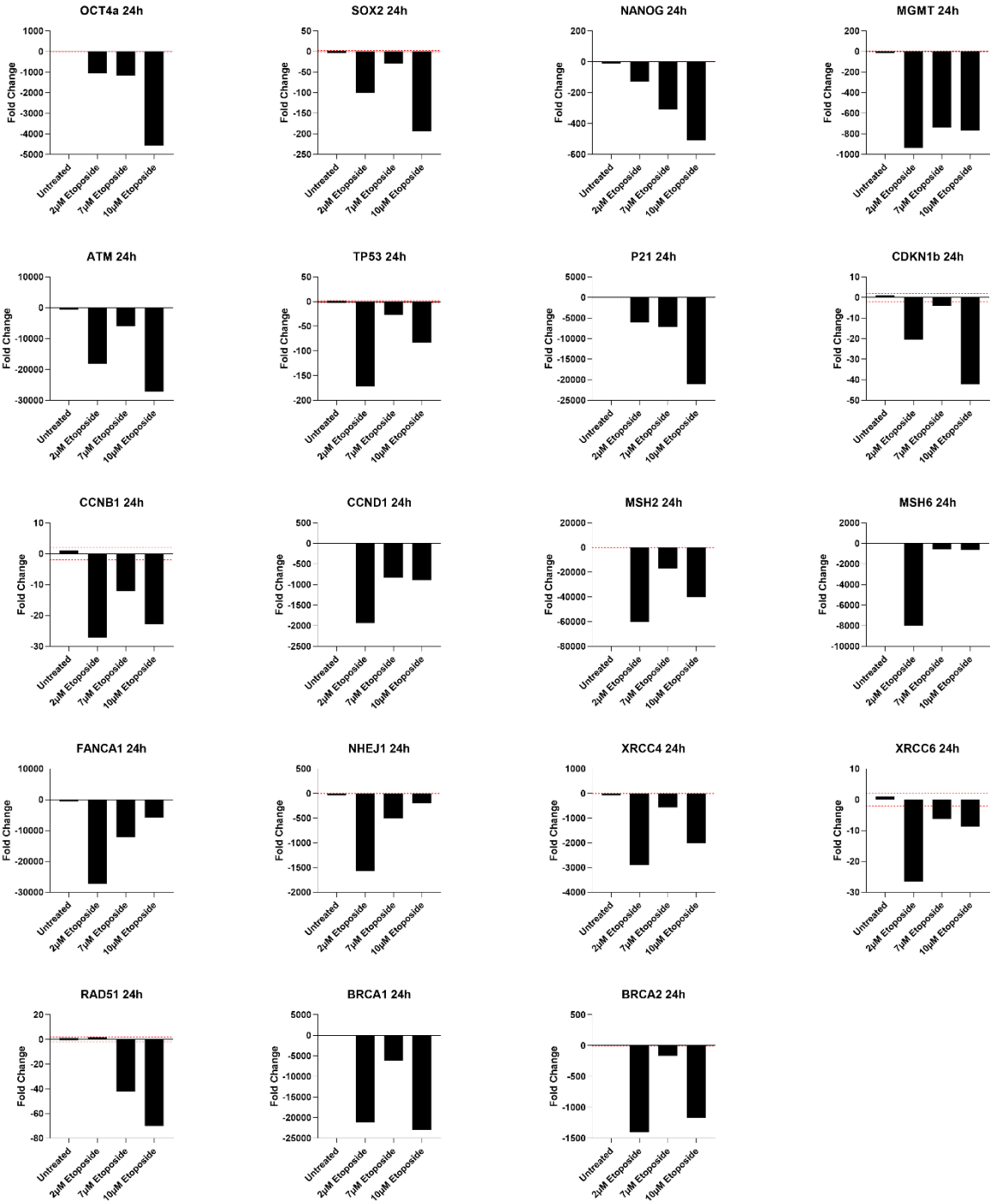
OCT4a 24h
SOX2 24h
NANOG 24h
MGMT 24h
ATM 24h
TP53 24h
P21 24h
CDKN1b 24h
CCNB1 24h
CCND1 24h
MSH2 24h
MSH6 24h
FANCA1 24h
NHEJ1 24h
XRCC4 24h
XRCC6 24h
RAD51 24h
BRCA1 24h
BRCA2 24h
Fold Change
Untreated
2μM Etoposide
7μM Etoposide
10μM Etoposide

B

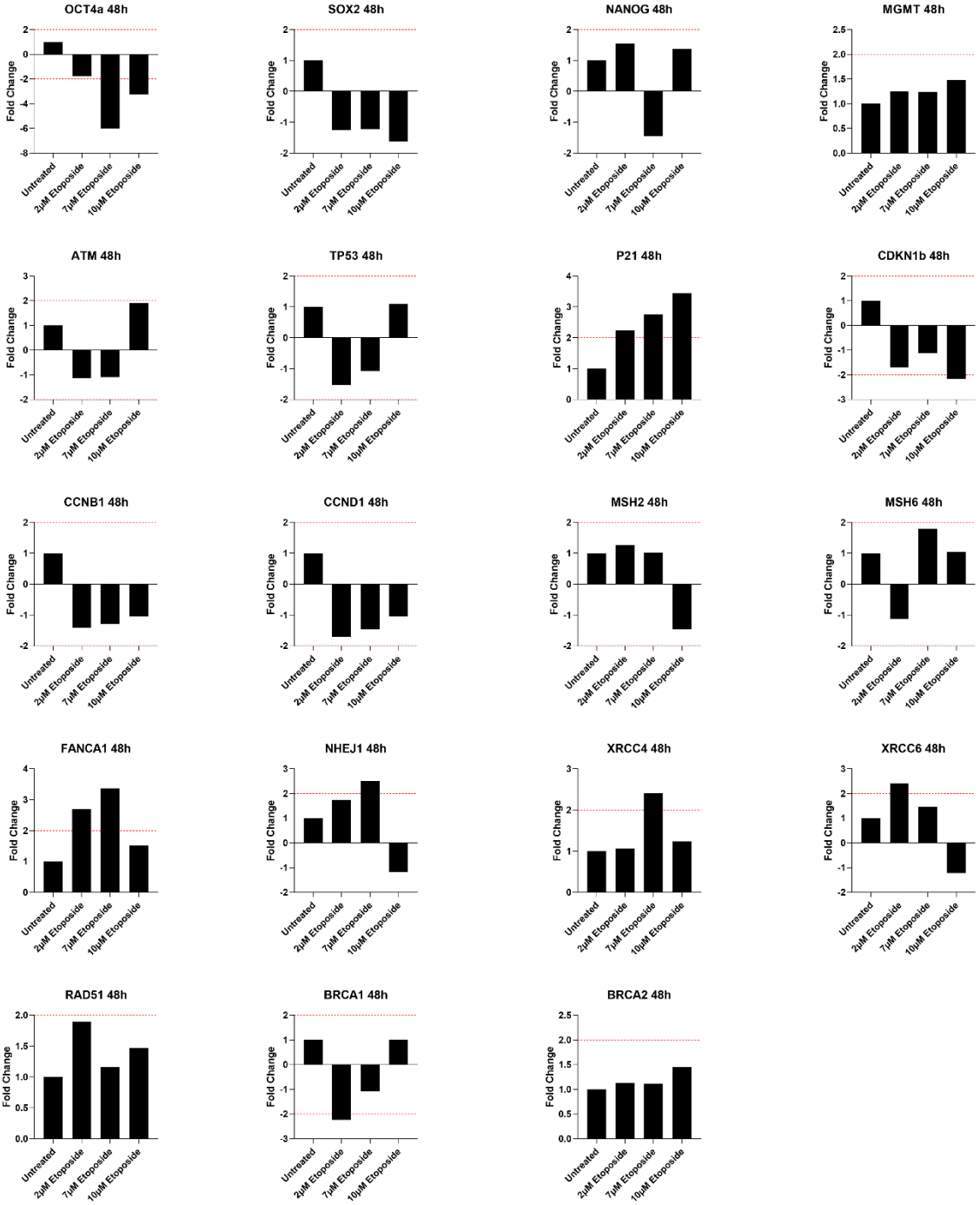

Figure 6: Analysis of DNA damage repair gene expression in iPSCs 24 h (A) and 48 h (B) after 24 h Etoposide treatment with varying concentrations (untreated, 2 µM, 7 µM and 10 µM). Data from one cell line (n = 1) was assessed by RT-qPCR. Fold changes are normalized to the untreated cells, represented as the baseline (Fold change = 1). Fold change was calculated using the $2^{-\Delta\Delta CT}$ method relative to the untreated control and normalized to the reference gene GAPDH. The red lines indicate the significance thresholds. 2 represents a two-fold increase and -2 represents a two-fold decrease. Abbreviations: ATM, ataxia telangiectasia-mutated kinase; BRCA1/2, breast cancer gene 1/2; CCNB1, cyclin B1; CCND1, cyclin D1; CDKN1b, cyclin-dependent kinase inhibitor 1b; FANCA1, fanconi anemia complementation group A; MGMT, O6-methyltransferase; MSH2/6, mismatch repair proteins 2/6; NHEJ1, non-homologous end joining factor 1; OCT4a, octamer-binding transcription factor 4A; P21, cyclin-dependent kinase inhibitor 1; RAD51, RAD51 homolog; SOX2, sex determining region Y-box 2; TP53, tumor protein P53 ; XRCC4/6, X-ray cross complementing protein group 4/6;

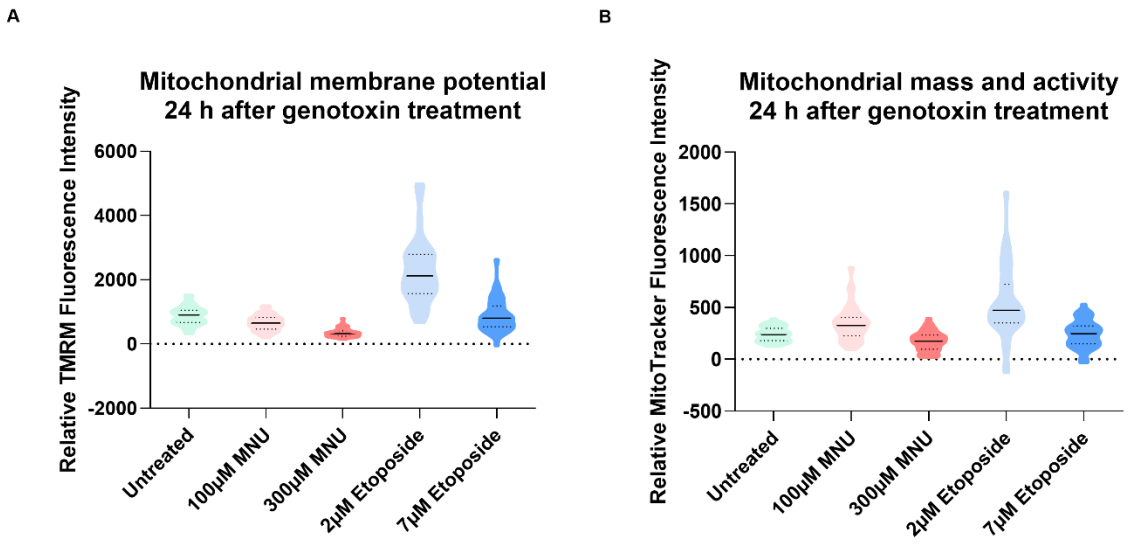

Figure 7: Mitochondrial membrane potential, mass and activity in iPSCs 24 h after treatment with MNU (1 h) or etoposide (24 h). Mitochondrial membrane potential was measured using fluorescent TMRM staining (A) while mitochondrial mass and activity was measured using fluorescent MitoTracker (B) in a single iPSC cell line. A total of 50 cells per condition were counted. Abbreviations: h, hour; MNU, N-methyl-N-nitrosourea; TMRM, tetramethylrhodamine methyl ester.

Mitochondrial membrane potential, mass and activity of iPSCs were assessed 24 h after MNU or etoposide treatment. Mitochondrial membrane potential measured via TMRM fluorescence intensity, showed a dose-dependent decrease following treatment with MNU. Notably, cells treated with 300 µM MNU exhibited the highest reduction in membrane potential. Treatment with 2 µM etoposide led to an increase in TMRM followed by a decrease to comparable levels to the untreated cells after treatment with 7 µM etoposide.

Mitochondrial mass and activity was evaluated through MitoTracker fluorescence intensity and also demonstrated similar dose-dependent effects as TMRM. Higher MNU concentrations were associated with a marked reduction in mitochondrial mass and activity compared to untreated cells. After treatment with 2 µM etoposide, first an increase in mitochondrial activity was assessed, which was reduced to comparable levels as the untreated control after treatment with 7 µM etoposide.

4.2. DNA Damage Response after Treatment of Cycling and Quiescent Cord Blood Hematopoietic Stem Cells with Distinct Genotoxic Noxae

Authors: Fabienne Becker, Meryem Ouzin, Stefanie Liedtke, Katharina Raba, Gesine Kögler

Published: Stem Cells

Impact Factor: 6.277

Own Work: 40%

Contribution: Fabienne Becker and Meryem Ouzin wrote, drafted and edited the manuscript, analyzed the data and illustrated the figures.

DNA Damage Response After Treatment of Cycling and Quiescent Cord Blood Hematopoietic Stem Cells With Distinct Genotoxic Noxae

Fabienne Becker, Meryem Ouzin, Stefanie Liedtke, Katharina Raba, Gesine Kogler

Stem Cells, 2024, **42**, 158–171
https://doi.org/10.1093/stmcls/sxad085
Advance access publication 14 November 2023
Original Research

DNA Damage Response After Treatment of Cycling and Quiescent Cord Blood Hematopoietic Stem Cells With Distinct Genotoxic Noxae

Fabienne Becker[*,1,‡], **Meryem Ouzin**[1,‡], **Stefanie Liedtke**[1], **Katharina Raba**[1], **Gesine Kogler**[1]

[1]Institute for Transplantation Diagnostics and Cell Therapeutics, University Hospital Düsseldorf, Heinrich Heine University Düsseldorf, Germany

[*]Corresponding author: Fabienne Becker, MSc, Moorenstr. 5. Tel: +49 211 81 04334. Email: fabienne.becker@med.uni-duesseldorf.de
[‡]Contributed equally.

Abstract

Hematopoietic stem cells (HSC) from cord blood can be applied as an alternative to bone marrow in transplantation to treat hematological diseases. Umbilical cord blood (UCB) consists of cycling and non-cycling $CD34^+/CD45^{low}$ cells needed for long-term and short-term engraftment. After sorting and subsequent in vitro culture, quiescent HSCs enter the cell cycle. This enables the analysis of HSCs in 2 different cell cycle stages and the comparison of their responses to different genotoxic noxae. To analyze different mechanisms of DNA damage induction in cells, 2 different genotoxins were compared: etoposide, a topoisomerase II inhibitor that targets mitosis in the S/G_2-phase of the cell cycle and the alkylating nitrosamine *N*-Nitroso-*N*-methylurea (MNU), which leads to the formation of methyl DNA adducts resulting in DNA double breaks during DNA replication and persistent mutations. Cycling cells recovered after treatment even with higher concentrations of etoposide (1.5µM/5µM/10µM), while sorted cells treated with MNU (0.1mM/0.3mM/0.5mM/1mM/3Mm/ 5mM) recovered after treatment with the lower MNU concentrations whereas high MNU concentrations resulted in apoptosis activation. Quiescent cells were not affected by etoposide treatment showing no damage upon entry into the cell cycle. Treatment with MNU, similarly to the cycling cells, resulted in a dose-dependent cell death. In conclusion, we found that depending on the genotoxic trigger and the cycling status, $CD34^+$cells have distinct responses to DNA damage. Cycling cells employ both DDR and apoptosis mechanisms to prevent damage accumulation. Quiescent cells predominantly undergo apoptosis upon damage, but their cell cycle status protects them from certain genotoxic insults.

Key words: hematopoietic stem cell; cell cycle; DNA damage response; cord blood; quiescence; genotoxins.

Graphical Abstract

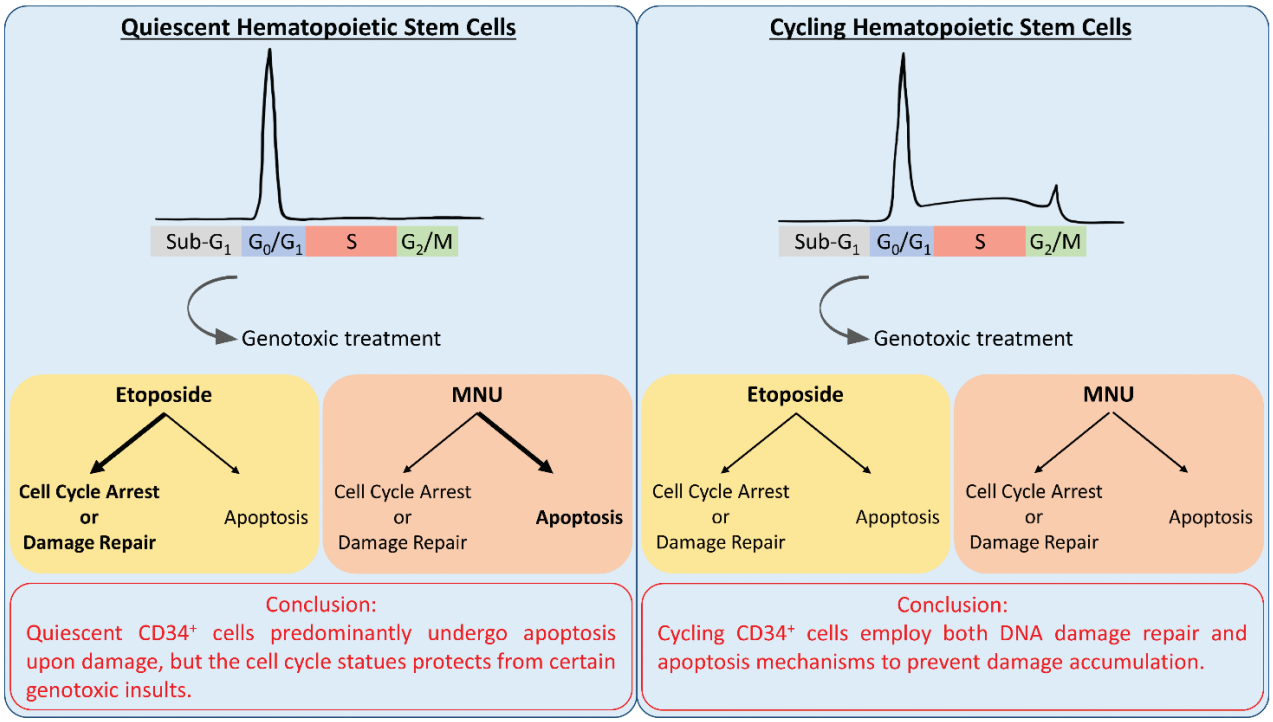

Received: 23 June 2023; Accepted: 6 November 2023.

Significance Statement

The neonatal HSCs isolated from cord blood are predominantly quiescent but their introduction into the cell cycle enables the comparison between quiescent and cycling cells, which differ in their response mechanisms to DNA damage, eg, replication stress/double-strand breaks. The differentiation between these populations is important during the toxicological assessment of therapeutical treatments in terms of hematotoxicity for a better prediction of genotoxic exposure but also to predict the contribution to carcinogenesis caused by nitrosamines, whose presence in food and pharmaceuticals is prohibited by the European Food Safety Authority (EFSA) and the European Medicines Agency (EMA).

Introduction

Every cell is constantly exposed to endogenous stress such as replication leading to daily DNA damage accumulation.[1] Additionally, exogenous triggers, such as genotoxic substances taken up through food, drug and environmental contaminants or during chemotherapy, can lead to major DNA damage.

UCB HSCs can be applied as an alternative source to bone marrow HSCs for stem cell transplantation. Although these cells have lower short-term engraftment capacity compared to peripheral blood stem cells or bone marrow, they have many advantages, eg, less-invasive collection procedure, low graft-versus-host disease (GvHD), and rapid availability.[2]

HSCs isolated from UCB are mainly maintained in a quiescent state to protect against exogenous and endogenous insults and avoid leukemic transformation and stem cell pool depletion.[3]

Moreover, mutations induced during chemotherapy are considered as the most severe side effects leading to myelosuppression and therapy-related AML (t-AML). The activation of the DNA damage repair (DDR) mechanisms results in one of 2 outcomes: damage repair with following genomic restoration and survival or damage persistence and following induction of apoptosis, senescence or cell cycle arrest thus preventing damage accumulation.[4]

Beside quiescence, HSCs are assumed to have additional evolutionary characteristics enabling protection against damage and resistance to acute injury. This is related to expression of different DDR genes and epigenetic factors. Milyavsky *et al.* reported a delayed DNA double-strand break (DSB) repair and persistent γH2AX-foci combined with an increased p53-dependent apoptosis upon γ-irradiation in HSCs compared to their progenitors allowing the in vivo repopulating HSC function.[5] Any DSB occurring during the quiescent cell stage is repaired via the non-homologous end-joining (NHEJ) pathway, which as an error-prone repair pathway, may be the cause for accumulated DNA damage, while DDR shifts toward homologous recombination (HR) upon cell cycle entry.[6,7]

In vitro, HSCs can be isolated from CB via enrichment/sorting of $CD34^+$ cells in their quiescent state.[8] The maintenance of HSCs and their progeny in vitro enables the investigation of DDR and the underlying intracellular mechanisms to various genotoxins.[9]

Etoposide, a cytostatic drug approved for treatment of various neoplasms, acts through the inhibition of topoisomerase II, resulting in DSB accumulation as the DNA unwinding, cleavage and re-ligation for the resolution of the topological tension is blocked.[10-14] The outcome varies from DSB repair to cell death depending on the severity of damage and needs to be considered as a key determinant of hematological toxicity of cytotoxic drugs.[15]

Nitrosamines are considered as a broad-acting group of carcinogens. Nitrosamine exposure occurs through diet, eg, cured meats and beer and are formed by the reaction of secondary amines, amides, and carbamates with the nitrogen in amino acids.[16] Moreover, increased awareness to nitrosamine impurities during the manufacturing process of several drugs, solvents, and catalysts was reported in 2018. This resulted in the establishment of a nitrosamine task force by the U.S. Food and Drug Administration (FDA) for guidance publication and development of testing methods for nitrosamine impurities. The EFSA provided a scientific opinion on the request of the European Commission to evaluate human health risks related to nitrosamine food contaminants.[17]

N-Methyl-*N*-nitrosourea (MNU) is an alkylating nitrosamine, which exerts its mutagenic effects by methylation of nucleotides, resulting in destabilization/breakage of DNA.[18] Without removal by the repair enzyme O^6-methylguanine-DNA methyl-transferase (MGMT), the modified base persists in the DNA and results in a point mutation, but could also induce epigenetic changes if a motif is lost.[19,20] Besides this risk, the presence of O^6-methylguanine might cause DSBs during replication.[21]

Although several DDR pathways have been identified for various cell types in vitro, it is important to analyze in detail how HSCs react to exogenous/endogenous insults with respect to their cell cycle status.[22]

DDR of both quiescent and cycling HSCs from cord blood was investigated. We hereby focused on 2 distinct genotoxins interfering in different cell cycle phases leading to DSBs.

Materials and Methods

Isolation of Hematopoietic Stem Cells

CB was collected from the umbilical cord with informed consent from the mother and donated to the José Carreras Cord Blood Bank Düsseldorf (Approval by the ethic commission 2975).

HSCs were isolated from CB by pre-enrichment of mononuclear cells. Density gradient centrifugation was performed using 1.077 g/cm^3 Histopaque-1077 Hybri-Max (Sigma-Aldrich). Cells were washed with PBS/EDTA (Miltenyi) and $CD34^+$cell fraction was isolated via magnetic-activated cell sorting using human CD34 MicroBead Kit (Miltenyi). Isolation was performed according to the manufacturer protocol.

Prior to MNU treatment, HSCs were subjected to fluorescence-activated cell sorting (FACS) to increase cell purity using the Moflo XDP (Beckmann Coulter). The instrument was used with standard optical configuration and samples were sorted using a 100-µm nozzle. First, live cells were selected based on FSC/SSC. Doublets were excluded by the SSC-width parameter and dead cells by staining with 7-aminoactinomycin D (Beckman Coulter). Phycoerythrin

(PE)-conjugated anti-CD34 antibodies (BD Bioscience) and fluorescein-isothiocyanate (FITC)-conjugated anti-CD45 antibodies (BD Bioscience) were used to determine HSCs. The HSC population was sorted via $CD34^{+}CD45^{low}$ (Supplementary Fig. S1).

Flow cytometry for CD34/CD45-markers was performed using a CytoFlex Flow Cytometer (Beckman Coulter) following the protocol according to the International Society of Hematotherapy and Graft Engineering (ISHAGE).[23]

Expansion of Hematopoietic Stem Cells

Cells were expanded on 24-well plates (Greiner AG) in CellGenix-GMP-SCGM medium (CellGenix) with 100 µg/mL penicillin (Lonza Group), 100 µg/mL streptomycin (Lonza Group), and 25 ng/mL of the following cytokines (Miltenyi): human stem cell factor (SCF), human Flt3-ligand (Flt3-L), human thrombopoietin (TPO), human interleukin 6 (IL-6), and human interleukin 3 (IL-3) and incubated at 37 °C in a humidified atmosphere with 5% CO_2.

Genotoxic Treatment of Cells

Quiescent $CD34^{+}$cells were subjected to treatment immediately after isolation, whereas cycling cells were expanded for 5 days prior to treatment.

One hundred millimolars and 1M stock solutions of Etoposide (TCI EUROPE NV) and MNU (MedChemExpress) were prepared in DMSO (Wak-Chemie Medical GmbH), respectively. Etoposide treatment was conducted for 24 h with following concentrations: 1.5 µM/5 µM/10 µM. MNU treatment was conducted for 1 h with following concentrations for qPCR: 1 mM/3 mM/5 mM and 0.1 mM/0.3 mM/0.5 mM for all other experiments. After treatment, cells were washed with PBS (Miltenyi) prior to further cultivation or subsequent analysis (Supplementary Fig. S2).

Coculture of Hematopoietic Stem Cells With Bone Marrow Mesenchymal Stromal Cells (BM-MSC Feeder)

One day before co-cultivation with $CD34^{+}$cells, BM-MSCs were plated on a 24-well plate in DMEM medium containing 30% FCS (Gibco GmbH), 100 µg/mL Penicillin (Lonza Group), and 100 µg/mL Streptomycin (Lonza Group) at a density of 1×10^5 cells/well. 2×10^5 cells/well $CD34^{+}$ cells were seeded on BM feeder and treated either with the feeder or before plating the cells on the feeder.

Cell Count and Assessment of Proliferation

Cell counting was performed using 10 µL trypan blue dye (Sigma-Aldrich), with 10 µL of cell suspension at different culture timepoints, and an improved Neubauer counting chamber (NanoEnTek). The cumulative population doublings (CPD) were performed applying the formula: PD = [log(n1/n0)]/log2; CPD = ΣPD; n1: number of counted cells. n0: number of plated cells.

Cell Fate Analysis

The subpopulations present in the $CD34^{+}$fraction were analyzed by flow cytometry using following monoclonal antibodies: CD34-PE (Miltenyi), CD38-APC (BD Pharmingen), CD10-PE-Cy™7 (BD Pharmingen), CD45Ra-APC-A750 (Beckman Coulter), CD90-FITC (Miltenyi), Propidium Iodide (BioLegend). Cells were co-stained with all antibodies for 15min and washed with PBS. For flow cytrometry, CytoFlex Flow Cytometer (Beckman Coulter) was used. The gating strategy is shown in Supplementary Fig. S3.

Cell Cycle Analysis

For cell cycle analysis, propidium iodide (PI) was applied for nuclear staining as described by C. Riccardi and I. Nicoletti [43]. 2.5×10^4 cells were washed twice with PBS (Miltenyi) (7 minutes/4 °C/550 g). Cells were resuspended in 25 µL staining solution and incubated in the dark for 1 h/4 °C prior to flow cytometry (Beckman Coulter).

Apoptosis Assay

Apoptosis detection/quantification was performed using Annexin V-FITC Apoptosis Detection Kit (BD Bioscience Pharmingen) according to the manufacturer protocol. Flow cytometry analysis was performed using CytoFlex Flow Cytometer (Beckman Coulter).

Total RNA Isolation and Reverse Transcription

At different timepoints during/after genotoxic treatment, cells from each condition were collected for total RNA isolation. RNeasy-Kit (Qiagen) was used according to the manufacturer instructions including the optional 15 minutes DNase digest. Determination of RNA concentrations and purity was carried out using a Nanodrop device (NanoDropTechnologies).

Reverse transcription was applied using the first-strand cDNA synthesis kit (Invitrogen) and oligo(dT) 20 primer (Thermo Fisher Scientific) following the manufacturer instructions. One microgram of total RNA was converted into first-strand cDNA in a 20-µL reaction.

Quantitative PCR Analysis

qPCR analysis was carried out with intron-spanning primers specific for each gene (Thermo Fisher Scientific). The respective primer sequences are given in Supplmentary Table S1. RPL13a was used as a reference gene.

Fifty nanograms of cDNA were applied for RT-PCR in a total volume of 25 µL containing Sybr Green PCR Mastermix (Thermo Fisher Scientific), 0.2 µM of primer (forward + reversed), distilled water, and 50 ng template (10 minutes/95 °C-15 s/95 °C-1 minutes/60 °C for 40 cycles).

To analyze the comparative CT experiments, Step One Software v.1.5.1 was used. Relative changes in gene expression were calculated by applying the comparative ΔΔCT method.[24] Differential gene expression was calculated by the formula $2^{-\Delta\Delta CT}$ normalized to untreated cells. Fold changes < 1 were transformed by the formula $-1/2^{-\Delta\Delta CT}$ in the case of downregulated genes and plotted together with positive fold changes and upregulated genes, respectively.

Immunocytochemistry

5×10^4 $CD34^{+}$cells were harvested at different timepoints (0.5-48 h) during treatment with MNU or etoposide. For the latter, a media change was performed 24 h after its addition by washing with PBS (550 g/4 °C/7 minutes). After resuspension in PBS/0.5% HSA, cells were transferred into a funnel (Thermo Fisher Scientific) of Cytospin3 (Thermo Shandon) inlets assembled with a microscope SuperFrost slide (Thermo Fisher Scientific) and a filter card (Epredia). Cells were transferred onto the glass slide (600g/5min/room temperature (RT)). A 8mm cloning ring (Merck) was placed on the slide and cells were fixed with 4% formaldehyde-solution

(AppliChem) for 15min, washed thrice with PBS for 5min, permeabilized with ice-cold methanol for 20min/-2 0°C and washed with PBS for 5 minutes. Non-specific antigen were incubation in blocking buffer (5%(v/v) NGS (Thermo Fisher Scientific) in PBS/0.3%(v/v) triton X-100 (Thermo Fisher Scientific)) for 1h. Primary antibody co-staining with anti-γH2AX (Ser139) (Merck) and anti-53BP1 rabbit polyclonal antibody (Cell Signaling Technology) was performed with 0.5µg/mL each in blocking buffer overnight at 4 °C. Afterward, cells were washed twice with PBS for 5min, once with PBS/0.4M NaCL for 2min, and once with PBST (PBS/0.3%(v/v) triton X-100) for 5min, before secondary antibody incubation with 0.5µg/mL of Alexa Fluor 488 AffiniPure Goat Anti-rabbit IgG (JacksonImmunoResearch) and Rhodamine Red™-X (RRX) AffiniPure Goat Anti-Mouse IgG (JacksonImmunoResearch) each in blocking buffer for 1h at RT in the dark. After washing thrice with PBS for 5min and rinsing twice with PBST, cloning rings were removed, Fluoromount-G™ mounting medium (Thermo Fisher Scientific) applied and slides covered with a coverslip. Cells were examined using Axio Observer 7 (Zeiss), and foci analysis was performed using (Fiji Is Just) ImageJ (Version 2.9.0).

Results

Characteristic Differences Between Quiescent and Cycling CD34⁺ Cells

Isolation of cells from CB via CD34 marker yields a heterogeneous cell population. To distinguish these subpopulations, a set of different markers was applied. Freshly isolated quiescent CD34⁺cells have a spherical morphology (Fig. 1A) and consist of 97.7% CD34⁺CD38⁺ (25.92% CLP, 1.4% LMPP, 0.65% CMP) and 0.91% CD34⁺CD38⁻ cells (2% LMPP, 5.14% MPP) (Fig. 1C). They are considerably smaller than their cycling counterpart and consist of 16.08% CD34⁺CD38⁺ (57.75% CLP, 5.7% LMPP, 7.97% CMP) and 77.91% CD34⁺CD38⁻ cells (77.65% LMPP, 14.83% MPP; Fig. 1C).

Directly after isolation, quiescent CD34⁺cells were primarily in the G_0/G_1-phase of the cell cycle (≥95%). Expansion with broad-acting cytokines induced cell cycle entry, where the majority of cells (72.55%) were still in the G_0/G_1-phase. However, there were also actively dividing cells in S-phase (14.15%) and G_2/M-phase (5.99%) and a smaller fraction of apoptotic cells (6.23%), represented by the sub-G_1-phase (Fig. 1B).

Dose-Dependent Damage of Cycling CD34⁺ Cells

Etoposide

Morphological analysis of cycling HSC, after treatment with various concentrations of etoposide (1.5 µM/5 µM/10 µM) for 24 h, revealed visible cell damage with different stages of apoptotic morphology, ie, membrane blebbing and formation of apoptotic membrane protrusions, in all conditions (Fig. 2A). Within 3 days, increasing signs of apoptosis were observed in a dose-dependent manner, ie, the cells treated with higher concentrations showed severe apoptotic blebbing/vesicles (Supplementary Fig. S4). Furthermore, on day 7, CD34⁺cells treated with 1.5 µM reached a fold change of 9.9, whereas 5 and 10 µM treatment resulted in a fold change of only 3.2 and 1.5, respectively, compared to the fold change of untreated cells (13.5) (Fig. 2B).

To investigate the origin of reduced cell count, both cell cycle analysis and apoptosis assay was used. The distribution of cells in each cell cycle phase did not fluctuate in the untreated control (on average 7.7% in the sub-G_1-phase, 54.8% in the G_0/G_1-phase, 22.4% in the S-phase, and 15.0% in the G_2/M-phase) (Fig. 2D). In comparison, cells treated with 1.5 µM etoposide showed a significant increase of cells in the G_2/M-phase (32.1%) and a decrease of cells in both G_0/G_1-phase (22.2%) and S-phase (16.5%) on day 1. On the following days, the distribution of cells in each cell cycle was comparable to that of untreated cells. Cells treated with 5 µM etoposide showed a similar trend of cell distribution in the cell cycle on d1 (18.3% in the G_0/G_1-phase, 15.6% in the S-phase, and 22.9% in the G_2/M-phase), except for a significant increase in cells in the sub-G_1 phase (43.1%). In the following 2 days, the amount of cells in sub-G_1-phase significantly increased (73.3%), whereas the overall cell numbers decreased. After treatment with 10 µM etoposide, most cells were in the sub-G_1-phase (61.2%) and only a small fraction was actively involved in the other cell cycle phases (22.1% in the G_0/G_1-phase, 13.1% in the S-phase, and only 3.4% in the G_2/M-phase) starting from day 1.

Dose-dependent increase of cells in the sub-G_1 phase was further characterized as cells undergoing apoptosis via Annexin V/PI staining, showing that over the 7 days, the number of cells in the late apoptotic stage increased with growing etoposide concentration, with more than 50% of cells undergoing apoptosis after exposure to 5 and 10 µM etoposide (Fig. 2E).

To study the effect of the microenvironment on damaged CD34⁺ cells, a co-cultivation experiment with BM-feeder was performed, with treatment of cells while they are in culture with the feeder. Analyzes revealed no significant contrast to the effect on cycling CD34⁺cells with the feeder present as compared to cells treated without the feeder (Supplementary Figs. S9 and S8).

MNU

Morphological analysis of cycling CD34⁺ cells after treatment with various concentrations of MNU (0.1 mM/0.3 mM/0.5 mM) for 1 h, revealed no visible cell damage on day 1 after treatment (Fig. 3A). At day 3, an extensive damage was visible, with different stages of apoptotic morphology observed in a dose-dependent manner, ie, cells treated with higher concentrations showed severe apoptotic-blebbing (Supplementary Fig. S7). Cell counts revealed a fold change of 18.5 in the untreated control, whereas treatment with 0.1 mM MNU resulted in a lower fold change of 15.3, and cells treated with both 0.3 and 0.5 mM MNU resulted in a near complete proliferation stop (Fig. 3B).

Cell cycle analysis showed that on day 1 both 0.3 and 0.5 mM treatment resulted in increased cell numbers in the sub-G_1-phase (62.45% and 78.24%, respectively). At day 7, cells treated with 0.3 mM were able to reconstitute their cell cycle, while most cells treated with 0.5 mM remained in the sub-G_1 phase (86.21%). In contrast, treatment with 0.1 mM showed no significant distinction in cell cycle distribution compared to the untreated control (Fig. 3D). Accordingly, apoptosis assay showed increased late apoptotic populations after treatment with 0.3 and 0.5 mM MNU until day 3. Between days 5 and 7, levels of apoptotic populations in all conditions were comparable to the untreated control (Fig. 3E).

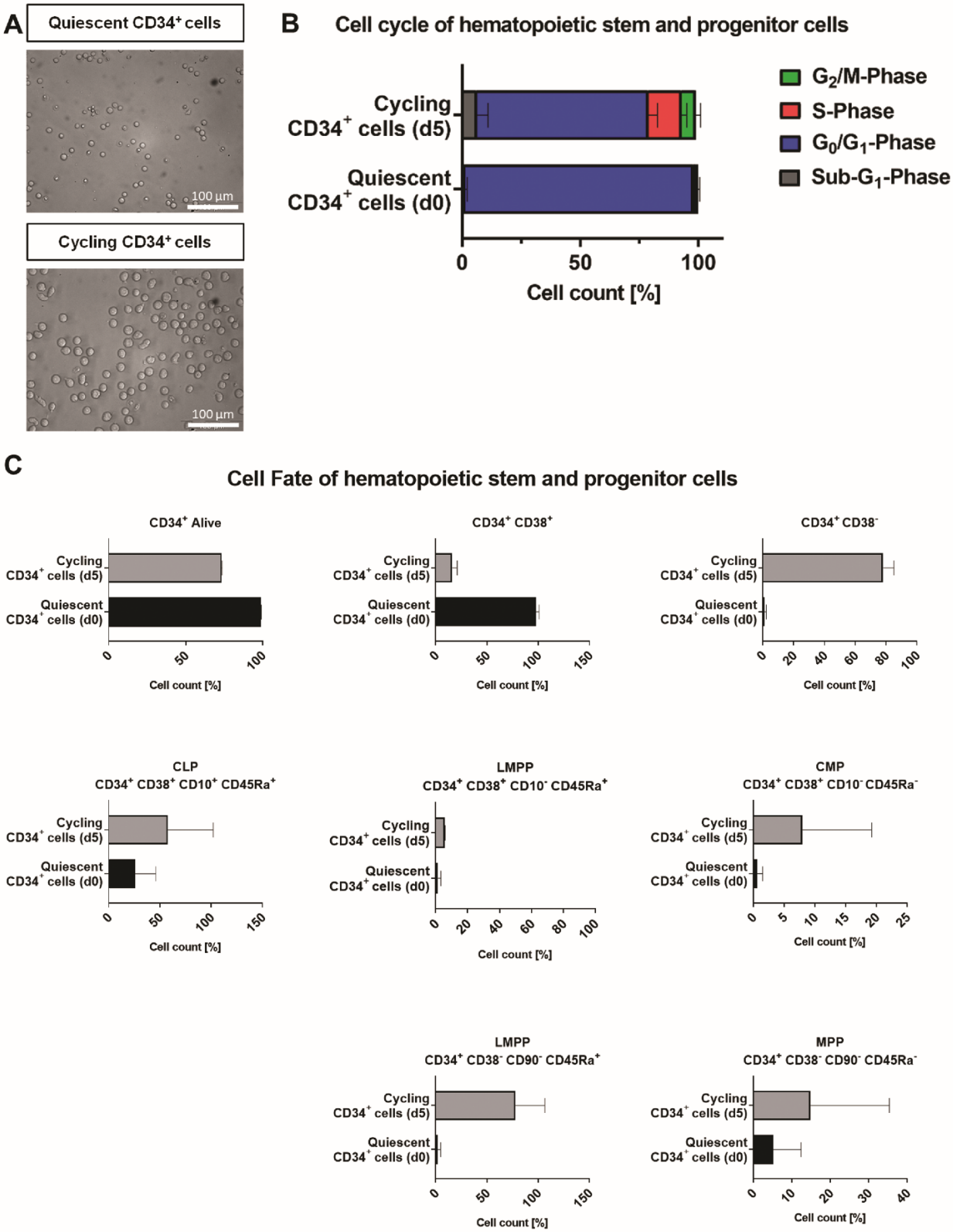

Figure 1. Characterization of quiescent and cycling hematopoietic stem and progenitor cell populations. (**A**) Representative morphology of untreated quiescent and cycling CD34+ cells. To ensure examination of quiescent CD34+ cells, they were immediately analyzed after isolation from cord blood; cycling cells were analyzed after 5 days of culture; scale bar = 100 µm. (**B**) Comparison of cell cycle analysis of untreated quiescent and cycling CD34+ cells. (**C**) Comparison of cell surface markers of quiescent and cycling CD34- cells. Abbreviations: CLP, common lymphoid progenitor; CMP, common myeloid progenitor; LMPP, lymphomyeloid-primed progenitor; MPP, multipotent progenitor.

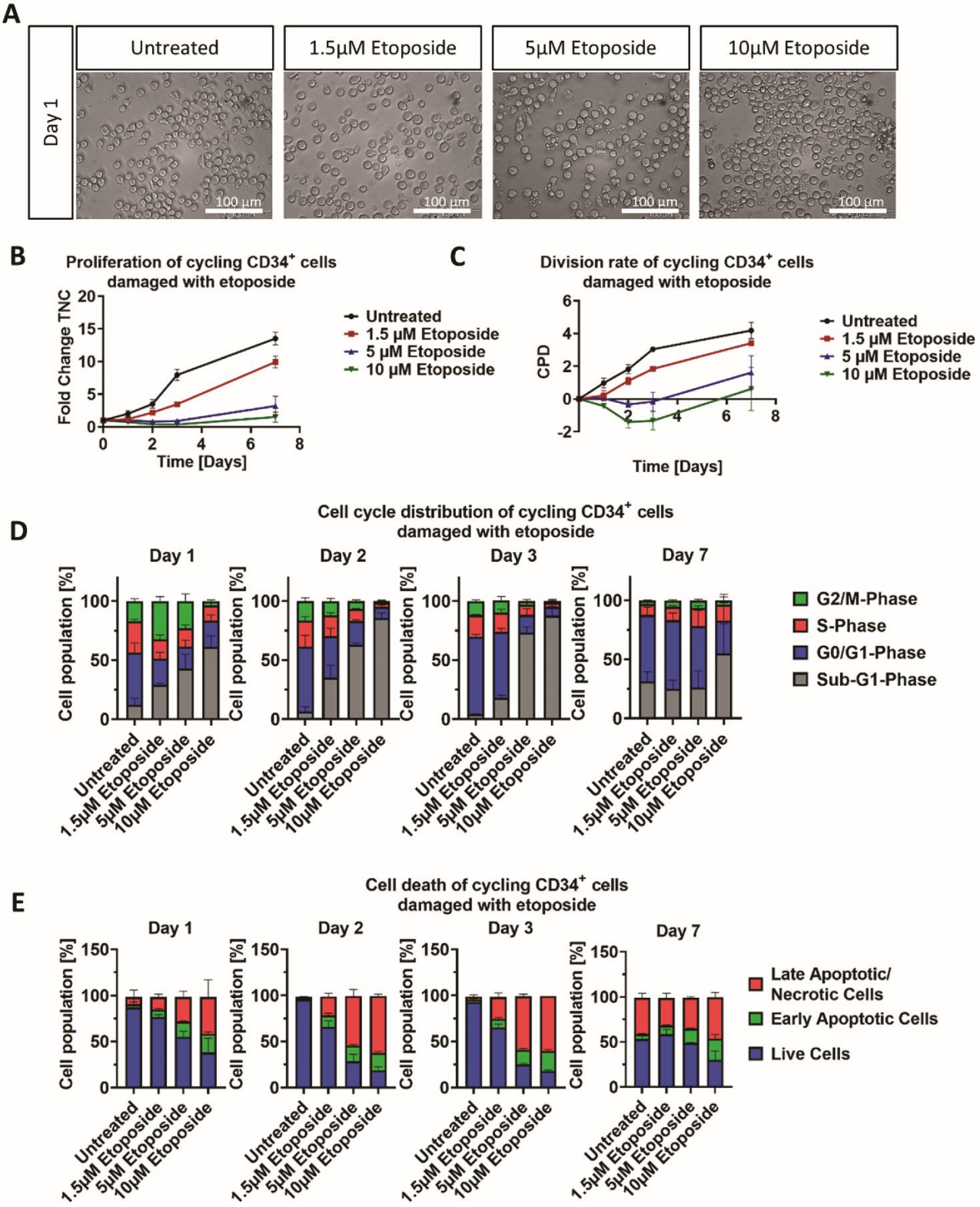

Figure 2. Effect of etoposide treatment on morphology, growth and cell cycle of cycling CD34+ cells. (**A**) Representative morphological images of untreated and with 1.5, 5, and 10 µM etoposide treated cycling CD34 + cells. Analysis was performed after 24 h treatment. Scale bars = 100 µm. (**B**, **C**) Representative growth kinetics depicted via the total fold change over time and the CPD. After treatment of cycling cells with different etoposide concentrations, the growth curves revealed a dose-dependent effect on cycling CD34+ cells. (**D**) Cell cycle analysis of treated cycling CD34+ cells via staining with PI and analysis by flow cytometry. (B-D) Representative data from 3 independent experiments with different CB donations. Abbreviations: CB, cord blood; CPD, cumulative population doubling, PI, propidium iodide.

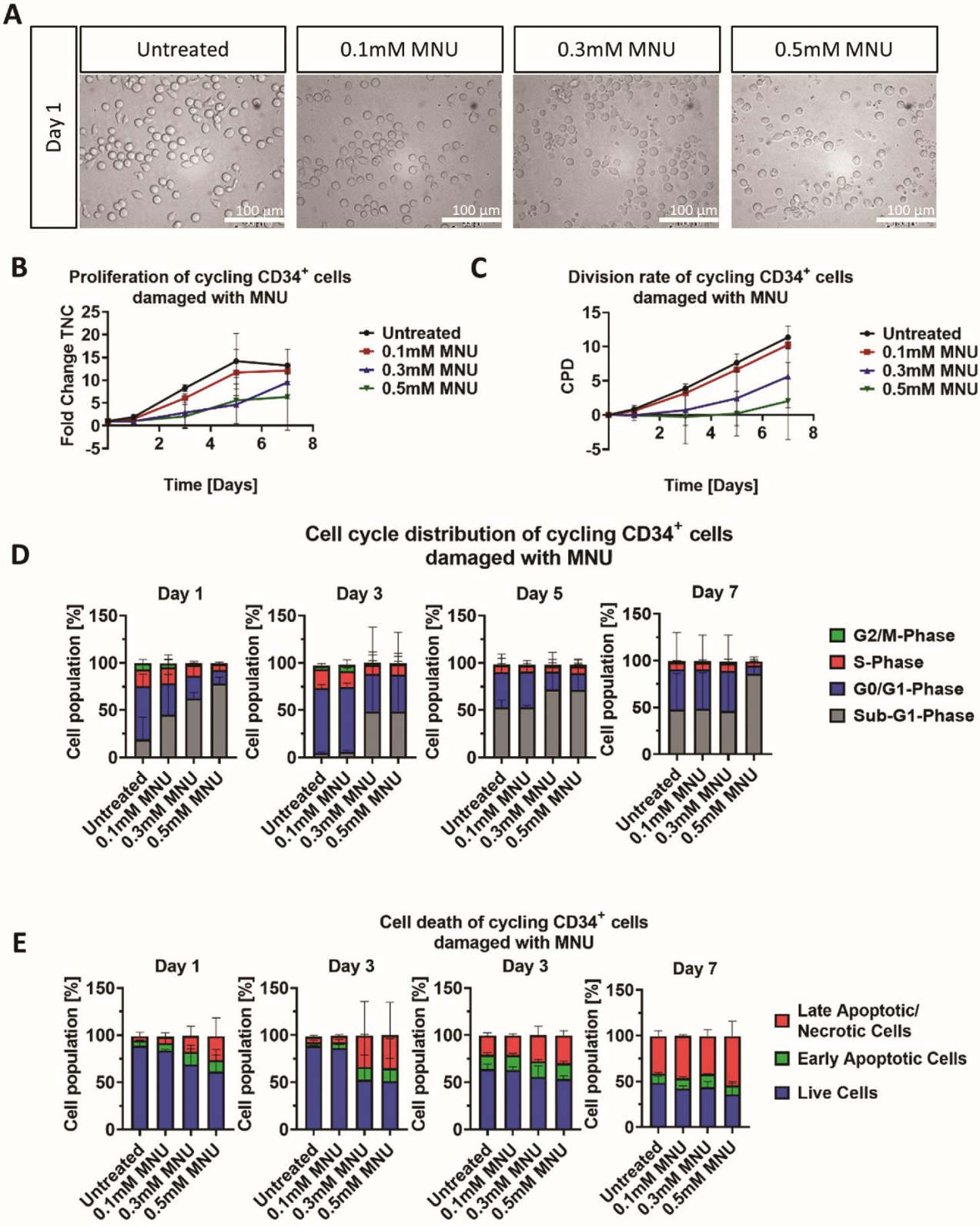

Figure 3. Effect of MNU treatment on morphology, growth and cell cycle of cycling CD34+ cells. (**A**) Representative morphological images of untreated and with 0.1, 0.3, and 0.5 mM MNU treated cycling CD34 + cells. Analysis was performed ~24 h after the 1 h treatment. Scale bars = 100 µm. (**B**, **C**) Representative growth kinetics depicted via the total fold change over time and the CPD. After treatment of cycling cells with different MNU concentrations, the growth curves revealed a dose-dependent effect on cycling CD34 cells. (**D**) Cell cycle analysis of treated cycling CD34+ cells via staining with PI and analysis by flow cytometry. (B-D) Shown are representative data from 3 independent experiments with different CB donations. Abbreviations: CB, cord blood; CPD, cumulative population doubling; MNU, *N*-methyl-*N*-nitrosurea; PI, propidium iodide.

Co-cultivation of cycling CD34+ with a BM-feeder was performed with 2 different treatment methods. After treating both CD34+ cells and the feeder, CD34+ cells showed no improved recovery after damage compared to cultivation without a feeder (Supplementary Figs S10 and S11). In contrast, transferring treated CD34+ cells onto a healthy feeder documented the protective capacity of the microenvironment on damaged cells, as all concentrations depicted the same morphology/cell count/cell cycle distribution/cell death tendencies as untreated cells (Supplementary Figs. S12 and S13).

Dose-Dependent Damage of Quiescent CD34+ Cells

Etoposide

Morphological analysis of quiescent HSC, after treatment with various concentrations of etoposide (1.5, 5, or 10 µM) for 24 h, revealed some smaller cells and few cells with membrane blebbing only in the fraction treated with 10 µM etoposide (Fig. 4A). Three days after treatment, no further signs of apoptosis were visible (Supplementary Fig. S5). Cell counts showed that quiescent CD34+ cells were not significantly damaged in their proliferative capacity, as fold changes at day 7 were comparable between all conditions (26.7 for untreated, 26.0 for 1.5 µM, 24.0 for 5 µM, 22.7 for 10 µM). However, proliferation start was delayed in a dose-dependent manner up to 2 days after culture start (Fig. 4B, C).

Cell cycle analysis revealed that only treatment with 1.5 µM resulted in comparable distribution of cells in each cell cycle to those of untreated cells (on average 13.6% in the subG$_1$-phase, 54.3% in the G$_0$/G$_1$-phase, 18.5% in the S-phase, and 10.5% in the G$_2$/M-phase). In contrast, 5 µM treatment resulted in a slight shift of cell distribution (34% in the sub-G$_1$-phase, 28.0% in the G$_0$/G$_1$-phase, 25.1% in the S-phase, and 12.8% in the G$_2$/M-phase), and treatment with 10 µM had a more significant dispersion, with an increase of cells in the sub-G$_1$-phase (49.7%), and a decrease in the G$_0$/G$_1$-phase(28.0%), the S-phase (15.9%), and the G$_2$/M-phase (6.4%). Both 5 and 10 µM etoposide treated cells regained a comparable distribution of cells in each cell cycle to that of untreated cells by day 7 (Fig. 4D). This slight shift of more sub-G$_1$ cells in a dose-dependent manner was further confirmed via apoptosis assay, showing increased levels of late apoptotic cells for 5 and 10 µM treatment. Nevertheless, as seen in cell cycle analysis, the apoptotic population levels in all conditions became comparable to those of untreated cells at day 7 (Fig. 4E).

MNU

Morphological analysis of quiescent CD34+cells, after treatment with various concentrations of MNU (0.1, 0.3, or 0.5 mM) for 1 h, revealed no visible cell damage upon treatment termination (Fig. 5A). Only after day 3, the extensive damage was visible, with different stages of apoptotic morphology observed in cells treated with 0.5 mM MNU ie, higher concentrations showed severe apoptotic blebbing and vesicles (Fig. 5A). Cell counts for quiescent CD34+cells treated with MNU revealed an overall fold change of 19.44 for the untreated control, treatment with 0.1 and 0.3 mM had a slightly lower fold change of 17.78 and 12.42, respectively, whereas 0.5 mM treated cells only reached a fold change of 0.33 at day 7 (Fig. 5B).

Although cell counts did not reveal any major discrepancy between untreated cells and 0.1/0.3 mM, cell cycle analysis revealed a severe cell cycle arrest in the G$_0$/G$_1$-phase (83.51% for 0.1 mM, 77.71% for 0.3 mM, 60.42% for 0.5 mM) at day 1 (Fig. 5C). However, this arrest was resolved for 0.1 mM/0.3 mM, whereas with 0.5 mM nearly all cells converted from cell cycle arrest into sub-G$_1$ phase (>95%), only a small fraction recovered at day 7.

Accordingly, apoptosis assay showed increased early and late apoptotic populations in a dose-dependent manner, with 0.5 mM treatment resulting in the highest number of apoptotic cells after cell cycle arrest (45.42%) at day 7 (Fig. 5E).

Treatment of Hematopoietic Stem and Progenitor Cells With Genotoxins Induces the Formation of γH2AX and 53BP1 Foci

To investigate DSB occurence after etoposide (1.5, 5, 10 µM) or MNU (0.1, 0.3, 0.5 mM) treatment, quiescent and cycling CD34+ cells were co-stained for γH2AX and 53BP1. Generally, 4 distinguished foci types were observed, (A) cells displaying only γH2AX-foci, (B) partial or complete co-localization of both γH2AX- and 53BP1-foci, and (C) rare instances with cells displaying only 53BP1-foci that resembled apoptotic rings (Supplementary Fig. S15). From the counted mean number of foci/nucleus, a threshold of ≥ 5 was selected as significant to determine the amount of foci positive cells. From this, co-localization of γH2AX/53BP1 was calculated. Complete co-localization was defined as ≥ 80% matching γH2AX/53BP1-foci, whereas partial co-localization was defined as < 80% γH2AX/53BP1-foci.

Analyzing the response of quiescent CD34+ cells to treatment with etoposide revealed a time- and dose-dependent foci formation (Fig. 6A, D). In cells treated with 1.5 µM, most foci were recorded 24 h after genotoxin addition, with more γH2AX-foci (45.4 ± 17.2) than 53BP1-foci (17.6 ± 10.2), which resulted in only partial co-localization. Treatment with 5 and 10 µM resulted in earlier foci detection, 6 and 1 h after addition of etoposide, respectively, with both conditions displaying highest numbers of foci/nucleus after 48 h. Furthermore, there were more γH2AX-foci (28.1 ± 13.7 for 5 µM, 39.6 ± 20.8 for 10 µM) than 53BP1-foci (9.5 ± 7.6 for 5 µM, 11.9 ± 11.8 for 10 µM) detected, with the majority only partially co-localized (~60%). On the other hand, cycling CD34+ cells treated with etoposide, displayed a similar foci formation time course for all concentrations, with foci detected between 0.5 and 1 h after addition of genotoxin and highest numbers of foci/nucleus at 24 h, after which only small numbers or no foci were counted (Fig. 6B, E). The overall number of foci was reduced compared to those counted in quiescent cells (γH2AX-foci/nucleus: 20.3 ± 9.5 for 1.5 µM, 18.5 ± 9.7 for 5 µM, 30.5 ± 15.8 for 10 µM). The difference to 53BP1-foci/nucleus was not as high (53BP1-foci/nucleus: 16.1 ± 9.7 for 1.5 µM, 27.9 ± 14.9 for 5 µM, 23.1 ± 16.8 for 10 µM) with both foci being completely and partially co-localized in cycling CD34+ cells. In contrast to the foci formation upon etoposide treatment, MNU treatment revealed no foci formation in quiescent cells and only low foci numbers in cycling cells with the majority being 53BP1-foci rather than γH2AX-foci (Fig. 6C, F and Supplementary Fig. S14).

Discussion

This work focuses on the characterization of CD34+ cell response to damage induced by 2 different genotoxic noxae,

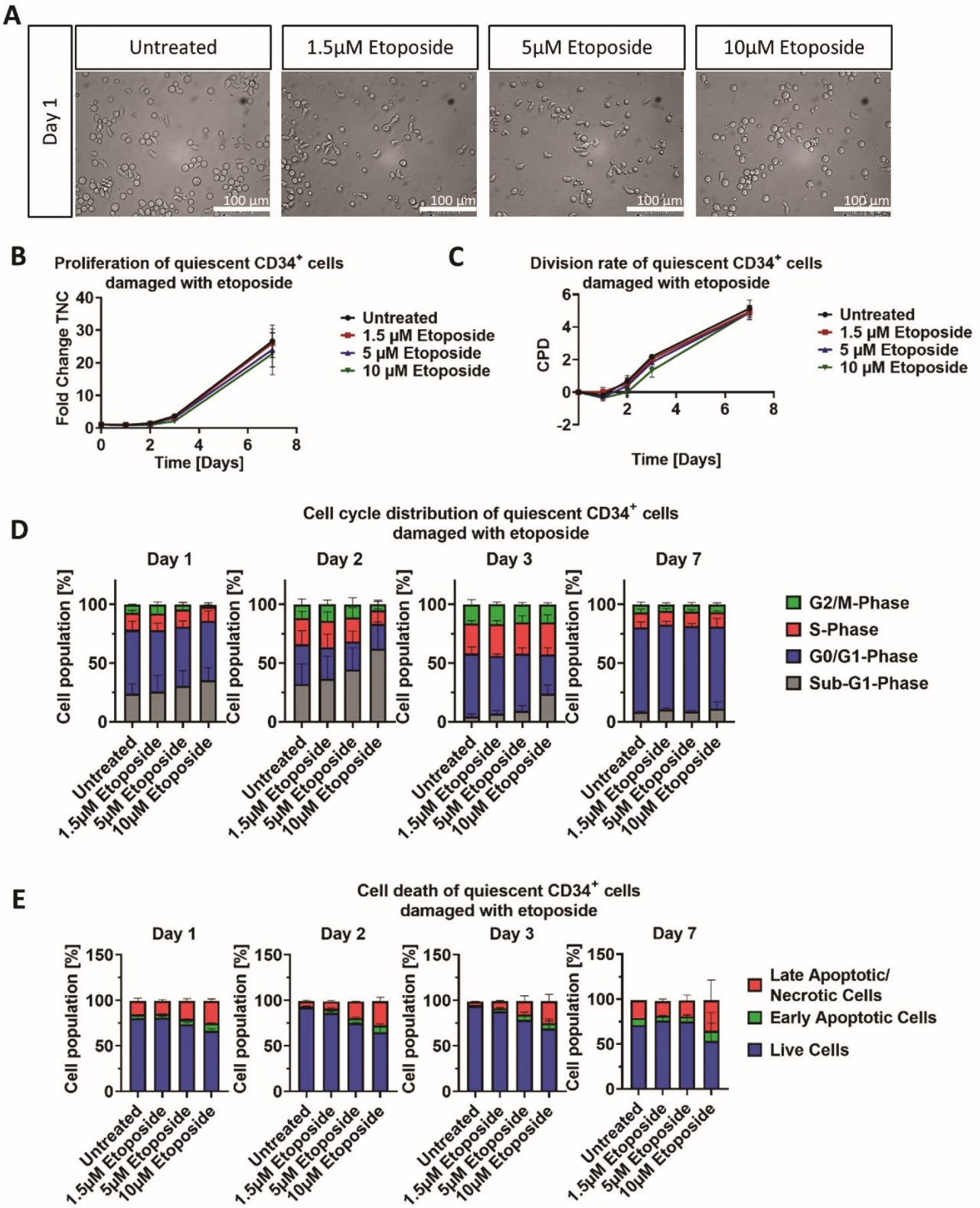

Figure 4. Effect of etoposide treatment on morphology, growth, and cell cycle of quiescent CD34+ cells. (**A**) Representative morphological images of untreated and with 1.5, 5, and 10 µM etoposide treated quiescent CD34+ cells. Analysis was performed after a 24 h treatment. Scale bars = 100 µm. (**B**, **C**) Representative growth kinetics depicted via the total fold change over time and the CPD. After treatment of quiescent cells with different etoposide concentrations, the growth curves revealed no significant effect on quiescent CD34+ cells. (**D**) Cell cycle analysis of treated quiescent CD34+ cells via staining with PI and analysis by flow cytometry. (B-D) Shown are representative data from 3 independent experiments with different CB donations. Abbreviations: CB, cord blood; CPD, cumulative population doubling, PI, propidium iodide.

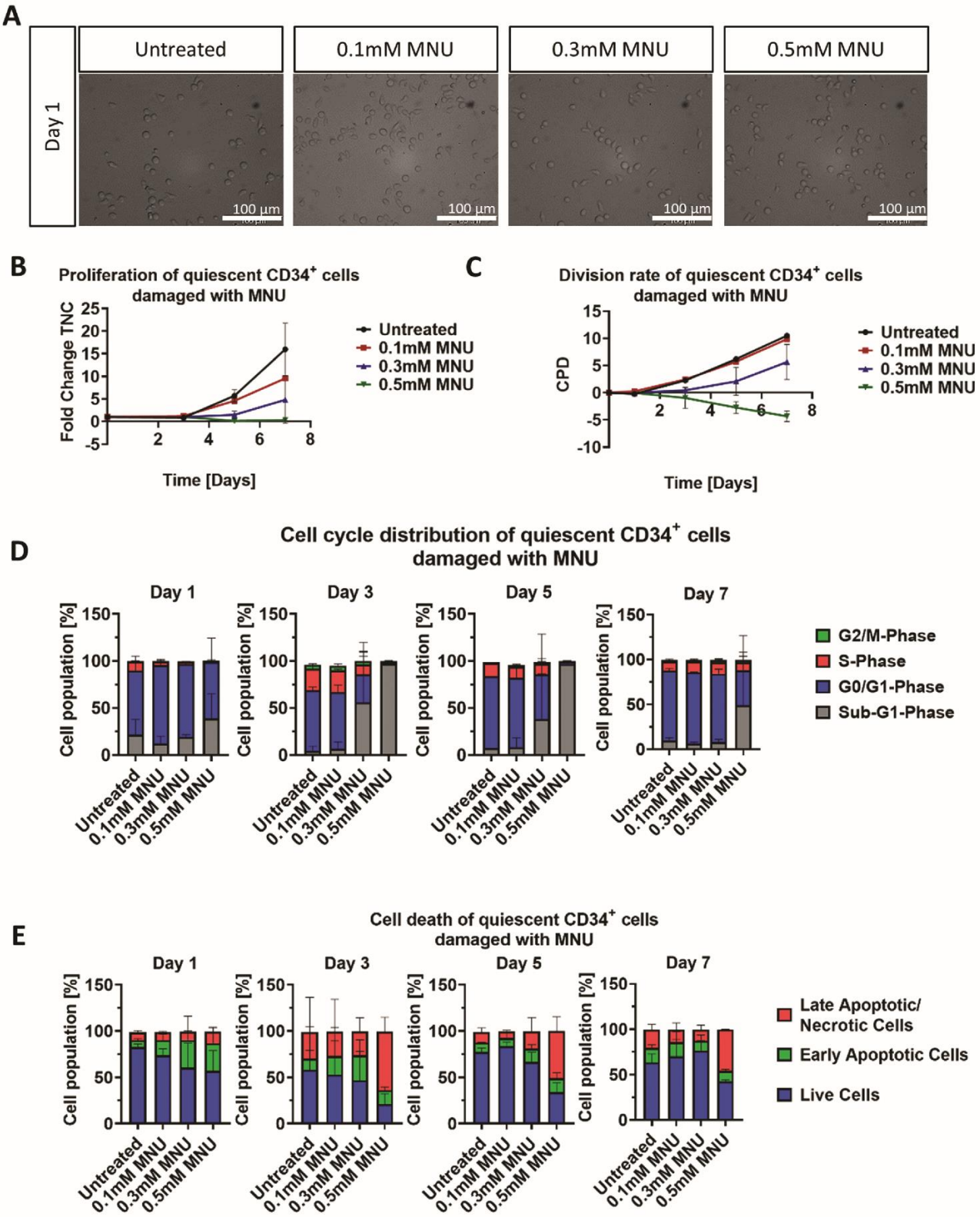

Figure 5. Effect of MNU treatment on morphology, growth and cell cycle of quiescent CD34+ cells. (**A**) Representative morphological images of untreated and with 0.1, 0.3, and 0.5 mM MNU treated quiescent CD34+ cells. Analysis was performed 24 h after the 1 h treatment. Scale bars = 100 µm. (**B**, **C**) Representative growth kinetics depicted via the total fold change over time and the CPD. After treatment of quiescent cells with different MNU concentrations, the growth curves revealed a dose-dependent effect on quiescent CD34+ cells. (**D**) Cell cycle analysis of treated quiescent CD34- cells via staining with PI and analysis by flow cytometry. (B-D) Shown are representative data from 3 independent experiments with different CB donations. Abbreviations: CB, cord blood; CPD, cumulative population doubling; MNU, *N*-methyl-*N*-nitrosurea; PI, propidium iodide.

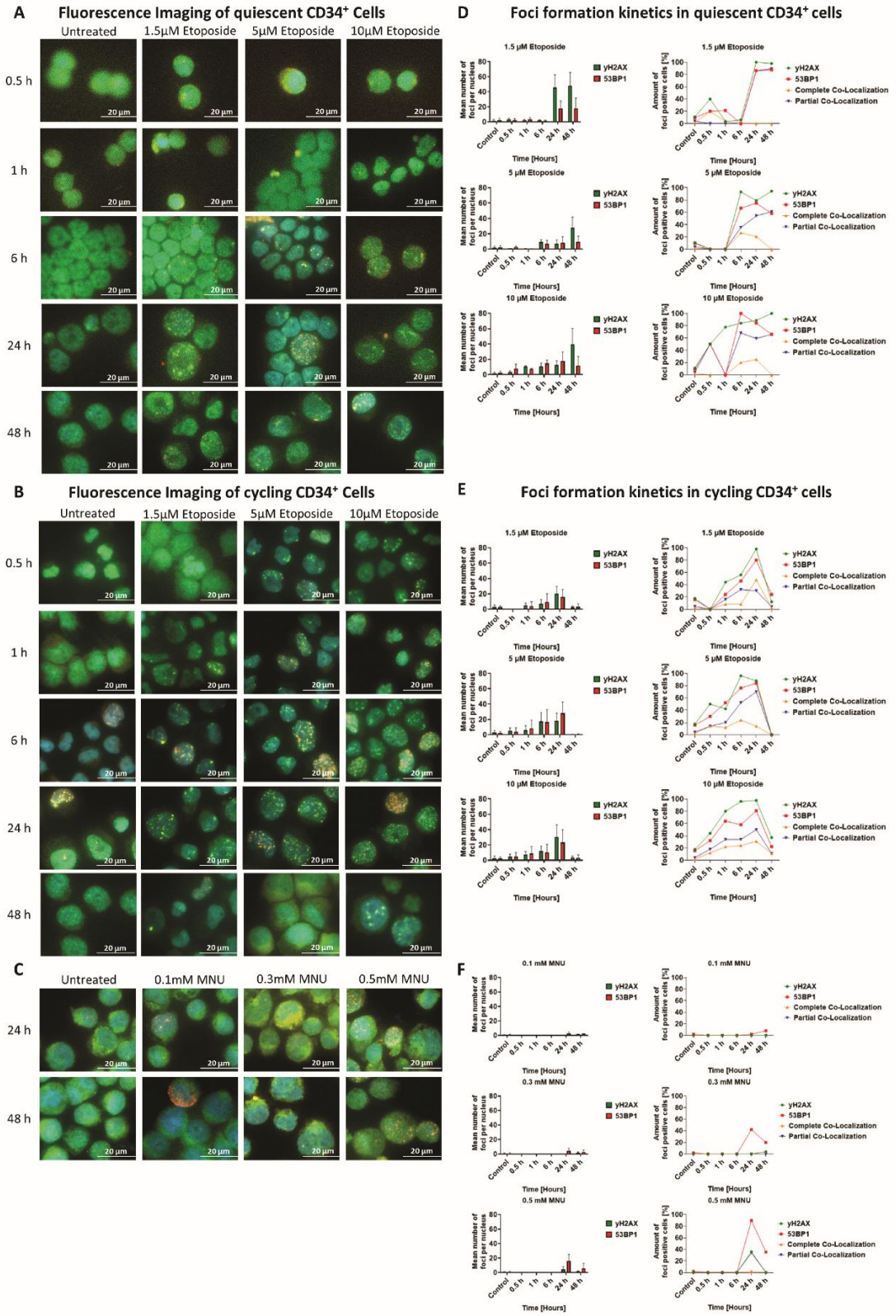

Figure 6. γH2AX and 53BP1 foci formation kinetics in CD34⁺ cells after treatment with genotoxic noxae etoposide or MNU. Quiescent or cycling CD34⁺ cells were treated with etoposide (1.5, 5, and 10 µM) or MNU (0.1, 0.3, and 0.5 mM), and harvested between 0.5 and 48 h and co-stained for γH2AX (green) and 53BP1 (red), using HOECHST (blue) to visualize the nucleus. Representative fluorescence co-staining images of (**A**) quiescent CD34⁺ cells treated with different doses of etoposide, (**B**) cycling CD34⁺ cells treated with different doses of etoposide, and selective images of (**C**) cycling CD34⁺ cells treated with different doses of MNU. Time course for the formation of different foci in (**D**) quiescent CD34⁺ cells treated with different doses of etoposide, (**E**) cycling CD34⁺ cells treated with different doses of etoposide, and (**F**) cycling CD34⁺ cells treated with different doses of MNU; the mean number of foci per nucleus includes at least 25 counted cells, from which the amount of foci positive cells (%) were determined. To determine positive stained cells, for either γH2AX or 53BP1, a threshold of ≥ 5 foci per nucleus was applied. From these, the co-localization of the 2 foci was calculated using a ≥ 80% overlap threshold of γH2AX and 53BP1 foci in one cell for the complete co-localization, and a < 80% overlap threshold of γH2AX and 53BP1 foci in one cell for the partial co-localization. Scale bars = 20 µm. Abbreviations: MNU, *N*-methyl-*N*-nitrosurea.

with special interest in deciphering the importance of cell cycle status in cell fate decision.[22]

Although the CD34+ cell population has been characterized to a certain degree in past works, differences in specific CD marker expression were found in this work.[25,26] CD38 expression was greatly upregulated in the tested CD34+ cells directly after isolation, with > 95% being CD34+CD38+. This would lead to the assumption that most cells isolated from UCB were already at a later differentiation state with no short-term (ST-HSC) or multipotent progenitors (MPPs) present. Contradictory to this, the CD34+CD38+ population was reduced during expansion, ie, ~80% CD34+CD38− cells detected after day 5, raising the question of a massive de-differentiation. As it is unlikely that the majority of cells spontaneously de-differentiate during culture, a possible approach was suggested by McKenzie *et al.*, where CD38 was described as a reversibly expressed HSC surface marker.[27]

DDR in CD34+cells is well studied in the adult counterpart, with other groups showing that adult quiescent CD34+ cells, residing in the bone marrow, accumulate DNA damage during aging thus triggering DDR when entering cell cycle.[28] Biechonski *et al.* emphasize the sensitivity of adult quiescent CD34+ cells to DNA damage, in contrast to their progeny, which in combination with the error-prone NHEJ used by the quiescent CD34+cells, leads to the drastically impaired regenerative capacity of these cells.[29]

We examined neonatal CD34+ cells, whose response to damage still needs to be extensively analyzed due to their clinical application in treatment of hematological malignancies.

DDR in Cycling CD34+ Cells

Cycling CD34+ cells were damaged in a dose-dependent manner when faced with distinct genotoxic noxae employing different mode of actions. Cells are sensitive to MNU due to its ability to methylate O^6-guanine. If the methylation is not removed through direct repair by MGMT or by the several other repair mechanisms, mutations can be accumulated during replication cycles and transferred to progeny. Mutation prevention is thus of great significance for neonatal CD34+ cells. Treatment resulted in a high abrogation of cell replication accompanied by the increase of the sub-G_1 cell fraction and cell cycle stop in a concentration-independent manner until 7 days post-treatment. This comes along with the upregulation of several DDR genes, eg, H2AX, BRCA2, XRCC6, and LIG4 to reduce damage accumulation after treatment with higher MNU concentrations (Supplementary Table S3). The damage increased 5 days after treatment and resulted in the complete cell death of cells treated with > 0.5 mM MNU. This is in accordance with gene expression showing upregulated expression of the pro-apoptotic gene BID and the autophagy-related gene BECN1.

Etoposide is a well-known cytostatic drug, applied to combat a variety of different neoplasms by inducing DSBs in cells through the inhibition of topoisomerase II during replication.[30] Cycling CD34+ cells treated with various concentrations of etoposide (1.5/5/10 µM) indicated different degrees of damage in a dose-dependent manner. Cells treated with 1.5 µM only exhibited signs of proliferation decrease merely directly after treatment. On the other hand, cells treated with both 5 and 10 µM showed different stages of apoptotic morphology, including membrane-bound apoptotic bodies, impaired replication capacity and a cell cycle distribution shift, with an increased sub-G_1-phase and a decreased S-/G_2-phase.

Our findings are in accordance with Tao et al., who showed that treatment of cycling HSCs with etoposide leads to apoptosis.[31] They postulate a DDR response in HSCs, which is tightly controlled by both pro-apoptotic genes, eg, BAX and FAS, and pro-survival genes, eg, BCL-2 and CDKN1A. Their upregulation suggests that, depending on the severity of the genotoxin-induced damage, the balance between the DDR players is altered and thus the fate of the cell determined. The analyzed genes study showed similar regulation upon etoposide exposure, as described by Tao et al., however, eventhough an upregulation of the cell cycle regulators CDKN1A and CCND1 in all conditions was registered, the cell used different DDR mechanisms depending on the applied concentration (Supplementary Table S2). While CDKN1A upregulation is reported to promote cell cycle arrest in both G_1/S- and G_2/M-transition to protect the cell from undergoing apoptosis after genotoxic stress,[32] CCND1 is reported to induce cell cycle re-entry after etoposide-induced cell cycle arrest.[30] The interplay of these different pro-apoptotic and pro-survival genes along with the analyzed dose-dependent proliferation halt and cell-cycle arrest, leads to the assumption that, while cycling CD34+cells treated with etoposide were damaged in a dose-dependent manner, at the time of damage, not all cells were actively cycling. Individual cells were still quiescent or predominantly in the G_1-phase at the time of damage. The initial response of CD34+cells to damage is a CDKN1A-induced cell cycle arrest, whereby the response rapidly shifts to the side of the pro-apoptotic players leading to apoptosis. The alleged recovery of cycling cells after treatment with etoposide can be explained by the fact that at the time of damage a small cell fraction was still quiescent and thus protected from the toxin. These CD34+cells could then start proliferation after toxin removal and could thus replenish the HSC pool in the culture. However, analysis of DSB markers γH2AX/53BP1 revealed that all conditions had severe numbers of DSBs accumulated in nearly all cells. In comparison to the extensively studied effect of irradiation on γH2AX/53BP1-foci formation with fast kinetics directly after exposure (1-3 minutes) and a disappearance of foci after 24-48 h,[33] etoposide treatment led to ambiguous results. With a 1 h delay in foci formation, all conditions displayed similar numbers of γH2AX/53BP1-foci, which did not persist for more than 24 h. This rapid loss of foci leads to the question whether DSBs have been repaired or cells appointed the apoptotic pathway to reduce damage in all conditions. The accurate interplay between γH2AX/53BP1 might also play an important role as we have found cells with only partially co-localized foci. De Feraudy *et al.* studied DSB response in human fibroblasts and suggested that a great number of cells do not display γH2AX/53BP1 co-localization postulating that γH2AX-foci alone might not be an accurate marker of DSBs. This leads to the assumption that only in cells where both foci are present, DDR leads to accurate repair of DSBs.[34]

DDR in Quiescent CD34+ Cells

Quiescent CD34+ cells have inherently different DDR mechanisms when faced with different genotoxic noxae. They may apply to either repair damage or protect the cell from transferring mutations to progeny by undergoing apoptosis. It was found that cell cycle statuses protect the cell differently from genotoxins depending on their mode of action. In recent years, nitrosamines have increasingly become the focus of research due to their potential carcinogenic effects. They have

also been found to pass the placental barrier, thus possibly posing a threat to neonatal HSCs,[35] evoking the necessity to study their effect on cord blood HSCs. Quiescent CD34⁺cells are sensitive to MNU treatment, in a dose-dependent manner. Proliferation and further cell cycle progression is affected, with cells being arrested in G_1 phase and predominantly undergoing apoptosis upon progression to S-phase when treated with high doses of MNU (0.5 mM) to stop the transfer of acquired mutations to progeny. This increase in apoptotic levels is in accordance with the upregulation of pro-apoptotic genes, eg, CAS3, CAS9, and FAS (Supplementary Table S5). In contrast, quiescent CD34⁺cells are mostly protected from cell cycle-specific agents, eg, etoposide, as it is believed that only cells that entered the cell cycle during the 24 h treatment would be affected. However, no significant damage of quiescent CD34⁺cells was observed in terms of morphology and cell counts. Apoptosis assay revealed a small dose-dependent increase in apoptotic cells, which is in accordance with the dose-dependent upregulation of CDKN1A and FAS in all conditions, thus explaining the cell cycle arrest and promotion of apoptosis (Supplementary Table S4). However, the immunocytochemical staining of γH2AX/53BP1-foci revealed the induction of DSBs for all concentrations of etoposide tested, with high numbers of γH2AX-foci detected, with only half as many 53BP1-foci. This raises again the question for further analyzes of DDR-specific genes on a protein basis to verify if repair mechanisms are successfully enacted only in cells with γH2AX/53BP1 co-localization.[34] The high number of γH2AX-single-foci might be an indicator, that once a DSB is detected in quiescent cells, the apoptotic pathway is directly activated, rather than further repair mechanisms, as it has been shown that non-chromatin-associated γH2AX sensitizes cells to undergo apoptosis, leading to the assumption that γH2AX might not only be a DSB-marker but also an apoptosis-related marker.[36]

Our findings suggest that neonatal CD34⁺cells similarly to their adult counterpart, have elaborated response mechanisms to DNA damage, which operate on a fine balance between pro-apoptotic and pro-survival signals. In contrast to adult CD34⁺ cells which repair accumulated damage after cell cycle entry, both quiescent and cycling neonatal CD34⁺ cells favor the apoptotic cell fate to prevent mutation accumulation and passaging to progeny especially in the case of persistent methylation damage. Nevertheless, the quiescent state of neonatal CD34⁺ cells greatly protects cells from toxins especially those operating in a cell cycle-dependent manner, thus allowing CD34⁺pool replenishment starting from the undamaged quiescent cell.

Funding

This work is supported by the Deutsche Forschungsgemeinschaft (DFG, German Research Foundation)—417677437/GRK2578 and the Jose Carreras Foundation for funding. We would like to thank the German José Carreras Leukemia Foundation (grant no. DJCLS18/R/2021) for their support and the Department of General Pediatrics, Neonatology and Pediatric Cardiology of the Medical Faculty in Düsseldorf for placing the fluorescence microscope at our disposal.

Conflict of Interest

All authors declared no potential conflicts of interest.

Author Contributions

F.B., M.O.: Conception and design, Collection and/or assembly of data, Data analysis and interpretation, Manuscript writing. S.L.: Conception and design, Data analysis and interpretation. K.R.: Collection and/or assembly of data. G.K.: Financial support, Administrative support, Provision of study material or patients, Final approval of manuscript.

Data Availability

The data supporting the findings of this study are available from the corresponding author upon reasonable request.

Supplementary Material

Supplementary material is available at *Stem Cells* online.

References

1. Yousefzadeh M, Henpita C, Vyas R, et al. DNA damage-how and why we age? *Elife*. 2021;10:e62852. https://doi.org/10.7554/eLife.62852
2. Rocha V, Broxmeyer HE. New approaches for improving engraftment after cord blood transplantation. *Biol Blood Marrow Transplant*. 2010;16(1 Suppl):S126-S132. https://doi.org/10.1016/j.bbmt.2009.11.001
3. Gudmundsson KO, Du Y. Quiescence regulation by normal haematopoietic stem cells and leukaemia stem cells. *FEBS J*. 2022;290(15):3708-3722. https://doi.org/10.1111/febs.16472
4. Vousden KH, Lane DP. p53 in health and disease. *Nat Rev Mol Cell Biol*. 2007;8(4):275-283. https://doi.org/10.1038/nrm2147
5. Milyavsky M, Gan OI, Trottier M, et al. A distinctive DNA damage response in human hematopoietic stem cells reveals an apoptosis-independent role for p53 in self-renewal. *Cell Stem Cell*. 2010;7(2):186-197. https://doi.org/10.1016/j.stem.2010.05.016
6. Mohrin M, Bourke E, Alexander D, et al. Hematopoietic stem cell quiescence promotes error-prone DNA repair and mutagenesis. *Cell Stem Cell*. 2010;7(2):174-185. https://doi.org/10.1016/j.stem.2010.06.014
7. Li T, Zhou ZW, Ju Z, Wang ZQ. DNA damage response in hematopoietic stem cell ageing. *Genomics Proteomics Bioinformatics*. 2016;14(3):147-154. https://doi.org/10.1016/j.gpb.2016.04.002
8. Jaatinen T, Laine J. Isolation of mononuclear cells from human cord blood by Ficoll-Paque density gradient. *Curr Protoc Stem Cell Biol*. 2007;1:2A.1.1-2A.1.4. https://doi.org/10.1002/9780470151808.sc02a01s1
9. Liedtke S, Koerschgen L, Kogler G. Good manufacturing practice-grade CD34+ selection from thawed cord blood and short-term expansion over 3–4 days as starting material for the generation of human leukocyte antigen homozygous induced pluripotent stem cells. *Stem Cells Transl Med*. 2019;8(S1):S20-S20. https://doi.org/10.1002/sctm.12563
10. O'Dwyer PJ, Leyland-Jones B, Alonso MT, Marsoni S, Wittes RE. Etoposide (VP-16-213) current status of an active anticancer drug. *N Engl J Med*. 1985;312(11):692-700. https://doi.org/10.1056/NEJM198503143121106
11. Belani CP, Doyle LA, Aisner J. Etoposide: current status and future perspectives in the management of malignant neoplasms. *Cancer Chemother Pharmacol*. 1994;34(Suppl):S118-S126. https://doi.org/10.1007/BF00684875
12. Chow KC, Ross WE. Topoisomerase-specific drug sensitivity in relation to cell cycle progression. *Mol Cell Biol*. 1987;7(9):3119-3123. https://doi.org/10.1128/mcb.7.9.3119-3123.1987
13. Burden DA, Osheroff N. Mechanism of action of eukaryotic topoisomerase II and drugs targeted to the enzyme. *Biochim Biophys Acta*. 1998;1400(1-3):139-154. https://doi.org/10.1016/s0167-4781(98)00132-8

14. Reyhanoglu G, Tadi P. *Etoposide*. StatPearls, Treasure Island (FL), 2022.
15. Soubeyrand S, Pope L, Hache RJ. Topoisomerase IIalpha-dependent induction of a persistent DNA damage response in response to transient etoposide exposure. *Mol Oncol*. 2010;4(1):38-51. https://doi.org/10.1016/j.molonc.2009.09.003
16. Lijinsky W. N-Nitroso compounds in the diet. *Mutat Res*. 1999;443(1-2):129-138. https://doi.org/10.1016/s1383-5742(99)00015-0
17. Schrenk D, Bignami M, Bodin L, et al. Risk assessment of N-nitrosamines in food. *EFSA J*. 2023;21(3):e07884. https://doi.org/10.2903/j.efsa.2023.7884
18. Swann PF, Magee PN. Nitrosamine-induced carcinogenesis the alklylation of nucleic acids of the rat by N-methyl-N-nitrosourea, dimethylnitrosamine, dimethyl sulphate and methyl methanesulphonate. *Biochem J*. 1968;110(1):39-47. https://doi.org/10.1042/bj1100039
19. Goth R, Rajewsky MF. Persistence of O6-ethylguanine in rat-brain DNA: correlation with nervous system-specific carcinogenesis by ethylnitrosourea. *Proc Natl Acad Sci USA*. 1974;71(3):639-643. https://doi.org/10.1073/pnas.71.3.639
20. Jones PA, Baylin SB. The fundamental role of epigenetic events in cancer. *Nat Rev Genet*. 2002;3(6):415-428. https://doi.org/10.1038/nrg816
21. Margison GP, Santibanez-Koref MF. O6-alkylguanine-DNA alkyltransferase: role in carcinogenesis and chemotherapy. *Bioessays*. 2002;24(3):255-266. https://doi.org/10.1002/bies.10063
22. Lane AA, Scadden DT. Stem cells and DNA damage: persist or perish? *Cell*. 2010;142(3):360-362. https://doi.org/10.1016/j.cell.2010.07.030
23. Sutherland DR, Anderson L, Keeney M, Nayar R, Chin-Yee I. The ISHAGE guidelines for CD34+ cell determination by flow cytometry International Society of Hematotherapy and Graft Engineering. *J Hematother*. 1996;5(3):213-226. https://doi.org/10.1089/scd.1.1996.5.213
24. Schmittgen TD, Livak KJ. Analyzing real-time PCR data by the comparative C(T) method. *Nat Protoc*. 2008;3(6):1101-1108. https://doi.org/10.1038/nprot.2008.73
25. Hordyjewska A, Popiołek L, Horecka A. Characteristics of hematopoietic stem cells of umbilical cord blood. *Cytotechnology*. 2015;67(3):387-396. https://doi.org/10.1007/s10616-014-9796-y
26. Sane MS, Tang H, Misra N, et al. Characterization of an umbilical cord blood sourced product suitable for allogeneic applications. *Regen Med*. 2019;14(8):769-789. https://doi.org/10.2217/rme-2019-0058
27. McKenzie JL, Gan OI, Doedens M, Dick JE. Reversible cell surface expression of CD38 on CD34-positive human hematopoietic repopulating cells. *Exp Hematol*. 2007;35(9):1429-1436. https://doi.org/10.1016/j.exphem.2007.05.017
28. Beerman I, Seita J, Inlay MA, Weissman IL, Rossi DJ. Quiescent hematopoietic stem cells accumulate DNA damage during aging that is repaired upon entry into cell cycle. *Cell Stem Cell*. 2014;15(1):37-50. https://doi.org/10.1016/j.stem.2014.04.016
29. Biechonski S, Yassin M, Milyavsky M. DNA-damage response in hematopoietic stem cells: an evolutionary trade-off between blood regeneration and leukemia suppression. *Carcinogenesis*. 2017;38(4):367-377. https://doi.org/10.1093/carcin/bgx002
30. Cheng T, Rodrigues N, Shen H, et al. Hematopoietic stem cell quiescence maintained by p21cip1/waf1. *Science*. 2000;287(5459):1804-1808. https://doi.org/10.1126/science.287.5459.1804
31. Tao W, Hangoc G, Hawes JW, et al. Profiling of differentially expressed apoptosis-related genes by cDNA arrays in human cord blood CD34+ cells treated with etoposide. *Exp Hematol*. 2003;31(3):251-260. https://doi.org/10.1016/s0301-472x(02)01083-4
32. Tanaka T, Halicka HD, Traganos F, Seiter K, Darzynkiewicz Z. Induction of ATM activation, histone H2AX phosphorylation and apoptosis by etoposide: relation to cell cycle phase. *Cell Cycle* 2007;6(3):371-376. https://doi.org/10.4161/cc.6.3.3835
33. Chronis F, Rogakou EP. Interplay between γH2AX and 53BP1 pathways inDNA double-strand break repair response. In: Gewirtz DA, Holt SF, Grant S, eds. *Apoptosis, Senescence, and Cancer*. Humana Press; 2007:243-63.
34. de Feraudy S, Revet I, Bezrookove V, Feeney L, Cleaver JE. A minority of foci or pan-nuclear apoptotic staining of gammaH2AX in the S phase after UV damage contain DNA double-strand breaks. *Proc Natl Acad Sci USA*. 2010;107(15):6870-6875. https://doi.org/10.1073/pnas.1002175107
35. Althoff J, Grandjean C, Pour P. Transplacental effect of nitrosamines in Syrian hamsters. *Z. Krebsforsch*. 1977;90(2):119-126.
36. Liu Y, Parry JA, Chin A, Duensing S, Duensing A. Soluble histone H2AX is induced by DNA replication stress and sensitizes cells to undergo apoptosis. *Mol Cancer*. 2008;7:61. https://doi.org/10.1186/1476-4598-7-61

Supporting Information

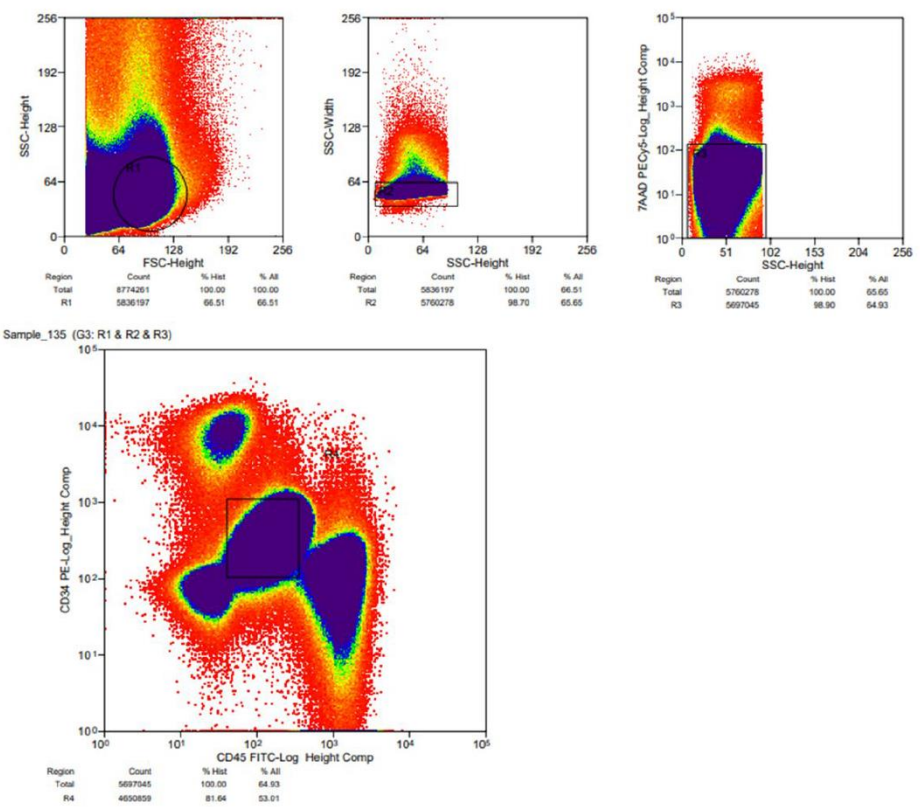

Figure S1: Sorting strategy of CD34⁺ CD45$^{+/low}$ quiescent HSCs after CliniMACS separation prior to MNU treatment. The figure shows representative scatterplots.

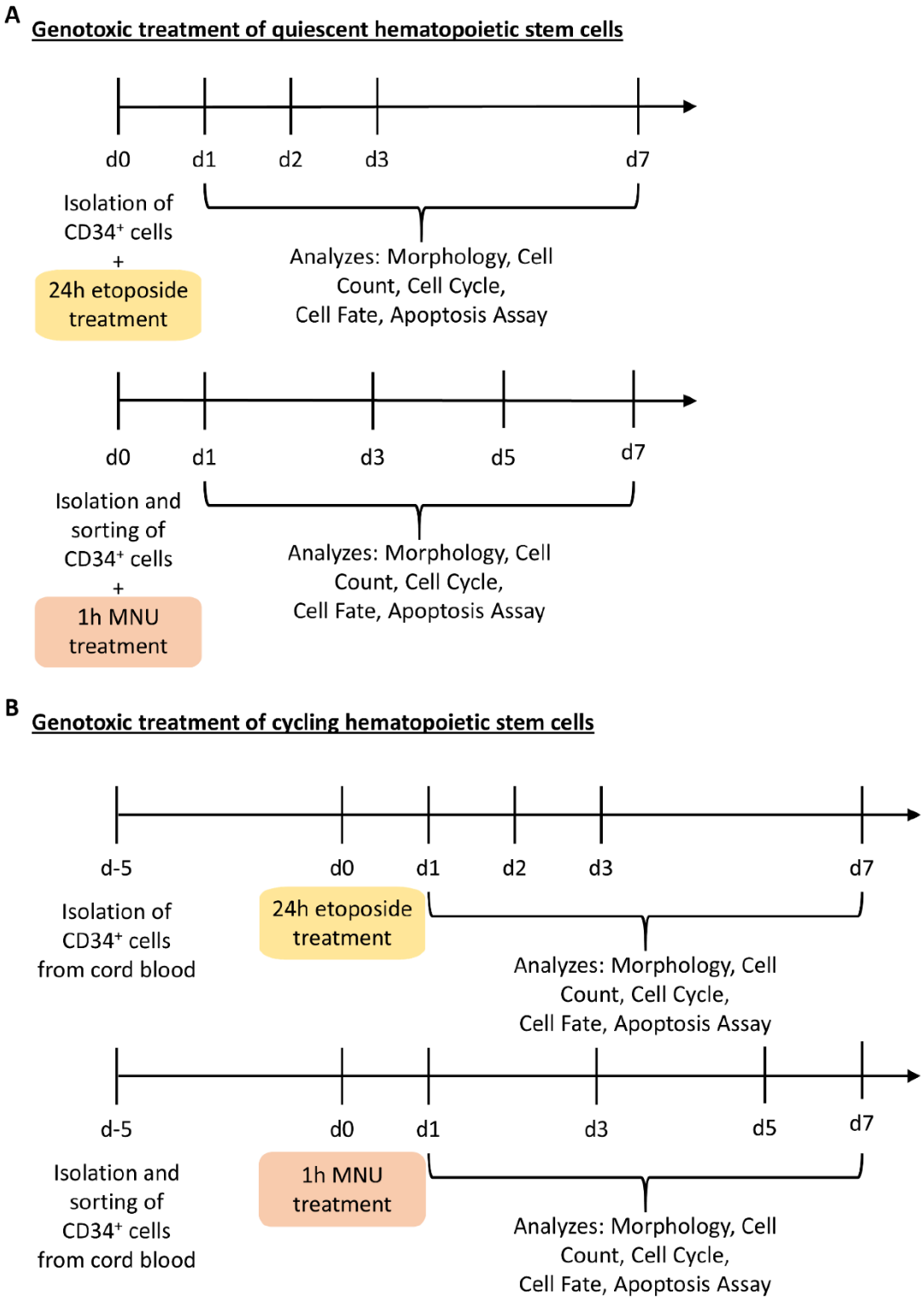

Figure S2: Schematic overview of the experimental setup of genotoxic treatment of quiescent and cycling CD34⁺ cells isolated from cord blood. (A) Quiescent HSCs were isolated from cord blood and directly treated with etoposide (24h) or MNU (1h). Analyzes were performed starting from d1. (B) Cycling HSCs were cultivated for 5 days after isolation from cord blood before treatment with etoposide (24h) or MNU (1h). Analyzes were performed starting from d1. Abbreviations: MNU, N-methyl-N-nitrosurea.

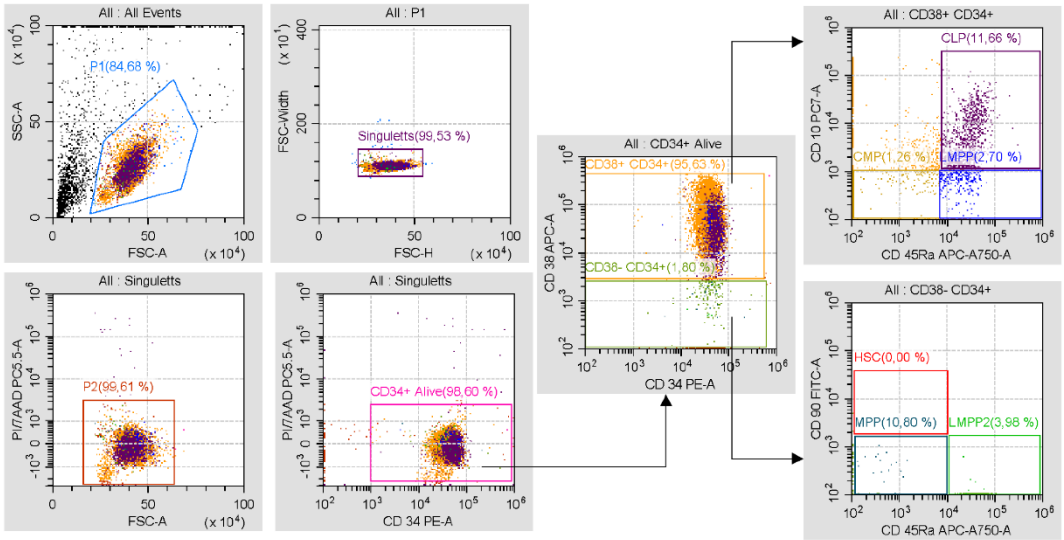

Figure S3: Gating strategy used for flow cytometric cell fate analysis. Alive cells were determined using PI staining (P2). Based on P2, the alive CD34⁺ population was determined. CD38⁺ CD34⁺ and CD38⁻ CD34⁺ populations were distinguished based on the FMO CD38 control. CLP (CD10⁺ CD45Ra⁺), CMP (CD10⁻ CD45Ra⁻) and LMPP (CD10⁻ CD45Ra⁺) were determined based on the CD38⁺ CD34⁺ population. HSC (CD90⁺ CD45Ra⁻), MPP (CD90⁻ CD45Ra⁻) and LMPP (CD90⁻ CD45Ra⁺) were determined based on the CD38⁻ CD34⁺ population. Abbreviations: CLP, common lymphoid progenitor; CMP, common myeloid progenitor; LMPP, lymphomyeloid-primed progenitor; FMO, fluorescence minus one; HSC, hematopoietic stem cell; MPP, multipotent progenitor.

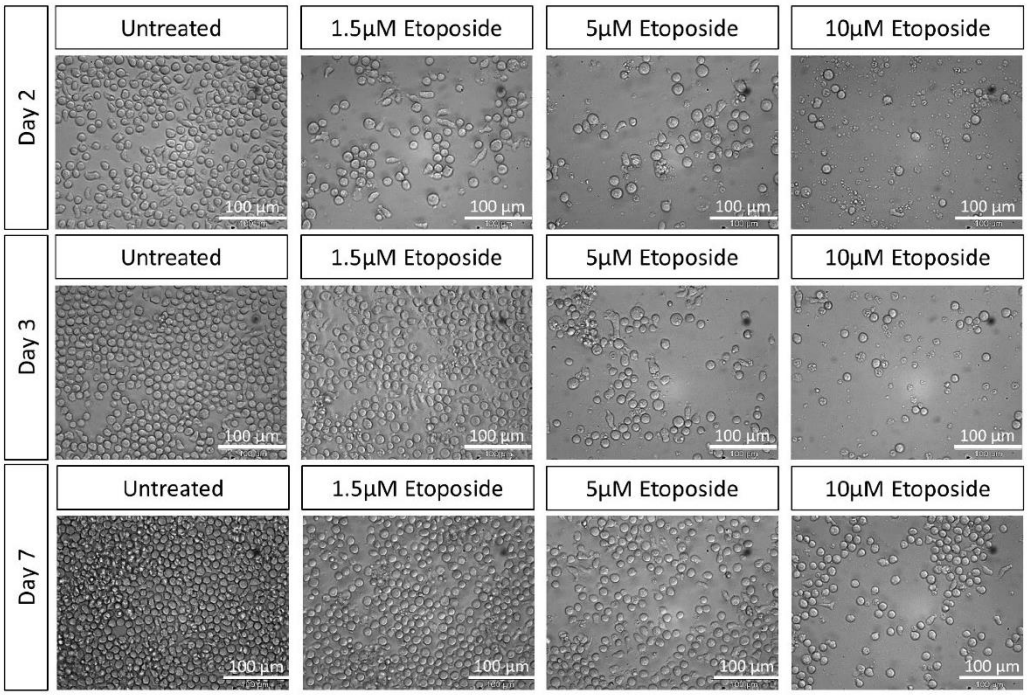

Figure S4: Representative morphological images of cycling CD34⁺ cells treated for 2 h with different etoposide concentrations (1.5µM, 5µM, and 10µM) in comparison to untreated cells. Changes were documented on day 2, 3 and 7 after the start of treatment. Scale bar = 100µm.

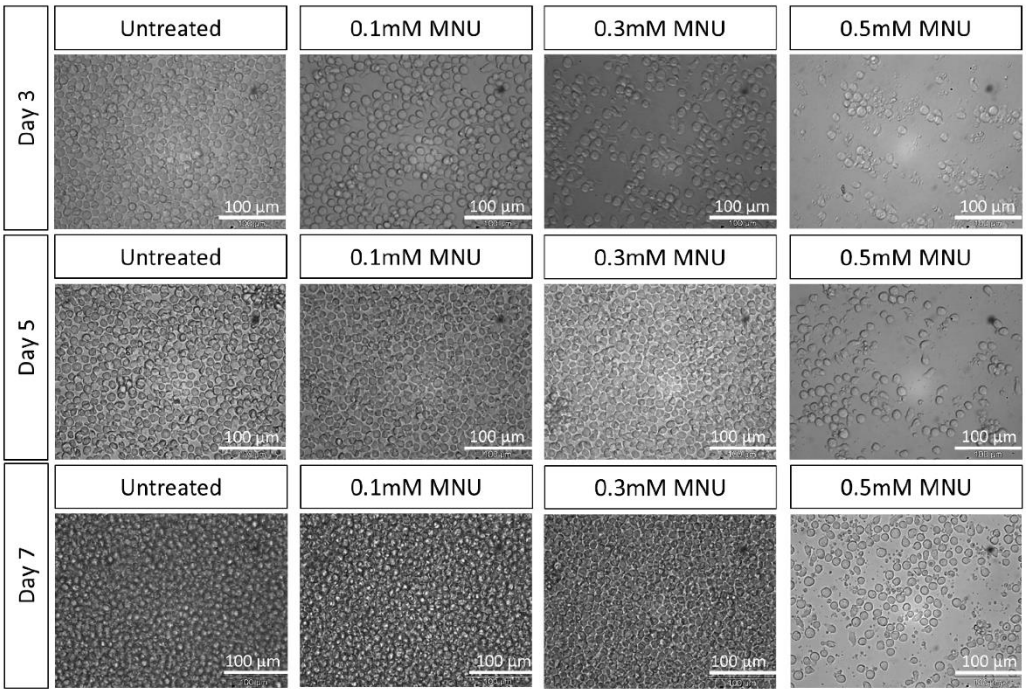

Figure S5: Representative morphological images of cycling CD34⁺ cells treated for 1h with different MNU concentrations (0.1mM, 0.3mM, and 0.5mM) in comparison to untreated cells. Changes were documented on day 3 and 5 after the start of treatment. Scale bar = 100µm. Abbreviations: MNU, N-methyl-N-nitrosurea.

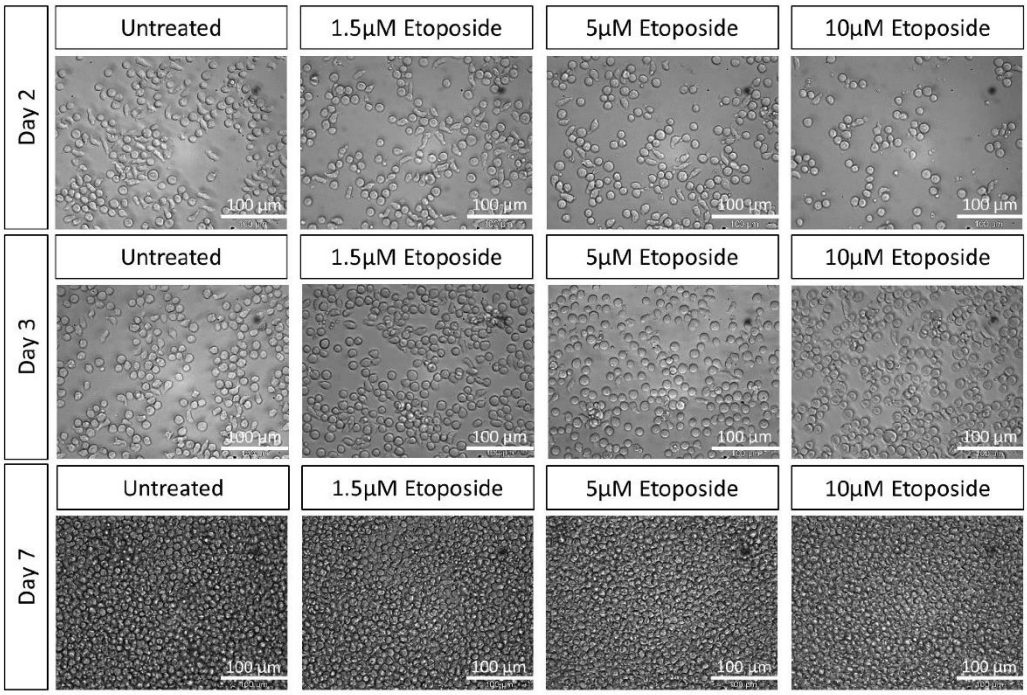

Figure S6: Representative morphological images of quiescent CD34⁺ cells treated for 24h with different etoposide concentrations (1.5µM, 5µM, and 10µM) in comparison to untreated cells. Changes were documented on day 2, 3 and 7 after the start of treatment. Scale bar = 100µm.

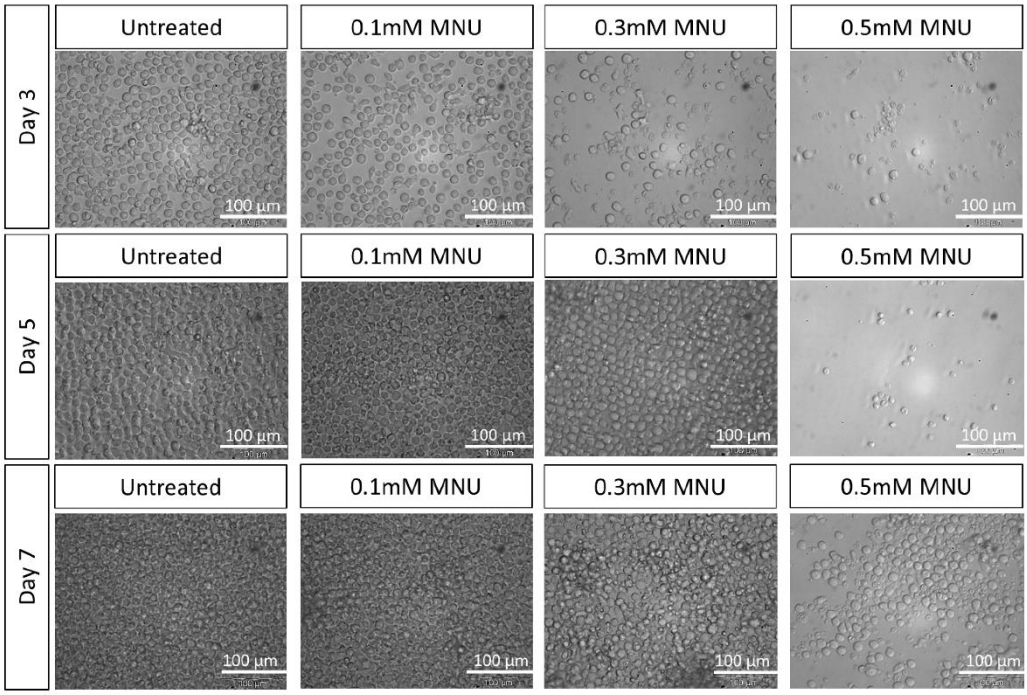

Figure S7: Representative morphological images of quiescent CD34⁺ cells treated for 1h with different MNU concentrations (0.1mM, 0.3mM, and 0.5mM) in comparison to untreated cells. Changes were documented on day 3 and 5 after the start of treatment. Scale bar = 100µm. Abbreviations: MNU, N-methyl-N-nitrosurea.

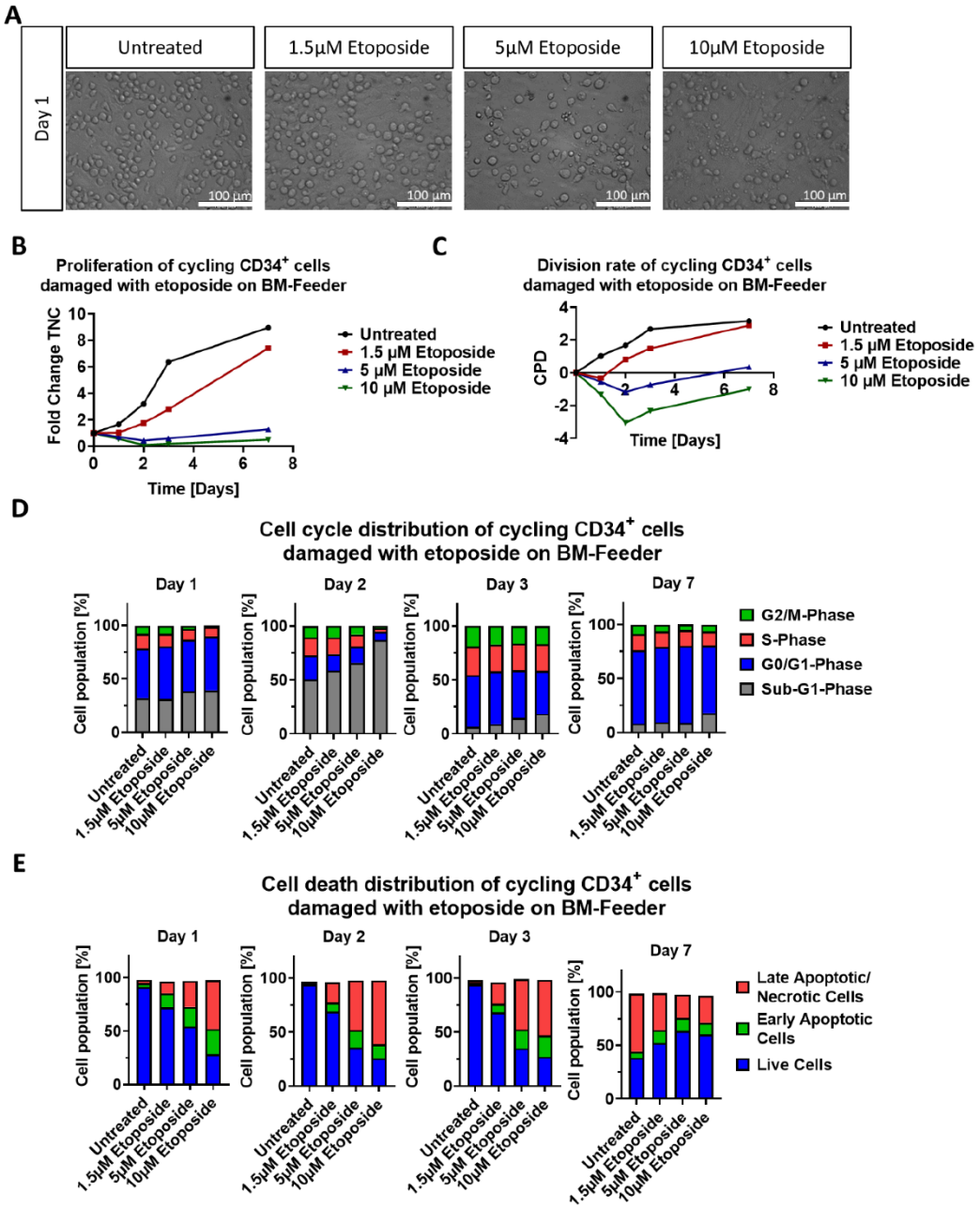

Figure S8: Effect of etoposide treatment on morphology, growth, cell cycle and cell death of cycling CD34⁺ cell on BM-Feeder. (A) Representative morphological images of untreated and with 1.5µM, 5µM and 10µM etoposide treated cycling CD34⁺ cells. Analysis was performed after a 24h treatment. Scale bars = 100µm. (B, C) Representative growth kinetics depicted via the total fold change over time and the CPD. After treatment of cycling cells with different etoposide concentrations, the growth curves revealed no significant effect on cycling CD34⁺ cells. (D) Cell cycle analysis of treated cycling CD34⁺ cells via staining with PI and analysis by flow cytometry. (E) Analysis of cell death levels of treated cycling CD34⁺ cells via Annexin V/PI staining. (B-E) Shown are representative data from three independent experiments with different CB donations. Abbreviations: BM-Feeder, bone marrow feeder; CB, cord blood; CPD, cumulative population doubling, PI, propidium iodide.

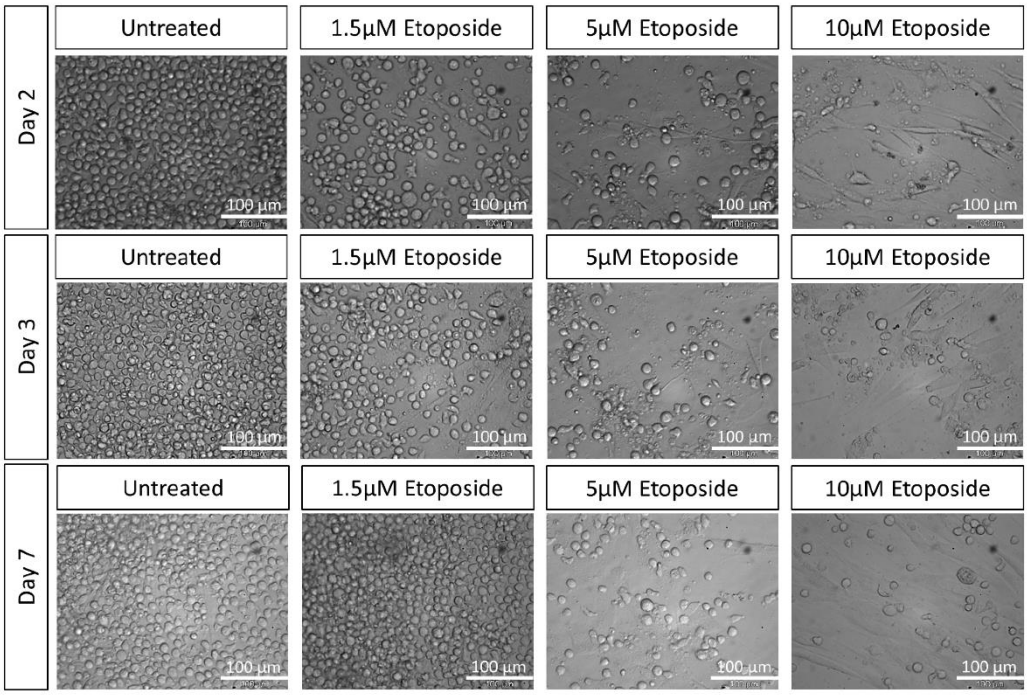

Figure S9: Representative morphological images of cycling CD34⁺ cells treated for 1h with different etoposide concentrations (1.5µM, 5µM, and 10µM) on BM-Feeder in comparison to untreated cells. Changes were documented on day 2, 5 and 7 after the start of treatment. Scale bar = 100µm.

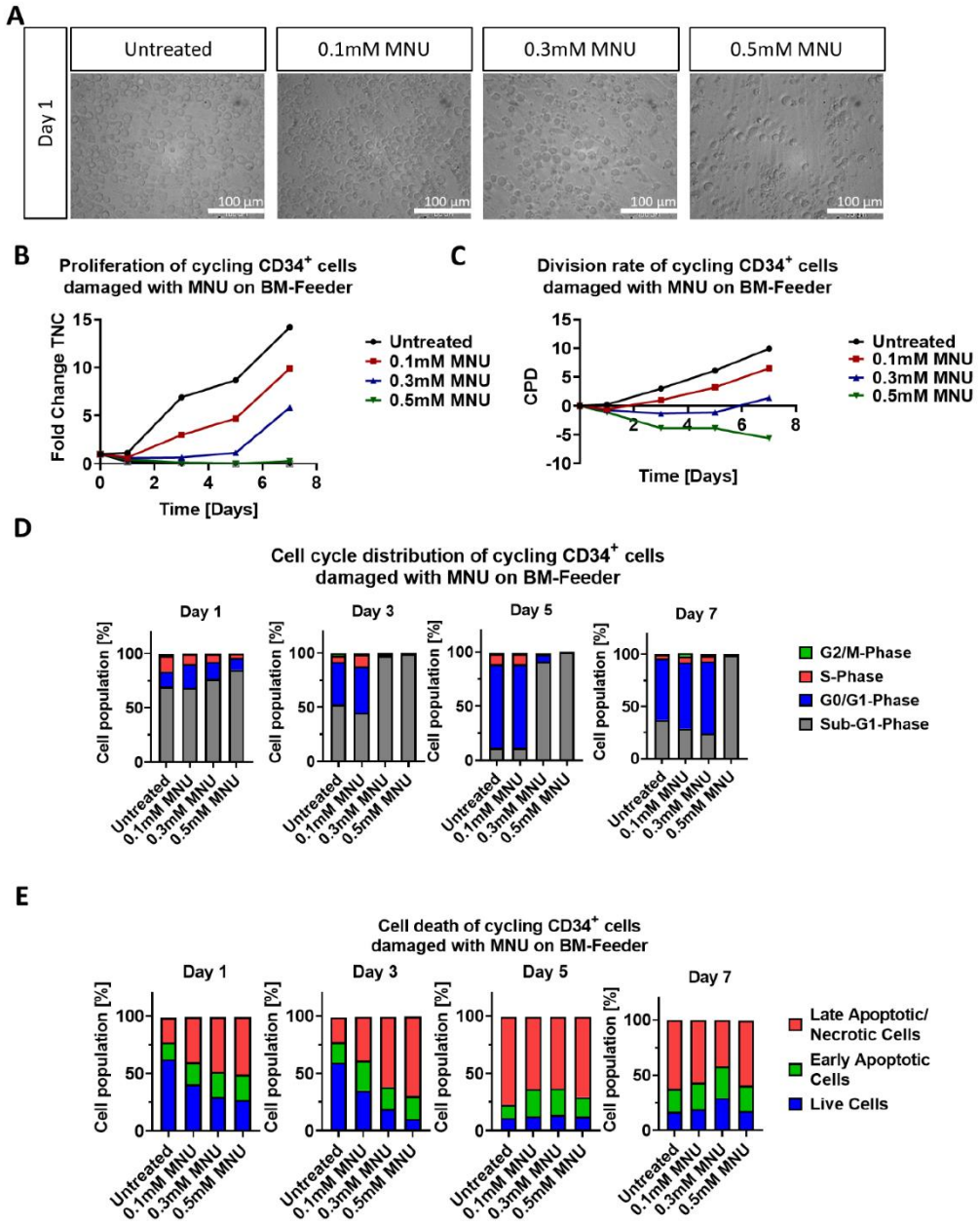

Figure S10: Effect of MNU treatment on morphology, growth, cell cycle and cell death of cycling CD34⁺ cell on BM-Feeder. (A) Representative morphological images of untreated and with 0.1mM, 0.3mM and 0.5mM MNU treated cycling CD34⁺ cells. Analysis was performed after a 1h treatment. Scale bars = 100µm. (B, C) Representative growth kinetics depicted via the total fold change over time and the CPD. After treatment of cycling cells with different MNU concentrations, the growth curves revealed no significant effect on cycling CD34⁺ cells. (D) Cell cycle analysis of treated cycling CD34⁺ cells via staining with PI and analysis by flow cytometry. (E) Analysis of cell death levels of treated cycling CD34⁺ cells via Annexin V/PI staining. (B-E) Shown are representative data from three independent experiments with different CB donations. Abbreviations: BM-Feeder, bone marrow feeder; CB, cord blood; CPD, cumulative population doubling, MNU, N-methyl-N-nitrosurea; PI, propidium iodide.

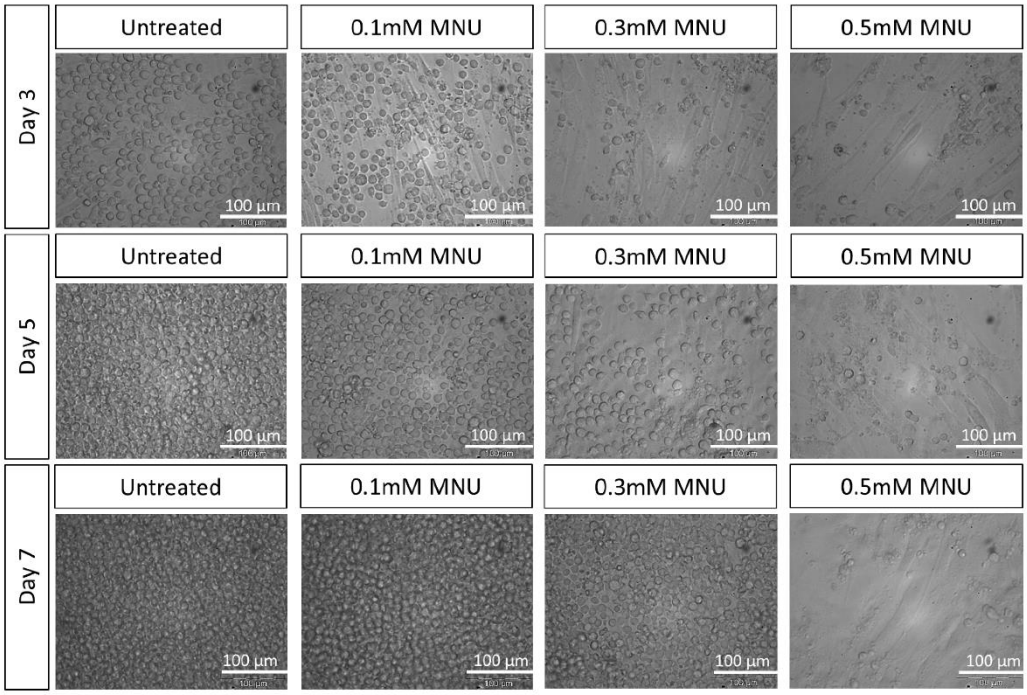

Figure S11: Representative morphological images of cycling CD34⁺ cells treated for 1h with different MNU concentrations (0.1mM, 0.3mM, and 0.5mM) on BM-Feeder in comparison to untreated cells. Changes were documented on day 3, 5 and 7 after the start of treatment. Scale bar = 100µm. Abbreviations: MNU, N-methyl-N-nitrosurea.

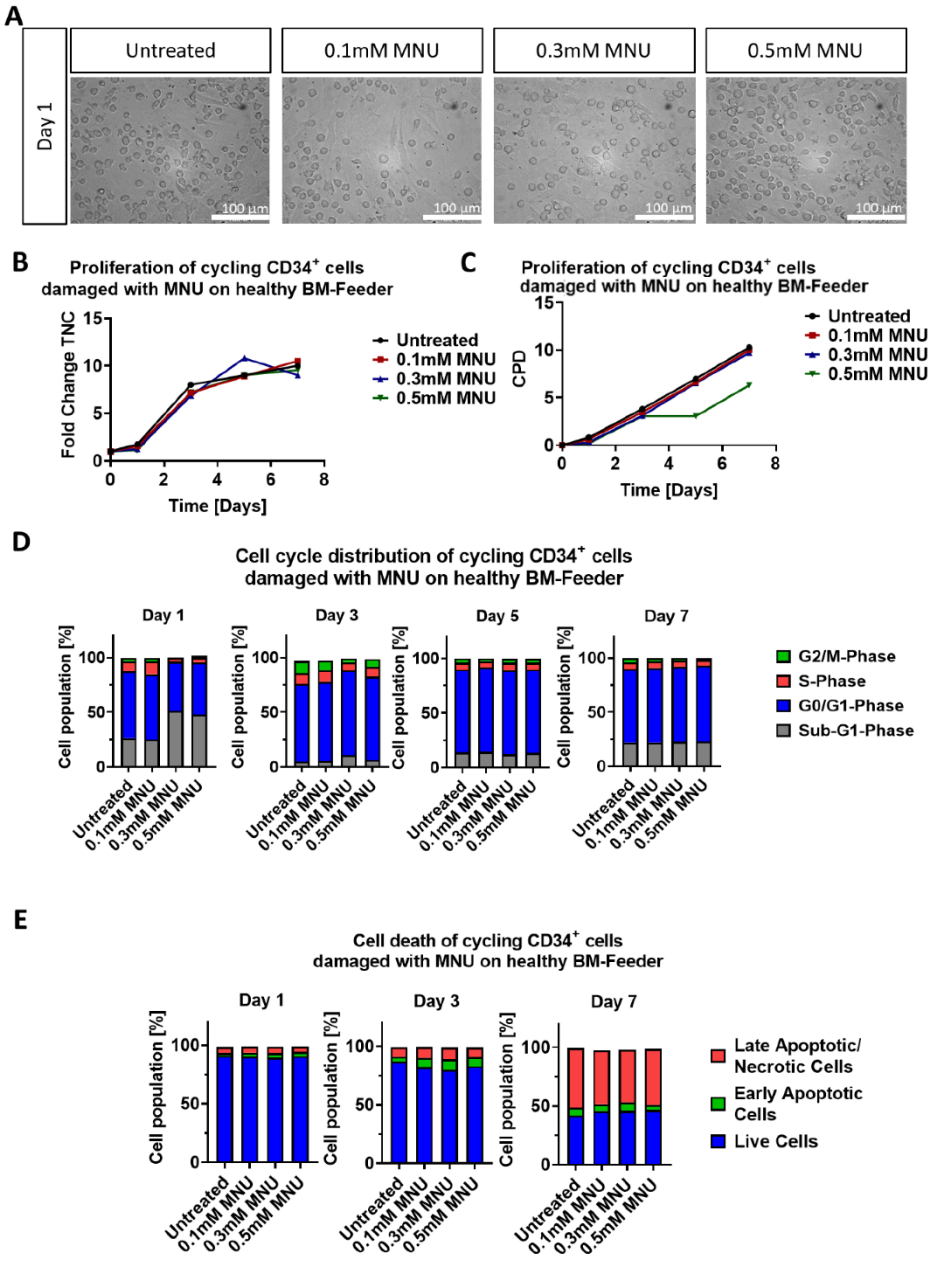

Figure S12: Effect of MNU treatment on morphology, growth, cell cycle and cell death of cycling CD34⁺ cell on healthy BM-Feeder. (A) Representative morphological images of untreated and with 0.1mM, 0.3mM and 0.5mM MNU treated cycling CD34⁺ cells. Analysis was performed after a 1h treatment. Scale bars = 100µm. (B, C) Representative growth kinetics depicted via the total fold change over time and the CPD. After treatment of cycling cells with different MNU concentrations, the growth curves revealed no significant effect on cycling CD34⁺ cells. (D) Cell cycle analysis of treated cycling CD34⁺ cells via staining with PI and analysis by flow cytometry. (E) Analysis of cell death levels of treated cycling CD34⁺ cells via Annexin V/PI staining. (B-E) Shown are representative data from three independent experiments with different CB donations. Abbreviations: BM-Feeder, bone marrow feeder; CB, cord blood; CPD, cumulative population doubling, MNU, N-methyl-N-nitrosurea; PI, propidium iodide.

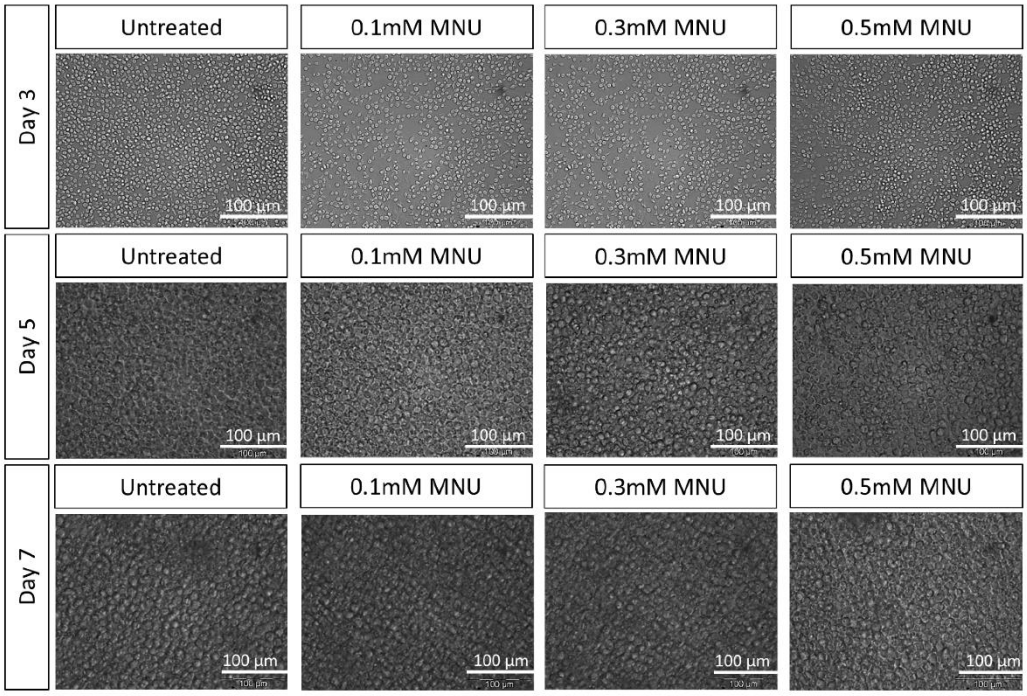

Figure S13: Representative morphological images of cycling CD34⁺ cells treated for 1h with different MNU concentrations (0.1mM, 0.3mM, and 0.5mM) and cultivated on healthy BM-Feeder in comparison to untreated cells. Changes were documented on day 3, 5 and 7 after the start of treatment. Scale bar = 100µm. Abbreviations: MNU, N-methyl-N-nitrosurea.

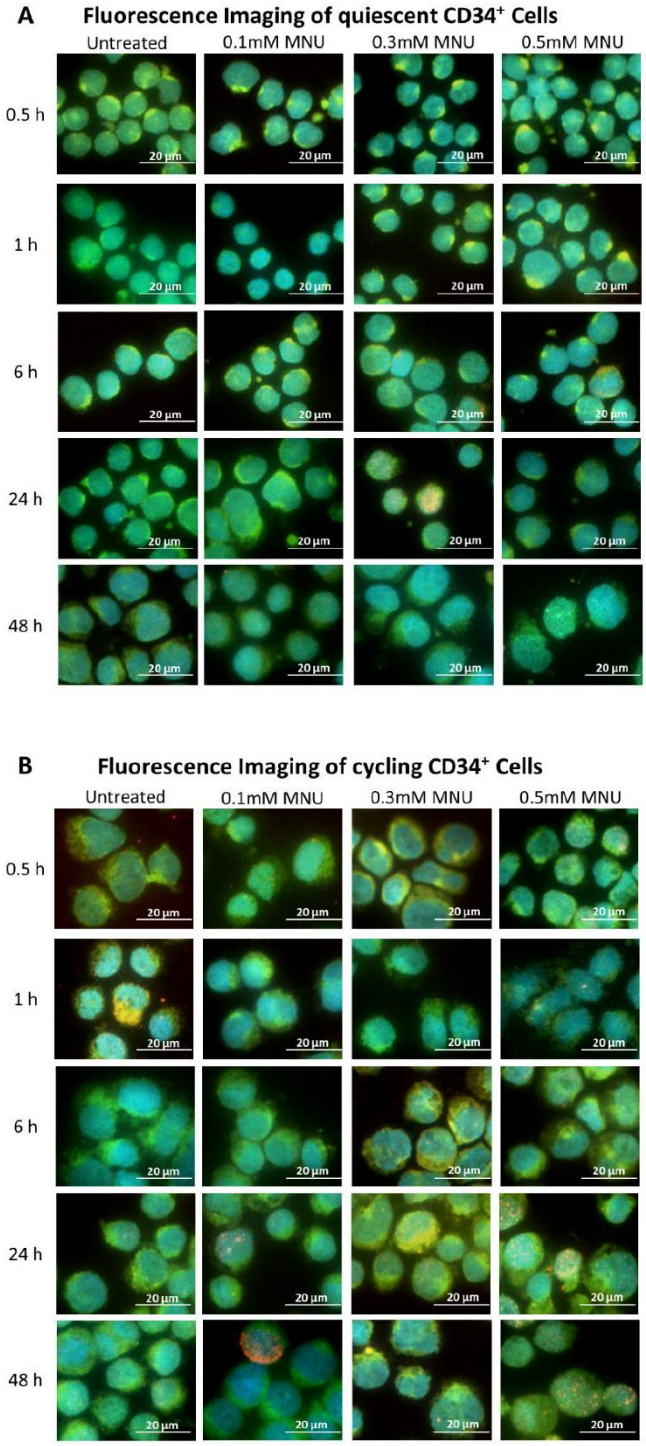

Figure S14: Representative fluorescence co-staining images of (A) quiescent CD34+ cells treated with different doses of MNU, and (B) cycling CD34+ cells treated with different doses of MNU. Cells were treated with 0.1mM, 0.3mM, or 0.5mM MNU, and harvested between 0.5h and 48h and co-stained for γH2AX (green) and 53BP1 (red), using HOECHST (blue) to visualize the nucleus. Scale bars = 20 µm.

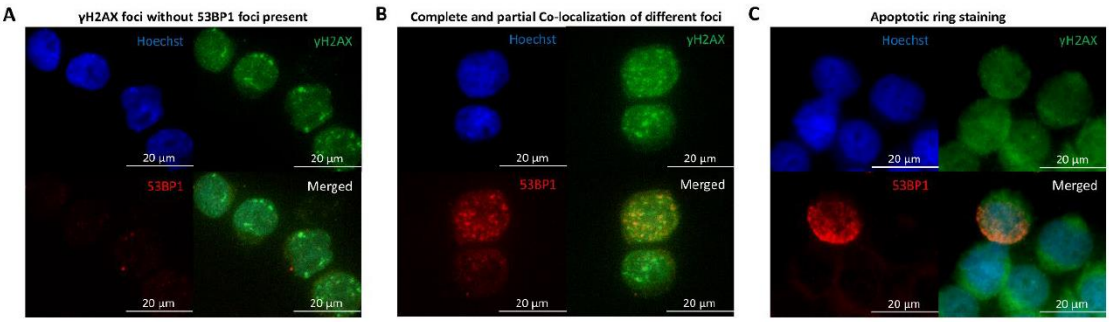

Figure S15: Representative fluorescent images of γH2AX and 53BP1 co-localization staining. CD34⁺ cells were treated with different genotoxic noxae (etoposide or MNU) and cells stained with γH2AX (green) and 53BP1 (red), using HOECHST (blue) to visualize the nucleus. Distinct γH2AX/53BP1 staining types were detected. These different types of foci were (A) only γH2AX with no 53BP1 foci present, (B) partial and complete co-localization of the γH2AX- and 53BP1-foci in a cell, and (C) apoptotic rings, where staining of 53BP1 revealed staining of the circuit of cells. Scale bars = 20 µm.

Table S1: List of utilized qRT-PCR primers. All primer sequences are listed from 5´ to 3´. All primers were obtained from Thermo Fisher Scientific.

Gene	Forward primer (5´-3´)	Reverse primer (5´-3´)
APEX1	*ACAAAGAGGCAGCAGGAGAG*	*CTGGGGCTTCTTCCTTTACC*
ATG3	*AGGACAATATAAGGCTTCAA*	*TTCCAACAATCCACTCTC*
ATM	*CCTTGTGCTAGTGGGCAGAA*	*ATGGGGAGCAAAGAACCCAG*
BAX	*CGGGGAGCAGCCCAG*	*GGAGTCTGTGTCCACGGC*
BCL-2	*GAACTGGGGGAGGATTGTGG*	*CCGTACAGTTCCACAAAGGC*
BECN1	*GGATGGAAGGGTCTAAGA*	*CTGTGGTAAGTAATGGAG*
BID	*GGGAAACTGTTGAGTGGCTGA*	*CAGCTCCGACTCACTCCTG*
BRCA1	*CCACAGATCAACTGGAATGG*	*GTAGAGTGCTACACTGTCCA*
BRCA2	*TTCTGAGGTGGACCTAATAGG*	*TGATTTGGATTCTGGTCGCC*
CAS3	*AGCAAACCTCAGGGAAACATT*	*CTCAGAAGCACACAAACAAAAC*
CAS8	*AATGTTGGAGGAAAGCAATC*	*CATAGTCGTTGATTATCTTCAGC*
CAS9	*AACCCTAGAAAACCTTACCCC*	*CATCACCAAATCCTCCAGAAC*
CCNB1	*GCATCTAAGATTGGAGAGGTTGAT*	*CAGGTAATGTTGTAGAGTTGGTG*
CCND1	*GATGCCAACCTCCTCAACGA*	*GGAAGCGGTCCAGGTAGTTC*
CDK1	*AAATTGAGCGGAGAGCGACG*	*TGGCTACCACTTGACCTGTAG*
CDK6	*TGGAGACCTTCGAGCACC*	*CACTCCAGGCTCTGGAACTT*
CDKN1A	*TACATCTTCTGCCTTAGT*	*TCTTAGGAACCTCTCATT*
CDKN1B	*ACAGCTCGAATTAAGAATA*	*CTTATACAGGATGTCCATT*
FAS	*TGTGTGATGAAGGACATGGCTTA*	*ACTTGGTGTTGCTGGTGAGT*
FANCA	*CGCAGGTCACGGTTGATGTA*	*CCACTGAACACTCCGAACCA*
FANCI	*CTGTGATATGAGCAACAATGG*	*TTCACTGCTTGATTCTGAAGG*
H2AX	*TTCTGGAAGACTTGGCCTTC*	*ACTCTTGCTGTCCACATAGC*
LIG4	*TTGCCCGAGGCCAGTTAAA*	*CACAAATCTGCAAAAGGAACGTG*
MGMT	*ACCGTTTGCGACTTGGTACT*	*GGGCTGGTGGAAATAGGCAT*
mKI67	*TCCTTTGGTGGGCACCTAAGACCTG*	*TGATGGTTGAGGCCTGTTCCTTGATG*
NHEJ1	*CCATTGTTGAAGGACGCTGC*	*CTAGCTCCCTCACTTGGCAC*
RAD51	*GCTGATGAGTTTGGTGTAGC*	*AACATAGCTTCAGCTTCAGG*
RPL13a	*GAGGTATGCTGCCCCACAAA*	*TTCAGACGCACGACCTTGAG*
TP53	*TTCCGAGAGCTGAATGAGGC*	*AATGTCAGTCTGAGTCAGGCC*
XPC	*GACCTCAAGAAGGCACACCA*	*TGGCTTCACAGGCAGAAGAG*
XPG	*TGCACCCCGGTCTTCCATTA*	*CCTCCCTGCTCCTACACAAC*
XRCC1	*GTCGCCATCTGTTCCCAAGA*	*AAGCCACTCAGCACCACTAC*
XRCC4	*CCTCAGGAGAATCAGCTTCAAGA*	*AAAGAGGTCTTCTGGGCTGC*
XRCC5	*AGCATAGACTGCATCCGAGC*	*TCCCCATACATCCACGACCT*
XRCC6	*TGCGTGGATTGTCGTCTTCT*	*CTTCTTCATCGCCCTCGGTT*

Table S2: Selection of genes involved in DNA damage repair, cell cycle regulation and apoptosis analyzed in cycling CD34⁺ treated with etoposide (1.5µM, 5µM, and 10µM). Fold changes in mRNA expression were analyzed using qPCR and calculated with the 2-ΔΔCT method relative to untreated CD34⁺ cells and normalized to the reference gene RPL13A. The value 1 corresponds to a basic expression as in untreated cells; Values above 2 are considered a significant upregulation (green) while values below -2 are considered a significant downregulation (red) of a gene in treated CD34⁺ cells. Abbreviations: ETO, Etoposide; HR, Homologous Repair; NHEJ, Non-Homologous End Joining; n.p., not performed.

		ETO 5h			ETO 16h			ETO 24h			ETO 48h			ETO 72h		
		1.5µM ETO	5µM ETO	10µM ETO	1.5µM ETO	5µM ETO	10µM ETO	1.5µM ETO	5µM ETO	10µM ETO	1.5µM ETO	5µM ETO	10µM ETO	1.5µM ETO	5µM ETO	10µM ETO
Pathways	**Gene**	**Fold Change**														
Cell cycle regulation	CDKN1A	3.853	17.372	17.395	8.962	27.429	27.505	10.095	30.143	53.995	16.058	30.960	54.927	13.139	11.133	18.198
	CDKN1B	1.063	1.647	-1.499	1.067	-1.047	-1.838	-1.198	1.277	1.112	-1.252	-1.433	-1.148	-1.842	-2.070	-3.040
	CCNB1	-1.164	-1.563	-2.793	1.009	-1.188	-3.802	1.140	-1.073	-1.883	-1.043	-1.294	-3.155	1.178	-1.319	-2.857
	CCND1	1.128	1.046	-1.282	1.501	1.886	1.618	3.301	13.588	5.572	3.041	4.542	2.779	6.566	7.875	4.440
	CDK1	-1.179	-2.899	-1.704	1.103	-1.130	-1.661	1.200	1.302	1.073	-1.214	-1.189	-1.063	1.071	-1.314	-3.759
Apoptosis	BAX	1.298	1.283	1.757	1.446	2.267	2.253	2.158	2.530	2.917	2.640	2.304	2.652	4.272	3.440	4.316
	BCL-2	1.123	-1.270	-1.426	-1.017	1.048	-1.398	-1.022	1.034	-1.120	-1.462	-1.454	-1.279	-1.117	-1.409	-1.881
	CAS3	1.182	-1.081	-1.171	-1.123	-1.391	-3.373	-1.152	-1.496	-1.972	-1.582	-1.439	-2.090	-1.054	-1.243	-2.237
	CAS9	1.228	1.012	-1.173	1.005	1.013	-1.848	-1.034	-1.162	-1.278	-1.384	-1.292	-1.021	1.091	1.048	1.176
	FAS	2.686	5.347	5.266	3.488	5.770	3.204	3.515	5.220	5.874	2.507	3.909	5.240	3.846	4.644	2.159
NHEJ	XRCC6	1.252	1.183	-1.200	-1.253	-1.515	-3.205	-1.131	-1.435	-1.634	-1.610	-2.024	-1.745	-1.089	-1.890	-3.086
	XRCC4	1.138	1.046	-1.181	-1.181	-1.245	-2.079	1.049	-1.155	-1.493	-1.048	-1.466	-1.404	-1.130	-1.748	-2.151
	XRCC5	1.115	-1.218	-1.081	-1.385	-1.508	-2.519	-1.076	-1.456	-1.560	-1.464	-1.675	-1.441	-1.035	-1.435	-1.302
	NHEJ1	1.134	-1.106	-1.292	-1.284	-1.414	-2.778	-1.071	-1.300	-1.377	-1.094	-1.333	-1.357	1.057	-1.486	-1.898
	LIG4	1.316	1.109	-1.408	-1.449	-1.464	-2.037	-1.114	1.122	-1.030	1.021	-1.332	1.209	1.734	1.484	1.172
HR	RAD51	-1.166	-1.290	-1.142	1.078	1.089	1.053	1.051	-1.065	-1.018	1.439	-1.499	-2.123	1.069	-1.004	-1.002
	BRCA1	-1.124	-1.068	-1.086	1.022	1.144	-1.401	-1.120	-1.311	-1.074	1.352	-1.502	-2.294	-1.003	1.014	1.220
	BRCA2	-1.209	-1.350	-1.203	1.036	-1.044	-1.024	-1.125	-1.088	1.189	1.186	-1.323	-2.110	1.045	-1.073	1.237
Involved in DDR	ATM	-1.170	-1.433	1.088	-1.319	-1.387	-1.626	-1.795	-1.608	-1.486	-1.727	-1.842	-1.957	-1.449	-1.351	-1.376
	TP53	1.142	1.663	-1.171	-1.120	-1.082	-2.119	-1.134	-1.351	-1.592	-1.812	-1.626	-1.490	-1.637	-2.208	-3.003
	FANCA	1.095	-1.065	1.032	-1.092	-1.040	-1.055	-1.410	-1.171	-1.092	1.185	-1.949	-3.257	-1.675	-1.379	-1.166

Table S3: Selection of genes involved in DNA damage repair, cell cycle regulation and apoptosis analyzed in cycling CD34⁺ treated with MNU (1mM, 3mM, and 5mM) for 1h. Fold changes in mRNA expression were analyzed using qPCR and calculated with the 2-ΔΔCT method relative to untreated CD34⁺ cells and normalized to the reference gene RPL13A. The value 1 corresponds to a basic expression as in untreated cells; Values above 2 are considered a significant upregulation (green) while values below -2 are considered a significant downregulation (red) of a gene in treated CD34⁺ cells. Abbreviations: HR, Homologous Repair; MNU, N-methyl-N-nitroso-urea; NHEJ, Non-Homologous End Joining; n.p., not performed.

		MNU d3		MNU d5	
		1mM MNU	3mM MNU	1mM MNU	3mM MNU
Pathways	**Gene**	**Fold Change**			
Direct repair	MGMT	1.033	1.331	1.909	2.868
Cell cycle regulation	CDKN1A	-1,894	1,903	3,540	6,878
	CDKN1B	-1.126	1.601	1.205	3.846
	CCNB1	-1.226	-1.403	-1.353	1.805
	CCND1	-1.249	1.382	-1.612	1.466
Apoptosis	BAX	1.061	2.000	1.336	5.039
	BCL-2	-1.303	-1.216	-1.658	1.715
	CAS3	1.082	1.570	1.629	11.397
	CAS9	-1.354	1.469	n.p.	n.p.
	CAS8	-1.473	-1.165	1.460	1.958
	FAS	-2.490	1.019	1.281	10.027
NHEJ	XRCC6	1.507	3.374	2.730	29.396
	XRCC4	1.356	1.241	2.017	5.186
	NHEJ1	-2.658	-1.414	2.316	15.138
	LIG4	1.716	3.278	-2.351	1.688
HR	RAD51	1.122	1.901	-1.251	2.378
	BRCA2	2.109	3.931	3.815	13.061
Autophagy	BID	1.863	3.014	n.p.	n.p.
	ATG3	1.594	2.110	1.803	8.467
	BECN1	1.130	2.758	n.p.	n.p.
NER	XPC	n.p.	n.p.	1,500	3,810
	XPG	n.p.	n.p.	1.737	4.365
Quiescence	mKi67	n.p.	n.p.	1.521	12.985
	CDK6	n.p.	n.p.	1.431	10.572
Involved in DDR	H2AX	2.348	4.295	1.043	3.493
	TP53	1.144	1.666	3.552	12.585
	APEX1	-3.681	-2.726	2.222	6.354
	XRCC1	n.p.	n.p.	1.554	4.052
	FANCI	n.p.	n.p.	2.897	26.101

Tabelle S4: Selection of genes involved in DNA damage repair, cell cycle regulation and apoptosis analyzed in quiescent CD34⁺ treated with etoposide (1.5µM, and 10µM). Fold changes in mRNA expression were analyzed using qPCR and calculated with the 2-ΔΔCT method relative to untreated CD34⁺ cells and normalized to the reference gene RPL13A. The value 1 corresponds to a basic expression as in untreated cells; Values above 2 are considered a significant upregulation (green) while values below -2 are considered a significant downregulation (red) of a gene in treated CD34⁺ cells. Abbreviations: ETO, Etoposide; HR, Homologous Repair; NHEJ, Non-Homologous End Joining.

		ETO 24h	
		1.5µM ETO	10µM ETO
Pathways	**Gene**	**Fold Change**	
Cell cycle regulation	CDKN1A	6.16	29.19
	CDKN1B	-1.02	-1.49
	CCNB1	-1.22	-2.77
	CCND1	1.18	1.16
Apoptosis	BAX	1.63	1.64
	BCL-2	-1.14	-1.41
	FAS	2.32	3.82
NHEJ	XRCC4	-1.09	-1.36
HR	RAD51	-1.18	-1.27
Involved in DDR	TP53	1.01	-1.14

Table S5: Selection of genes involved in DNA damage repair, cell cycle regulation and apoptosis analyzed in quiescent CD34⁺ treated with MNU (1mM, 3mM, and 5mM) for 1h. Fold changes in mRNA expression were analyzed using qPCR and calculated with the 2-ΔΔCT method relative to untreated CD34⁺ cells and normalized to the reference gene RPL13A. The value 1 corresponds to a basic expression as in untreated cells; Values above 2 are considered a significant upregulation (green) while values below -2 are considered a significant downregulation (red) of a gene in treated CD34⁺ cells. Abbreviations: HR, Homologous Repair; MNU, N-methyl-N-nitroso-urea; NHEJ, Non-Homologous End Joining; n.p., not performed.

		MNU d1		MNU d3	
		1mM MNU	3mM MNU	1mM MNU	3mM MNU
Pathways	**Gene**	**Fold Change**			
Direct repair	MGMT	-1.877	-1.841	-1.170	1.249
Cell cycle regulation	CDKN1A	7.707	6.219	1.142	5.943
	CDKN1B	-1.720	-1.506	-293.575	-265.398
	CCNB1	-2.126	-1.569	-4.108	-4.772
	CCND1	-2.602	-3.058	-1.234	1.500
Apoptosis	BAX	-1.301	-1.034	-886.362	-371.693
	BCL-2	-1.914	-2.004	-1.707	1.789
	CAS3	-2.054	-1.370	-1.136	2.304
	CAS9	-1.351	1.060	1.059	3.759
	CAS8	-1.436	-1.104	-1.350	-1.714
	FAS	1.633	4.628	1.630	3.683
	BID	1.102	1.667	n.p.	n.p.
NHEJ	XRCC6	-1.304	-1.365	-1.363	2.774
	XRCC4	-1.786	-1.951	-307.726	-230.717
	LIG4	-1.217	1.242	1.497	4.897
	NHEJ1	-1.412	-128.783	1.135	1.935
HR	RAD51	-1.337	-1.259	-1.058	1.555
	BRCA1	-4.492	-6.207	1.131	2.377
	BRCA2	-1.265	-1.452	1.064	2.112
Autophagy	ATG3	-1.429	-1.460	-1.312	2.190
	BECN1	-1.220	-1.096	1.033	2.508
Quiescence	mKi67	n.p.	n.p.	1.356	2.882
	CDK6	n.p.	n.p.	1.247	3.462
Involved in DDR	H2AX	-1.996	-2.295	n.p.	n.p.
	TP53	-1.435	-1.406	1.221	1.960
	APEX1	-1.684	-2.218	-1.252	1.665
	FANCA2	-1.140	1.074	n.p.	n.p.

4.3. Impact of Genotoxin-Induced Stress on Cord Blood Hematopoietic Stem Cell Colony Formation Capacity of Quiescent and Cycling HSCs

This chapter presents additional, unpublished data that further supports the findings discussed in Chapter 4.2. Specifically, it highlights the impact of genotoxin-induced stress on the colony formation capacity of cord blood HSCs, both in quiescent and cycling states. These results provide further insight into the genotoxic effects on the differentiation capacity of HSCs and complement the observations made in the previous section.

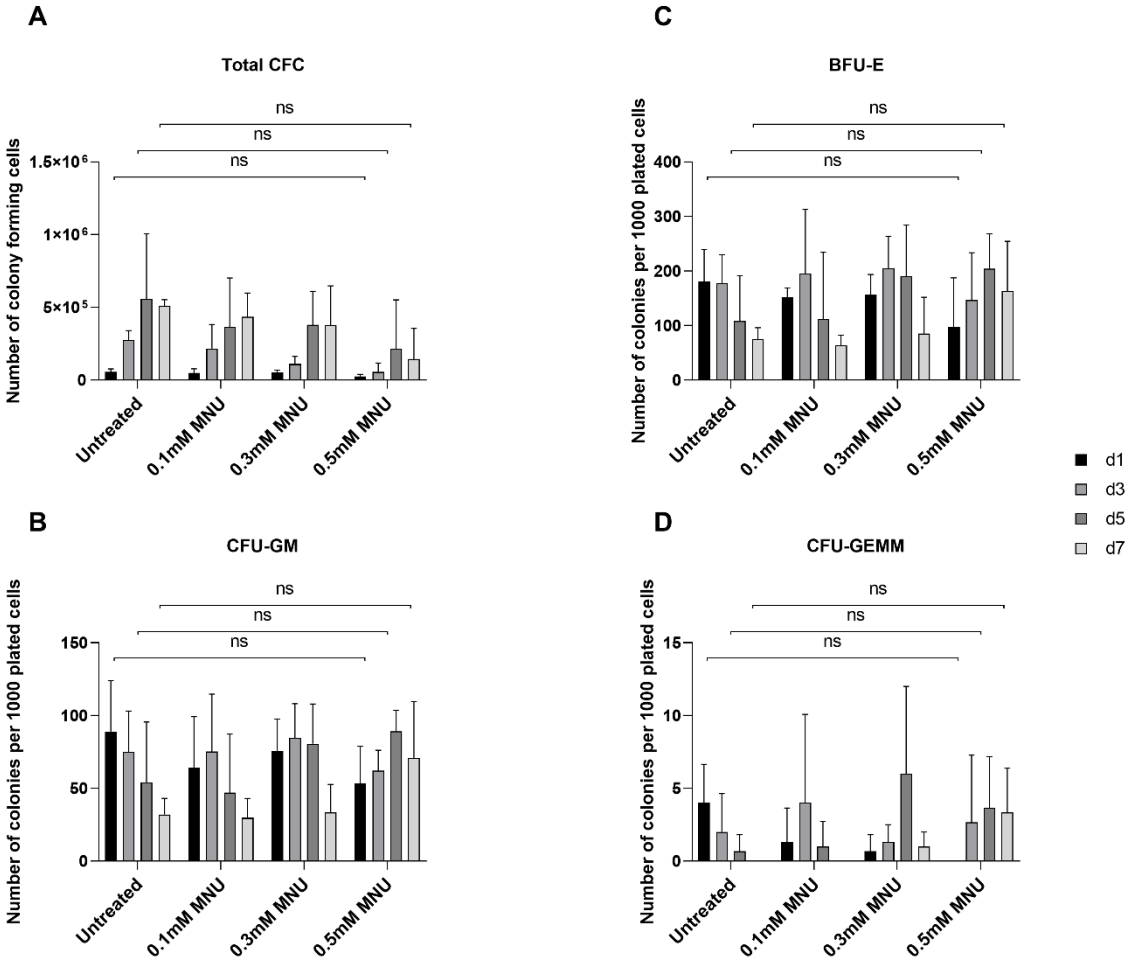

Figure 8: Colony-forming unit (CFU) assay of quiescent CD34⁺ HSCs treated with MNU. Cells were collected on d1, d3, d5 and d7 post-treatment for CFU assay, which was evaluated 14 days after assay start. Total CFC (up left), BFU-E (top right), CFU-GM (bottom left) and CFU-GEMM (bottom right) were counted. Data represent the mean ± standard deviation from three independent experiments, each performed with cells derived from different cord blood donations (n=3). Abbreviations: CFC, colony forming cell; BFU-E, burst-forming unit-erythroid; CFU-GM, colony-forming unit-granulocyte-macrophage; CFU-GEMM, colony-forming unit-granulocyte-erythroid-macrophage-megakaryocyte; d, day; MNU, N-methyl-N-nitrosourea; ns, non-significant.

Figure 8A illustrates that no significant impact on the colony-forming capacity of CD34⁺ HSCs was able to be evaluated on a period of seven days post-treatment on d0. Quiescent CD34⁺ HSCs demonstrated a resilient ability to form colonies under various doses of MNU. This suggests that the hematopoietic stem cells may possess mechanisms that protect against the immediate effects of genotoxic agents, or that the

extent of damage induced by MNU within this period was insufficient to affect the colony-forming ability.

BFU-E colonies arise from erythroid progenitors that represent an early stage of erythrocyte development. Same as the CFC, BFU-E, CFU-GM and CFU-GEMM colonies did not show any significant differences between untreated and MNU-treated samples showing no effect of MNU on the formation of erythrocytes, granulocytes, monocytes and multipotent progenitors (Figure 8B-D).

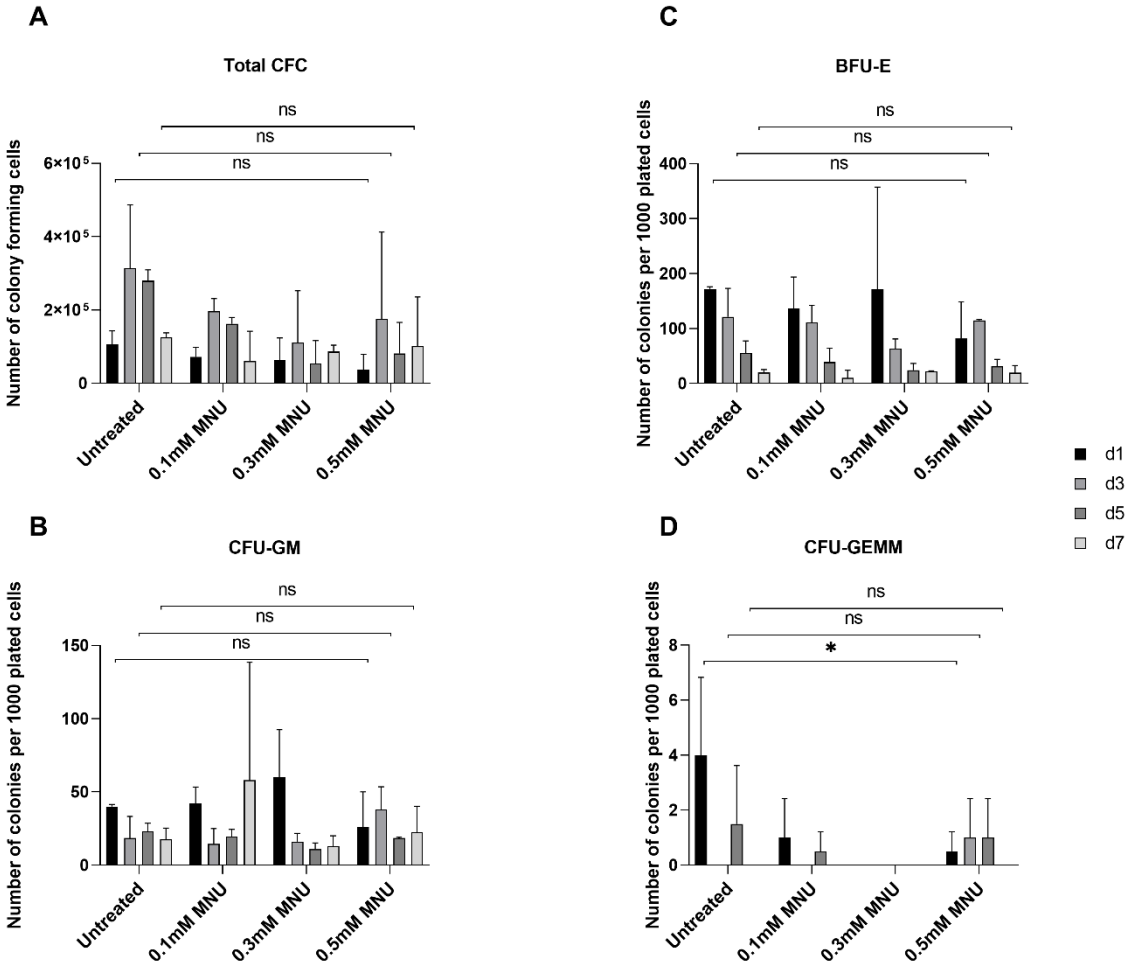

*Figure 9: Colony-forming unit (CFU) assay of cycling CD34⁺ HSCs treated with MNU. Cells were collected on d1, d3, d5 and d7 post-treatment for CFU assay, which was evaluated 14 days after assay start. Total CFC (A), CFU-GM (B), BFU-E (C), and CFU-GEMM (D) were counted. Data represent the mean ± standard deviation from two independent experiments, each performed with cells derived from different cord blood donations (n=2). * denotes p ≤ 0.05. Abbreviations: CFC, colony forming cell; BFU-E, burst-forming unit-erythroid; CFU-GM, colony-forming unit-granulocyte-macrophage; CFU-GEMM, colony-forming unit-granulocyte-erythroid-macrophage-megakaryocyte; d, day; MNU, N-methyl-N-nitrosourea; ns, non-significant.*

As shown on Figure 9, total CFC numbers were not significantly reduced in cells treated with MNU over the course of 7 days post-treatment (Figure 9A). Similarly to MNU-treated quiescent HSCs, the capacity to build BFU-E and CFU-GM colonies was not significantly affected (Figure 9B-C), whereas the CFU-GEMM colonies were significantly reduced in all MNU treated samples on d1 post-treatment (Figure 9D). This trend, however, was not seen on d3 to d7 post-treatment.

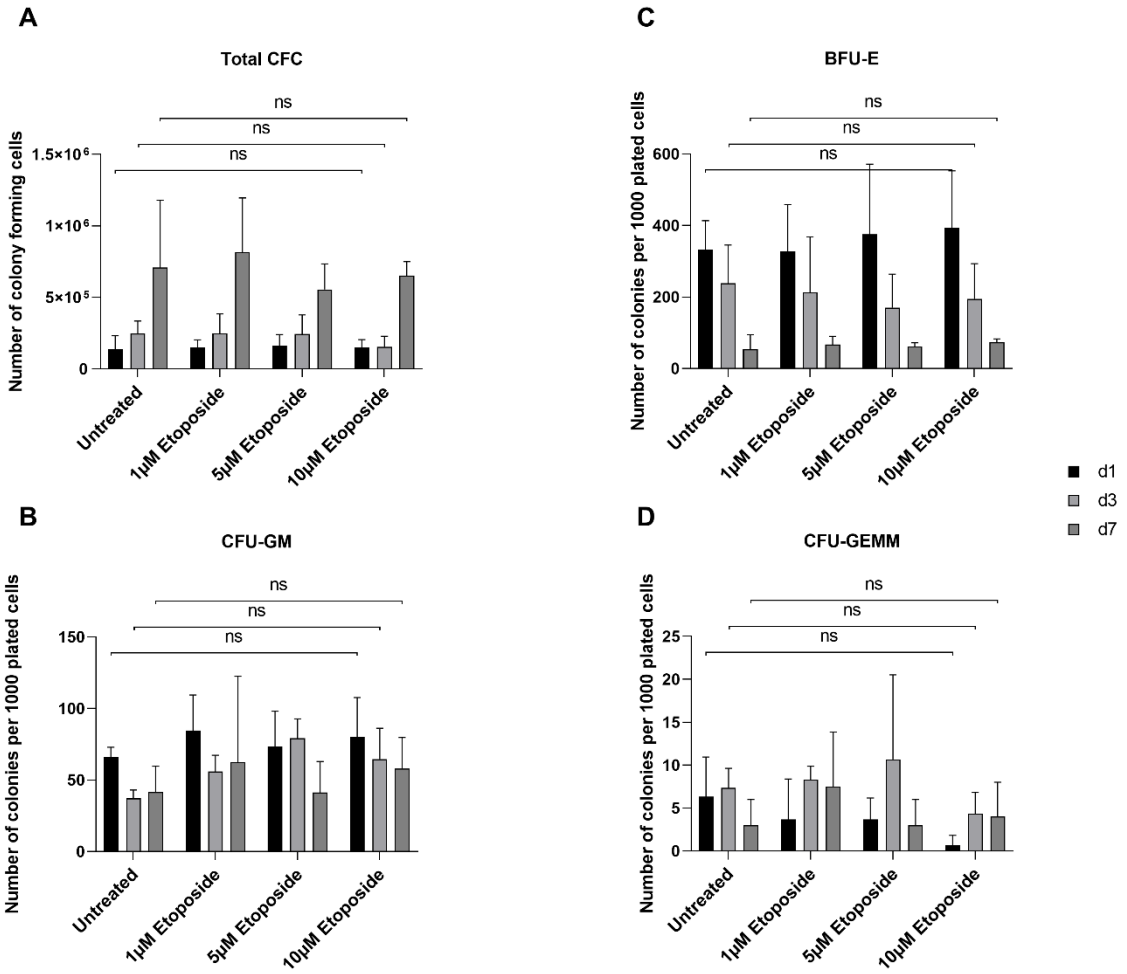

Figure 10: Colony-forming unit (CFU) assay of quiescent CD34⁺ HSCs treated with etoposide. Cells were collected on d1, d3 and d7 post-treatment for CFU assay, which was evaluated 14 days after assay start. Total CFC (A), CFU-GM (B), BFU-E (C), and CFU-GEMM (D) were counted. Data represent the mean ± standard deviation from three independent experiments, each performed with cells derived from different cord blood donations (n=3). Abbreviations: CFC, colony forming cell; BFU-E, burst-forming unit-erythroid; CFU-GM, colony-forming unit-granulocyte-macrophage; CFU-GEMM, colony-forming unit-granulocyte-erythroid-macrophage-megakaryocyte; d, day; ns, non-significant.

Etoposide treatment of CD34⁺ cells directly after their isolation showed no significant effect on their colony-forming capacity over 7 days post-treatment. Total CFC, CFU-GM, BFU-E and CFU-GEMM remained unaffected across all tested conditions and time points, indicating that etoposide does not impair differentiation CD34+ HSCs under the testes genotoxin doses.

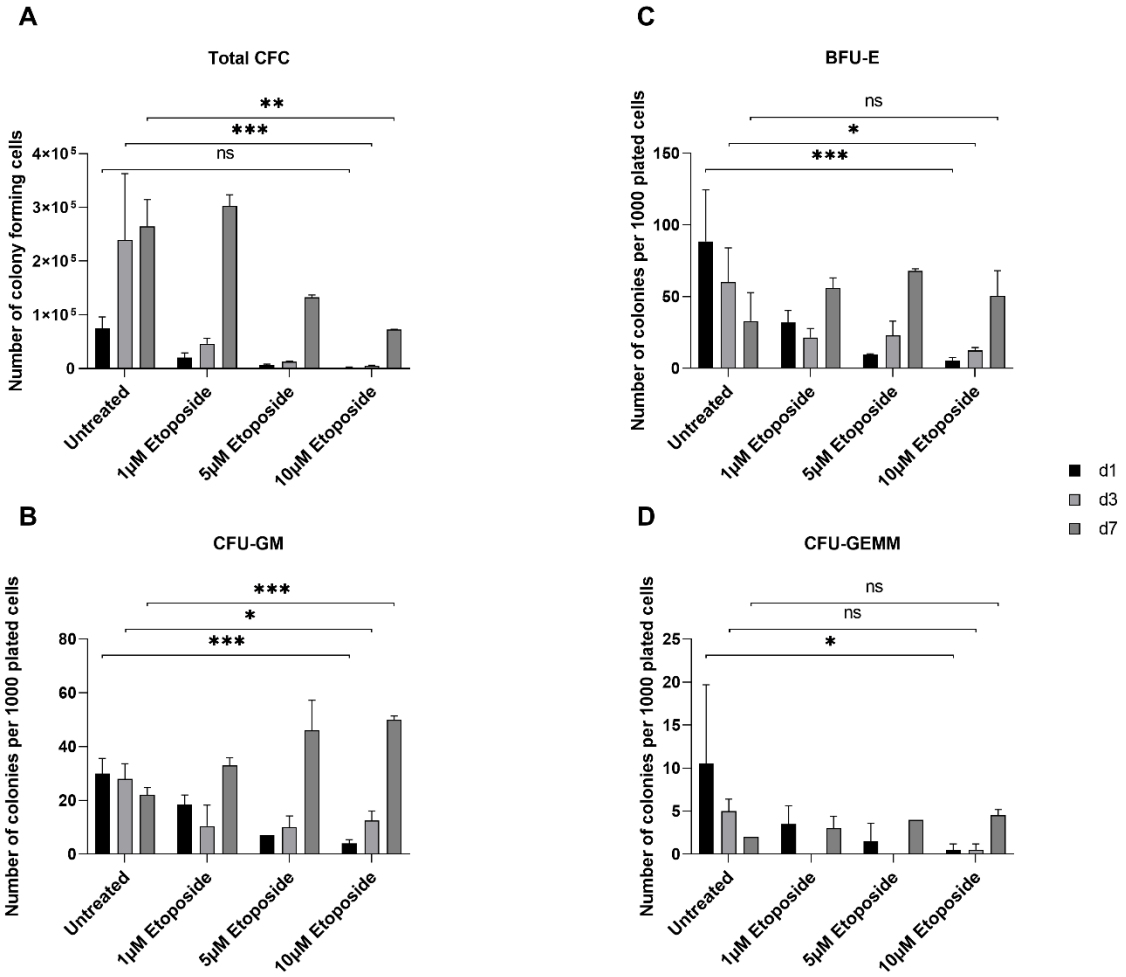

*Figure 11: Colony-forming unit (CFU) assay of cycling CD34⁺ HSCs treated with etoposide. Cells were collected on d1, d3 and d7 post-treatment for CFU assay, which was evaluated 14 days after assay start. Total CFC (A), CFU-GM (B), BFU-E (C), and CFU-GEMM (D) were counted. Data represent the mean ± standard deviation from two independent experiments, each performed with cells derived from different cord blood donations (n=2). * denotes p ≤ 0.05, ** denotes p ≤ 0.01 and *** denotes p ≤ 0.001. Abbreviations: CFC, colony forming cell; BFU-E, burst-forming unit-erythroid; CFU-GM, colony-forming unit-granulocyte-macrophage; CFU-GEMM, colony-forming unit-granulocyte-erythroid-macrophage-megakaryocyte; d, day; ns, non-significant.*

Opposite of the quiescent CD34⁺ HSCs, cycling cells treated with etoposide on d5 were significantly affected by genotoxin treatment. Total CFC significantly decreased with increasing etoposide dose on d3 and d7 post-treatment, whereas no significant decrease was assessed on d1. CFU-GM colonies were significantly reduced upon all treatment conditions and time points. BFU-E colony numbers significantly dropped with increasing etoposide concentrations with a recovery on d7 post-treatment to comparable levels as the untreated cells. The CFU-GEMM colonies showed a slight decrease on d1 post-treatment and showed no significant difference compared to the untreated control on d3 and d7 post-treatment.

4.4. Evaluation of Genotoxic Effects of MNU and Etoposide on the Differentiation Potential of MSCs from Umbilical Cord Blood and Bone Marrow

Authors: Meryem Ouzin, Sebastian Wesselborg, Gerhard Fritz and Gesine Kögler

Published: Cells

Impact Factor: 5.1

Own Work: 80%

Contribution: Meryem Ouzin performed all experiments, wrote, drafted and edited the manuscript, analyzed the data and illustrated the figures.

cells

MDPI

Article

Evaluation of Genotoxic Effects of N-Methyl-N-Nitroso-Urea and Etoposide on the Differentiation Potential of MSCs from Umbilical Cord Blood and Bone Marrow

Meryem Ouzin [1,*], Sebastian Wesselborg [2], Gerhard Fritz [3] and Gesine Kogler [1]

[1] Institute for Transplantation Diagnostics and Cell Therapeutics, University Hospital, Heinrich Heine University Düsseldorf, Moorenstraße 5, 40225 Düsseldorf, Germany; gesine.koegler@med.uni-duesseldorf.de
[2] Institute for Molecular Medicine I, University Hospital, Heinrich Heine University Düsseldorf, Universitätsstraße 1, 40225 Düsseldorf, Germany; sebastian.wesselborg@uni-duesseldorf.de
[3] Institute of Toxicology, University Hospital, Heinrich Heine University Düsseldorf, Universitätsstraße 1, 40225 Düsseldorf, Germany; fritz@uni-duesseldorf.de
* Correspondence: meryem.ouzin@hhu.de

Abstract: The present study investigates the influence of nitrosamines and etoposide on mesenchymal stromal cells (MSCs) in a differentiation state- and biological age-dependent manner. The genotoxic effects of the agents on both neonatal and adult stem cell populations after treatment, before, or during the course of differentiation, and the sensitivity of the different MSC types to different concentrations of MNU or etoposide were assessed. Hereby, the multipotent differentiation capacity of MSCs into osteoblasts, adipocytes, and chondrocytes was analyzed. Our findings reveal that while all cell types exhibit DNA damage upon exposure, neonatal CB-USSCs demonstrate enhanced resistance to genotoxic damage compared with their adult counterparts. Moreover, the osteogenic differentiation of MSCs was more susceptible to genotoxic damage, whereas the adipogenic and chondrogenic differentiation potentials did not show any significant changes upon treatment with genotoxin. Furthermore, we emphasize the cell-specific variability in responses to genotoxic damage and the differences in sensitivity and reaction across different cell types, thus advocating the consideration of these variabilities during drug testing and developmental biological research.

Keywords: mesenchymal stromal cells; osteogenesis; adipogenesis; chondrogenesis; nitrosamines; etoposide

Citation: Ouzin, M.; Wesselborg, S.; Fritz, G.; Kogler, G. Evaluation of Genotoxic Effects of N-Methyl-N-Nitroso-Urea and Etoposide on the Differentiation Potential of MSCs from Umbilical Cord Blood and Bone Marrow. *Cells* **2024**, *13*, 2134. https://doi.org/10.3390/cells13242134

Academic Editor: Alessandro Poggi

Received: 2 December 2024
Revised: 19 December 2024
Accepted: 20 December 2024
Published: 23 December 2024

1. Introduction

Mesenchymal stromal cells (MSCs) are a heterogeneous population that was originally identified in the bone marrow [1,2] but has also been discovered in various other tissues, such as adipose tissue, umbilical cord blood, or placenta, thus offering unique advantages regarding accessibility for clinical applications [3–5]. Due to their low expression of the Major Histocompatibility Complex (MHC) I and lack of the MHC II, MSCs are recognized for their immunomodulatory properties on T-cell alloreactive responses and proliferation but also for their ability to secrete bioactive molecules such as cytokines, chemokines and growth factors that promote tissue repair and regeneration [6]. This versatility makes them a focal point in regenerative medicine and tissue engineering, offering promising approaches for the treatment of a wide range of diseases and injuries.

Beyond these immunomodulatory capacities, MSCs are also known for their multipotent differentiation capacity, which allows them to differentiate into a variety of cell types, including osteoblasts, chondrocytes, and adipocytes. All these properties make them ideal candidates for cell-based therapies aiming for tissue repair or replacement in conditions such as osteoarthritis, cardiovascular diseases, and neurodegenerative disorders. This ability is driven by complex signaling pathways and micro-environmental cues, highlighting

the importance of understanding these mechanisms to harness the full therapeutic potential of MSCs. This knowledge can furthermore be exploited in the field of toxicological risk assessment. The use of MSCs for drug testing represents a significant advancement in pharmacological and toxicological research, offering a reliable and human-relevant model for evaluating drug toxicity. The multilineage differentiation potential of MSCs allows for comprehensive testing across different tissue types, thus providing more accurate predictions of a drug impact, enhances the predictive power of preclinical studies and, moreover, reduces the reliance on animal models, which often fail to reflect human physiology.

MSCs are integral components of the bone marrow niche and thus play a crucial role in supporting hematopoiesis by providing essential signals and a supportive microenvironment for the proliferation and differentiation of hematopoietic stem cells (HSCs). This unique interaction underscores their importance in drug toxicity testing, as they can influence the hematopoietic response to chemical substances. Thus, evaluating drug effects on MSCs is essential for understanding potential toxicities and side effects on the bone marrow and overall hematopoietic function, thereby enhancing the safety and efficacy profiles of new therapeutic agents.

Biological age is a crucial factor in drug testing since it influences how cells and tissues respond to chemical compounds. Cells from younger sources with a lower biological age typically exhibit higher proliferative capacity, robust regenerative properties, and predictable responses to drugs for an accurate assessment of drug efficacy and toxicity [7,8]. Conversely, cells with a higher biological age often have accumulated genetic and epigenetic changes, reduced regenerative capacity, and altered metabolic profiles that can affect drug metabolism and efficacy [9]. Incorporating the concept of biological age into drug testing helps to ensure that the models used closely mimic the intended patient populations, thus enhancing the relevance and reliability of preclinical studies. This approach can lead to better predictions of clinical outcomes, reduce the incidence of adverse effects, and improve the overall success rate of new drug development. The ability to isolate MSCs from various sources provides a unique opportunity to analyze age-dependent reactions to toxins. This versatility allows the comparison of MSC responses across different age groups, from neonatal to adult, thereby gaining insights into how age-related cellular and molecular changes influence responses to drugs. This is also crucial for developing age-specific drug safety profiles, optimizing therapeutic strategies, and minimizing adverse effects in different patient populations, ultimately leading to more personalized and effective treatments.

The biological age difference between cord blood MSCs (CB-MSCs), cord blood unrestricted somatic stem cells (CB-USSCs), and bone marrow MSCs (BM-MSCs) is a critical factor influencing their therapeutic potential and functionality. MSCs derived from cord blood (CB-MSCs and CB-USSCs) are derived from a perinatal source, making them biologically younger and more primitive compared with BM-MSCs, which are obtained from adult tissues. This is associated with a higher proliferative capacity, greater telomerase activity, and enhanced differentiation potential [10]. Additionally, CB-USSCs and -MSCs exhibit lower immunogenicity and a greater ability to modulate immune responses, which can be advantageous in clinical applications. In contrast, adult BM-MSCs, although well studied and widely used, may have reduced regenerative abilities due to the aging process and accumulation of environmental stress-induced damage. Understanding these differences is crucial for optimizing the selection of MSC sources for specific therapeutic and risk assessment purposes.

Nitrosamines are a class of chemical compounds typically formed through the reaction of nitrites and secondary amines, often found in processed meats, tobacco smoke, and certain industrial settings. These compounds are potent carcinogens, known for their ability to induce DNA damage through alkylation, leading to mutations that can initiate cancer development [11,12]. Upon metabolic activation, nitrosamines produce reactive intermediates that form adducts with DNA, resulting in mutagenesis and potentially triggering a cascade of cellular malfunctions. Chronic exposure to nitrosamines has been

linked to various cancers, including those of the liver, esophagus, and stomach, highlighting the importance of monitoring and limiting exposure to these toxic substances to mitigate their health risks [13–15].

Etoposide is a chemotherapeutic agent commonly used to treat various cancers, including testicular cancer, lung cancer, and lymphoma. It functions primarily by inhibiting the enzyme topoisomerase II, which is crucial for DNA replication and transcription. By stabilizing the DNA-topoisomerase II complex, etoposide induces DNA double-strand breaks (DSBs) and prevents their re-ligation, leading to DSB accumulation. This disruption in DNA integrity triggers cell cycle arrest and apoptosis in rapidly dividing cancer cells [16]. However, the toxic effects of etoposide also extend to normal, healthy cells, particularly those with high proliferation rates, such as bone marrow cells, leading to side effects like myelosuppression, increased risk of secondary hematological malignancies, and other systemic toxicities [17,18]. The ability of etoposide to cause DNA damage underpins its effectiveness as a cancer treatment but also necessitates careful management to mitigate adverse effects on healthy tissue.

Drug and chemical testing on both target cancer cells and their surrounding non-cancer cells is crucial to comprehensively assess the safety and efficacy of new therapies. While specifically targeting diseased cells is essential for therapeutic efficacy, the impact on neighboring healthy cells must also be evaluated to predict potential side effects and systemic toxicity. Understanding how chemicals affect the microenvironment, including supportive stromal cells, immune cells, and endothelial cells, helps to identify unintended harmful effects that could compromise patient health. This holistic approach ensures that treatments are not only effective against the intended targets but also safe for the overall cellular milieu, leading to more reliable and effective therapeutic strategies with minimized adverse effects. Furthermore, this study emphasized the need to evaluate not only direct cytotoxicity on healthy tissues but also the influence of genotoxins both on the differentiation capacity of tissue stem cells and on the responses to genotoxic damage at different stages of cellular development. By conducting analyses at various time points following the induction of differentiation, we sought to evaluate the effects of genotoxin treatment on the initiation and progression of MSC differentiation. Additionally, this approach allows comparing the susceptibility of undifferentiated with differentiated MSCs. This dual focus provides insights into the potential risks posed by genotoxins in terms of regenerative processes and mature tissue functionality.

2. Materials and Methods

2.1. Generation and Expansion of CB-MSCs and CB-USSCs

Cord blood was collected from umbilical cord vein with informed consent of the mother. Briefly, mononuclear cells (MNC) were obtained by Ficoll® (Biochrom, Berlin, Germany, density 1.077 g/cm^3) gradient separation following lysis of RBCs by ammonium chloride. A total of 5–7 × 10^6 CB-MNC/mL was cultured in low-glucose Dulbecco's modified Eagle's medium (DMEM) (Lonza, Basel, Switzerland) with 30% fetal calf serum (FCS) (Perbio, Bonn, Germany), 10^{-7} M dexamethasone (Sigma-Aldrich, St-Louis, MO, USA), and penicillin/streptomycin (Lonza) until detection of adherent growing colonies. Cells were expanded without dexamethasone in a closed system applying cell stacks (Corning, New York, NY, USA), incubated at 37 °C in 5% CO_2 in a humidified atmosphere. After reaching 80% confluency, cells were detached with 0.25% trypsin (Lonza) and re-plated 1:3. CB-USSCs were distinguished from CB-MSCs by analysis of their HOX gene expression pattern by PCR [19]. CB-USSCs lack most HOX gene clusters. The used CB-MSC and CB-USSC cell lines are listed in Table S1.

2.2. Generation of BM-MSCs

Bone marrow from healthy adult donors was directly plated for the generation of MSCs in DMEM low glucose with 30% FCS and PS until adherent colonies appeared. Cells were expanded without dexamethasone in a closed system applying cell stacks (Corning),

incubated at 37 °C in 5% CO_2 in a humidified atmosphere. After reaching 80% confluency, cells were detached with 0.25% trypsin (Lonza) and re-plated 1:3. The used BM-MSC cell lines are listed in Table S1.

2.3. Generation and Expansion of iPSCs

Clinical-grade iPSCs were generated from selected cord blood units based on informed re-consenting of the donors as described by Terheyden-Keighley et al. [20].

2.4. MNU Treatment

Prior to treatment of cultivated cells with MNU (MedChemExpress, Monmouth Junction, NJ, USA), cells were washed twice with PBS (Lonza) and incubated for 7 min at 37 °C. After removal of PBS, different concentrations of MNU (stock solution: 1 M in DMSO) were added to the cells. After 1 h treatment, MNU was removed prior to further cultivation or differentiation.

2.5. Etoposide Treatment

Treatment with etoposide (TCI Europe N. V., Zwijndrecht, Belgium) was conducted for 24 h in culture medium. After treatment with different etoposide concentrations (stock solution: 100 µM in DMSO), cells were washed with PBS prior to further cultivation or differentiation.

2.6. Cell Viability Assay

Resazurin staining was used to determine cell viability 4 days after cytotoxic treatment (1 h MNU or 24 h Etoposide). Resazurin is reduced to fluorescent resorufin by metabolically active cells. Cells were cultured in 96-well plates, treated with resazurin solution after 4 days, and incubated for 2–4 h. The fluorescence intensity, which is proportional to the number of living cells, was measured using a fluorescence microplate reader (excitation wavelength: 560 nm; emission wavelength: 590 nm).

2.7. Assessment of MSC Growth

To evaluate the cumulative population doublings (CPD), the following formula was applied: $PD = [\log(n_1/n_0)]/\log_2$ $CPD = \Sigma PD$, where n_1 is the number of harvested cells, and n_0 is the number of plated cells. Cells were treated 1 h with MNU or 24 h with etoposide, and proliferation measurements were carried out for several passages.

2.8. In Vitro Osteogenic Differentiation and Alizarin Staining

In vitro osteogenic differentiation was conducted as described by Liedtke et al. [21]. Uninduced cells were used as a negative control. After culturing for 14 days, the cells were fixed with 4% paraformaldehyde at 4 °C for 20 min. Next, the fixed cells were stained with 40 mM Alizarin Red S (Sigma-Aldrich) for 30 min at room temperature and observed under an inverted microscope.

For quantification of calcium deposition, 800 µL 10% (*v*/*v*) acetic acid was added to the cells, incubated at room temperature for 30 min with shaking until scaffolds detached, and collected. After vortexing for 30 s, the samples were heated to exactly 85 °C for 10 min, transferred to ice for 5 min, and centrifuged at 345× *g* for 15 min. The supernatant was removed into a collecting tube, and 200 µL of 10% (*v*/*v*) ammonium hydroxide was added to neutralize the acid. OD was measured in triplicates at 405 nm on a 96-well plate.

2.9. In Vitro Adipogenic Differentiation and Oil Red O Staining

In vitro adipogenic differentiation was conducted as described by Liedtke et al. [21]. Uninduced MSCs were used as a negative control. The cells were maintained for 21 days and then fixed with 37% formaldehyde at room temperature for 10 min. Finally, the cells were examined under an inverted microscope after staining with 0.3% Oil Red O (Sigma-Aldrich) in 60% isopropanol for 20 min.

For quantification, Oil Red O was extracted by adding 500 µL isopropanol. OD was measured in triplicated at 500 nm on a 96-well-plate.

2.10. In Vitro Chondrogenic Differentiation and Safranin O Staining

In vitro adipogenic differentiation was conducted as described by Liedtke et al. [21]. The spheroidal chondrogenic pellets were embedded in Tissue Freezing Medium (Leica, Wetzlar, Germany) and frozen at −80 °C before cutting them into sections of 6 µm using a cryotome (Leica). The areas and diameters of the pellets were measured on days 7, 14, and 21 of differentiation using AVISO CellCelector analySIS image software (Version 2.7). For each time point, a minimum of n = 7 pellets were measured, and the arithmetic mean and standard deviation (SD) were calculated.

2.11. Total RNA Extraction and Reverse Transcription

Total RNA was extracted from the cell pellets in a 30 µL volume applying the RNeasy Kit (Qiagen, Hilden, Germany) according to the manufacturer's instructions, including the optional 15 min DNase digest. RNA from differentiated cells was isolated using the TRI Reagent® RNA Isolation reagent (Sigma-Aldrich) following a standard protocol of a phenol–chloroform extraction. Determination of RNA concentrations and purity was carried out using a Nanodrop device (NanoDropTechnologies, Wilmington, NC, USA). Reverse transcription was applied using the first-strand cDNA synthesis kit (Invitrogen, Waltham, MA, USA) and oligo(dT)$_{20}$ primer (Thermo Fisher Scientific, Waltham, MA, USA) following the manufacturer's instructions. A total of 1 µg of total RNA was converted into first-strand cDNA in a 20 µL reaction.

2.12. Quantitative PCR Analysis (RT-qPCR)

RT-qPCR analysis was carried out with intron-spanning primers specific to each gene (Thermo Fisher Scientific). The respective primer sequences are given in Table S2. RPL13a was used as a reference gene. A total of 50 ng of cDNA was applied for RT-qPCR in a total volume of 25 µL containing Sybr Green PCR Mastermix (Thermo Fisher Scientific), 0.2 µM of primer (forward + reverse), and distilled water (10 min/95 °C–15 s/95 °C–1 min/60 °C for 40 cycles).

To analyze the comparative CT experiments, Step One Software v.1.5.1 was used. Relative changes in gene expression were calculated by applying the comparative ΔΔCT method. Differential gene expression was calculated by the formula $2^{-\Delta\Delta CT}$ normalized to untreated cells. Fold changes < 1 were transformed by the formula $-1/2^{-\Delta\Delta CT}$ in the case of downregulated genes and plotted together with positive fold changes and upregulated genes, respectively.

2.13. Alkaline Comet Assay

A total of 1–2 × 10^6 cells were washed with PBS, pelleted, and stored on ice or at −20 °C. The cell number used for the assay is fixed upon all samples to be compared. A total of 10 µL of the cell suspension was added to 120 µL LMP-Agarose (37 °C), placed on an object slide, and covered with a coverslip, which was then cooled for 5 min at 4 °C. Next, the coverslip was carefully laterally removed and incubated for 1 h in precooled lysis buffer (2.5 M NaCl, 100 mM EDTA, 10 mM Tris, 1% lauroylsarcosine, Triton X-100, DMSO) at 4 °C. The slides were removed from the lysis buffer, allowed to drain, and placed into an electrophoresis chamber before overlayering (2–3 mm) with precooled electrophoresis buffer. After an incubation step of 25 min for alkaline denaturation of DNA at 4 °C, electrophoresis was carried out (25 min, 25 V, and 300 mA) on ice. Subsequently, the slides were removed from the chamber, allowed to drain, and three times overlayered with neutralization buffer (400 mM Tris) for 5 min each. Next, the slides were immersed in ddH_2O, followed by 5 min incubation in 80–100% ethanol. Next, the slides were diagonally tilted and dried overnight. For imaging, 50 µL PI solution was added onto the slide and covered with a coverslip. A minimum of 50 comets per condition were counted.

2.14. Statistical Analysis

Statistical analysis was performed using one-way analysis of variance (ANOVA) to evaluate the differences between groups in response to nitrosamines and etoposide exposure. Quantitative data are presented as means ± SD. Differences were considered significant at $p \leq 0.05$. * denotes $p \leq 0.05$, ** denotes $p \leq 0.01$, *** denotes $p \leq 0.001$, and **** denotes $p \leq 0.0001$.

3. Results

3.1. Determination of Sublethal Treatment Doses of MNU and Etoposide

Based on the resazurin reduction assay, doses ranging from 1 to 5 mM (for MNU treatment) and 1 to 10 µM (for etoposide treatment) for CB-USSC, CB-MSC, and BM-MSC cell lines were used for further experiments (Figure 1). IPSCs showed a higher sensitivity to both genotoxic agents compared with MSCs, with an IC_{50} of 220 µM for MNU and 14.9 nM for etoposide. When compared with neonatal MSC cell lines, iPSCs showed a lower expression of DNA damage repair (DDR) genes and DDR-related factors (Figure S1). This comes in accordance with their higher vulnerability to genotoxin-induced damage.

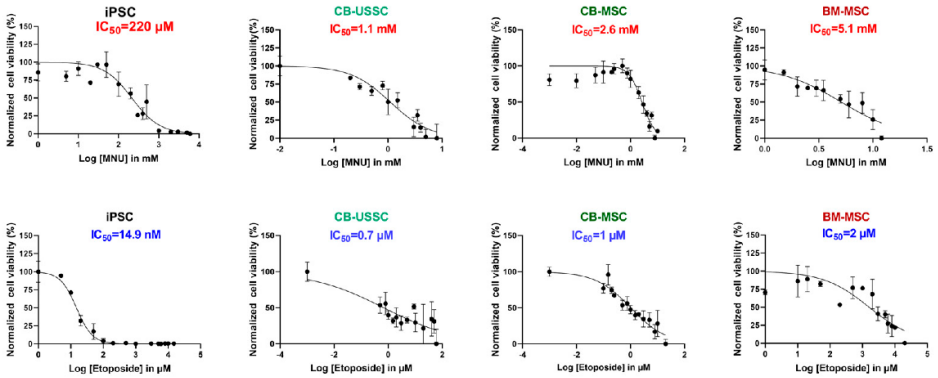

Figure 1. Cell viability and corresponding IC_{50} values after MNU or etoposide treatment measured by resazurin reduction assay. Representative data from an MSC from each source and an iPSC cell line is shown (Mean ± SD from N = 2, n = 3). Abbreviations: CB, cord blood; BM, bone marrow; iPSC, induced pluripotent stem cell; MNU, N-methyl-N-nitroso-urea; USSC; unrestricted somatic stem cells.

3.2. Effects of DNA Damage Resulting from MNU or Etoposide Treatment on MSC Morphology and Proliferation Kinetics

MSCs from all sources showed an impaired morphology after treatment with 5 mM MNU or 10 µM etoposide (Figure 2A). The untreated cells have a more elongated and organized morphology, whereas the treated cells are less compact, indicating the effect of the genotoxin treatment on cell proliferation already 72 h after treatment independently of the biological age. Additionally, MNU treatment has a notable decrease in MSC proliferation kinetics, shown by the CPDs traced after treatment and subsequent culture over the course of 20 to 30 days (Figure 2B). CB-USSCs treated with 3 mM and 5 mM MNU only reached a CPD of 2.9 and −3.3, respectively, after 20 days of cultivation. Expansion after 20 days was not possible due to too low cell numbers. CB-MSCs treated with 3 mM MNU reached a CPD of −5.16 after 28 days of culture, whereas treatment of BM-MSCs with 5 mM MNU showed a CPD of −3.18 already after 20 days of cultivation. Treatment with low etoposide concentrations led to a senescent state in CB-USSC and -MSC. Again, adult BM-MSCs show a highly impaired proliferation compared with neonatal MSCs similar to MNU treatment. Treatment of neonatal cells with 10 µM etoposide led to negative CPD values already after the first passaging. Comet assay analysis revealed high amounts of DSBs 24 h after MNU treatment and 48 h after etoposide treatment, especially in CB-USSCs and CB-MSCs (Figure 2C).

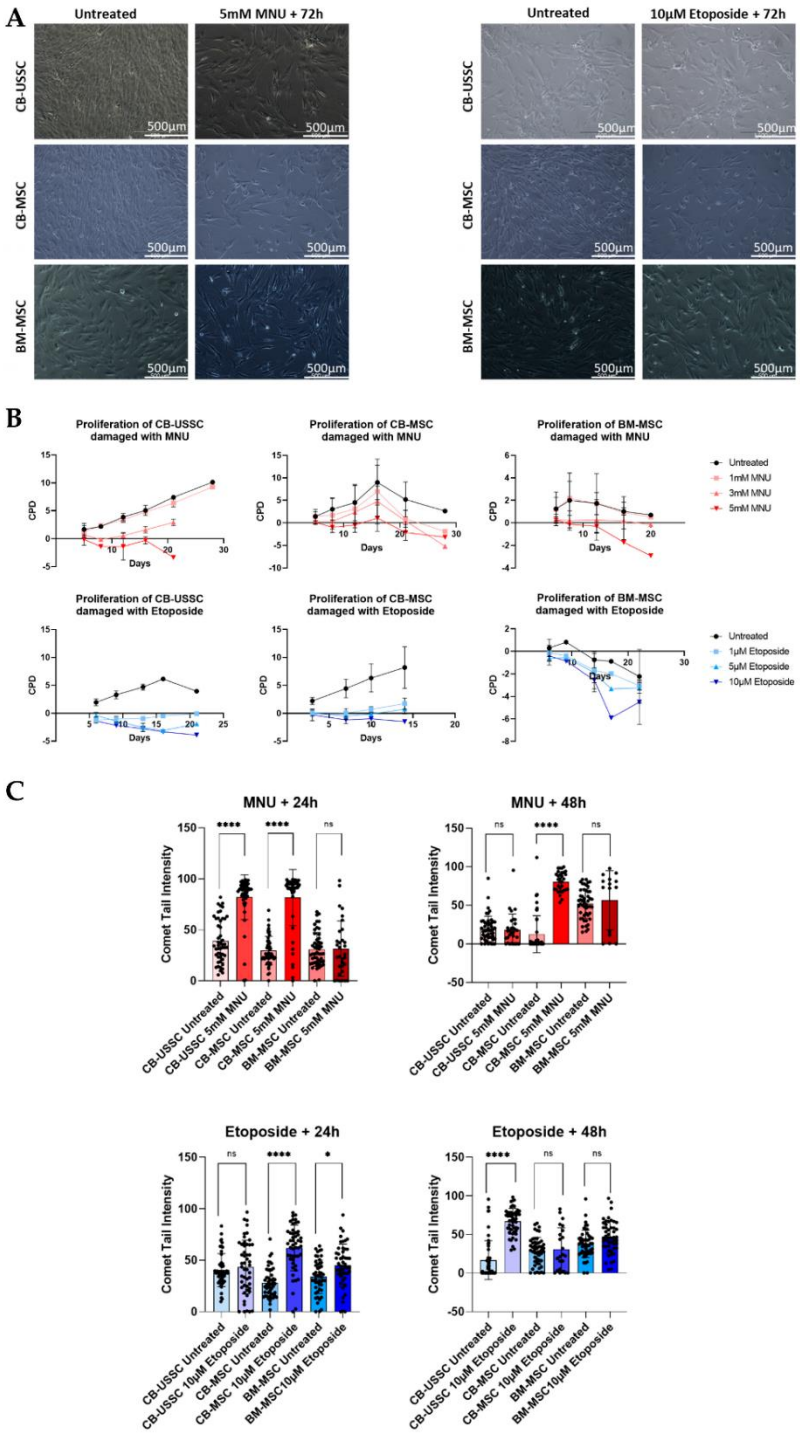

Figure 2. (**A**) Morphological changes in MSCs from different sources 72 h after treatment with 5 mM MNU for 1 h or 10 µM etoposide for 24 h in comparison with the untreated cells. Morphology was representatively analyzed 72 h after 5 mM MNU or 10 µM etoposide treatment. Scale bars = 500 µm. (**B**) Dose-dependent impact of genotoxic stress induced by MNU or etoposide on proliferation kinetics of CB-USSC, CB-MSC, and BM-MSC. To determine long-term growth kinetics, cells were exposed to different doses of MNU (untreated, 1 mM, 3 mM, and 5 mM) or etoposide (untreated, 1 µM, 5 µM, 10 µM), and cell numbers were counted after each passage. CPDs are shown (Mean ± SD from N = 3). (**C**) Analysis of DNA damage in MSCs after MNU or etoposide treatment by alkaline comet assay.

For each condition, the intensity of 50 comets was assessed. CB-USSC2, CB-USSC3, CB-USSC4, CB-MSC1, CB-MSC2, CB-MSC3, CB-MSC4, BM-MSC2, BM-MSC3. Quantitative data are presented as means ± SD. * denotes $p \leq 0.05$ and **** denotes $p \leq 0.0001$. Abbreviations: BM, bone marrow; CB, cord blood; CPD, cumulative population doublings; MNU, N-methyl-N-nitroso-urea; ns, no significance; USSC; unrestricted somatic stem cells.

3.3. Effects of DNA Damage on the Multilineage Differentiation Potential of MSCs

3.3.1. Effects of MNU Treatment on Day 0

- *Osteogenic Differentiation*

In order to determine the effect of MNU treatment on the osteogenic differentiation potential of MSCs, cells were damaged at d0 before osteogenesis induction and subsequent culture until the final readout on d14. Hereby, CB-USSC, CB-MSC, and BM-MSC were compared. The calcification level, which is an indicator of the osteogenic capacity, was assessed by Alizarin staining on d14.

MSCs from all sources showed a decreased osteogenic differentiation potential after treatment with MNU on d0 before induction of differentiation (Figure 3). A more than 2-fold decrease in calcification was traced by Alizarin staining after treatment with 5 mM MNU before induction of osteogenic differentiation. Expression levels of osteogenic genes were analyzed at d7 and d14 after induction of osteogenic differentiation. Runt-related transcription factor 2 (RUNX2), which is considered the master regulator of osteogenic differentiation and the stimulator of Osterix (OSX) expression [22], did not show any significant downregulation in the treated samples on both d7 and 14, whereas OSX levels at d14 were downregulated after treatment with high MNU doses in both CB-USSCs and CB-MSCs to reach levels comparable to the uninduced negative control (Figure S2). BM-MSCs first showed an upregulation of OSX levels after treatment with 1 mM or 3 mM MNU and a downregulation in the case of treatment with 5 mM MNU.

- *Adipogenic Differentiation*

The low amount of characteristic lipid droplets formed during the adipogenic formation of BM–MSCs may be related to the possibly high passage number used for adipogenic differentiation. In contrast to osteogenic differentiation, MNU treatment on d0 had no effect on adipogenic differentiation of CB- and BM-MSCs (Figure 4). CB-USSCs were not assessed since they lack the ability to differentiate into adipocytes [23].

Late adipogenic genes CCAAT/enhancer-binding-proteins (CEBPα and CEBPβ), which play a role in terminal adipocyte differentiation and maturation, showed a dose-dependent increase in MNU-treated cells, whereas the peroxisome proliferator-activated receptor γ (PPARγ), which is considered as the key regulator of adipogenic differentiation, was not significantly dysregulated in treated samples (Figure S3).

- *Chondrogenic Differentiation*

The effects of 3 mM MNU treatment on the chondrogenic differentiation, in particular, pellet area and pellet diameter of CB-USSC, CB-MSC, and BM-MSC over a period of 7, 14, and 21 days, were assessed. In CB-USSCs, both untreated and MNU-treated conditions showed no significant difference in pellet size over the course of differentiation, indicating no impact of MNU on chondrogenic differentiation (Figure 5). Untreated CB-MSCs showed higher condensation levels compared with the MNU-treated samples, which showed no changes in size over the course of differentiation. However, untreated BM-MSCs exhibit a decreased condensation level compared with the CB-derived cell types. This baseline variation complicates the interpretation of MNU-related effects in BM-MSCs.

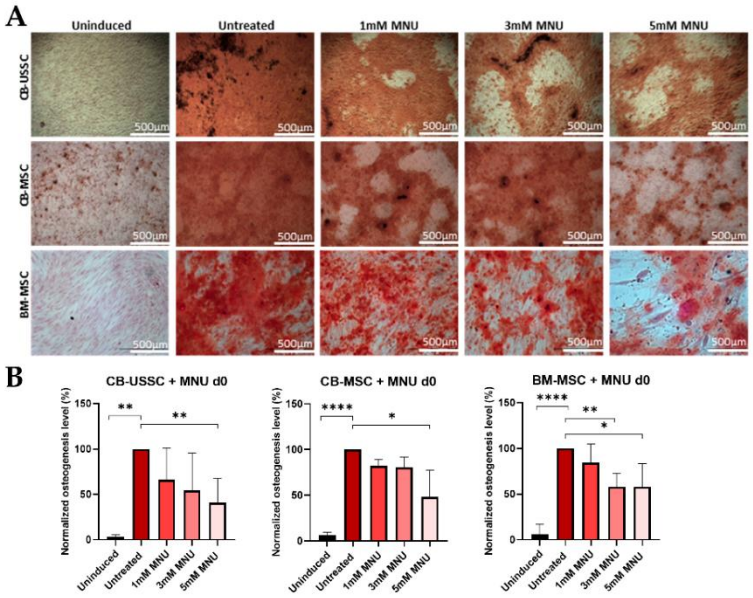

Figure 3. (**A**) Osteogenic differentiation of MSCs after MNU treatment on d0. Representative data (CB-USSC3-CB-MSC3-BM-MSC1) after Alizarin Red S staining on d14 of osteogenic differentiation is shown. Scale bars = 500 µm. (**B**) Osteogenic differentiation of MSCs after 1 h MNU treatment with different doses (untreated, 1 mM, 3 mM, and 5 mM) on d0. Quantitative determination of Alizarin Red S staining on d14 of osteogenic differentiation is shown. Quantitative data are presented as means ± SD of N = 3, n = 3. Differences were considered significant at $p \leq 0.05$. * denotes $p \leq 0.05$, ** denotes $p \leq 0.01$ and **** denotes $p \leq 0.0001$. Abbreviations: BM, bone marrow; CB, cord blood; d, day; MNU, N-methyl-N-nitroso-urea; USSC; unrestricted somatic stem cells.

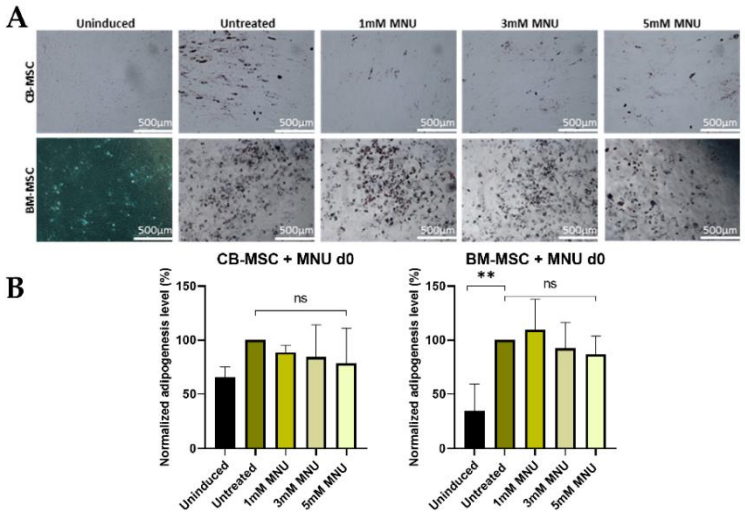

Figure 4. (**A**) Adipogenic differentiation of MSCs after MNU treatment on d0. Representative data (CB-MSC3-BM-MSC4) after Oil Red O staining on d21 of adipogenic differentiation is shown. The induced samples successfully underwent adipogenesis, while the uninduced sample was devoid of characteristic lipid droplet formation after 21 days of differentiation. Scale bars = 500 µm. (**B**) Adipogenic differentiation of MSCs after 1 h MNU treatment with different doses (untreated, 1 mM, 3 mM, and 5 mM) on d0. Quantitative determination of Oil Red O staining on d21 of adipogenic differentiation is shown. Quantitative data are presented as means ± SD of N = 3, n = 3. Differences were considered significant at $p \leq 0.05$. ** denotes $p \leq 0.01$, and ns denotes non-significant. Abbreviations: BM, bone marrow; CB, cord blood; d; day; MNU, N-methyl-N-nitroso-urea.

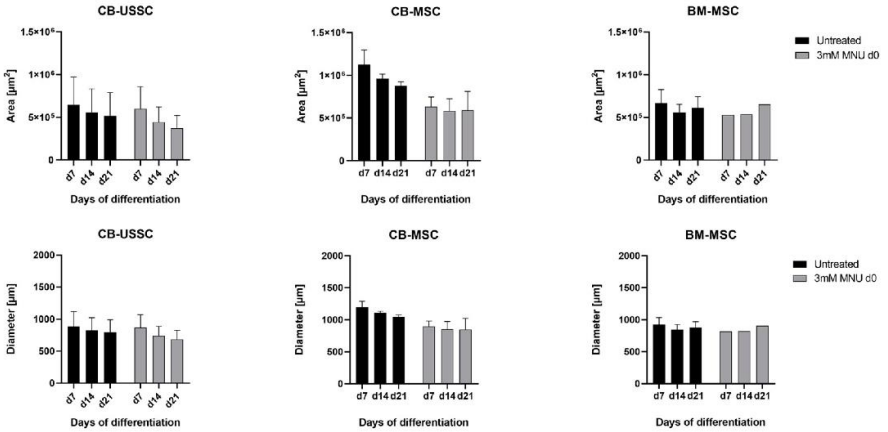

Figure 5. Chondrogenic differentiation of MSCs after 1 h MNU treatment on d0 of differentiation. Areas and diameters of the chondrogenic pellets were measured on d7, d14, and d21 of chondrogenic differentiation (Mean + SD N = 3, n = 3). Abbreviations: BM, bone marrow; CB, cord blood; d; day; MNU, N-methyl-N-nitroso-urea; USSC; unrestricted somatic stem cells.

3.3.2. Effects of Etoposide Treatment on Day 0

- *Osteogenic Differentiation*

Similarly to MNU treatment on d0, etoposide treatment on d0 led to an impaired osteogenic differentiation potential of CB-USSCs and BM-MSCs but had no significant impact on the osteogenic differentiation potential of CB-MSCs (Figure 6).

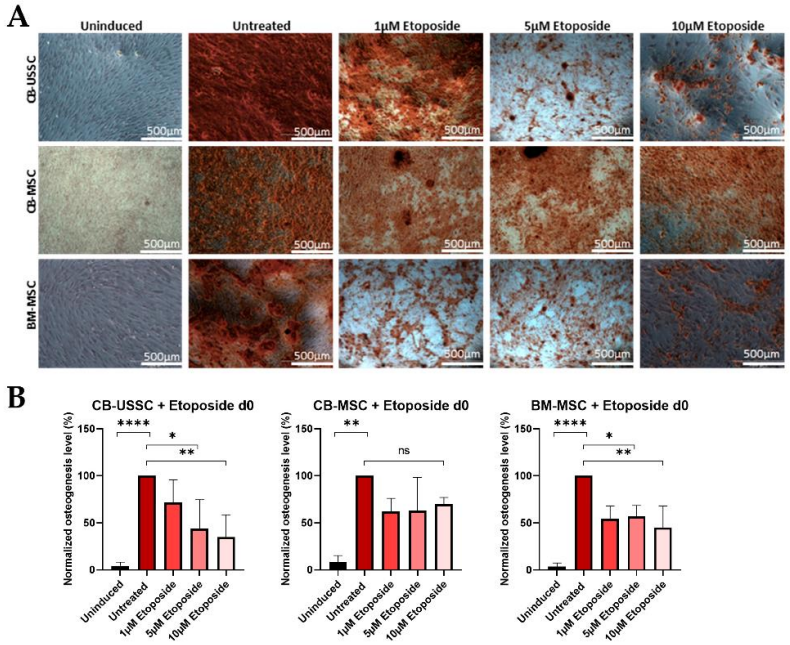

Figure 6. (**A**) Osteogenic differentiation of MSCs after 24 h etoposide treatment on d0. Representative data (CB-USSC4-CB-MSC2- BM-MSC1) after Alizarin Red S staining on d14 of osteogenic differentiation is shown. Scale bars = 500 µm. (**B**) Osteogenic differentiation of MSCs after 24 h etoposide treatment with different doses (untreated, 1 µM, 5 µM, and 10 µM) on d0. Quantitative determination of Alizarin Red S staining on d14 of osteogenic differentiation is shown. Quantitative data are presented as means ± SD of N = 3, n = 3. Differences were considered significant at $p \leq 0.05$. * denotes $p \leq 0.05$, ** denotes $p \leq 0.01$, **** denotes $p \leq 0.0001$ and ns denotes non-significant. Abbreviations: BM, bone marrow; CB, cord blood; USSC, unrestricted somatic stem cells.

Etoposide treatment on d0 led to a downregulation of RUNX2 and OSX expression on d14, especially with high genotoxin doses, in contrast to MNU treatment on d0 (Figure S4).

- *Adipogenic Differentiation*

The results indicate that etoposide treatment on d0 has differing effects on the outcome of CB-MSC and BM-MSC adipogenic differentiation. CB-MSCs showed no significant difference in adipogenic potential following MNU treatment, whereas BM-MSCs exhibited a reduced adipogenic potential in response to MNU. Notably, even under untreated conditions, the adipogenic potential of BM-MSCs was inherently lower than that of CB-MSCs, suggesting an intrinsic difference between the two cell types (Figure 7). CB-MSCs show a high upregulation of CEBPα and PPARγ after treatment with 5 µM etoposide on d0 of adipogenic differentiation, whereas BM-MSCs exhibit no significant change in all conditions. CEBPβ levels showed no significant changes under all treatment conditions (Figure S5).

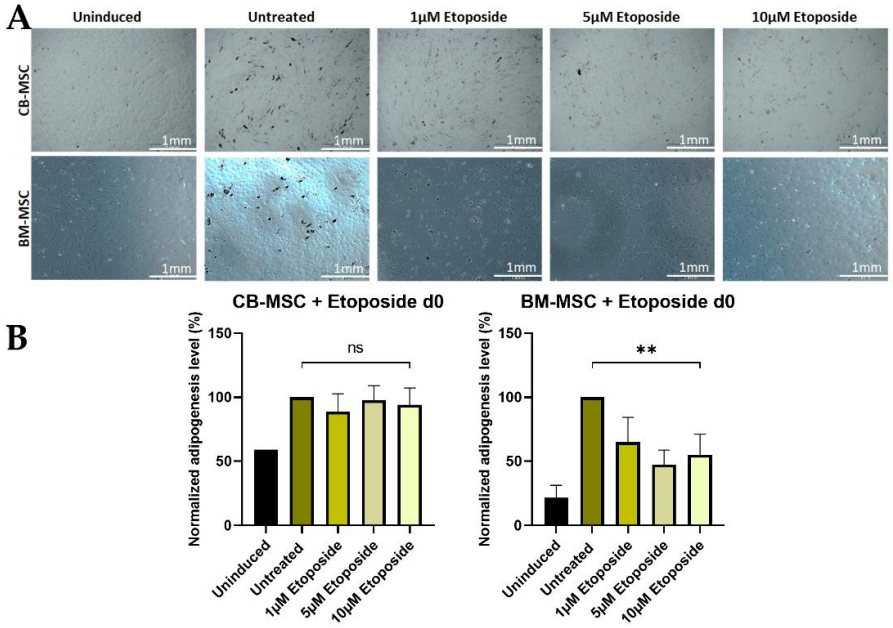

Figure 7. (**A**) Adipogenic differentiation of MSCs after 24 h etoposide treatment on d0. Representative data (CB-MSC2-BM-MSC2) after Oil Red O staining on d21 of adipogenic differentiation is shown. The induced samples successfully underwent adipogenesis, while the uninduced sample was devoid of characteristic lipid droplet formation after 21 days of differentiation. Scale bars = 1 mm. (**B**) Adipogenic differentiation of MSCs after 24 h etoposide treatment with different doses (untreated, 1 µM, 5 µM, and 10 µM) on d0. Quantitative determination of Oil Red O staining on d21 of adipogenic differentiation is shown. Quantitative data are presented as means ± SD of N = 3, n = 3. Differences were considered significant at $p \leq 0.05$. ** denotes $p \leq 0.01$, and ns denotes non-significant. Abbreviations: BM, bone marrow; CB, cord blood.

- *Chondrogenic Differentiation*

A total of 10 µM etoposide treatment on d7 of chondrogenic differentiation did not affect pellet condensation of CB-USSC and BM-MSC but led to an increase in the diameter and area of chondrogenic pellets derived from CB-MSCs (Figure 8).

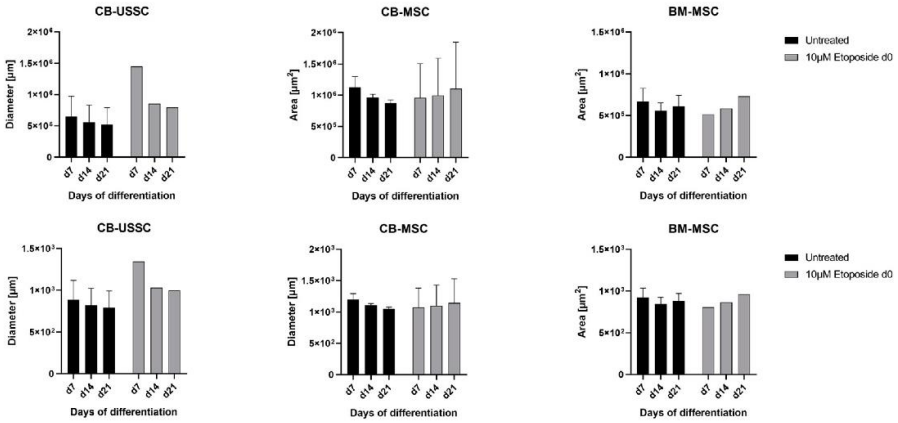

Figure 8. Chondrogenic differentiation of MSCs after 24 h etoposide treatment on d0 of differentiation. Areas and diameters of the chondrogenic pellets were measured on d7, d14, and d21 of chondrogenic differentiation (Mean + SD N = 3, n = 3). Abbreviations: BM, bone marrow; CB, cord blood; d; day; MNU, N-methyl-N-nitroso-urea; USSC; unrestricted somatic stem cells.

3.3.3. Effects of MNU Treatment on Day 7 of Differentiation

- *Osteogenic Differentiation*

MSC treatment with MNU on d7 after induction of osteogenic differentiation had no significant effect on osteogenesis of CB-USSCs and BM-MSCs but led to a significant decrease in calcification levels of CB-MSCs (Figure 9).

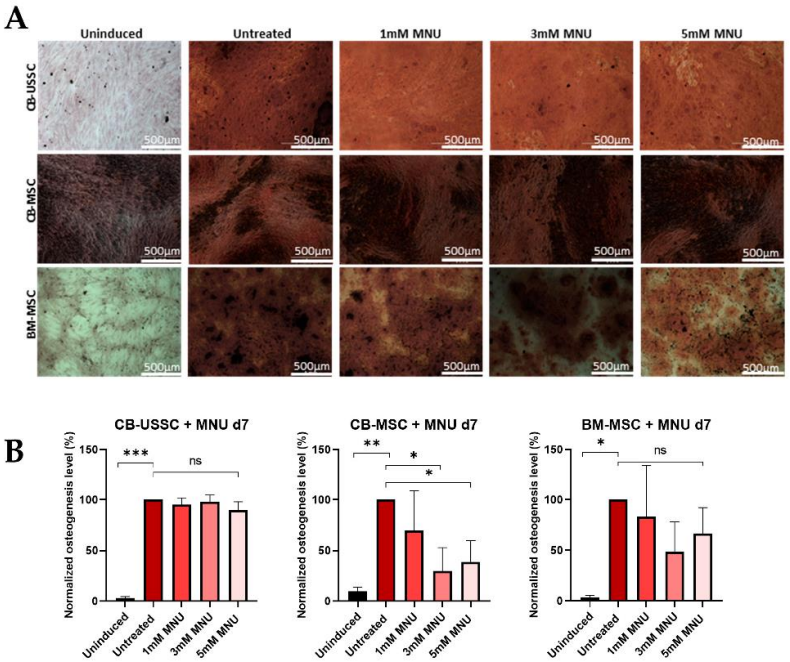

Figure 9. (**A**) Osteogenic differentiation of MSCs after 1 h MNU treatment on d7. Representative data (CB-USSC4-CB-MSC4-BM-MSC4) after Alizarin Red S staining on d14 of osteogenic differentiation is shown. Scale bars = 500 µm. (**B**) Osteogenic differentiation of MSCs after 1 h MNU treatment with different doses (untreated, 1 mM, 3 mM, and 5 mM) on d7. Quantitative determination of Alizarin Red S staining on d14 of osteogenic differentiation is shown. Quantitative data are presented as means ± SD of N = 3, n = 3. Differences were considered significant at $p \leq 0.05$. * denotes $p \leq 0.05$, ** denotes $p \leq 0.01$, *** denotes $p \leq 0.001$ and ns denotes non-significant. Abbreviations: BM, bone marrow; CB, cord blood; d, day; MNU, N-methyl-N-nitroso-urea; USSC, unrestricted somatic stem cells.

RUNX2 levels did not show any significant dose-dependent changes upon MNU treatment on d7. In contrast, OSX was downregulated in a dose-dependent manner in CB-USSCs and CB-MSCs. BM-MSCs showed increasing OSX levels with increasing genotoxin dose (Figure S6).

- *Adipogenic Differentiation*

Treatment of CB-MSCs with MNU on d7 of adipogenic differentiation had no significant effect on their adipogenic potential. BM-MSCs showed a decreased adipogenic potential after MNU treatment of d7 only after treatment with the highest genotoxin dose. Here, again, CB-MSCs showed a reduced adipogenic differentiation potential compared with the adult BM-MSCs (Figure 10). No significant changes regarding CEBPβ and PPARγ gene expression were registered upon MNU treatment (Figure S7).

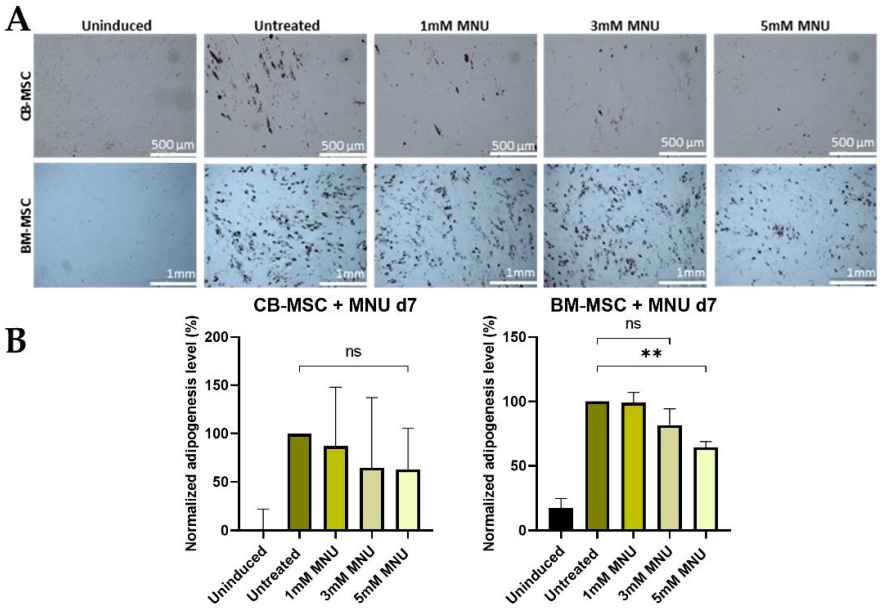

Figure 10. (**A**) Adipogenic differentiation of MSCs after 1 h MNU treatment on d7. Representative data (CB-MSC3-BM-MSC1) after Oil Red O staining on d21 of adipogenic differentiation is shown. The induced samples successfully underwent adipogenesis, while the uninduced sample was devoid of characteristic lipid droplet formation after 21 days of differentiation. Scale bars = 500 µm or 1 mm. (**B**) Adipogenic differentiation of MSCs after 1 h MNU treatment with different doses (untreated, 1 mM, 3 mM, and 5 mM) on d7. Quantitative determination of Oil Red O staining on d21 of adipogenic differentiation is shown. Quantitative data are presented as means ± SD of N = 3, n = 3. Differences were considered significant at $p \leq 0.05$. ** denotes $p \leq 0.01$, and ns denotes non-significant. Abbreviations: BM, bone marrow; CB, cord blood; d, day; MNU, N-methyl-N-nitroso-urea.

- *Chondrogenic Differentiation*

Treatment of MSCs with 3 mM MNU on d7 of chondrogenic differentiation had no impact on CB-USSC but led to a condensation impairment in the case of CB-MSCs. The chondrogenic condensation of BM-MSCs was, in general, not as pronounced as in the neonatal MSCs (Figure 11).

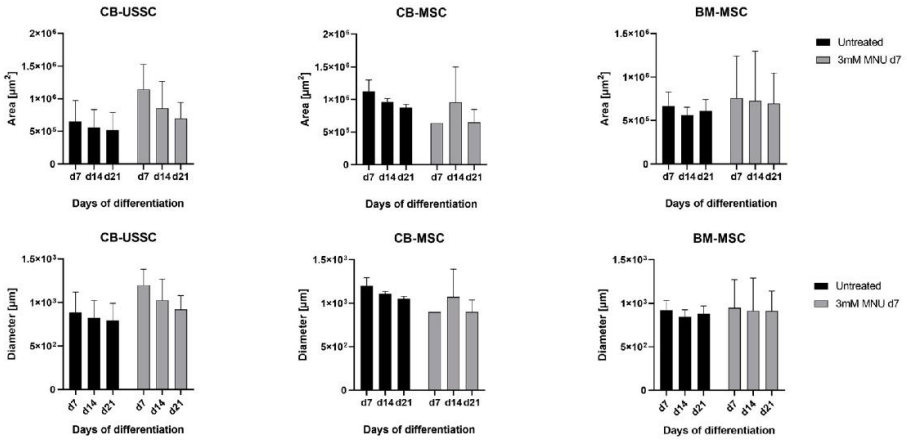

Figure 11. Chondrogenic differentiation of MSCs after 1 h MNU treatment on d7 of differentiation. Areas and diameters of the chondrogenic pellets were measured on d7, d14, and d21 of chondrogenic differentiation (Mean + SD N = 3, n = 3). Abbreviations: BM, bone marrow; CB, cord blood; d; day; MNU, N-methyl-N-nitroso-urea; USSC; unrestricted somatic stem cells.

3.3.4. Effects of Etoposide Treatment on Day 7 of Differentiation

- *Osteogenic Differentiation*

Etoposide treatment of all MSC cell types on d7 of osteogenic differentiation had no effect on their ability to differentiate into osteocytes (Figure 12).

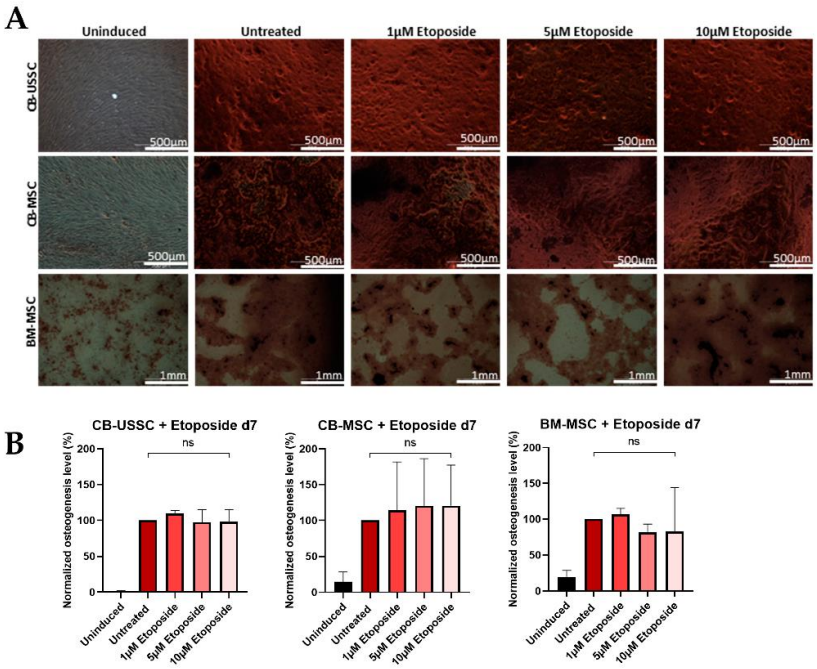

Figure 12. (**A**) Osteogenic differentiation of MSCs after 24 h etoposide treatment on d7. Representative data (CB-USSC4-CB-MSC3-BM-MSC6) after Alizarin Red S staining on d14 of osteogenic differentiation is shown. Scale bars = 1 mm. (**B**) Osteogenic differentiation of MSCs after 24 h etoposide treatment with different doses (untreated, 1 µM, 5 µM, and 10 µM) on d7. Quantitative determination of Alizarin Red S staining on d14 of osteogenic differentiation is shown. Quantitative data are presented as means ± SD of N = 3, n = 3. Differences were considered significant at $p \leq 0.05$. ns denotes non-significant. Abbreviations: BM, bone marrow; CB, cord blood; d, day; USSC, unrestricted somatic stem cells.

RUNX2 showed a genotoxic damage-dependent downregulation in CB-MSCs and BM-MSCs, whereas OSX levels were not significantly dysregulated in CB-USSCs and BM-MSCs, although a slight increase was registered in CB-MSCs (Figure S8).

- *Adipogenic Differentiation*

Etoposide treatment of all MSC types on d7 had no effect on the outcome of adipogenic differentiation (Figure 13). CEBPα showed no differences between treated and untreated samples (Figure S9). CEBPβ levels on d21 showed no significant changes in BM-MSCs, whereas an upregulation was registered on d21 in CB-MSCs in a dose-dependent manner. PPARγ levels were slightly increased in CB-MSCs with increasing genotoxic dose, whereas no significant change was seen in BM-MSCs.

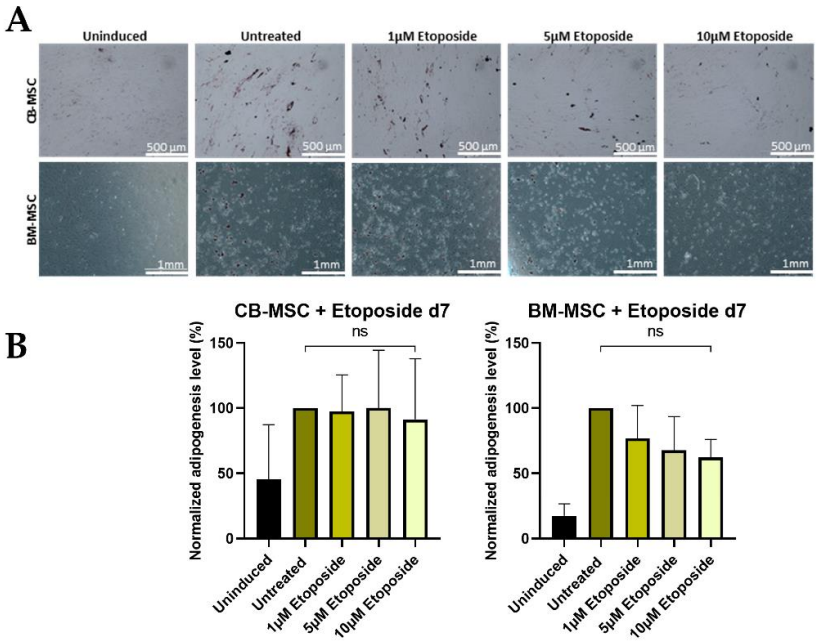

Figure 13. Adipogenic differentiation of MSCs after 24 h etoposide treatment on d7. (**A**) Representative data (CB-MSC3-BM-MSC2) after Oil Red O staining on d21 of adipogenic differentiation is shown. The induced samples successfully underwent adipogenesis, while the uninduced sample was devoid of characteristic lipid droplet formation after 21 days of differentiation. Scale bars = 500 µm or 1 mm. (**B**) Adipogenic differentiation of MSCs after 24 h etoposide treatment with different doses (untreated, 1 µM, 5 µM, and 10 µM) on d7. Quantitative determination of Oil Red O staining on d21 of adipogenic differentiation is shown. Quantitative data are presented as means ± SD of N = 3, n = 3. ns denotes non-significant. Abbreviations: BM, bone marrow; CB, cord blood; d, day.

- *Chondrogenic Differentiation*

The results indicate that treatment with 10 µM etoposide on d7 of differentiation affects CB-USSCs, CB-MSCs, and BM-MSCs differently. While treated CB-USSCs and BM-MSCs showed an even higher condensation than the untreated control, CB-MSCs showed increasing pellet size over the differentiation period after etoposide treatment (Figure 14). This suggests that CB-MSCs may have a unique response to etoposide treatment, potentially reflecting a differential sensitivity or the presence of adaptation mechanisms in CB-MSCs as compared with CB-USSCs and BM-MSCs.

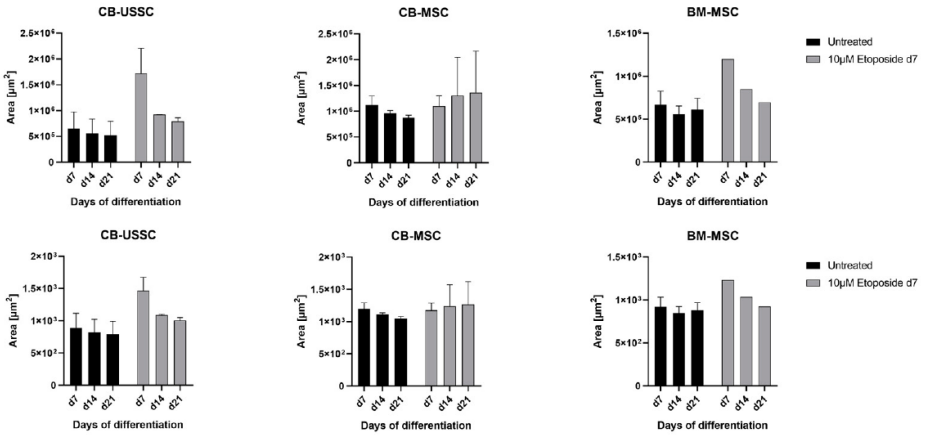

Figure 14. Chondrogenic differentiation of MSCs after 24 h etoposide treatment on d7 of differentiation. Areas and diameters of the chondrogenic pellets were measured on d7, d14, and d21 of chondrogenic differentiation (Mean + SD N = 3, n = 3). Abbreviations: BM, bone marrow; CB, cord blood; d, day; USSC, unrestricted somatic stem cell.

4. Discussion

In order to maintain their genomic integrity, cells developed adequate responses to DNA damage. This is of particular interest in the context of cell differentiation. For this, MSCs are an ideal in vitro model for studying genotoxin-induced stress responses due to their multipotency and the possibility of testing cells of different biological ages.

Our results show that iPSCs, which were used as controls for their embryonic similar age, exhibit a higher sensitivity towards the genotoxic agents MNU and etoposide compared with MSCs. This increased sensitivity could be due to more active cell division compared with MSCs and a lower DSB repair capacity of iPSCs. Others have reported that in spite of fast DNA damage repair capacity, iPSCs are more prone to apoptosis [24]. Furthermore, their DNA repair capacities are more heterogeneous depending on their source as compared with progenitor cells [24]. Moreover, the reprogramming process of iPSCs imposes oxidative stress and other cellular changes that can diminish their overall DNA repair efficiency [25].

In contrast to iPSCs, all types of MSCs were more resistant to the DNA-damaging agents MNU and etoposide. Due to their prolonged lifespan, they usually acquire high amounts of damage and may have specific damage coping mechanisms in order to avoid loss of functional activity. Others have shown that this resistance is associated with an induction of p53, proliferation arrest, or temporary G_2/M cell cycle arrest upon genotoxic damage [26]. Despite the lower sensitivity of MSCs to damage, high MNU or etoposide concentrations led to significant morphological changes, indicating functional changes and impaired cell proliferation, regardless of the biological age, thus underlining the significant effect of genotoxic substances on cell integrity. Genotoxin treatment additionally led to decreased proliferation kinetics, which was more pronounced in adult BM-MSCs, even though this effect was not seen after analysis by comet assay. This is partly due to their lower basal proliferation activity compared with neonatal MSCs but might also be reinforced by the prior accumulated damage burden and the age-related decrease in their DNA repair capacity during the aging process.

The multilineage potential of MSCs is a valuable parameter that can be used for testing drug effects on cell differentiation. This parameter, however, has not been previously studied. Genotoxin treatment on d0 prior to the induction of osteogenic differentiation showed more severe effects compared with genotoxin treatment on d7, with the exception of etoposide-treated CB-MSCs. No significant changes were registered in the mRNA expression of RUNX2 and OSX, although others have described RUNX2 involvement in

DDR by regulation of H2AX phosphorylation and its accumulation after genotoxic stress in muscular smooth muscle cells, thus leading to vascular calcification [27].

Genotoxin treatment applied on d0, prior to the induction of adipogenic and chondrogenic differentiation, did not significantly influence the differentiation outcomes in these lineages, unlike in osteogenic differentiation, which appears to be more susceptible to DNA damage at early time points of the differentiation process. This finding suggests that adipogenic and chondrogenic pathways may have greater resilience to genotoxic stress applied at early time points of differentiation, potentially due to differences in lineage-specific DNA repair mechanisms or stress response pathways that protect these differentiation routes from early-stage damage. In accordance with this hypothesis, no significant decreased levels in the expression of the adipogenic genes CEBPα, CEBPβ, and PPARγ were assessed. An exception was observed within CB-MSCs, which displayed a higher sensitivity to genotoxin treatment compared with CB-USSCs and BM-MSCs, suggesting an intrinsic vulnerability that may be due to differences in DNA repair efficiency or stress response pathways. This enhanced sensitivity of CB-MSCs highlights the need to consider cell-source-specific and age-related responses when evaluating the impact of genotoxins on the differentiation potential of MSCs.

Interestingly, genotoxic noxae administered on d7 after induction of differentiation appear to exert a generally reduced impact on MSC differentiation potential compared with treatment on d0, suggesting that cells might have adapted protective mechanisms during the late stages of differentiation, e.g., transcription-coupled repair or nucleotide excision repair [28]. Among the conditions tested, only MNU treatment on d7 showed an effect on osteogenic differentiation, specifically in CB-MSCs, underscoring their unique sensitivity to DNA damage even at later stages of differentiation induction. For other MSC types (CB-USSCs and BM-MSCs), no significant changes were observed across all differentiation lineages following MNU or etoposide treatment on d7.

Regarding chondrogenic differentiation, genotoxic stress on d0 did not affect this lineage significantly, and the same held true for treatment on d7, further reinforcing the idea that the chondrogenic pathway may possess a greater inherent resilience to DNA damage compared with the osteogenic pathway. This observed resistance in chondrogenic differentiation could indicate either an enhanced capacity for DNA repair in this lineage or a differential reliance on DDR pathways, e.g., non-homologous end joining, which may mitigate the effects of genotoxic agents. The extracellular matrix (ECM) synthesized during chondrogenic differentiation may play a protective role against genotoxic agents when treatment is applied to d7 of differentiation. This matrix, rich in proteoglycans, collagen, and other structural proteins, creates a dense, supportive environment that may help shield the cells from harmful agents. The ECM could act as a physical barrier, limiting the penetration and diffusion of genotoxic compounds into the cells and thus reducing their effective concentration at the cellular level. Additionally, the matrix might interact with cellular signaling pathways, potentially modulating cell responses to DNA damage and enhancing their resilience during later stages of differentiation. This potentially protective effect of the ECM may partially explain the reduced impact of genotoxin treatment on chondrogenic differentiation compared with earlier treatments in other lineages.

Our findings contribute significantly to the understanding of MSC differentiation and its therapeutic potential by highlighting genotoxin effects on undifferentiated and differentiated MSCs. By analyzing these effects at various differentiation time points, we have demonstrated that MNU- and etoposide-induced damage can not only impair cell viability and proliferation but might also affect the ability of MSCs to progress through their differentiation pathway, which is a critical factor for their therapeutic application in tissue repair and regeneration. Moreover, we have provided evidence about the resilience of differentiated MSCs compared with their undifferentiated counterparts, showing that the timing of genotoxic stress influences treatment outcomes. This is important to consider in the context of drug testing and safety assessment, and a deeper understanding of the

responses at different stages of differentiation allows the development of more refined in vitro models to better mimic physiological conditions.

Nevertheless, a limitation of this study is the relatively small sample size and the inherent variability in donor characteristics accentuating MSC-related heterogeneity. These factors may influence the observed responses among the different cell lines. While efforts were made to minimize these effects, individual donor variability, including genetic and epigenetic differences, could still contribute to variations in the results. Future studies with larger sample sizes and more standardized donor selection criteria will be essential to validate and generalize these findings.

5. Conclusions

The insights obtained from this study emphasize the critical need to consider the effects of genotoxic damage on cell differentiation in an agent- and biological age-specific manner when conducting toxicological studies and during drug development. Neonatal MSCs, with their enhanced proliferative capacity, differentiation potential, and lower immunogenicity, present a significant promise for regenerative therapies and are a valuable tool for new approach methodologies to avoid animal testing compared with adult MSCs. Furthermore, in addition to therapy-related hematotoxicity, adverse effects on MSCs, which are the main components of the hematopoietic stem cell niche, also need to be considered.

Supplementary Materials: The following supporting information can be downloaded at: https://www.mdpi.com/article/10.3390/cells13242134/s1, Table S1: List of used CB-USSC, CB-MSC and BM-MSC cell lines; Table S2: List of used primers for RT-qPCR; Figure S1: Expression pattern of DDR of an iPSC cell line (R26) compared to MSCs from different sources; Figure S2: Expression pattern of early and late osteogenic genes in CB-USSC, CB-MSC and BM-MSC on d7 or d14 after induction of osteogenic differentiation and 1 h treatment with MNU on d0 of differentiation; Figure S3: Expression pattern of late adipogenic genes in CB-MSC and BM-MSC on d21 after induction of adipogenic differentiation and 1 h treatment with MNU on d0 of differentiation; Figure S4: Expression pattern of early and late osteogenic genes in CB-USSC, CB-MSC and BM-MSC on d7 or d14 after induction of osteogenic differentiation and 24h treatment with etoposide on d0 of differentiation; Figure S5: Expression pattern of late adipogenic genes in CB-MSC and BM-MSC on d21 after induction of adipogenic differentiation and 24 h treatment with etoposide on d0 of differentiation; Figure S6: Expression pattern of early and late osteogenic genes in CB-USSC, CB-MSC and BM-MSC on d14 after induction of osteogenic differentiation and 1 h treatment with MNU on d7 of differentiation; Figure S7: Expression pattern of late adipogenic genes in CB-MSC and BM-MSC on d21 after induction of adipogenic differentiation and 1 h treatment with MNU on d7 of differentiation; Figure S8: Expression pattern of early and late osteogenic genes in CB-USSC, CB-MSC and BM-MSC on d14 after induction of osteogenic differentiation and 24 h treatment with etoposide on d7 of differentiation; Figure S9: Expression pattern of late adipogenic genes in CB-MSC and BM-MSC on d21 after induction of adipogenic differentiation and 1 h treatment with MNU on d7 of differentiation.

Author Contributions: Conceptualization, M.O., G.K. and G.F.; methodology, M.O.; validation, M.O., investigation, G.K., G.F. and S.W.; data curation, M.O.; writing—original draft preparation, M.O. All authors have read and agreed to the published version of the manuscript.

Funding: This work is supported by the Deutsche Forschungsgemeinschaft (DFG, German Research Foundation)—417677437/GRK2578 (to G.F., G.K. and S.W.) and the Deutsche José Carreras Leukämie-Stiftung (DJCLS 18R/2021) to G.K.

Institutional Review Board Statement: The study was conducted in accordance with the Declaration of Helsinki and approved by the Institutional Review Board (or Ethics Committee) of University Hospital Düsseldorf (ethic commissions 3484 and 2020-1144).

Informed Consent Statement: Informed consent was obtained from all subjects involved in the study.

Data Availability Statement: The original contributions presented in the study are included in the article, further inquiries can be directed to the corresponding author.

Acknowledgments: We would like to express our sincere gratitude to Catalent for their generous providence with reprogrammed iPSCs. Additionally, we would also like to thank Lena Abbey from the Institute of Toxicology for her assistance with the Comet Assay. This support and resources have been invaluable in achieving the objectives of this research.

Conflicts of Interest: The authors declare no conflicts of interest.

References

1. Pittenger, M.F.; Mackay, A.M.; Beck, S.C.; Jaiswal, R.K.; Douglas, R.; Mosca, J.D.; Moorman, M.A.; Simonetti, D.W.; Craig, S.; Marshak, D.R. Multilineage potential of adult human mesenchymal stem cells. *Science* **1999**, *284*, 143–147. [CrossRef] [PubMed]
2. Caplan, A.I. Mesenchymal stem cells. *J. Orthop. Res.* **1991**, *9*, 641–650. [CrossRef] [PubMed]
3. Zuk, P.A.; Zhu, M.; Mizuno, H.; Huang, J.; Futrell, J.W.; Katz, A.J.; Benhaim, P.; Lorenz, H.P.; Hedrick, M.H. Multilineage cells from human adipose tissue: Implications for cell-based therapies. *Tissue Eng.* **2001**, *7*, 211–228. [CrossRef]
4. Erices, A.; Conget, P.; Minguell, J.J. Mesenchymal progenitor cells in human umbilical cord blood. *Br. J. Haematol.* **2000**, *109*, 235–242. [CrossRef]
5. Soncini, M.; Vertua, E.; Gibelli, L.; Zorzi, F.; Denegri, M.; Albertini, A.; Wengler, G.S.; Parolini, O. Isolation and characterization of mesenchymal cells from human fetal membranes. *J. Tissue Eng. Regen. Med.* **2007**, *1*, 296–305. [CrossRef]
6. Jacobs, S.A.; Pinxteren, J.; Roobrouck, V.D.; Luyckx, A.; van't Hof, W.; Deans, R.; Verfaillie, C.M.; Waer, M.; Billiau, A.D.; Van Gool, S.W. Human multipotent adult progenitor cells are nonimmunogenic and exert potent immunomodulatory effects on alloreactive T-cell responses. *Cell Transplant.* **2013**, *22*, 1915–1928. [CrossRef] [PubMed]
7. Zaim, M.; Karaman, S.; Cetin, G.; Isik, S. Donor age and long-term culture affect differentiation and proliferation of human bone marrow mesenchymal stem cells. *Ann. Hematol.* **2012**, *91*, 1175–1186. [CrossRef] [PubMed]
8. Choudhery, M.S.; Badowski, M.; Muise, A.; Pierce, J.; Harris, D.T. Donor age negatively impacts adipose tissue-derived mesenchymal stem cell expansion and differentiation. *J. Transl. Med.* **2014**, *12*, 8. [CrossRef]
9. Smith, N.; Shirazi, S.; Cakouros, D.; Gronthos, S. Impact of Environmental and Epigenetic Changes on Mesenchymal Stem Cells during Aging. *Int. J. Mol. Sci.* **2023**, *24*, 6499. [CrossRef]
10. Guillot, P.V.; Gotherstrom, C.; Chan, J.; Kurata, H.; Fisk, N.M. Human first-trimester fetal MSC express pluripotency markers and grow faster and have longer telomeres than adult MSC. *Stem Cells* **2007**, *25*, 646–654. [CrossRef] [PubMed]
11. Druckrey, H.; Preussmann, R.; Ivankovic, S.; Schmahl, D. [Organotropic carcinogenic effects of 65 various N-nitroso- compounds on BD rats]. *Z. Krebsforsch.* **1967**, *69*, 103–201. [CrossRef] [PubMed]
12. Kaina, B.; Christmann, M.; Naumann, S.; Roos, W.P. MGMT: Key node in the battle against genotoxicity, carcinogenicity and apoptosis induced by alkylating agents. *DNA Repair* **2007**, *6*, 1079–1099. [CrossRef] [PubMed]
13. Sandercock, L.E.; Hahn, J.N.; Li, L.; Luchman, H.A.; Giesbrecht, J.L.; Peterson, L.A.; Jirik, F.R. Mgmt deficiency alters the in vivo mutational spectrum of tissues exposed to the tobacco carcinogen 4-(methylnitrosamino)-1-(3-pyridyl)-1-butanone (NNK). *Carcinogenesis* **2008**, *29*, 866–874. [CrossRef] [PubMed]
14. Jakszyn, P.; Gonzalez, C.A. Nitrosamine and related food intake and gastric and oesophageal cancer risk: A systematic review of the epidemiological evidence. *World J. Gastroenterol.* **2006**, *12*, 4296–4303. [CrossRef] [PubMed]
15. Song, P.; Wu, L.; Guan, W. Dietary Nitrates, Nitrites, and Nitrosamines Intake and the Risk of Gastric Cancer: A Meta-Analysis. *Nutrients* **2015**, *7*, 9872–9895. [CrossRef]
16. Nitiss, J.L.; Beck, W.T. Antitopoisomerase drug action and resistance. *Eur. J. Cancer* **1996**, *32A*, 958–966. [CrossRef]
17. Papiez, M.A. The effect of quercetin on oxidative DNA damage and myelosuppression induced by etoposide in bone marrow cells of rats. *Acta Biochim. Pol.* **2014**, *61*, 7–11. [CrossRef] [PubMed]
18. Bellomo, M.J.; Cabrol, C.; Beris, P.; Mermillod, B.; Zulian, G.B.; Alberto, P. Etoposide and secondary haematological malignancies: Coincidence or causality? *Ann. Oncol.* **1993**, *4*, 559–566. [CrossRef] [PubMed]
19. Liedtke, S.; Buchheiser, A.; Bosch, J.; Bosse, F.; Kruse, F.; Zhao, X.; Santourlidis, S.; Kögler, G. The HOX Code as a "biological fingerprint" to distinguish functionally distinct stem cell populations derived from cord blood. *Stem Cell Res.* **2010**, *5*, 40–50. [CrossRef] [PubMed]
20. Terheyden-Keighley, D.; Hühne, M.; Berger, T.; Hiller, B.; Martins, S.; Gamerschlag, A.; Sabour, D.; Meffert, A.; Kislat, A.; Slotta, C.; et al. GMP-compliant iPS cell lines show widespread plasticity in a new set of differentiation workflows for cell replacement and cancer immunotherapy. *Stem Cells Transl. Med.* **2024**, *13*, 898–911. [CrossRef]
21. Liedtke, S.; Sacchetti, B.; Laitinen, A.; Donsante, S.; Klockers, R.; Laitinen, S.; Riminucci, M.; Kogler, G. Low oxygen tension reveals distinct HOX codes in human cord blood-derived stromal cells associated with specific endochondral ossification capacities in vitro and in vivo. *J. Tissue Eng. Regen. Med.* **2017**, *11*, 2725–2736. [CrossRef] [PubMed]
22. Tsao, Y.T.; Huang, Y.J.; Wu, H.H.; Liu, Y.A.; Liu, Y.S.; Lee, O.K. Osteocalcin Mediates Biomineralization during Osteogenic Maturation in Human Mesenchymal Stromal Cells. *Int. J. Mol. Sci.* **2017**, *18*, 159. [CrossRef]
23. Kluth, S.M.; Buchheiser, A.; Houben, A.P.; Geyh, S.; Krenz, T.; Radke, T.F.; Wiek, C.; Hanenberg, H.; Reinecke, P.; Wernet, P.; et al. DLK-1 as a marker to distinguish unrestricted somatic stem cells and mesenchymal stromal cells in cord blood. *Stem Cells Dev.* **2010**, *19*, 1471–1483. [CrossRef] [PubMed]

24. Luo, L.Z.; Gopalakrishna-Pillai, S.; Nay, S.L.; Park, S.-W.; Bates, S.E.; Zeng, X.; Iverson, L.E.; O'Connor, T.R. DNA Repair in Human Pluripotent Stem Cells Is Distinct from That in Non-Pluripotent Human Cells. *PLoS ONE* **2012**, *7*, e30541. [CrossRef]
25. Turinetto, V.; Orlando, L.; Giachino, C. Induced Pluripotent Stem Cells: Advances in the Quest for Genetic Stability during Reprogramming Process. *Int. J. Mol. Sci.* **2017**, *18*, 1952. [CrossRef]
26. Lützkendorf, J.; Wieduwild, E.; Nerger, K.; Lambrecht, N.; Schmoll, H.J.; Müller-Tidow, C.; Müller, L.P. Resistance for Genotoxic Damage in Mesenchymal Stromal Cells Is Increased by Hypoxia but Not Generally Dependent on p53-Regulated Cell Cycle Arrest. *PLoS ONE* **2017**, *12*, e0169921. [CrossRef]
27. Cobb, A.M.; Yusoff, S.; Hayward, R.; Ahmad, S.; Sun, M.; Verhulst, A.; D'Haese, P.C.; Shanahan, C.M. Runx2 (Runt-Related Transcription Factor 2) Links the DNA Damage Response to Osteogenic Reprogramming and Apoptosis of Vascular Smooth Muscle Cells. *Arterioscler. Thromb. Vasc. Biol.* **2021**, *41*, 1339–1357. [CrossRef]
28. Hanawalt, P.C. Subpathways of nucleotide excision repair and their regulation. *Oncogene* **2002**, *21*, 8949–8956. [CrossRef] [PubMed]

Supplementary Materials:

Table S1: List of used CB-USSC, CB-MSC and BM-MSC cell lines, all derived from different donors and were numbered independently of the donor. The donor age of BM-MSCs is listed. Abbreviations: BM, bone marrow; CB, cord blood; d, day; USSC, unrestricted somatic stem cell; N.K., not known;

Cell type	Number	Name	Donor age
CB-USSC	1	SA5/73	Neonatal
	2	SA8/25	
	3	SA10/36	
	4	USSC86b	
CB-MSC	1	SA6/51	
	2	SA8/39	
	3	USSC63	
	4	USSC120a	
BM-MSC	1	KM9-14	23
	2	KM9-15	32
	3	KM114	43
	4	KM120	N.K.
	5	KM8/06	52
	6	KM1/23	36
	7	KM2/23	31
	8	KM3/23	24

Table S2: List of used primers for RT-qPCR. Abbreviations: ATM, Ataxia Telangiectasia Mutated; BRCA1, Breast Cancer 1; BRCA2, Breast Cancer 2; CEBP, CCAAT/Enhancer Binding Protein Alpha; O_6-Methylguanine-DNA Methyltransferase; NHEJ1, Non-Homologous End Joining Factor 1; OSX: Osterix; P21, Cyclin-Dependent Kinase Inhibitor 1A (CDKN1A); PPARγ, Peroxisome Proliferator-Activated Receptor Gamma; RAD51, RAD51 Recombinase; RPL13a, Ribosomal Protein L13a; RUNX2, Runt-Related Transcription Factor 2; TP53, Tumor Protein 53 (p53); XRCC: X-Ray Repair Cross-Complementing;

Target	Forward sequence 5´- 3´	Reverse sequence 5´- 3´
ATM	CCTTGTGCTAGTGGGCAGAA	ATGGGGAGCAAAGAACCCAG
BRCA1	CCACAGATCAACCTGGAATGG	GTAGAGTGCTACACTGCTCA
BRCA2	TTCTGAGGTGGACCTAATAGG	TGATTTGGATTCTGGTCGCC
CEBPα	GAGTCACACCAGAAAGCTAG	GATGGACTGATCGTGCTTC
CEBPβ	TTTCGAAGTTGATGCAATCG	ACAGCAACAAGCCCGTAGG
MGMT	ACCGTTTGCGACTTGGTACT	GGGCTGGTGGAAATAGGCAT
NHEJ1	CCATTGTTGAAGGACGCTGC	CTAGCTCCCTCACTTGGCAC
OSX	TGCTTGAGGAGGAAGTTCAC	CTGAAAGGTCACTGCCCAC
P21	TACATCTTCTGCCTTAGT	TCTTAGGAACCTCTCATT
PPARγ	TCCATGCTGTTATGGGTGAA	TCAAAGGAGTGGGAGTGGTC
RAD51	GCTGATGAGTTTGGTGTAGC	AACATAGCTTCAGCTTCAGG
RPL13a	GAGGTATGCTGCCCCACAAA	TTCAGACGCACGACCTTGAG
RUNX2	GAGTGGACGAGGCAAGAG	GGACACCTACTCTCATACTG
TP53	TTCCGAGAGCTGAATGAGGC	AATGTCAGTCTGAGTCAGGCC
XRCC4	CCTCTAGGAGAATCAGCTTCAAGA	AAAGAGGTCTTCTGGGCTGC
XRCC5	AGCATAGACTGCATCCGAGC	TCCCCATACATCCACGACCT
XRCC6	TGCGTGGATTGTCGTCTTCT	CTTCTTCATCGCCCTCGGTT

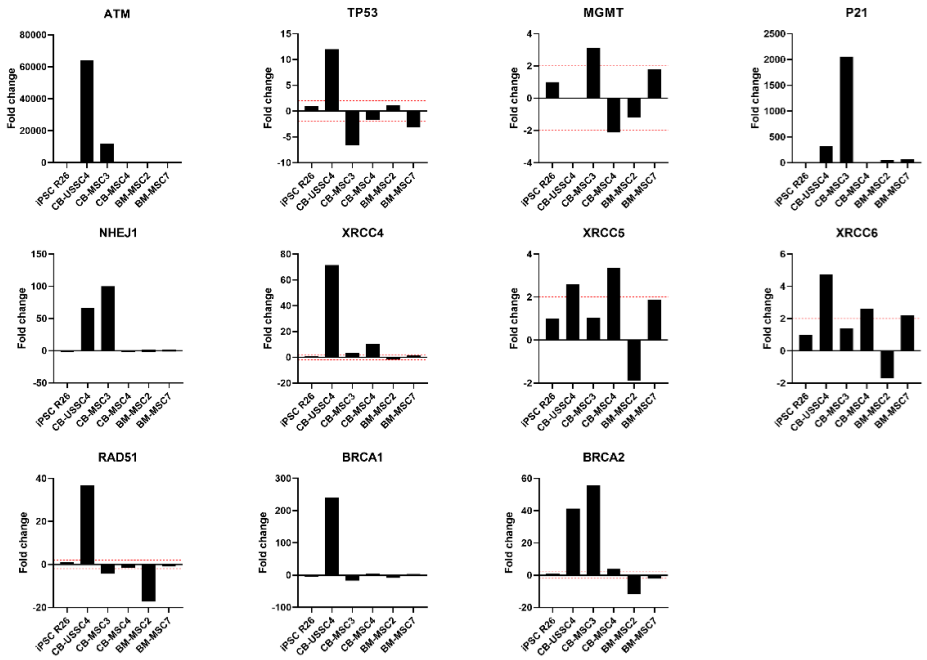

Figure S1: Expression pattern of DDR of an iPSC cell line (R26) compared to MSCs from different sources. Fold change was calculated using the $2^{-\Delta\Delta CT}$ method relative to the untreated control and normalized to the reference gene RPL13a. 2 represents a two-fold increase and -2 represents a two-fold decrease. Abbreviations: BM, bone marrow; CB, cord blood; iPSC, induced pluripotent stem cell; MSC, mesenchymal stromal cell; USSC, unrestricted somatic stem cell;

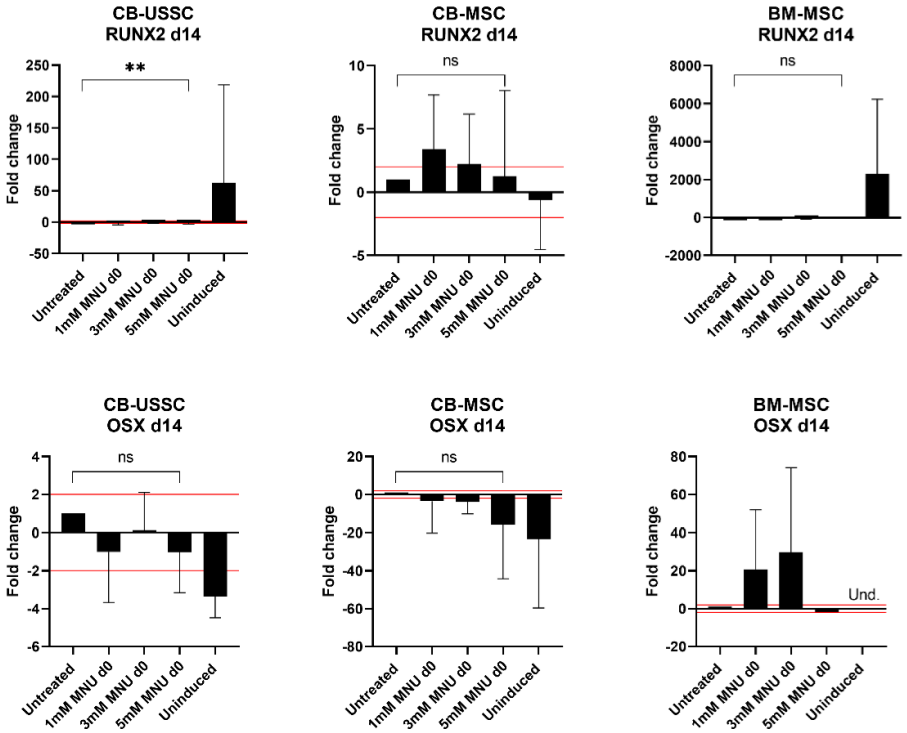

Figure S2: Expression pattern of early and late osteogenic genes in CB-USSC, CB-MSC and BM-MSC on d7 or d14 after induction of osteogenic differentiation and 1 h treatment with MNU on

d0. Fold change was calculated using the $2^{-\Delta\Delta CT}$ method relative to the untreated control and normalized to the reference gene RPL13a. The red lines indicate the significance thresholds. 2 represents a two-fold increase and -2 represents a two-fold decrease. Abbreviations: d, day; RUNX2, Runt-related transcription factor 2; OSX, Osterix; Und., undetermined;

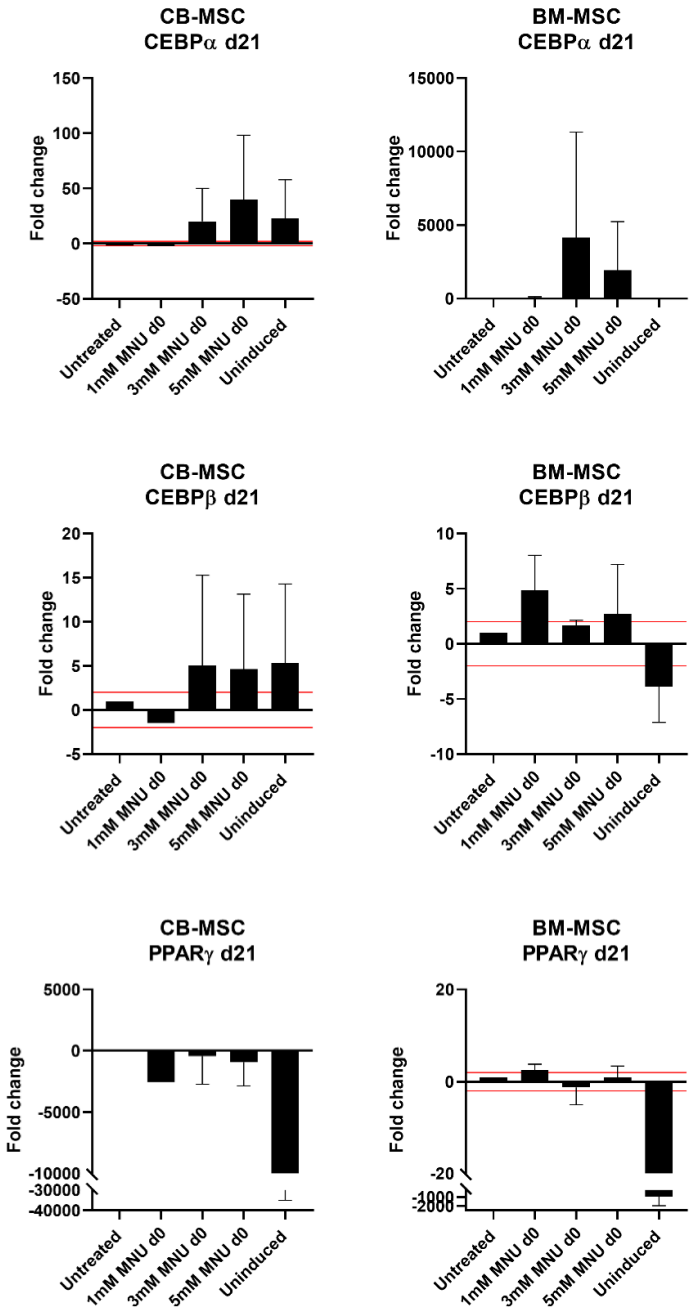

Figure S3. Expression pattern of late adipogenic genes in CB-MSC and BM-MSC on d21 after induction of adipogenic differentiation and 1 h treatment with MNU on d0. Fold change was calculated using the $2^{-\Delta\Delta CT}$ method relative to the untreated control and normalized to the reference gene RPL13a. The red lines indicate the significance thresholds. 2 represents a two-fold increase and -2 represents a two-fold decrease. Abbreviations: PPARγ, Peroxisome proliferator-activated receptor gamma; CEBP, CCAAT-enhancer-binding protein; d, day; MNU, N-methyl-N-nitroso-urea;

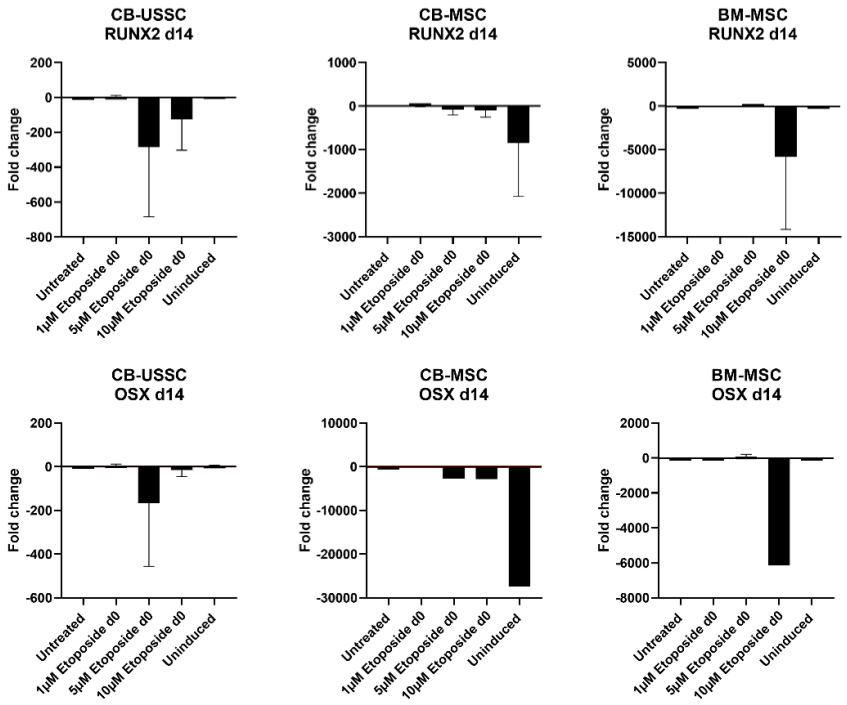

Figure S4. Expression pattern of early and late osteogenic genes in CB-USSC, CB-MSC and BM-MSC on d7 or d14 after induction of osteogenic differentiation and 24h treatment with etoposide. Fold change was calculated using the $2^{-\Delta\Delta CT}$ method relative to the untreated control and normalized to the reference gene RPL13a. The red lines indicate the significance thresholds. 2 represents a two-fold increase and -2 represents a two-fold decrease. Abbreviations: d, day; RUNX2, Runt-related transcription factor 2; OSX, Osterix;

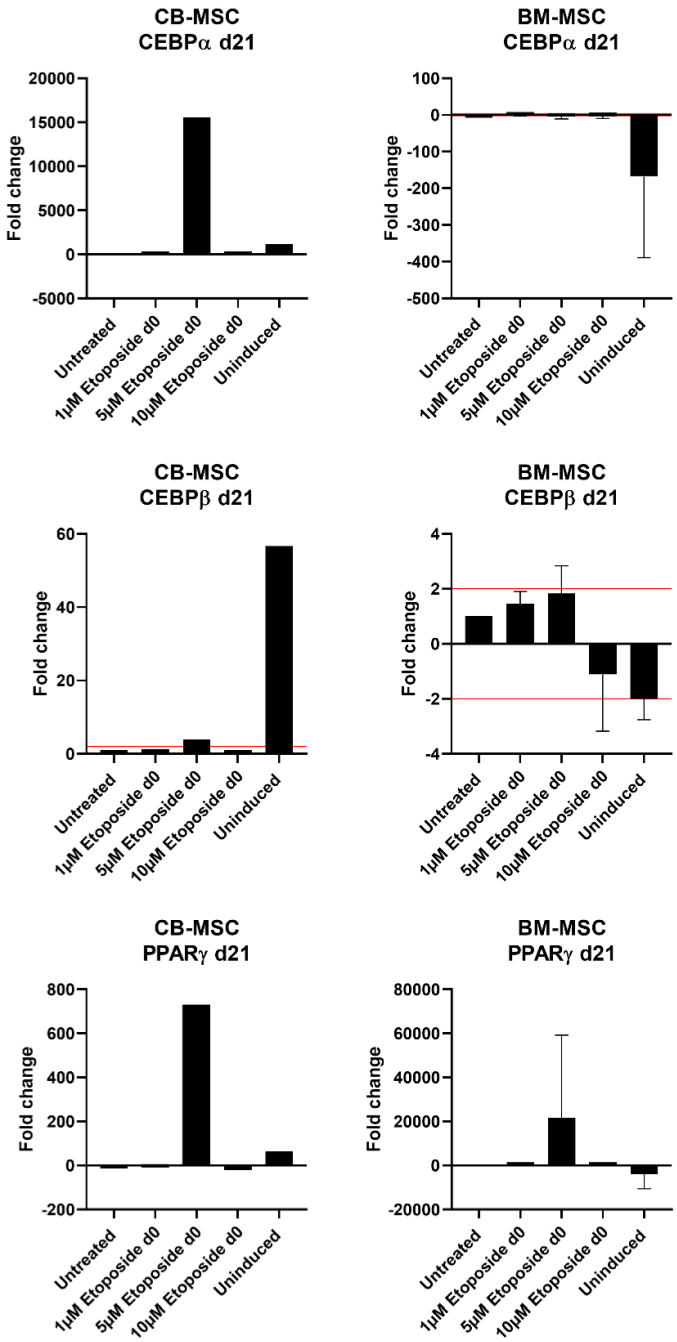

Figure S5. Expression pattern of late adipogenic genes in CB-MSC and BM-MSC on d21 after induction of adipogenic differentiation and 24 h treatment with etoposide on d0. Fold change was calculated using the $2^{-\Delta\Delta CT}$ method relative to the untreated control and normalized to the reference gene RPL13a. The red lines indicate the significance thresholds. 2 represents a two-fold increase and -2 represents a two-fold decrease. Abbreviations: PPARγ, Peroxisome proliferator-activated receptor gamma; CEBP, CCAAT-enhancer-binding protein; d, day;

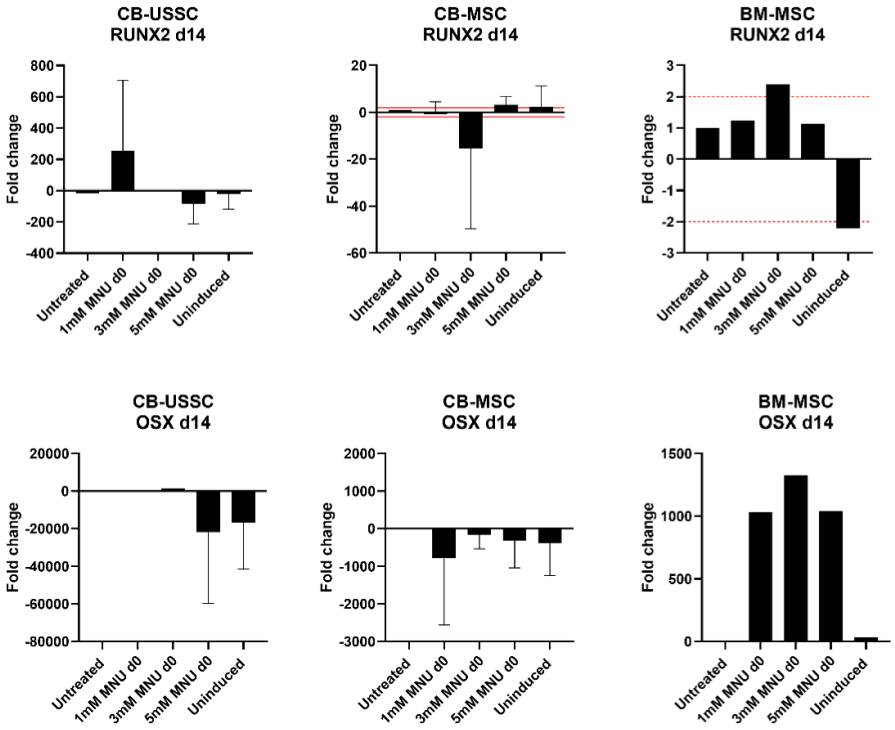

Figure S6. Expression pattern of early and late osteogenic genes in CB-USSC, CB-MSC and BM-MSC on d14 after induction of osteogenic differentiation and 1 h treatment with MNU on d7 of differentiation. Fold change was calculated using the $2^{-\Delta\Delta CT}$ method relative to the untreated control and normalized to the reference gene RPL13a. The red lines indicate the significance thresholds. 2 represents a two-fold increase and -2 represents a two-fold decrease. Abbreviations: d, day; RUNX2, Runt-related transcription factor 2; OSX, Osterix;

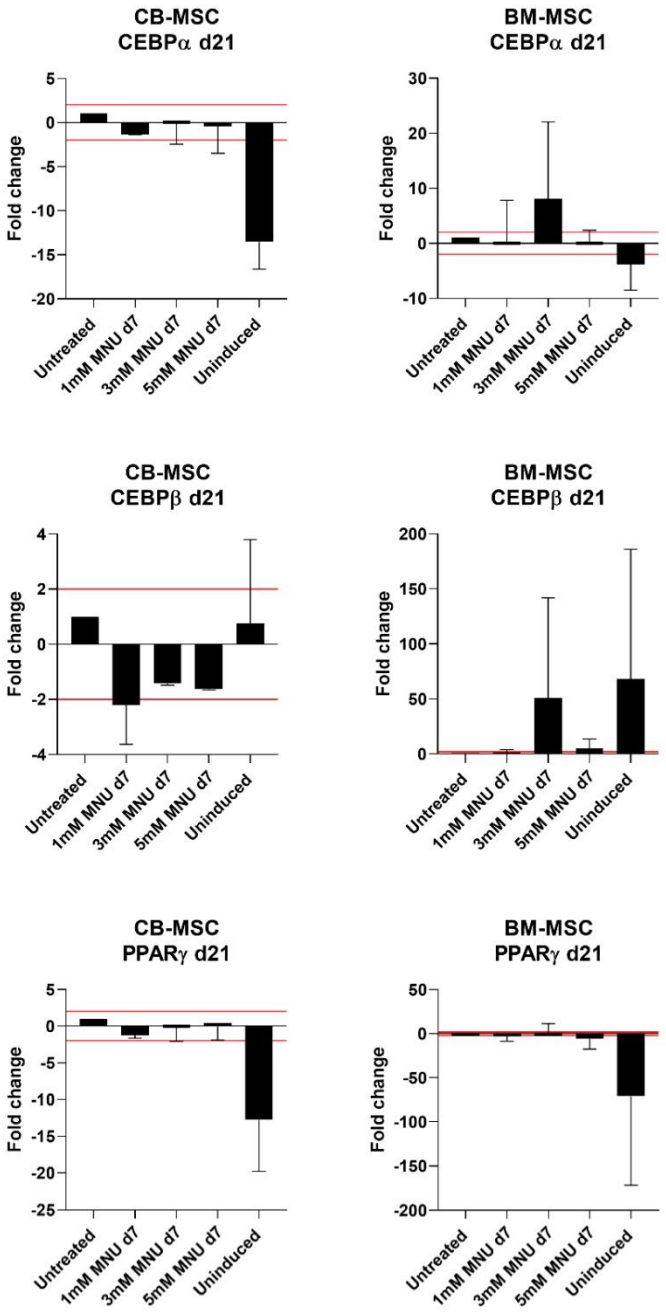

Figure S7. Expression pattern of late adipogenic genes in CB-MSC and BM-MSC on d21 after induction of adipogenic differentiation and 1 h treatment with MNU on d7. Fold change was calculated using the $2^{-\Delta\Delta CT}$ method relative to the untreated control and normalized to the reference gene RPL13a. The red lines indicate the significance thresholds. 2 represents a two-fold increase and -2 represents a two-fold decrease. Abbreviations: PPARγ, Peroxisome proliferator-activated receptor gamma; CEBP, CCAAT-enhancer-binding protein; d, day;

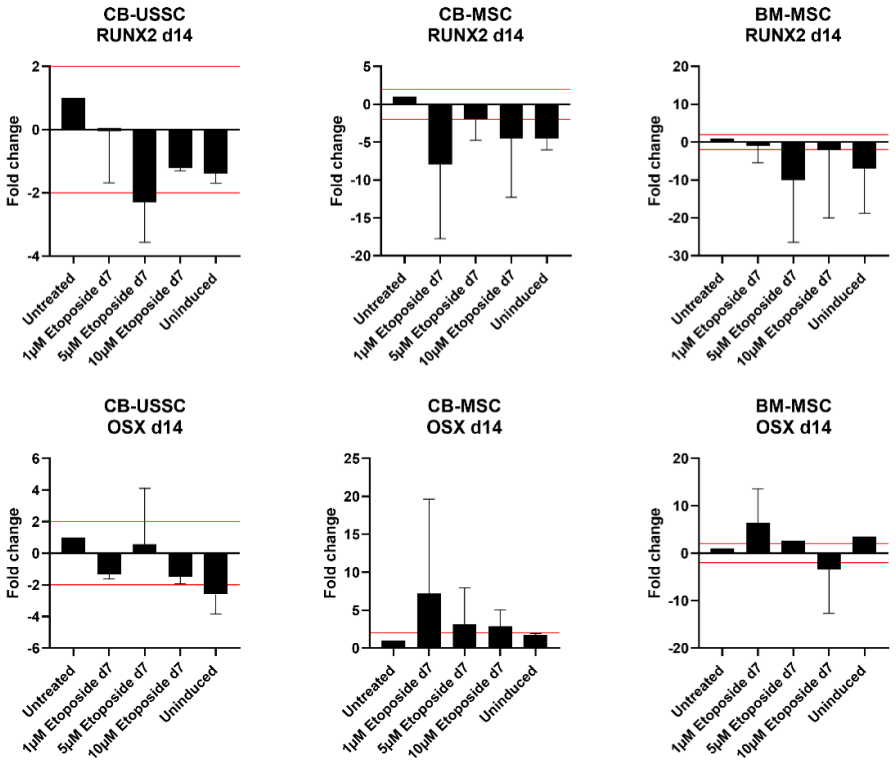

Figure S8. Expression pattern of early and late osteogenic genes in CB-USSC, CB-MSC and BM-MSC on d14 after induction of osteogenic differentiation and 24 h treatment with etoposide on d7 of differentiation. Fold change was calculated using the $2^{-\Delta\Delta CT}$ method relative to the untreated control and normalized to the reference gene RPL13a. The red lines indicate the significance thresholds. 2 represents a two-fold increase and -2 represents a two-fold decrease. Abbreviations: d, day; RUNX2, Runt-related transcription factor 2; OSX, Osterix;

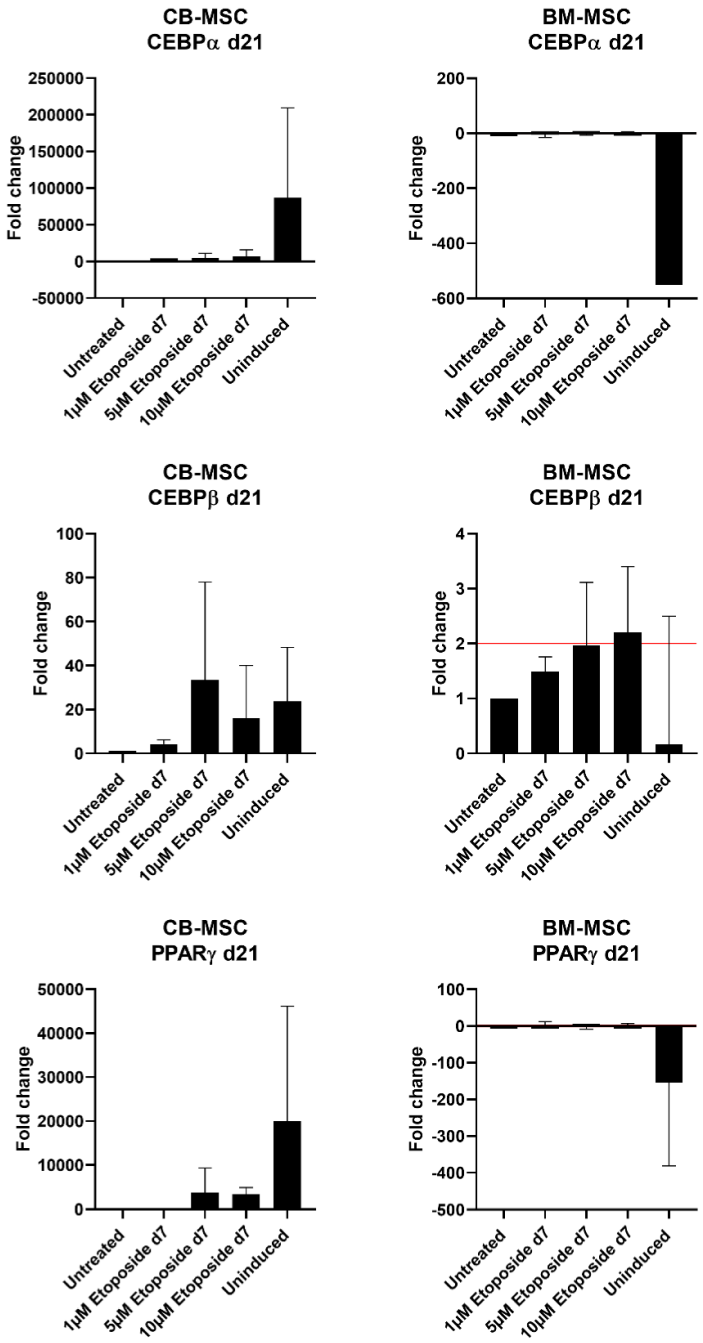

Figure S9. Expression pattern of late adipogenic genes in CB-MSC and BM-MSC on d21 after induction of adipogenic differentiation and 1 h treatment with MNU on d7. Fold change was calculated using the $2^{-\Delta\Delta CT}$ method relative to the untreated control and normalized to the reference gene RPL13a. The red lines indicate the significance thresholds. 2 represents a two-fold increase and -2 represents a two-fold decrease. Abbreviations: PPARγ, Peroxisome proliferator-activated receptor gamma; CEBP, CCAAT-enhancer-binding protein; d, day;

4.5. Effects of MNU and Etoposide Treatment of MSCs on the Expression Pattern of Differentiation-related Genes

This chapter presents unpublished results that complement the findings from Chapter 4.4. Specifically, it examines the effects of genotoxic stress on several additional osteogenic and adipogenic differentiation-related genes. These data provide further insights into the broader implications of genotoxic stress on stem cell differentiation and enhance the understanding of the findings discussed in the preceding section.

Osteogenic Differentiation

Besides RUNX2 and OSX (Chapter 4.4), several other osteogenic differentiation-related genes were tested upon MNU or etoposide treatment on d0 or d7.

Bone morphogenetic proteins (BMPs) including BMP2 and BMP4 are members of the TGF-β family and are required for proper bone formation during MSC differentiation into osteoblasts in vitro and in vivo. Disruptions in the BMP signaling results in a variety of skeletal and extra-skeletal anomalies. BMP2 plays a role in the induction of osteogenesis regulating bone matrix microenvironment while BMP4 induces osteoprogenitor differentiation into mature osteoblasts and additionally stimulates osteoblasts to produce ECM. BMP2 and BMP4 RNA expression were analyzed upon MNU or etoposide treatment on d0 or on d7 of osteogenic differentiation.

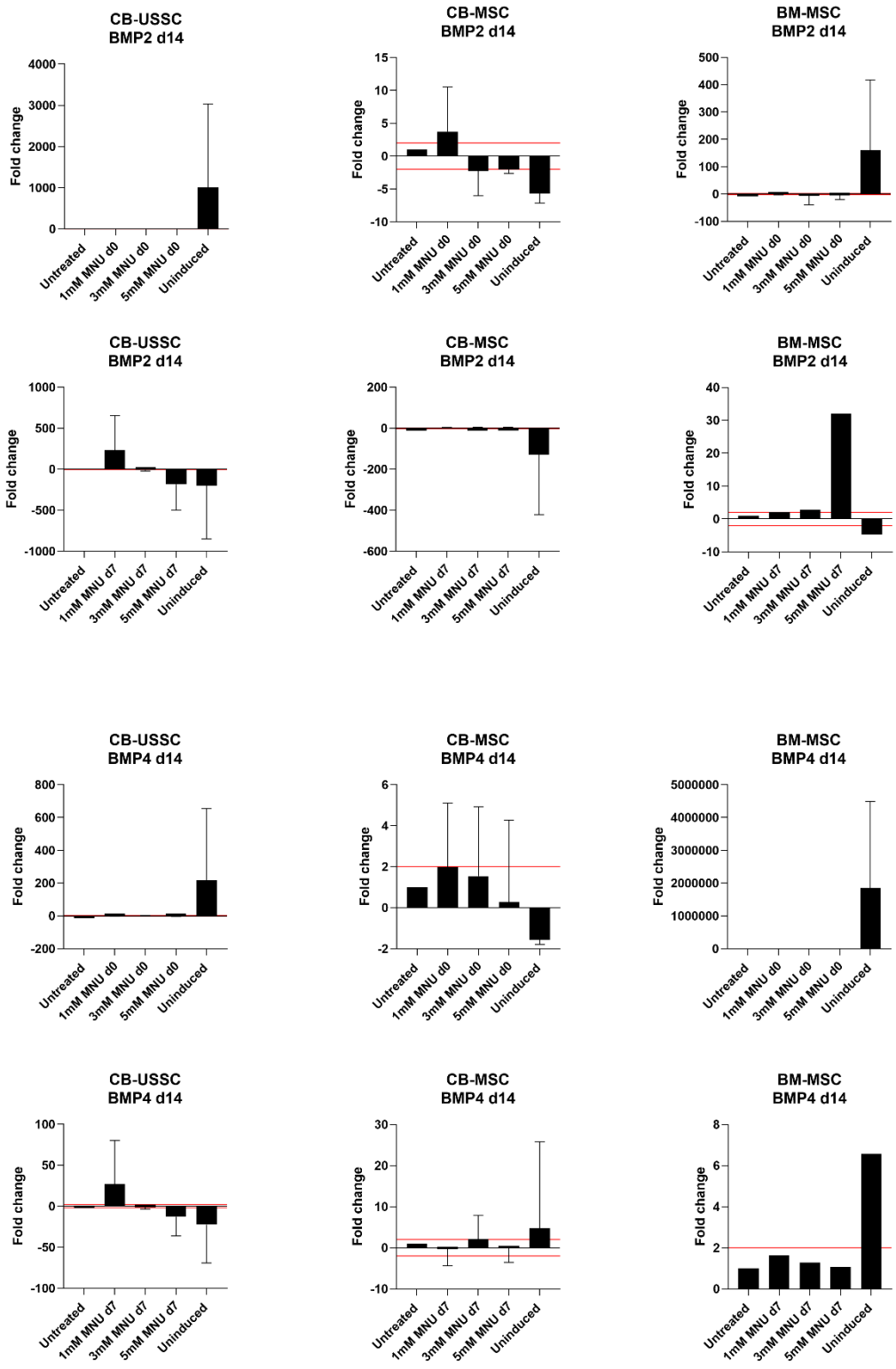

Figure 12: Expression pattern of BMP2 and BMP4 in CB-USSC, CB-MSC and BM-MSC on d14 after induction of osteogenic differentiation and 1 h treatment with MNU on d0 or on d7. Fold change was calculated using the $2^{-\Delta\Delta CT}$ method relative to the untreated control and normalized to the reference gene RPL13a. The red lines indicate the significance thresholds. 2 represents a two-fold increase and -2 represents a two-fold decrease. Abbreviations: BMP, bone morphogenetic protein; BM, bone marrow; CB, cord blood; d, day; MNU, N-methyl-N-nitrosourea; MSC, mesenchymal stromal cell; USSC, unrestricted somatic stem cell;

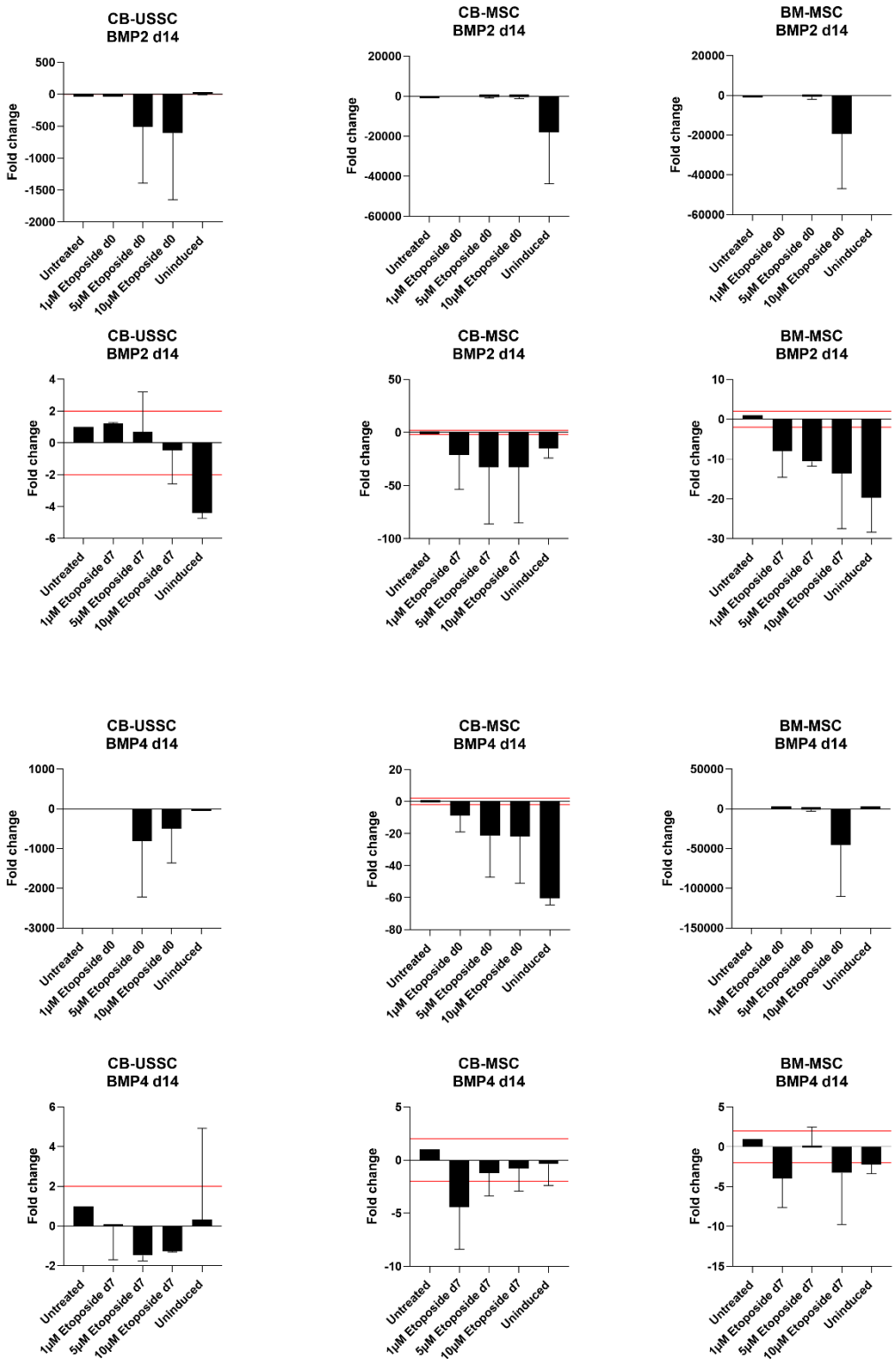

Figure 13: Expression pattern of BMP2 and BMP4 in CB-USSC, CB-MSC and BM-MSC on d14 after induction of osteogenic differentiation and 24 h treatment with etoposide on d0 or on d7. Fold change was calculated using the $2^{-\Delta\Delta CT}$ method relative to the untreated control and normalized to the reference gene RPL13a. The red lines indicate the significance thresholds. 2 represents a two-fold increase and -2 represents a two-fold decrease. Abbreviations: BMP, bone morphogenetic protein; BM, bone marrow; CB, cord blood; d, day; MSC, mesenchymal stromal cell; USSC, unrestricted somatic stem cell;

MNU treatment on d0 or d7 did not result in any significant changes in the expression levels of BMP2 and BMP4 across the analyzed cell types. The observed fold changes remained within the variability range indicating that MNU exposure at these time points

did not notably affect BMP-induced differentiation pathways (Figure 12). Etoposide treatment on d0 lead to a downregulation of BMP2 expression at high doses of etoposide and to a dose-dependent downregulation of BMP4, whereas etoposide treatment at d7 lead to the downregulation of BMP2 in a dose-dependent manner in CB-MSCs and BM-MSCs but not in CB-USSCs and had no significant impact on BMP4 expression (Figure 13).

Bone sialoprotein (BSP) is one of the non-collagenous proteins in the bone ECM and plays an important role in mineralization and osteoclast adherence to bone but is also a marker for osteogenic differentiation.

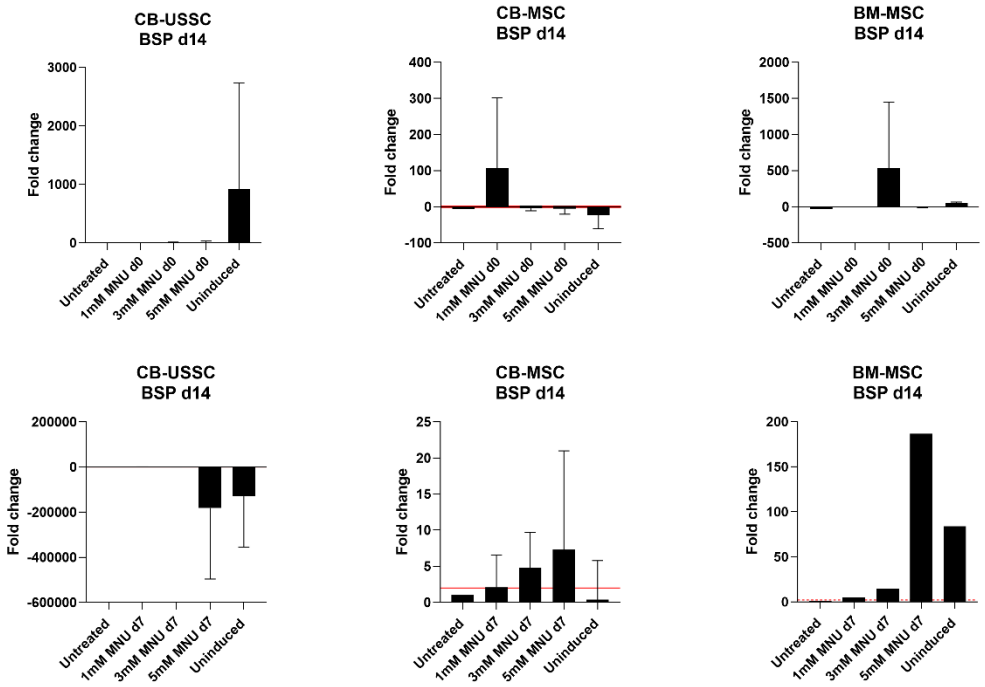

Figure 14: Expression pattern of BSP in CB-USSC, CB-MSC and BM-MSC on d14 after induction of osteogenic differentiation and 1 h treatment with MNU on d0 or on d7. Fold change was calculated using the $2^{-\Delta\Delta CT}$ method relative to the untreated control and normalized to the reference gene RPL13a. The red lines indicate the significance thresholds. 2 represents a two-fold increase and -2 represents a two-fold decrease. Abbreviations: BSP, bone sialoprotein; BM, bone marrow; CB, cord blood; d, day; MNU, N-methyl-N-nitrosourea; MSC, mesenchymal stromal cell; USSC, unrestricted somatic stem cell;

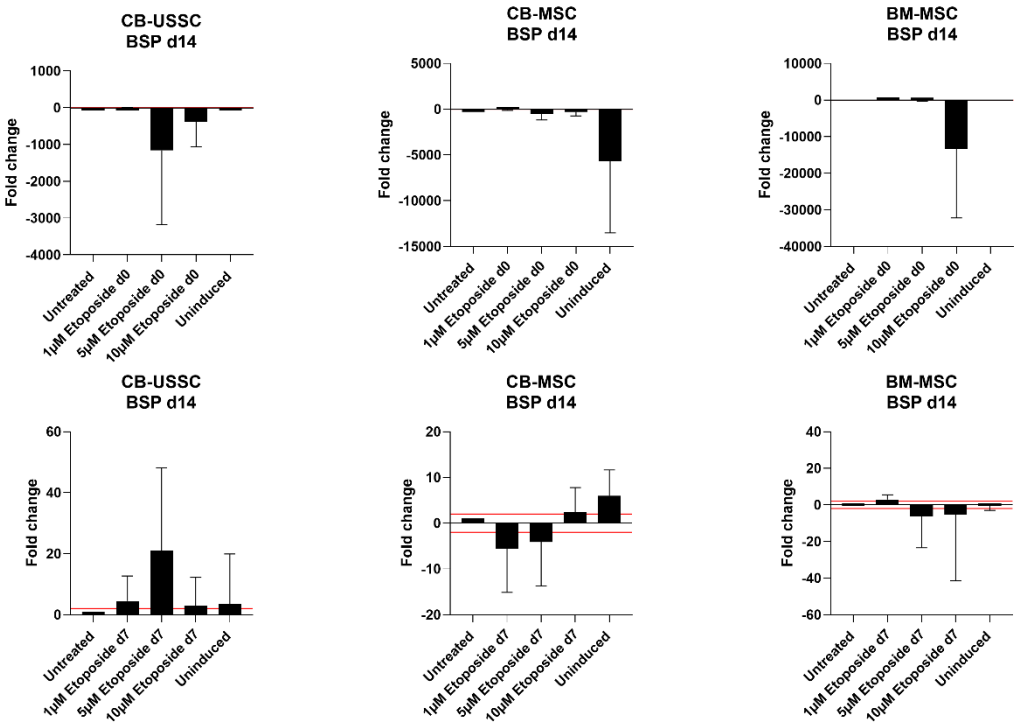

Figure 15: Expression pattern of BSP in CB-USSC, CB-MSC and BM-MSC on d14 after induction of osteogenic differentiation and 24 h treatment with etoposide on d0 or on d7. Fold change was calculated using the $2^{-\Delta\Delta CT}$ method relative to the untreated control and normalized to the reference gene RPL13a. The red lines indicate the significance thresholds. 2 represents a two-fold increase and -2 represents a two-fold decrease. Abbreviations: BSP, bone sialoprotein; BM, bone marrow; CB, cord blood; d, day; MSC, mesenchymal stromal cell; USSC, unrestricted somatic stem cell;

MNU treatment on d0 did not lead to any significant changes in the expression pattern of BSP whereas MNU treatment on d7 lead to a downregulation of BSP in CB-USSCs after 5mM MNU on d7 and an upregulation of BSP in CB-MSCs and BM-MSCs in a dose-dependent manner (Figure 14). Etoposide treatment on d0 lead to a downregulation of BSP in a dose-dependent manner in CB-USSCs and BM-MSCs but no significant changes in CB-MSCs. Etoposide treatment on d7 lead to the upregulation of BSP in CB-USSCs but not to significant changes in BSP expression in CB-MSCs and BM-MSCs (Figure 15).

Osteonectin (ON), osteocalcin (OCN) and osteopontin (OPN) are matrix proteins and markers for mature osteoblasts. ON is involved in the first mineralization steps of skeletal tissue. It is found in active osteoblasts and osteoprogenitors and in young osteocytes but not in aged and quiescent osteocytes thus being a marker for functional osteoblastic differentiation. OCN is the most abundant non-collagenous bone matrix protein and is synthesized by mature osteoblasts. OPN is also produced by mature osteoblasts but its role in bone formation and remodeling is not yet understood.

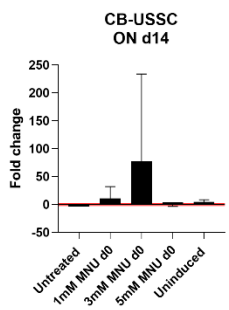
CB-USSC
ON d14
Fold change
250
200
150
100
50
0
-50
Untreated
1mM MNU d0
3mM MNU d0
5mM MNU d0
Uninduced

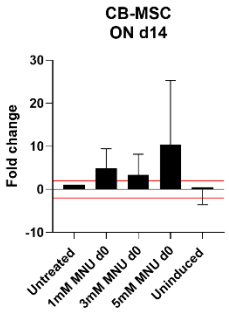
CB-MSC
ON d14
Fold change
30
20
10
0
-10
Untreated
1mM MNU d0
3mM MNU d0
5mM MNU d0
Uninduced

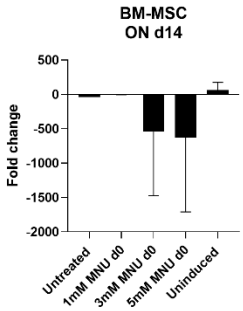
BM-MSC
ON d14
Fold change
500
0
-500
-1000
-1500
-2000
Untreated
1mM MNU d0
3mM MNU d0
5mM MNU d0
Uninduced

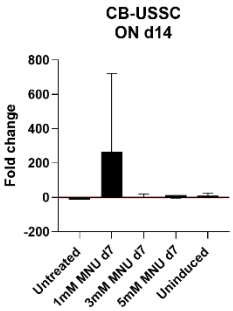
CB-USSC
ON d14
Fold change
800
600
400
200
0
-200
Untreated
1mM MNU d7
3mM MNU d7
5mM MNU d7
Uninduced

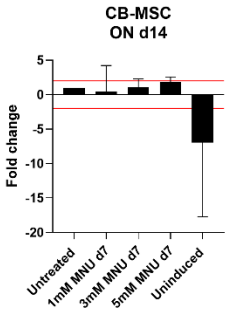
CB-MSC
ON d14
Fold change
5
0
-5
-10
-15
-20
Untreated
1mM MNU d7
3mM MNU d7
5mM MNU d7
Uninduced

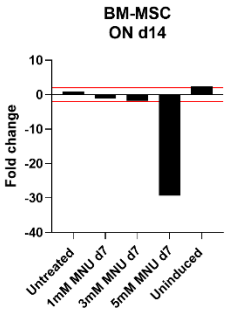
BM-MSC
ON d14
Fold change
10
0
-10
-20
-30
-40
Untreated
1mM MNU d7
3mM MNU d7
5mM MNU d7
Uninduced

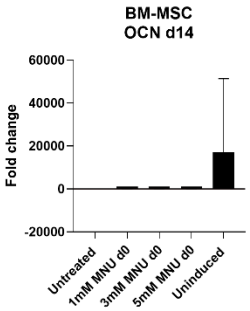
BM-MSC
OCN d14
Fold change
60000
40000
20000
0
-20000
Untreated
1mM MNU d0
3mM MNU d0
5mM MNU d0
Uninduced

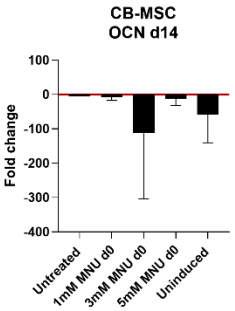
CB-MSC
OCN d14
Fold change
100
0
-100
-200
-300
-400
Untreated
1mM MNU d0
3mM MNU d0
5mM MNU d0
Uninduced

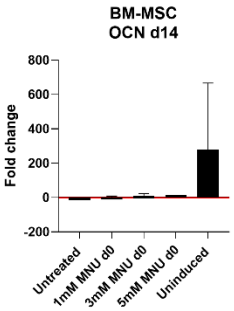
BM-MSC
OCN d14
Fold change
800
600
400
200
0
-200
Untreated
1mM MNU d0
3mM MNU d0
5mM MNU d0
Uninduced

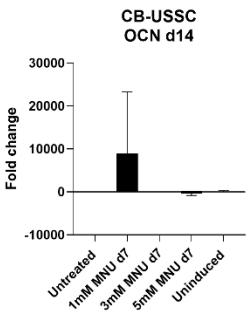
CB-USSC
OCN d14
Fold change
30000
20000
10000
0
-10000
Untreated
1mM MNU d7
3mM MNU d7
5mM MNU d7
Uninduced

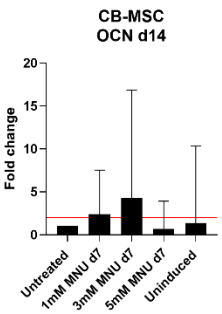
CB-MSC
OCN d14
Fold change
20
15
10
5
0
Untreated
1mM MNU d7
3mM MNU d7
5mM MNU d7
Uninduced

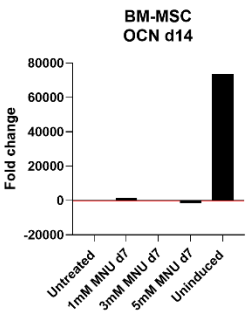
BM-MSC
OCN d14
Fold change
80000
60000
40000
20000
0
-20000
Untreated
1mM MNU d7
3mM MNU d7
5mM MNU d7
Uninduced

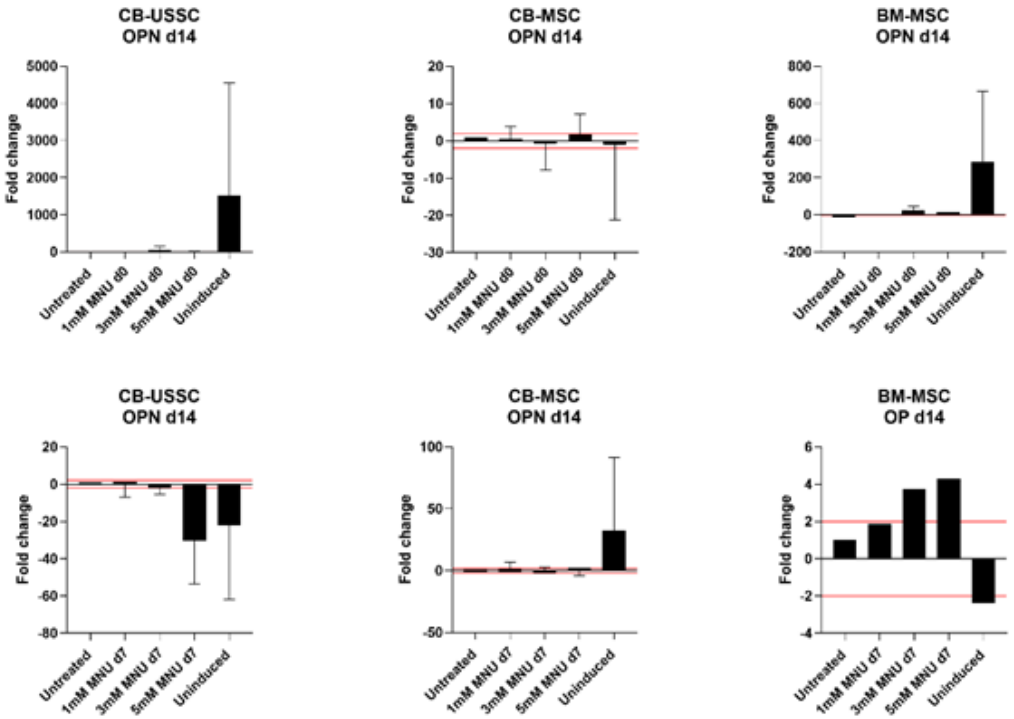

Figure 16: Expression pattern of ON, OCN and OPN in CB-USSC, CB-MSC and BM-MSC on d14 after induction of osteogenic differentiation and 1 h treatment with MNU on d0 or on d7. Fold change was calculated using the $2^{-\Delta\Delta CT}$ method relative to the untreated control and normalized to the reference gene RPL13a. The red lines indicate the significance thresholds. 2 represents a two-fold increase and -2 represents a two-fold decrease. Abbreviations: BM, bone marrow; CB, cord blood; d, day; MNU, N-methyl-N-nitrosourea; MSC, mesenchymal stromal cell; OCN, osteocalcin; ON, osteonectin; OPN, osteopontin; USSC, unrestricted somatic stem cell;

MNU treatment on d0 lead to the upregulation of ON in CB-USSCs and BM-MSCs and its downregulation in BM-MSCs whereas MNU treatment on d7 lead to ON downregulation after treatment with 5mM MNU in BM-MSCs but no significant changes in CB-USSCs and CB-MSCs. MNU treatment generally did not significantly affect OCN and OPN expression except treatment with 5mM MNU on d7 of CB-USSCs, which lead to the downregulation of OPN (Figure 16).

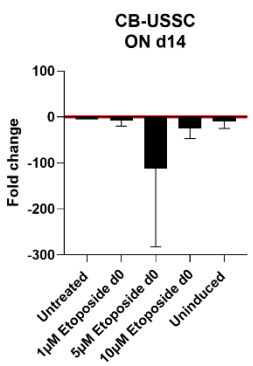
CB-USSC
ON d14
Fold change
100
0
-100
-200
-300
Untreated
1µM Etoposide d0
5µM Etoposide d0
10µM Etoposide d0
Uninduced

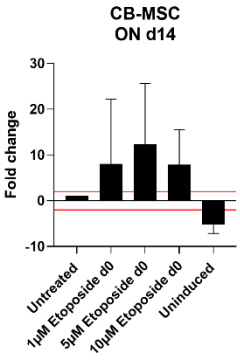
CB-MSC
ON d14
Fold change
30
20
10
0
-10
Untreated
1µM Etoposide d0
5µM Etoposide d0
10µM Etoposide d0
Uninduced

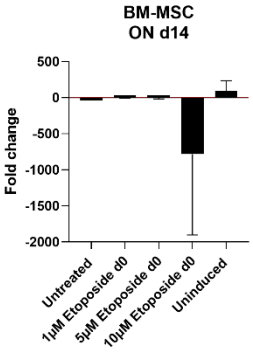
BM-MSC
ON d14
Fold change
500
0
-500
-1000
-1500
-2000
Untreated
1µM Etoposide d0
5µM Etoposide d0
10µM Etoposide d0
Uninduced

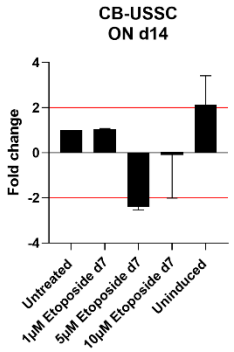
CB-USSC
ON d14
Fold change
4
2
0
-2
-4
Untreated
1µM Etoposide d7
5µM Etoposide d7
10µM Etoposide d7
Uninduced

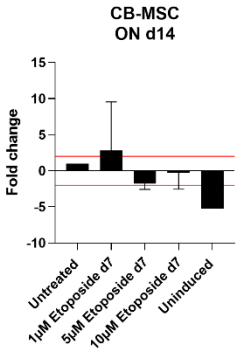
CB-MSC
ON d14
Fold change
15
10
5
0
-5
-10
Untreated
1µM Etoposide d7
5µM Etoposide d7
10µM Etoposide d7
Uninduced

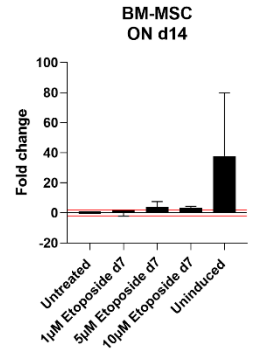
BM-MSC
ON d14
Fold change
100
80
60
40
20
0
-20
Untreated
1µM Etoposide d7
5µM Etoposide d7
10µM Etoposide d7
Uninduced

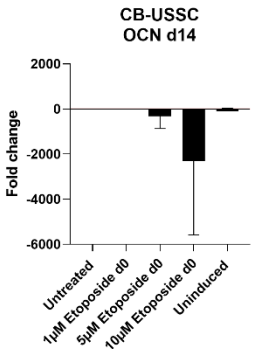
CB-USSC
OCN d14
Fold change
2000
0
-2000
-4000
-6000
Untreated
1µM Etoposide d0
5µM Etoposide d0
10µM Etoposide d0
Uninduced

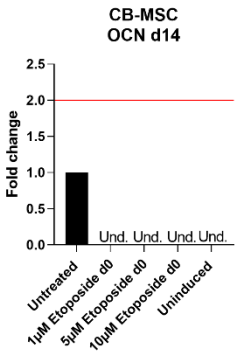
CB-MSC
OCN d14
Fold change
2.5
2.0
1.5
1.0
0.5
0.0
Und. Und. Und. Und.
Untreated
1µM Etoposide d0
5µM Etoposide d0
10µM Etoposide d0
Uninduced

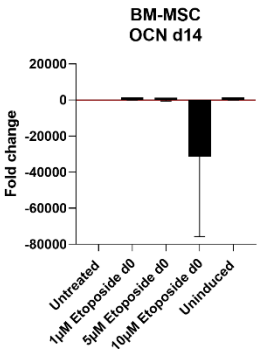
BM-MSC
OCN d14
Fold change
20000
0
-20000
-40000
-60000
-80000
Untreated
1µM Etoposide d0
5µM Etoposide d0
10µM Etoposide d0
Uninduced

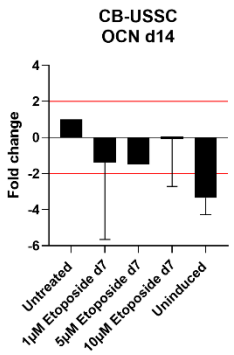
CB-USSC
OCN d14
Fold change
4
2
0
-2
-4
-6
Untreated
1µM Etoposide d7
5µM Etoposide d7
10µM Etoposide d7
Uninduced

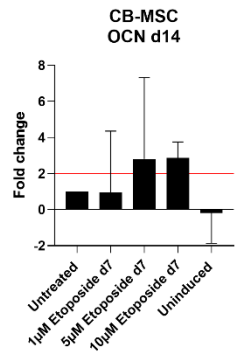
CB-MSC
OCN d14
Fold change
8
6
4
2
0
-2
Untreated
1µM Etoposide d7
5µM Etoposide d7
10µM Etoposide d7
Uninduced

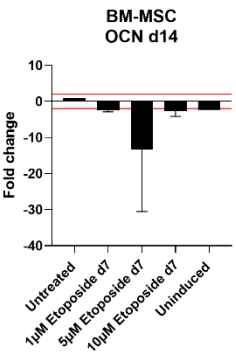
BM-MSC
OCN d14
Fold change
10
0
-10
-20
-30
-40
Untreated
1µM Etoposide d7
5µM Etoposide d7
10µM Etoposide d7
Uninduced

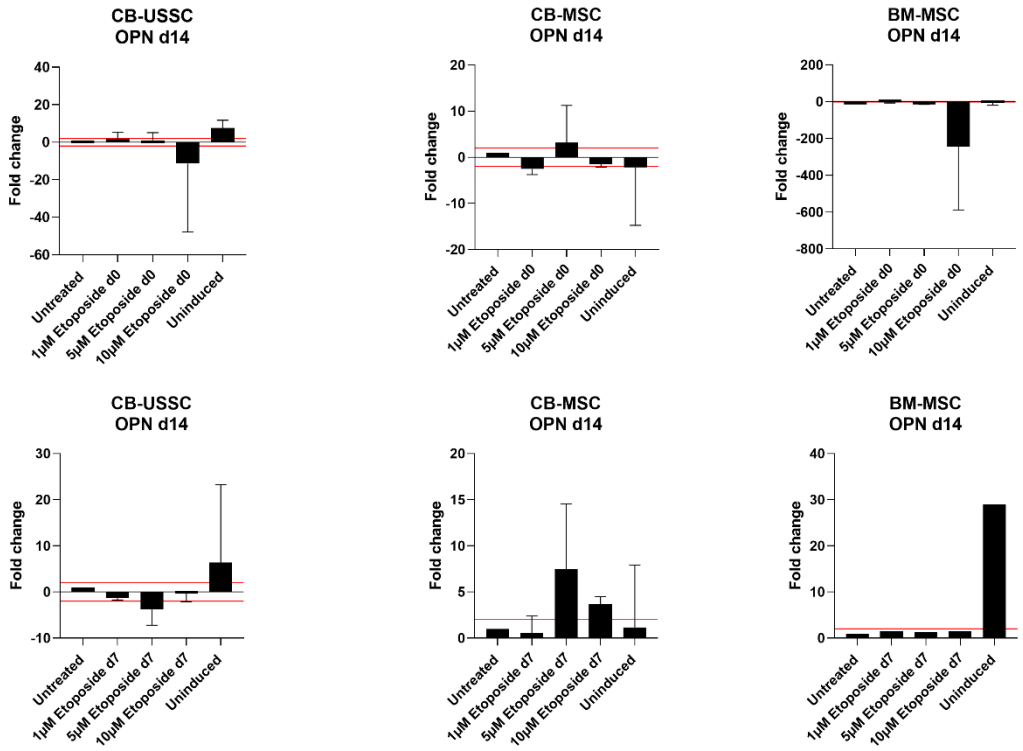

Figure 17: Expression pattern of ON, OCN and OPN in CB-USSC, CB-MSC and BM-MSC on d14 after induction of osteogenic differentiation and 24 h treatment with etoposide on d0 or on d7. Fold change was calculated using the $2^{-\Delta\Delta CT}$ method relative to the untreated control and normalized to the reference gene RPL13a. The red lines indicate the significance thresholds. 2 represents a two-fold increase and -2 represents a two-fold decrease. Abbreviations: BM, bone marrow; CB, cord blood; d, day; MSC, mesenchymal stromal cell; OCN, osteocalcin; ON, osteonectin; OPN, osteopontin; Und., undetermined; USSC, unrestricted somatic stem cell;

ON expression levels were not affected by etoposide treatment on d7 in all types of MSCs whereas etoposide treatment on d0 lead to the downregulation of ON in CB-USSCs and BM-MSCs, while it was upregulated in CB-MSCs in a dose-dependent manner. OCN expression levels were downregulated after treatment with the highest etoposide dose on d0 in CB-USSCs and BM-MSCs and no changes after treatment on d7 were recorded. OPN showed a decreased expression only after treatment with 10µM etoposide on d0 in BM-MSCs whereas etoposide treatment on d7 showed an increase in OPN expression in CB-MSCs in a dose-dependent manner (Figure 17).

Adipogenic Differentiation

To further assess the impact of genotoxic damage on adipogenic differentiation, the expression of key adipogenic markers PLIN1, ADIPOQ and FABP4 were assessed following exposure to MNU or etoposide at d0 or d7 of adipogenic differentiation in addition to C/EBPα, C/EBPβ and PPARγ shown in chapter 4.4. These genes play essential role in lipid storage, adipocyte function and terminal differentiation and their impairment may suggest potential disruptions in adipogenic commitment and maturation and can provide insights into how DNA damage may impair adipocyte formation and metabolic function.

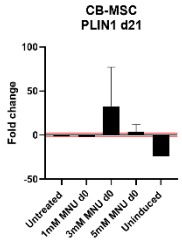
CB-MSC
PLIN1 d21
Fold change
100
50
0
-50
Untreated
1mM MNU d0
3mM MNU d0
5mM MNU d0
Uninduced

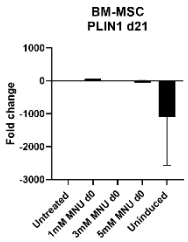
BM-MSC
PLIN1 d21
Fold change
1000
0
-1000
-2000
-3000
Untreated
1mM MNU d0
3mM MNU d0
5mM MNU d0
Uninduced

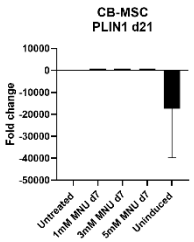
CB-MSC
PLIN1 d21
Fold change
10000
0
-10000
-20000
-30000
-40000
-50000
Untreated
1mM MNU d7
3mM MNU d7
5mM MNU d7
Uninduced

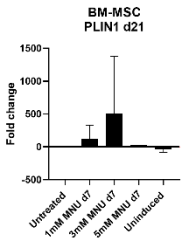
BM-MSC
PLIN1 d21
Fold change
1500
1000
500
0
-500
Untreated
1mM MNU d7
3mM MNU d7
5mM MNU d7
Uninduced

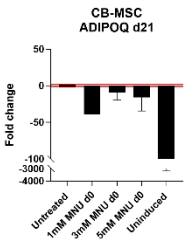
CB-MSC
ADIPOQ d21
Fold change
50
0
-50
-100
-3000
-4000
Untreated
1mM MNU d0
3mM MNU d0
5mM MNU d0
Uninduced

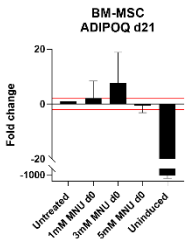
BM-MSC
ADIPOQ d21
Fold change
20
0
-20
-1000
Untreated
1mM MNU d0
3mM MNU d0
5mM MNU d0
Uninduced

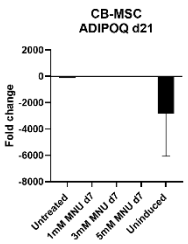
CB-MSC
ADIPOQ d21
Fold change
2000
0
-2000
-4000
-6000
-8000
Untreated
1mM MNU d7
3mM MNU d7
5mM MNU d7
Uninduced

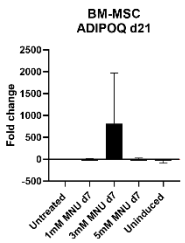
BM-MSC
ADIPOQ d21
Fold change
2500
2000
1500
1000
500
0
-500
Untreated
1mM MNU d7
3mM MNU d7
5mM MNU d7
Uninduced

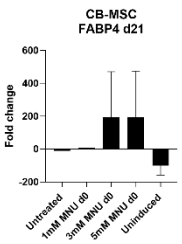
CB-MSC
FABP4 d21
Fold change
600
400
200
0
-200
Untreated
1mM MNU d0
3mM MNU d0
5mM MNU d0
Uninduced

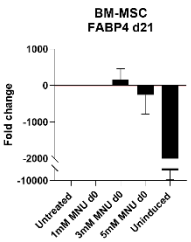
BM-MSC
FABP4 d21
Fold change
1000
0
-1000
-2000
-10000
Untreated
1mM MNU d0
3mM MNU d0
5mM MNU d0
Uninduced

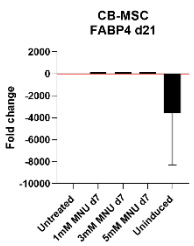
CB-MSC
FABP4 d21
Fold change
2000
0
-2000
-4000
-6000
-8000
-10000
Untreated
1mM MNU d7
3mM MNU d7
5mM MNU d7
Uninduced

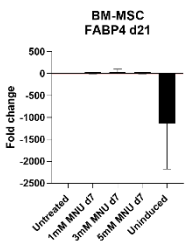
BM-MSC
FABP4 d21
Fold change
500
0
-500
-1000
-1500
-2000
-2500
Untreated
1mM MNU d7
3mM MNU d7
5mM MNU d7
Uninduced

Figure 18: Expression pattern of PLIN1, ADIPOQ and FABP4 in CB-MSC and BM-MSC on d21 after induction of adipogenic differentiation and 1 h treatment with MNU on d0 or on d7. Fold change was calculated using the $2^{-\Delta\Delta CT}$ method relative to the untreated control and normalized to the reference gene RPL13a. The red lines indicate the significance thresholds. 2 represents a two-fold increase and -2 represents a two-fold decrease. Abbreviations: ADIPOQ, adiponectin; BM, bone marrow; CB, cord blood; d, day; FABP4, fatty acid binding protein 4; MNU, N-methyl-N-nitrosourea; MSC, mesenchymal stromal cell; PLIN1, perilipin 1;

MNU treatment on d0 did not result in any changes in the expression pattern of PLIN1 whereas ADIPOQ was downregulated in CB-MSCs and upregulated in BM-MSCs and FABP4 was upregulated in CB-MSCs and downregulated in BM-MSCs. MNU treatment on d7 induced the upregulation of PLIN1 in BM-MSCs treated with 1mM and 3mM MNU whereas no changes in the expression of ADIPOQ and FABP4 both in CB-MSCs and BM-MSCs were recorded (Figure 18).

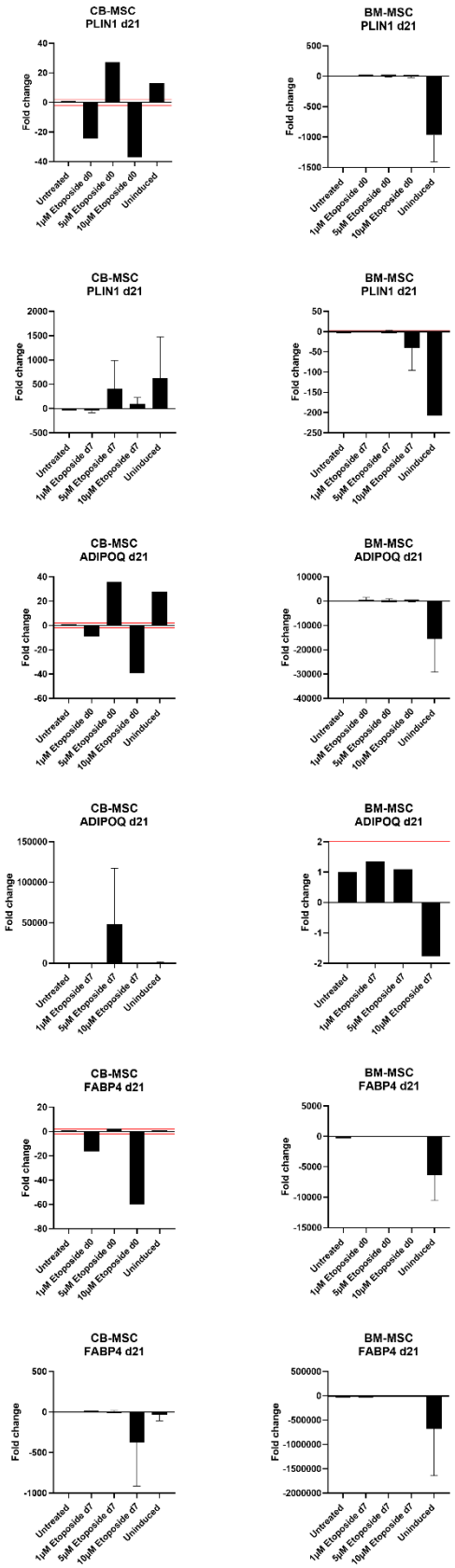

Figure 19: Expression pattern of PLIN1, ADIPOQ and FABP4 in CB-MSC and BM-MSC on d21 after induction of adipogenic differentiation and 24 h treatment with etoposide on d0 or on d7. Fold change was calculated using the $2^{-\Delta\Delta CT}$ method relative to the untreated control and normalized to the reference gene RPL13a. The red lines indicate the significance thresholds. 2 represents a two-fold increase and -2 represents a two-fold decrease. Abbreviations:

ADIPOQ, adiponectin; BM, bone marrow; CB, cord blood; d, day; FABP4, fatty acid binding protein 4; MSC, mesenchymal stromal cell; PLIN1, perilipin 1;

Etoposide treatment on d0 lead to a distorted expression of PLIN1, ADIPOQ and FABP4 in CB-MSCs but to no significant changes in the expression of these genes in BM-MSCs. Etoposide treatment on d7 resulted in the downregulation of PLIN1 in BM-MSCs and FABP4 in CB-MSCs after 10µM etoposide whereas no significant changes in the expression of ADIPOQ were registered.

4.6. Characterization and MNU treatment of MSCs differentiated from iPSCs (iMSCs) generated from CD34⁺ HSCs

To evaluate the developmental identity of iMSCs, the expression of HOX genes was analysed and compared to that of BM-MSCs, which express all four HOX gene clusters (A-D). HOX genes play a crucial role in embryonic development and positional identity and their expression patterns serve as molecular markers for the developmental origin of mesenchymal populations. The comparative analysis aimed to determine whether iMSCs exhibit a similar HOX code to BM-MSCs or if reprogramming and re-differentiation lead to altered or incomplete HOX gene expression.

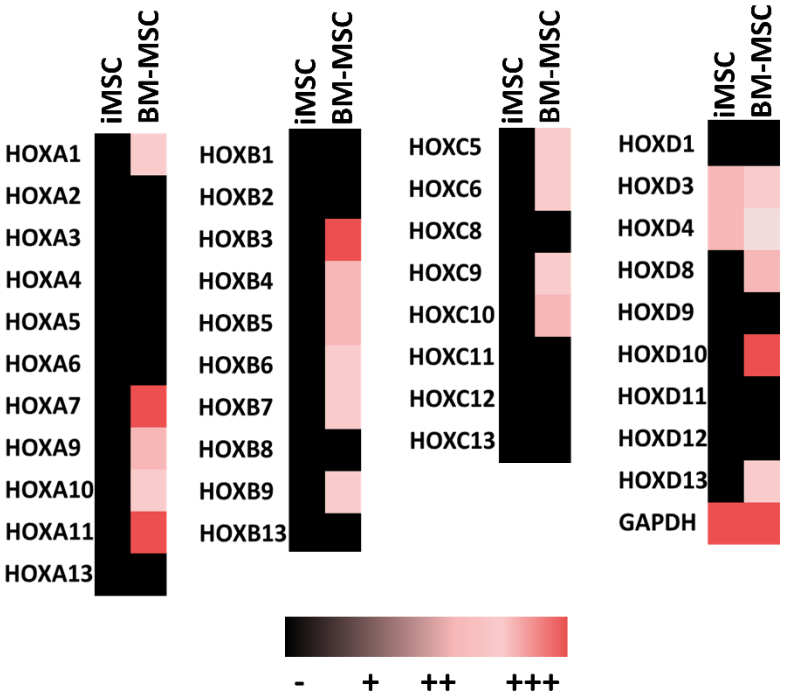

Figure 20: Comparison of HOX gene cluster (A-D) expression profiles of iMSCs to BM-MSCs. Analysis occurred by PCR followed by gel electrophoresis. Representative analysis of one cell line. GAPDH was used as a reference gene. Abbreviations: GAPDH, glyceraldehyde 3-phosphate dehydrogenase; HOX, homeobox; iMSC, MSCs differentiated from induced pluripotent stem cells; MSC, mesenchymal stromal cell;

As shown in Figure 20, the analyzed iMSCs exhibited no expression of genes from the HOXA, HOXB, or HOXC clusters, in contrast to BM-MSCs, which express all HOX clusters. Only a weak expression of HOXD3 and HOXD4 was detected in iMSCs, consistent with their low expression levels in BM-MSCs.

MSC secretome plays a critical role in the maintenance and regulation of HSCs within the bone marrow niche. MSCs secrete a diverse array of growth factors, cytokines and extracellular matrix proteins that influence HSC self-renewal, quiescence and differentiation. Key components of the MSC secretome such as vascular endothelial growth factor (VEGF) and angiopoietins provide essential signalling cues, which are essential for the preservation of hematopoietic homeostasis. Therefore, it is important to test whether the secretome of iMSCs is comparable to that of BM-MSCs as this could reveal their potential to functionally support HSCs in a similar manner.

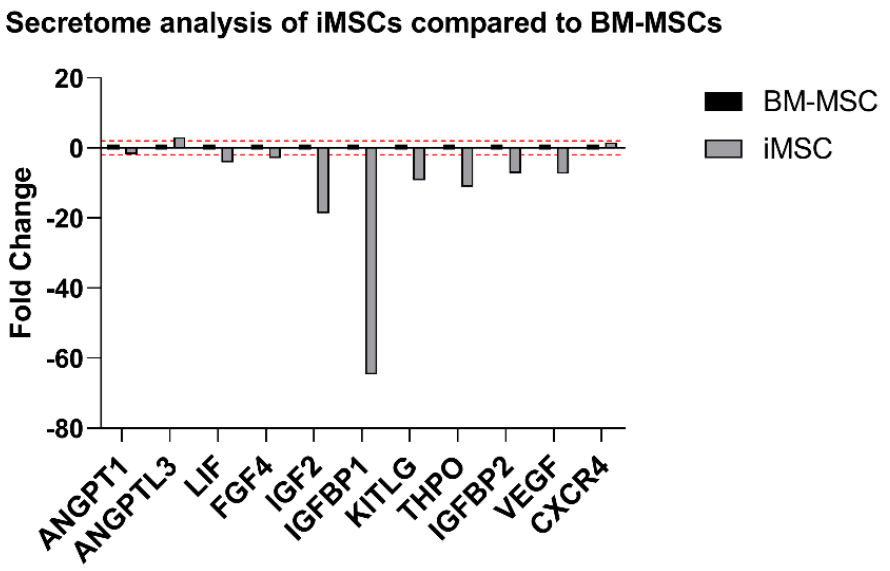

Figure 21: Comparative secretome analysis of iMSCs compared to BM-MSCs by RT-qPCR. Fold changes are normalized to BM-MSCs, represented as the baseline (Fold change = 1). Fold change was calculated using the $2^{-\Delta\Delta CT}$ method relative to the untreated control and normalized to the reference gene GAPDH. The red lines indicate the significance thresholds. 2 represents a two-fold increase and -2 represents a two-fold decrease. Abbreviations: ANGPT1, angiopoietin 1; ANGPTL3, angiopoietin like 3; CXCR4, CXC motif chemokine receptor 4; FGF4, fibroblast growth factor; IGF2, insulin-like growth factor 2; IGFBP1, insulin-like growth factor binding protein 1; IGFBP2, insulin-like growth factor binding protein 2; KITLG; tyrosine kinase receptor ligand; LIF, leukemia inhibitory factor; THPO, thrombopoietin; VEGF, vascular endothelial growth factor A;

Figure 21 illustrates a comparative analysis of the expression of secretome-related genes between BM-MSCs and iMSCs, as determined by RT-qPCR. iMSCs showed a downregulated RNA expression of several genes involved in tissue vascularization, cellular signaling and cell growth pathways. Notably, the expression of IGF2 and IGFBP1 is markedly reduced in iMSCs compared to BM-MSCs. Others genes such as KITLG, THPO, IGFBP2 and VEGF are moderately downregulated. Conversely, the expression of ANGPTL1, ANGPTL3 and FGF4 are comparable between two cell types. These results indicate a divergence in the secretory profile of iMSCs potentially reflecting their cellular origin and functional properties.

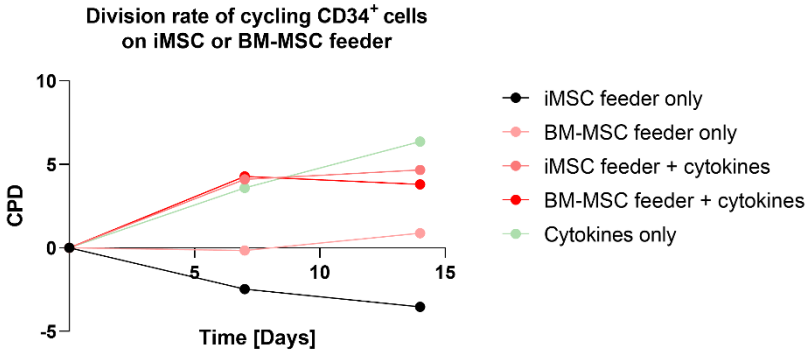

Figure 22: Division rate of cycling $CD34^+$ HSCs cultured on iMSC or BM-Feeder with or without cytokines (TPO, SCF, IL-6, FLT3-L, IL-3). To determine long-term growth kinetics, $CD34^+$ HSCs were counted after 7 and 14 days. CPDs are shown (Mean ± SD from N=2 for iMSCs and N=1 for BM-MSC). Abbreviations: BM-MSC, bone marrow mesenchymal stromal cell; CPD, cumulative population doubling time; iMSC, mesenchymal stromal cell from iPSC;

BM-MSCs are known to secrete factors that support the proliferation of CD34⁺ HSCs. This experiment aimed to determine whether iMSCs possess a similar ability to support CD34⁺ HSC proliferation. To investigate that, the division rate of cycling CD34⁺ cells was analyzed after co-culture on BM-MSC feeder and compared to iMSC feeder, either in the presence or in absence of broad-acting cytokines.

The results showed that CD34⁺ HSCs cultivated on the iMSC feeder alone exhibited the lowest division rates over 15 days of culture, with a declining proliferation capacity. In contrast, cells co-cultured on the BM-MSC feeder without cytokines demonstrated a moderate increase in division rates, reflecting the supportive role of BM-MSCs in promoting cell proliferation. When cytokines were added to the to the culture conditions, both iMSC and BM-MSC feeders supported similar levels of CD34⁺ HSCs proliferation, indicating that cytokines compensated the limited support provided by iMSCs alone. Interestingly, the highest proliferation rates were observed in the condition where CD34⁺ HSCs were cultured with cytokines only, without any feeder cells. This finding highlights the strong proliferative effect of cytokines on CD34⁺ HSCs.

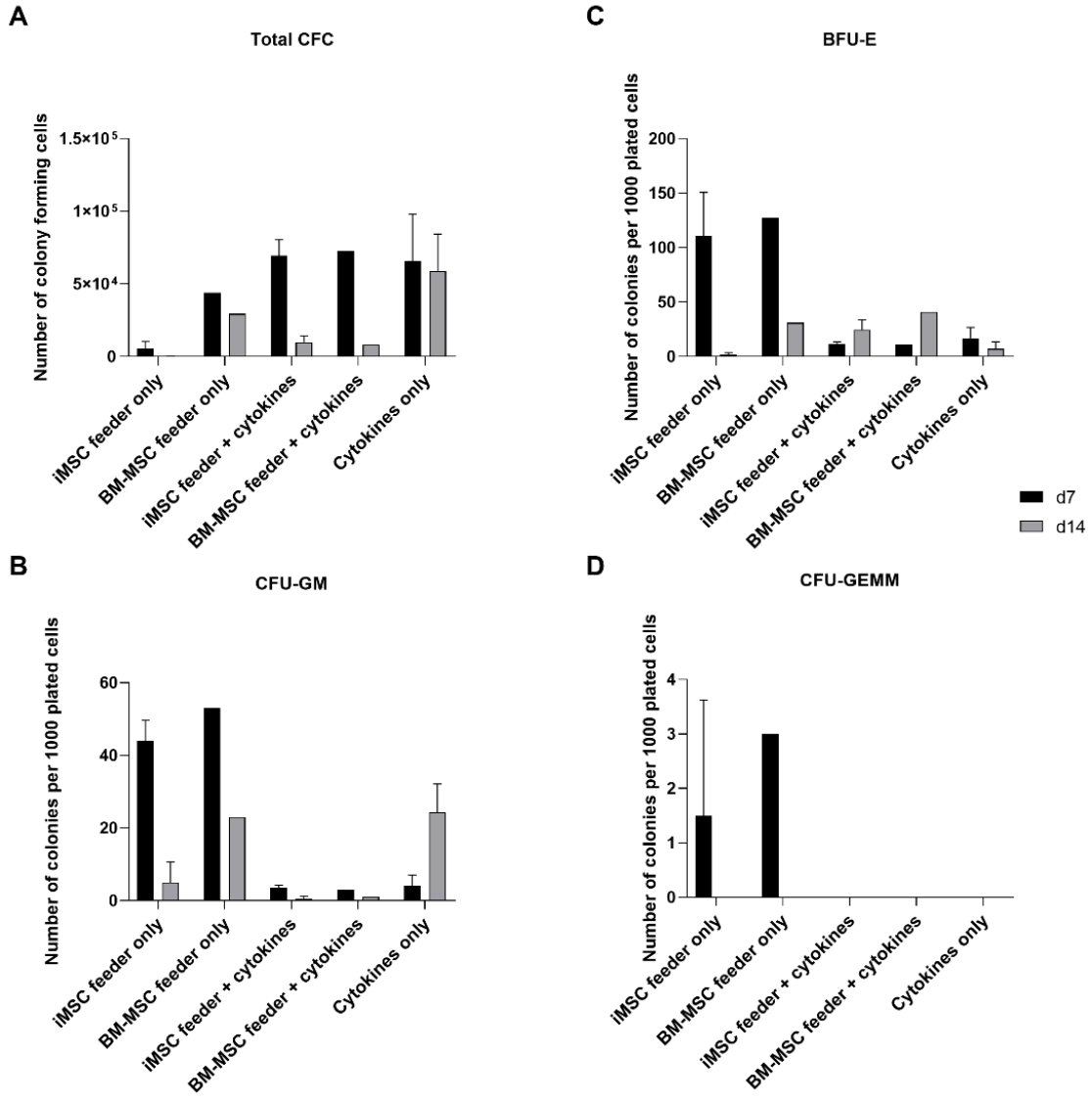

Figure 23: Colony-forming unit (CFU) assay of cycling CD34+ HSCs cultured on iMSC feeder compared to BM-MSC feeder. Cells were collected on d7 and d14 for CFU assay, which was evaluated 14 days after assay start. Total CFC (A), CFU-GM (B), BFU-E (C), and CFU-GEMM (D) were counted. Data represent the mean ± standard

deviation from two iMSC cell lines and one BM-MSC cell line. Abbreviations: BFU-E, burst-forming unit-erythroid; BM-MSC, bone marrow mesenchymal stromal cell; CFC, colony forming cell; CFU-GM, colony-forming unit-granulocyte-macrophage; CFU-GEMM, colony-forming unit-granulocyte-erythroid-macrophage-megakaryocyte; d, day;

Furthermore, the colony-forming capacity of $CD34^+$ HSCs cultured on iMSC feeder was analyzed and compared to that of cells cultured on BM-MSC feeder (Figure 23). The total colony forming cell numbers on d7 and d14 were significantly lower in the iMSC feeder-only condition compared to BM-MSC feeder-only condition on both days. However, the addition of cytokines rescued the total CFC numbers to comparable levels between the two feeder conditions.

Looking at specific colony types, CFU-GM numbers were similar between the iMSC feeder and BM-MSC feeder on d7 but were reduced on d14 in the iMSC feeder condition. Interestingly, in the presence of cytokines, CFU-GM numbers were much lower compared to the feeder-only conditions. The numbers of BFU-E colonies were comparable between the two feeder conditions on both d7 and d14, but a notable reduction was observed when cytokines were added. A similar trend was seen in CFU-GEMM colonies, where comparable numbers were counted between the iMSC and BM-MSC feeders, but the addition of cytokines resulted in lower colony numbers.

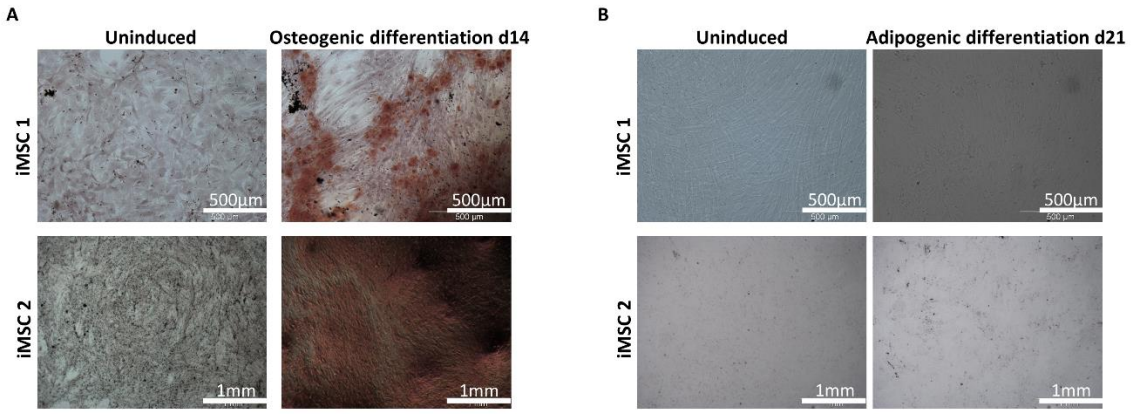

Figure 24: Differentiation of iMSCs into osteogenic and adipogenic Lineages. Comparison of uninduced and induced conditions at d14 for osteogenesis analyzed by Alizarin Red staining (A) and d21 for adipogenesis analyzed by Oil Red O staining (B).

The osteogenic and adipogenic differentiation potential of two iMSC cell lines was assessed using the standard protocols, which were also applied on MSCs (Figure 24). However, the differentiation observed in the iMSC cell lines was weaker compared to MSCs. Specifically, only iMSC2 cell line exhibited an osteogenic differentiation potential as evidenced by Alizarin staining on d14 but this was more limited compared to MSCs. In contrast, neither of the iMSC cell lines displayed any visible Adipogenic differentiation as seen after Oil Red O staining on d21.

To further investigate whether iMSCs respond differently to genotoxic stress compared to primary MSCs, iMSCs were subjected to MNU treatment under the same conditions used for BM-MSCs, CB-MSCs and CB-USSCs. Given the molecular and functional differences observed between iMSCs and primary MSC populations, the investigation focused on whether these discrepancies translate into altered sensitivity to DNA damage. This comparison could provide important insights into the genomic stability of iMSCs and their potential suitability for therapeutic applications, especially in genotoxic

environments such as those encountered in cancer therapies or chronic inflammatory conditions.

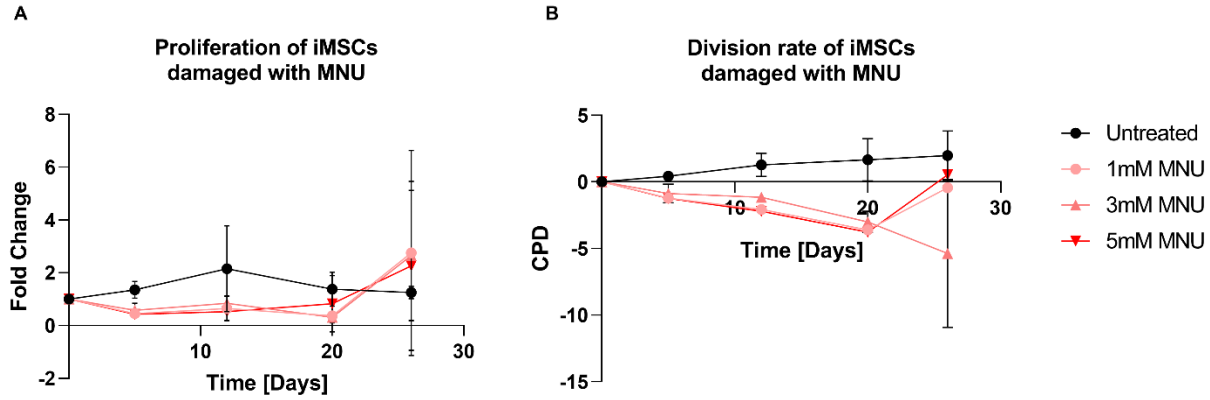

Figure 25: Dose-dependent impact of genotoxic stress induced by MNU on proliferation kinetics (A) and division rate of iMSCs (B). To determine long-term growth kinetics, cells were exposed to different doses of MNU (untreated, 1 mM, 3 mM and 5 mM), and cell numbers were counted after each passage. Fold change of cell numbers and CPDs are shown (Mean ± SD from N=2). Abbreviations: CPD, cumulative population doubling time; MNU, N-methyl-N-nitrosourea; iMSC, mesenchymal stromal cell from iPSC;

The results presented in Figure 25A and B illustrate the effects of MNU treatment on the proliferation and division rate of iMSCs. The fold change in cell numbers over time shows a dose-dependent suppression of proliferation with increasing MNU concentrations while untreated cells exhibit steady growth with a fold change maximum on day 20. Cells treated with MNU display reduced proliferation with the most pronounced suppression of proliferation recorded after treatment with 5 mM MNU where cell numbers fail to recover beyond initial seeding density. As measured by CPDs, Figure 25B further quantifies the impact of MNU on the division rate of iMSCs. Untreated cells maintain a positive CPD over 30 days, indicative of continued cell division. In contrast, cells treated with MNU show a marked decline in CPD with higher doses resulting in negative CPDs, suggesting cell death or a cessation of proliferation. This trend is particularly evident a 3 mM and 5 mM MNU where the division rates drop until day 20 and fail to recover. These results confirm the cytotoxic and anti-proliferative effects of MNU on iMSCs in a dose- and time-dependent manner.

5. Discussion

To maintain genomic integrity, cells have developed complex and finely tuned mechanisms and distinct responses to DNA damage. These mechanisms are particularly important in the context of cell proliferation, cell cycle progression and cell differentiation. Evaluating this impact of genotoxicity is crucial in toxicological risk assessment studies during pharmacological testing and safety profile testing of new drugs to ensure compliance with regulatory guidelines. DNA damage responses are tightly linked to the regulation of the cell cycle with the checkpoints preventing the propagation of DNA damage. For instance, proliferating cells, which are actively dividing have a different response than non-dividing quiescent cells [120, 121]. For this, testing cells at different states allows the understanding of how genotoxic agents affect cells dependently on their cell cycle status. Moreover, reaction to DNA damage differs between undifferentiated and more mature cells thus the importance of a comparative analysis of the effects of toxins on different cell types with different maturation status [122]. To obtain a comprehensive evaluation, it is crucial to conduct these assessments not only on different cell types, but also on cells derived from various sources to account the influence of developmental age. Furthermore, including cells from multiple donors helps minimizing the effects of donor variability ensuring that the findings are more representative and applicable across diverse populations. This multifaceted approach enhances the reliability of toxicological studies and contributes to more accurate safety evaluations of pharmaceutical compounds.

In this work, MNU and etoposide were selected as inducers of DSBs due to their well-characterized mechanism of action and of genotoxicity and their relevance in the experimental and clinical setting. MNU is a direct-acting alkylating agent that induces DNA damage primarily through the formation of O^6-methylguanine adducts, which can lead to replication stress and to the generation of DSBs, if left unrepaired. This compound is widely used in genotoxicity studies due to its ability to mimic endogenous and environmental mutagenic insults. Moreover, it has been established that nitrosamines are capable of crossing the placental barrier, raising concerns about their potential effects on embryonal development [123]. Exposure to nitrosamines during pregnancy could pose a significant risk to embryonic and fetal cells, which are highly proliferative and particularly sensitive to DSB-induced damage. Additionally, proper cell differentiation is crucial for normal embryo development thus the need of investigation genotoxin effect on the process of cell differentiation. Understanding how these compounds influence differentiation pathways can provide valuable insights into their potential role in developmental disorders and teratogenic effects. This is particularly relevant in the context of prenatal exposure, where low levels of genotoxic stress could have lasting consequences on tissue formation and organogenesis. Etoposide, on the other hand, is a topoisomerase II inhibitor that prevents the re-ligation of cleaved DNA strands resulting in DSB accumulation. It is a commonly used therapeutic agent thus the high relevance of understanding its effect not only on the targeted population but also on stem cell populations particularly in the context of therapy-related toxicity. The use of two agents with distinct mechanisms of action allowed for a comprehensive assessment of the DDR in iPSCs, HSCs, MSCs and iMSCs, and their capacity to maintain genomic integrity under various genotoxic stress conditions. IPSCs are considered as promising candidates for future applications especially in personalized regenerative medicine. However, their high mutational load,

genetic abnormalities and their unpredictable responses to DNA damage remain major concerns since little is known about the mechanisms governing their genomic stability under genotoxic stress.

Before assessing the effects of genotoxic stress, the iPSCs used in this work were first characterized by evaluating their capacity of expression of key pluripotency markers, namely OCT4a, SOX2, Nanog, TRA-1-60 and TRA-1-81. This step was essential to confirm that the used iPSCs maintained the undifferentiated state prior to treatment with genotoxins. These results confirmed robust expression of these markers, indicating that the iPSCs retained their pluripotent identity prior to treatment. This characterization was a critical prerequisite for our study, ensuring that any observed effects of genotoxic agents on differentiation or DNA damage response were not influenced by variability in pluripotency status. Moreover, our results show that the iPSCs, which served in this work as a negative control due to their embryonic-like age, are more sensitive to the genotoxic agents MNU and etoposide compared to MSCs. This heightened sensitivity may be aggravated by their higher rate of cell division compared to MSCs leading to high replicative stress, as well as their reported lower capacity for DSB repair [124]. Previous research has shown that despite rapid DDR, iPSCs are more prone to apoptosis, which appears as their primary defense mechanism to counteract and avoid genomic instability and de-differentiation [125]. IPSC source might also influence their DDR capacity as the intrinsic properties of the donor cells can affect genomic instability and stress response mechanisms. The iPSCs used in this work were derived from umbilical cord blood HSCs, which are known for their relatively low mutational burden and high proliferative potential. Additionally to their source, the reprogramming process of iPSCs induces oxidative stress, DSBs and other cellular changes that reduce their overall DNA repair efficiency. González et. al. showed that ectopic expression of reprogramming factors increases the level of phosphorylated histone H2AX as one of the earliest cellular responses to DSBs independently of viral integration or use of oncogenic transcriptional factors [126]. Moreover, the reprogramming process also promotes replication and oxidative stress. This can be counteracted by increasing the levels of the checkpoint kinase 1 (CHK1) or nucleoside supplementation [127]. The observed decrease in DDR gene expression with increasing MNU doses in iPSCs may be attributed to several factors namely the increasing cellular toxicity due to the high levels of genotoxic stress potentially damages the transcriptional machinery or causes widespread degradation of RNA. Severe DNA damage also leads cells towards apoptosis or necrosis thus globally downregulating transcription. Additionally, cells might employ protective mechanisms such as transcriptional shutdown to prevent errors caused by transcribing damaged DNA. Furthermore, high levels of DNA damage might overwhelm DDR pathways resulting in feedback inhibition or exhaustion of repair mechanisms further reducing their gene expression. The contrasting expression patterns observed between the 24 h and the 48 h analysis time points reflect the different stages of the cellular responses to MNU-induced genotoxic stress. The initial decrease in DDR gene expression at 24 h could be due to the acute toxicity of MNU, impairing transcriptional activity or causing widespread RNA degradation. In contrast, the increased expression of specific DDR genes such as XRRC5 and XRCC6 at 48 h may indicate activation of delayed repair mechanisms or adaptive stress responses as the cells attempt to cope with the accumulated DNA damage. 24 h after etoposide treatment, no significant changes in

the expression of several DDR genes could be assessed, which might have occurred since etoposide treatment was conducted for 24 h, which correlates with the population doubling time of the iPSCs. A replication cycle is necessary to arouse the effect of etoposide. A similar pattern to the MNU treated cells was observed 48 h after etoposide treatment, where the upregulation of FANCA1 and XRCC4 has been observed at low etoposide doses, which again might indicate a delayed upregulation of some DDR mechanisms. In this study, the impact of genotoxic damage induced by MNU or etoposide on iPSC mitochondria to determine whether DNA damage influences mitochondrial function was also assessed. Surprisingly, no significant differences were observed between the untreated and treated samples in terms of mitochondrial membrane potential, mass and overall activity, suggesting that the mitochondrial function remained largely unaffected by the genotoxic stress. This was in contrast to the clear morphological changes observed in the treated cells indicating that while nuclear and cytoskeletal integrity were compromised, mitochondrial homeostasis appeared to be maintained. These findings suggest a potential decoupling of mitochondrial function from genotoxic stress responses induced by MNU or etoposide in iPSCs or a high degree of mitochondrial resilience in these cells. Furda et. al. showed that mouse embryonic fibroblasts treated with oxidants showed a rapid loss of mitochondrial DNA and mitochondrial dysfunction whereas the alkylating agent methyl-methanesulfonate did not induce mitochondrial DNA loss, mitochondrial dysfunction or decreasing levels of nuclear-encoded mitochondrial subunits [128]. Further studies are however, necessary to explore whether alternative stress response mechanisms, such as metabolic adaptations or enhanced mitophagy, contribute to the maintenance of mitochondrial integrity under these conditions.

HSCs are particularly sensitive to DNA damage due to their pivotal role in hematopoiesis and their ability to self-renew. Most of the published studies investigate DDR of HSCs derived from adult sources such as the bone marrow or mobilized peripheral blood [120, 129]. In contrast, relatively few studies have examined the DDR of HSCs derived from neonatal sourced particularly those isolated from umbilical cord blood. Given the fundamental differences in the proliferative capacity, self-renewal potential, and metabolic state between neonatal and adult HSCs, it is crucial to understand how neonatal HSCs respond to genotoxic stress. Understanding these differences could provide valuable insights into age-related variations in HSC function and their implications for hematopoietic regeneration, transplantation and therapeutic applications.

HSCs play a crucial role in understanding the impact of genotoxic stress, as they are integral to blood regeneration and immune function. The $CD34^+$ HSCs used in this work were first characterized and differences were found in their expression of CD markers compared to other studies [130, 131]. CD38 expression was significantly upregulated suggesting that HSCs derived from cord blood are in a more differentiated state and lack short-term HSCs (ST-HSCs) or multipotent progenitors (MPPs) [132]. The $CD34^+$ $CD38^+$ population decreased over the time of expansion with an increase in the $CD34^+$ $CD38^-$ population. This raises the question of whether a substantial de-differentiation process occurred during cell culture or if the CD38 marker is a reversible surface marker as described by McKenzie and colleagues [133]. This characterization is essential to ensure reliable and biologically relevant results. As demonstrated by

Casorelli et al., $CD34^+$ hematopoietic stem and progenitor cells exhibit distinct DNA repair gene expression profiles compared to their more differentiated counterparts, which are $CD34^-$ [134]. In their study, freshly isolated $CD34^+$ cells displayed higher expression levels of genes involved in MMR, BER, and DSB repair, suggesting a more robust DNA damage response compared to $CD34^-$ cells [134]. However, these differences were not observed after $CD34^+$ cells were expanded in cytokine-rich medium, indicating that cellular state and culture conditions can significantly influence DNA repair capacity [134]. Furthermore, when exposed to MNU, cycling $CD34^+$ and $CD34^-$ cells exhibited similar levels of apoptosis, emphasizing that cellular sensitivity to DNA damage may depend on proliferation status rather than initial stemness markers [134]. These findings highlight the importance of thoroughly characterizing our cell populations, as variations in gene expression, differentiation state, and cycling status can significantly impact their response to genotoxic stress. Understanding these factors allows for a more precise interpretation of experimental outcomes and ensures that any observed effects are attributed to the intended experimental conditions rather than intrinsic cellular differences.

The results indicate that HSCs exhibit increased sensitivity to genotoxic agents such as MNU and etoposide. This heightened sensitivity could be linked to their high proliferative capacity and the need for tight regulation of cell cycle progression to ensure proper hematopoietic function. Furthermore, the DDR mechanisms in HSCs may differ from those of other progenitor cells, potentially leading to a reduced ability to cope with genotoxic stress. In this study, a comparative analysis of the genotoxic effects on $CD34^+$ cells derived from the neonatal cord blood by distinguishing between quiescent and cycling populations was conducted. Quiescent cells are generally more resistant to genotoxic stress due to their reduced replication-associated damage, whereas cycling cells, which are actively proliferating, may be more vulnerable due to increased DNA replication stress and a higher likelihood of replication fork collapse. To gain insights into the impact of cell cycle status on sensitivity to genotoxic agents, these two populations were compared.

MNU treatment of cycling $CD34^+$ HSCs resulted in the abrogation of cell replication accompanied by an increase in the Sub-G_1 population and dose-independent cell cycle stop, which remained persistent until 7 days post-treatment. Additionally, several DDR genes were upregulated e.g. H2AX, BRCA2, XRCC6 and LIG4 in an attempt to reduced damage accumulation induced by MNU. The severity of the damage persisted for 5 days and finally resulted in complete cell death at high MNU doses, which comes in accordance with the gene expression showing the upregulation of the pro-apoptotic gene BID and the autophagy-related gene BECN1. Cycling cells treated with etoposide showed dose-dependent reactions with cells treated with low concentrations showing a decrease in proliferation capacity and cells treated with high concentrations showing an apoptotic morphology that manifests by the appearance of apoptotic bodies and vesicles, a reduced replicative capacity and a shift from the Sub-G_1 to the S/G_2 phase. These findings come in accordance with the results of Tao and colleagues, who showed that cycling cord blood $CD34^+$ HSCs utilize pro-apoptotic pathways such as P53, BAX, FAS and TRAIL in response to etoposide treatment in order to arrest cell cycle progression at several checkpoints stop proliferation and induce apoptosis but also induce pro-survival pathways e.g. BCL-2 and CDKN1A suggesting a dose- and

severity-dependent response controlling the cell fate [135]. Beside CDKN1A upregulation, which correlates with protection from apoptosis by the promotion of cell cycle arrest in both G_1/S- and G_2/M-transition, an increase in CCDN1 was registered, which in turn correlates with the induction of the re-entry into cell cycle after the formerly registered cell cycle arrest [136, 137]. This interplay between pro-apoptotic and pro-survival genes in response to etoposide along with the dose-dependent decrease of proliferation and the registered cell cycle arrest might be attributed to the existence of cells at different cycle status in the culture. The initial response of the still quiescent or G_1-phase cells was a cell cycle arrest by the upregulation of CDKN1A, whereas the cycling cells rather induce pro-apoptotic genes. This might explain the recovery of the cycling cells after etoposide exposure, originating from the protected quiescent cell fraction that could replenish the stem cell pool. A potential experiment to further investigate this would involve the synchronization of the cell cycle before exposure to the DNA damaging agents. This can be achieved by various methods such as serum starvation for a G_0/G_1 block or nocodazole treatment for a G_2/M arrest. However, it is important to consider that cell synchronization itself might introduce additional stress, which in turn may influence the response to genotoxin damage potentially confounding the results of genotoxicity studies. DSBs were analyzed using the γH2AX/53BP1 markers that revealed a high accumulation of DSB breaks both in cycling cells treated with MNU and etoposide and nearly all cells were affected. In the etoposide-treated cells, these lesions started already after 1 h and persisted only for 24 h. This rapid loss of foci either implies that the DSBs have been repaired or the cells have undergone apoptosis to reduced the impact of the damage. This however does not come in accordance with results deduced from cells exposed to irradiation, where γH2AX/53BP1 foci formation kinetics were fast, already appeared after 1-3 min and disappeared in the first 48 h. Additionally to cells with co-localizing γH2AX/53BP1 foci, also cells with single foci were registered. This confirms the suggestion of De Feraudy and colleagues postulating that γH2AX foci alone might not be the accurate marker for DSBs [138]. Its coupling with 53BP1 ensures a more precise identification of DSBs since it is a key protein involved in NHEJ and is more selective for true DSBs thus providing additional structural information about the nature of the break.

Quiescent $CD34^+$ HSCs exhibit distinct DDR mechanisms when exposed to genotoxic damage. Depending on the type of damage and the mechanism of action of the damaging agent, they either attempt to repair the damage of initiate apoptosis if the risk of passing mutations to progeny is important. Quiescent $CD34^+$ HSCs studied in this work exhibited a dose-dependent sensitivity to MNU. Exposure to high doses of MNU affects cell proliferation and disrupts cell cycle progression leading to a cell cycle arrest in G_1 subsequently undergoing apoptosis when entering the S-phase likely as a protective measure to prevent the transmission of damage to progeny. This increase in apoptotic populations correlated with the upregulation of pro-apoptotic genes such as CAS3, CAS9 and FAS. In contrast to MNU, quiescent $CD34^+$ HSCs appear to be largely protected from the cell cycle-specific agent etoposide. Etoposide primarily affects actively cycling cells. For this, only cells that have entered the cell cycle during the 24 h treatment period have been impacted. Morphological analysis and cell numbers did not indicate significant damage to quiescent cells and apoptosis assays showed only a low dose-dependent increase in apoptotic cells. This aligns with the dose-dependent upregulation of CDKN1A and FAS under all conditions, suggesting

that etoposide exposure induces cell cycle arrest and promotes apoptosis in quiescent CD34$^+$ HSCs. However, immunocytochemical staining for γH2AX and 53BP1 foci revealed the induction of double-strand breaks (DSBs) at all tested etoposide concentrations. A high number of γH2AX foci were detected, but only about half as many 53BP1 foci were observed. This raises the question of whether DDR pathways are fully engaged in cells where γH2AX and 53BP1 co-localization is present, warranting further analysis of DDR-related proteins at the protein level. The abundance of γH2AX foci without corresponding 53BP1 foci suggests that once a DSB is detected in quiescent cells, the apoptotic pathway may be preferentially activated rather than DNA repair mechanisms. This aligns with previous findings that non-chromatin-bound γH2AX can sensitize cells to apoptosis, raising the possibility that γH2AX is not solely a marker of DSBs but may also play a role in apoptosis signaling.

In terms of differentiation capacity, cycling CD34$^+$ HSCs displayed a significant reduction in multipotent progenitors (CFU-GEMM) one day post MNU treatment suggesting that multipotent progenitors might be particularly susceptible to MNU-induced damage at this early stage. However, this effect did not persist in later time points, indicating a potential recovery or compensatory mechanism over time. Similarly, cycling CD34$^+$ cells treated with etoposide showed a significant reduction in total CFC numbers, particularly on d3 and d7 post-treatment, while no immediate effect was observed on d1. The impact on specific progenitor lineages varied: granulocyte-macrophage (CFU-GM) colonies were consistently reduced across all conditions, while erythroid (BFU-E) colonies exhibited a dose-dependent decrease followed by a partial recovery by d7. Interestingly, CFU-GEMM colonies showed only a slight initial decrease on d1 but no significant difference was detected in later time points. Our findings also indicate that the colony-forming capacity of quiescent CD34$^+$ HSCs remained largely unaffected by MNU treatment over a period of 7 days. The ability of these cells to form colonies across different hematopoietic lineages including erythroid (BFU-E), granulocyte-macrophage (CFU-GM) and multipotent progenitors (CFU-GEMM) was not significantly impaired. This suggests that quiescent HSCs may possess intrinsic protective mechanisms against immediate genotoxic stress or that the extent of MNU-induced damage within this timeframe was insufficient to compromise their colony-forming ability. Similarly, etoposide treatment of quiescent CD34$^+$ HSCs did not significantly alter their differentiation potential as no notable effects on total CFC numbers or specific progenitor colonies were observed. These results indicate that quiescent HSCs exhibit a remarkable resistance to both MNU and etoposide, at least within the tested doses and observation period. Together, these results highlight the differential sensitivity of cycling and quiescent CD34$^+$ HSCs to genotoxic agents. While quiescent cells appear more resistant, possibly due to their inherit DDR mechanisms and reduced reliance on replication-dependent repair pathways, cycling cells are more vulnerable particularly at later analysis time points where damage accumulation might interfere with proliferation and differentiation. The observed recovery trends in certain progenitor populations further suggest that HSCs may activate compensatory mechanisms that allow for the maintenance of hematopoietic function despite genotoxic stress. These findings underscore the importance of considering cell cycle status when evaluating the impact of genotoxins on HSCs and their potential long-term effects on hematopoiesis.

In vivo, MSCs play a crucial role in supporting HSCs within the bone marrow niche. To investigate how this support is affected under genotoxic stress, HSCs were cultured on a BM-MSC feeder layer, which was either untreated or also exposed to MNU or etoposide and assessed their proliferation. Our findings revealed that when the MSC feeder was also damaged by genotoxins, HSCs exhibited a proliferation response similar to that of HSCs cultured without a feeder, suggesting that a compromised MSC layer fails to provide its usual protective support. In contrast, when HSCs were cultivated on a healthy MSC feeder, even those exposed to genotoxic treatment maintained a proliferation rate comparable to untreated HSCs. This suggests that an intact MSC feeder may secrete additional cytokines or growth factors that enhance HSC proliferation and mitigate the detrimental effects of genotoxic stress. These results highlight the importance of a functional MSC microenvironment in maintaining HSC resilience and suggest that the protective role of MSCs is compromised when they themselves are subjected to genotoxic damage.

The results of this study also provide important insights into the effects of genotoxic stress induced by MNU or etoposide on different types of MSCs. Our findings demonstrate that MSCs exhibit a certain level of resistance to the genotoxic agents MNU and etoposide compared to the iPSCs, which displayed significantly higher sensitivity, as reflected in their lower IC_{50} values. This observation aligns with previous studies that have reported increased genomic instability in pluripotent stem cells compared to more differentiated cell types. The relative resistance of MSCs may be attributed to their intrinsic DNA repair mechanisms, which have been suggested to be more robust in adult stem cells, compared to pluripotent cells and may be due to their prolonged lifespan acquiring high amounts of damage thus the need of specific damage coping mechanisms. Lützkendorf and colleagues have shown that this resistance in MSCs is associated with an induction of P53 and P21, proliferation arrest or temporary G_2/M cell cycle arrest upon genotoxic damage [139].

Interestingly, variations in sensitivity among different MSC subtypes were observed, with CB-MSCs and BM-MSCs showing distinct responses to genotoxic stress. 24 h and 48 h after MNU or etoposide damage, BM-MSCs showed a less amount of damage compared to CB-USSCs and CB-MSCs, as shown by comet assay. This variability suggests that the tissue of origin and the developmental age may play a role in determining the extent of DNA damage and repair capacity, a notion supported by prior studies highlighting differences in proliferation rates, differentiation potential and senescence onset among MSC populations. While our findings are consistent with these reports, further mechanistic studies are needed to elucidate the molecular pathways underlying these differences.

The multilineage potential of MSCs makes them a valuable model for assessing the impact of drugs and toxins on cell differentiation. However, this aspect has not yet been extensively investigated. Exposure to genotoxic agents on d0 before the initiation of osteogenic differentiation, led to more pronounced effects compared to treatment on d7, except in the case of etoposide-treated CB-MSCs. Despite this, no significant changes were observed in the mRNA expression levels of RUNX2, OSX, BMP2 and BMP4. This contrasts with previous findings suggesting that RUNX2 plays a role in the DNA damage response by regulating H2AX phosphorylation and promoting its accumulation following genotoxic stress in smooth muscle cells, a process linked to

vascular calcification [140]. Etoposide treatment on d0 and d7 lead to the downregulation of BMP2 and BMP4, which are major regulators during osteogenic differentiation. Moreover, genotoxic treatment applied on d0 before the initiation of adipogenic and chondrogenic differentiation did not significantly affect the differentiation outcomes in these lineages. In contrast, osteogenic differentiation appeared to be more sensitive to early DNA damage, suggesting that adipogenic and chondrogenic pathways may possess a higher resistance to genotoxic stress at early differentiation stages. This resilience could be attributed to lineage-specific differences in DNA repair mechanisms or stress response pathways that help protect these differentiation processes from early-stage damage. Supporting this idea, no notable reduction was observed in the expression of key adipogenic genes including CEBPα, CEBPβ and PPARγ. However, CB-MSCs exhibited greater sensitivity to genotoxic treatment compared to CB-USSCs and BM-MSCs, indicating an intrinsic vulnerability that may stem from variations in DNA repair capacity or stress response pathways. This heightened sensitivity of CB-MSCs underscores the importance of considering cell source-specific and age-related factors when assessing the effects of genotoxins on MSC differentiation potential. Interestingly, administering MNU or etoposide on d7 after the initiation of the differentiation process had a generally lower impact on MSC differentiation potential compared to treatment on d0. This suggests that cells may develop protective mechanisms during the later stages of differentiation such as transcription-coupled repair or nucleotide excision repair. Among the tested conditions, only MNU treatment on d7 affected the osteogenic differentiation, particularly in CB-MSCs, highlighting their distinct sensitivity to DNA damage even at later differentiation stages. In contrast, no significant effects were observed in CB-USSCs and BM-MSCs across any differentiation lineage following treatment with MNU or etoposide on d7.

Chondrogenic differentiation remained largely unaffected by genotoxic stress, whether applied on d0 or d7, suggesting that this lineage may have a greater intrinsic resistance to DNA damage compared to the osteogenic pathway. This resilience could be attributed to an enhanced ability to repair DNA damage or a distinct dependence on DDR mechanisms such as NHEJ, which may help counteract the effects of genotoxic agents. Additionally, the ECM produced during chondrogenic differentiation might play a protective role when genotoxic treatment was applied on d7. Composed of proteoglycans, collagen and structural proteins, this dense matrix may serve as a physical shield, limiting the penetration and diffusion of harmful agents, thereby reducing their effective concentration within the cells. Moreover, the ECM could influence cellular signaling pathways, modulating the response to DNA damage and further reinforcing the resilience of chondrogenic cells at later differentiation stages. This protective effect of the ECM may help explain why chondrogenic differentiation appears to be less affected by genotoxic stress compared to other lineages, particularly during later time points.

These results enhance the understanding of MSC differentiation and its therapeutic relevance by shedding light on the impact of genotoxic agents on both undifferentiated and differentiated MSCs. By examining these effects at different stages of differentiation, it was shown that damage induced by MNU and etoposide not only compromises cell viability and proliferation but may also interfere with the ability of MSCs to successfully complete their differentiation process, which is an essential

factor for their potential use in tissue repair and regeneration. Furthermore, our findings highlight the greater resilience of differentiated MSCs compared to their undifferentiated counterparts, emphasizing that the timing of genotoxic exposure plays a crucial role in determining its effects. These insights are particularly relevant for drug testing and safety evaluations, as they underscore the need for considering differentiation stage-specific responses. A deeper understanding of these mechanisms will contribute to the refinement of in vitro models that more accurately replicate physiological conditions.

Despite these insights, our study has certain limitations. The in vitro nature of our experiments does not fully recapitulate the complex microenvironment of MSCs in vivo, where interactions with niche factors and immune cells may influence their response to genotoxic agents. Additionally, while DNA damage responses were assessed, further work is required to evaluate the long-term consequences of genotoxic stress, such as potential senescence, apoptosis, or malignant transformation. Future studies should aim to integrate in vivo models and single-cell sequencing approaches to provide a more comprehensive understanding of MSC behavior under genotoxic stress.

Overall, our study contributes to the growing body of literature on MSC biology by highlighting their differential responses to genotoxic agents and emphasizing the need for careful evaluation of their genomic stability in therapeutic settings. These findings provide a basis for further investigations into the molecular mechanisms governing MSC resistance to DNA damage and offer important considerations for their clinical application.

The characterization of iMSCs revealed notable differences compared to primary MSC populations, which are crucial to consider when evaluating their therapeutic applicability. Unlike BM-MSCs and CB-MSCs, which express HOX genes, iMSCs are HOX-negative, a feature they share with CB-USSCs. This lack of HOX gene expression may contribute to the impaired differentiation potential observed in these cells, as previously described for CB-USSCs, which also fail to undergo adipogenic differentiation. Consistently, iMSCs displayed a marked inability to differentiate into adipocytes and exhibited only minimal osteogenic differentiation under the same conditions successfully applied to BM-MSCs and CB-MSCs. Furthermore, the cytokine secretion profile of iMSCs was altered, with several key cytokines downregulated compared to BM-MSCs. This reduced cytokine expression may underlie the decreased hematopoietic support function of iMSCs, as reflected by significantly lower CFC numbers when $CD34^+$ HSCs were cultured on the iMSC feeder. Altogether, these findings highlight that although iMSCs share phenotypic similarities with MSCs, their molecular and functional discrepancies, particularly in HOX gene expression, cytokine secretion, and differentiation capacity must be carefully considered before proposing them as reliable alternatives for clinical applications.

In the context of therapeutic applications, the accurate identification of iMSCs is crucial to ensure their reliability and effectiveness in clinical settings. Proper characterization of these cells helps to distinguish them from other stem cell types and ensures consistency in their functional properties. Additionally, establishing precise and standardized differentiation protocols is essential to achieve reproducible and

trustworthy outcomes. Without well-defined guidelines, variations in differentiation efficiency and cellular behavior could compromise the safety and efficacy of iMSC-based therapies. Therefore, rigorous validation of identification markers and optimization of differentiation protocols are fundamental steps to enhance the clinical applicability of iMSCs and maximize their therapeutic potential.

6. List of Figures

7. List of Tables

8. References

1. Wolff, I.A. and A.E. Wasserman, *Nitrates, Nitrites, and Nitrosamines.* Science, 1972. **177**(4043): p. 15-19.
2. GRAY, J.I. and L.R. DUGAN JR., *FORMATION OF N-NITROSAMINES IN LOW MOISTURE SYSTEMS.* Journal of Food Science, 1974. **39**(3): p. 474-478.
3. Keeper, L.K. and P.P. Roller, *N-Nitrosation by Nitrite Ion in Neutral and Basic Medium.* Science, 1973. **181**(4106): p. 1245-1247.
4. Abe, Y., et al., *Temperature-Dependent Formation of N-Nitrosodimethylamine during the Storage of Ranitidine Reagent Powders and Tablets.* Chem Pharm Bull (Tokyo), 2020. **68**(10): p. 1008-1012.
5. Lundberg, J.O. and E. Weitzberg, *Biology of nitrogen oxides in the gastrointestinal tract.* Gut, 2013. **62**(4): p. 616-29.
6. Lu, Y. and A.I. Cederbaum, *CYP2E1 and oxidative liver injury by alcohol.* Free Radic Biol Med, 2008. **44**(5): p. 723-38.
7. Beranek, D.T., *Distribution of methyl and ethyl adducts following alkylation with monofunctional alkylating agents.* Mutat Res, 1990. **231**(1): p. 11-30.
8. Kolarić, K., *Combination chemotherapy with 1-methyl-1-nitrosourea (MNU) and cyclophosphamide in solid tumors.* Zeitschrift für Krebsforschung und Klinische Onkologie, 1977. **89**(3): p. 311-319.
9. Clark, A.S., et al., *Antitumor imidazotetrazines. 32. Synthesis of novel imidazotetrazinones and related bicyclic heterocycles to probe the mode of action of the antitumor drug temozolomide.* J Med Chem, 1995. **38**(9): p. 1493-504.
10. Zak, P., K. Kleibl, and F. Laval, *Repair of O6-methylguanine and O4-methylthymine by the human and rat O6-methylguanine-DNA methyltransferases.* J Biol Chem, 1994. **269**(1): p. 730-3.
11. Kleihues, P. and P. Margison, *Brief Communication: Carcinogenicity of N-Methyl-N-nitrosourea: Possible Role of Excision Repair of O6-Methylguanine From DNA.* JNCI: Journal of the National Cancer Institute, 1974. **53**(6): p. 1839-1841.
12. Becker, K., et al., *Targeted expression of human O(6)-methylguanine-DNA methyltransferase (MGMT) in transgenic mice protects against tumor initiation in two-stage skin carcinogenesis.* Cancer Res, 1996. **56**(14): p. 3244-9.
13. Becker, K., et al., *DNA repair protein MGMT protects against N-methyl-N-nitrosourea-induced conversion of benign into malignant tumors.* Carcinogenesis, 2003. **24**(3): p. 541-6.
14. Wirtz, S., et al., *Both base excision repair and O6-methylguanine-DNA methyltransferase protect against methylation-induced colon carcinogenesis.* Carcinogenesis, 2010. **31**(12): p. 2111-7.
15. Dumenco, L.L., et al., *The prevention of thymic lymphomas in transgenic mice by human O6-alkylguanine-DNA alkyltransferase.* Science, 1993. **259**(5092): p. 219-22.
16. Lijinsky, W., et al., *Effects of inhibition of O6-alkylguanine-DNA alkyltransferase in rats on carcinogenesis by methylnitrosourea and ethylnitrosourea.* Jpn J Cancer Res, 1994. **85**(3): p. 226-30.
17. Nakatsuru, Y., et al., *O6-methylguanine-DNA methyltransferase protects against nitrosamine-induced hepatocarcinogenesis.* Proc Natl Acad Sci U S A, 1993. **90**(14): p. 6468-72.
18. Koike, G., et al., *Purification, structure, and biochemical properties of human O6-methylguanine-DNA methyltransferase.* J Biol Chem, 1990. **265**(25): p. 14754-62.

19. Xu-Welliver, M. and A.E. Pegg, *Degradation of the alkylated form of the DNA repair protein, O(6)-alkylguanine-DNA alkyltransferase.* Carcinogenesis, 2002. **23**(5): p. 823-30.
20. Meier, B., et al., *Mutational signatures of DNA mismatch repair deficiency in C. elegans and human cancers.* Genome Res, 2018. **28**(5): p. 666-675.
21. Lin, D.P., et al., *An Msh2 point mutation uncouples DNA mismatch repair and apoptosis.* Cancer Res, 2004. **64**(2): p. 517-22.
22. Yang, G., et al., *Dominant effects of an Msh6 missense mutation on DNA repair and cancer susceptibility.* Cancer Cell, 2004. **6**(2): p. 139-50.
23. Yoshioka, K., Y. Yoshioka, and P. Hsieh, *ATR kinase activation mediated by MutSalpha and MutLalpha in response to cytotoxic O6-methylguanine adducts.* Mol Cell, 2006. **22**(4): p. 501-10.
24. Roos, W.P., et al., *Brca2/Xrcc2 dependent HR, but not NHEJ, is required for protection against O(6)-methylguanine triggered apoptosis, DSBs and chromosomal aberrations by a process leading to SCEs.* DNA Repair (Amst), 2009. **8**(1): p. 72-86.
25. Mao, Z., et al., *Comparison of nonhomologous end joining and homologous recombination in human cells.* DNA Repair, 2008. **7**(10): p. 1765-1771.
26. Bremer, K., et al., *Etoposide and etoposide-ifosfamide therapy for refractory testicular tumors.* Cancer Treatment Reviews, 1982. **9**: p. 79-84.
27. Nagano, H., et al., *Patients with Advanced Ovarian Cancer Administered Oral Etoposide following Taxane as Maintenance Chemotherapy.* Case Rep Oncol, 2016. **9**(1): p. 195-204.
28. Hofmann, W.K., et al., *Intensive chemotherapy with idarubicin, cytarabine, etoposide, and G-CSF priming in patients with advanced myelodysplastic syndrome and high-risk acute myeloid leukemia.* Ann Hematol, 2004. **83**(8): p. 498-503.
29. Celsing, F., et al., *Addition of etoposide to CHOP chemotherapy in untreated patients with high-grade non-Hodgkin's lymphoma.* Ann Oncol, 1998. **9**(11): p. 1213-7.
30. Kushner, B.H., K. Kramer, and N.K. Cheung, *Oral etoposide for refractory and relapsed neuroblastoma.* J Clin Oncol, 1999. **17**(10): p. 3221-5.
31. Caubet, M., et al., *Carboplatin-etoposide combination chemotherapy in metastatic castration-resistant prostate cancer: A retrospective study.* Mol Clin Oncol, 2015. **3**(6): p. 1208-1212.
32. Grunberg, S.M., et al., *Extended administration of oral etoposide and oral cyclophosphamide for the treatment of advanced non-small-cell lung cancer: a Southwest Oncology Group study.* J Clin Oncol, 1993. **11**(8): p. 1598-601.
33. Ardizzoni, A., et al., *The combination of etoposide and cisplatin in non-small-cell lung cancer (NSCLC).* Ann Oncol, 1999. **10 Suppl 5**: p. S13-7.
34. Haim, N., et al., *Peroxidase-catalyzed metabolism of etoposide (VP-16-213) and covalent binding of reactive intermediates to cellular macromolecules.* Cancer Res, 1987. **47**(22): p. 5835-40.
35. Lovett, B.D., et al., *Etoposide Metabolites Enhance DNA Topoisomerase II Cleavage near Leukemia-Associated MLL Translocation Breakpoints.* Biochemistry, 2001. **40**(5): p. 1159-1170.
36. Zhang, W., et al., *Etoposide, an anticancer drug involved in therapy-related secondary leukemia: Enzymes at play.* Transl Oncol, 2021. **14**(10): p. 101169.
37. Grieder, A., R. Maurer, and H. Stahelin, *Effect of an epipodophyllotoxin derivative (VP 16-213) on macromolecular synthesis and mitosis in mastocytoma cells in vitro.* Cancer Res, 1974. **34**(8): p. 1788-93.

38. Colombo, T., et al., *Comparison between VP 16 and VM 26 in Lewis lung carcinoma of the mouse.* European Journal of Cancer and Clinical Oncology, 1986. **22**(2): p. 173-179.
39. Roed, H., et al., *The effect of the two epipodophyllotoxin derivatives etoposide (VP-16) and teniposide (VM-26) on cell lines established from patients with small cell carcinoma of the lung.* Cancer Chemotherapy and Pharmacology, 1987. **19**(1): p. 16-20.
40. Kasahara, K., et al., *Determinants of Response to the DNA Topoisomerase II Inhibitors Doxorubicin and Etoposide in Human Lung Cancer Cell Lines.* JNCI: Journal of the National Cancer Institute, 1992. **84**(2): p. 113-118.
41. Sciascia, N., et al., *Suppressing proteasome mediated processing of topoisomerase II DNA-protein complexes preserves genome integrity.* eLife, 2020. **9**: p. e53447.
42. Szlachta, K., et al., *Topoisomerase II contributes to DNA secondary structure-mediated double-stranded breaks.* Nucleic Acids Research, 2020. **48**(12): p. 6654-6671.
43. Tsuda, M., et al., *Repair of trapped topoisomerase II covalent cleavage complexes: Novel proteasome-independent mechanisms.* Nucleosides, Nucleotides & Nucleic Acids, 2020. **39**(1-3): p. 170-184.
44. Anuranjani and M. Bala, *Concerted action of Nrf2-ARE pathway, MRN complex, HMGB1 and inflammatory cytokines - Implication in modification of radiation damage.* Redox Biology, 2014. **2**: p. 832-846.
45. Thompson, L.H. and D. Schild, *Homologous recombinational repair of DNA ensures mammalian chromosome stability.* Mutation Research/Fundamental and Molecular Mechanisms of Mutagenesis, 2001. **477**(1): p. 131-153.
46. Lambert, S. and B.S. Lopez, *Inactivation of the RAD51 recombination pathway stimulates UV-induced mutagenesis in mammalian cells.* Oncogene, 2002. **21**(25): p. 4065-4069.
47. Popova, T., et al., *Ploidy and Large-Scale Genomic Instability Consistently Identify Basal-like Breast Carcinomas with BRCA1/2 Inactivation.* Cancer Research, 2012. **72**(21): p. 5454-5462.
48. Shin, H.-J., et al., *Etoposide induced cytotoxicity mediated by ROS and ERK in human kidney proximal tubule cells.* Scientific Reports, 2016. **6**(1): p. 34064.
49. Zhang, W., et al., *Etoposide, an anticancer drug involved in therapy-related secondary leukemia: Enzymes at play.* Translational Oncology, 2021. **14**(10): p. 101169.
50. Lucca, C., et al., *Sch9S6K controls DNA repair and DNA damage response efficiency in aging cells.* Cell Reports, 2024. **43**(6): p. 114281.
51. Annett, K., et al., *An investigation of DNA mismatch repair capacity under normal culture conditions and under conditions of supra-physiological challenge in human CD4+T cell clones from donors of different ages.* Exp Gerontol, 2005. **40**(12): p. 976-81.
52. Sargent, R.G., M.A. Brenneman, and J.H. Wilson, *Repair of site-specific double-strand breaks in a mammalian chromosome by homologous and illegitimate recombination.* Mol Cell Biol, 1997. **17**(1): p. 267-77.
53. Okawa, A., et al., *Differential expression of DNA-dependent protein kinase catalytic subunit in the brain of neonatal mice and young adult mice.* Proc Jpn Acad Ser B Phys Biol Sci, 2020. **96**(5): p. 171-179.
54. Kim, K.-H., et al., *The role of Rad51 in safeguarding mitochondrial activity during the meiotic cell cycle in mammalian oocytes.* Scientific Reports, 2016. **6**(1): p. 34110.
55. Li, Z., et al., *Impaired DNA double-strand break repair contributes to the age-associated rise of genomic instability in humans.* Cell Death Differ, 2016. **23**(11): p. 1765-1777.

56. Takahashi, K. and S. Yamanaka, *Induction of Pluripotent Stem Cells from Mouse Embryonic and Adult Fibroblast Cultures by Defined Factors.* Cell, 2006. **126**(4): p. 663-676.
57. Takahashi, K., et al., *Induction of pluripotent stem cells from adult human fibroblasts by defined factors.* Cell, 2007. **131**(5): p. 861-72.
58. Yu, J., et al., *Induced pluripotent stem cell lines derived from human somatic cells.* Science, 2007. **318**(5858): p. 1917-20.
59. Laurent, L.C., et al., *Dynamic changes in the copy number of pluripotency and cell proliferation genes in human ESCs and iPSCs during reprogramming and time in culture.* Cell Stem Cell, 2011. **8**(1): p. 106-18.
60. Schofield, R., *The relationship between the spleen colony-forming cell and the haemopoietic stem cell.* 1978.
61. Till, J.E. and C.E. Mc, *A direct measurement of the radiation sensitivity of normal mouse bone marrow cells.* Radiat Res, 1961. **14**: p. 213-22.
62. Spangrude, G.J., S. Heimfeld, and I.L. Weissman, *Purification and characterization of mouse hematopoietic stem cells.* Science, 1988. **241**(4861): p. 58-62.
63. Gluckman, E., et al., *Hematopoietic reconstitution in a patient with Fanconi's anemia by means of umbilical-cord blood from an HLA-identical sibling.* N Engl J Med, 1989. **321**(17): p. 1174-8.
64. Barker, J.N., D.J. Weisdorf, and J.E. Wagner, *Creation of a double chimera after the transplantation of umbilical-cord blood from two partially matched unrelated donors.* N Engl J Med, 2001. **344**(24): p. 1870-1.
65. Erices, A., P. Conget, and J.J. Minguell, *Mesenchymal progenitor cells in human umbilical cord blood.* Br J Haematol, 2000. **109**(1): p. 235-42.
66. Le Blanc, K., et al., *Mesenchymal stem cells inhibit and stimulate mixed lymphocyte cultures and mitogenic responses independently of the major histocompatibility complex.* Scand J Immunol, 2003. **57**(1): p. 11-20.
67. Knutsen, A.P. and D.A. Wall, *Umbilical cord blood transplantation in severe T-cell immunodeficiency disorders: two-year experience.* J Clin Immunol, 2000. **20**(6): p. 466-76.
68. Kögler, G., et al., *A new human somatic stem cell from placental cord blood with intrinsic pluripotent differentiation potential.* J Exp Med, 2004. **200**(2): p. 123-35.
69. Kluth, S.M., et al., *DLK-1 as a Marker to Distinguish Unrestricted Somatic Stem Cells and Mesenchymal Stromal Cells in Cord Blood.* Stem Cells and Development, 2010. **19**(10): p. 1471-1483.
70. Liedtke, S., et al., *The HOX Code as a "biological fingerprint" to distinguish functionally distinct stem cell populations derived from cord blood.* Stem Cell Res, 2010. **5**(1): p. 40-50.
71. Kluth, S.M., T.F. Radke, and G. Kögler, *Increased Haematopoietic Supportive Function of USSC from Umbilical Cord Blood Compared to CB MSC and Possible Role of DLK-1.* Stem Cells Int, 2013. **2013**: p. 985285.
72. Handschel, J., et al., *Comparison of ectopic bone formation of embryonic stem cells and cord blood stem cells in vivo.* Tissue Eng Part A, 2010. **16**(8): p. 2475-83.
73. Uchida, K., et al., *Bone Marrow-Engrafted Cells after Mice Umbilical Cord Blood Transplantation Differentiate into Osteoblastic Cells in Response to Fracture and Placement of Titanium Screws.* Experimental Animals, 2012. **61**(4): p. 427-433.
74. Friedenstein, A.J., S. Piatetzky, II, and K.V. Petrakova, *Osteogenesis in transplants of bone marrow cells.* J Embryol Exp Morphol, 1966. **16**(3): p. 381-90.

75. Noël, D., et al., *Cell specific differences between human adipose-derived and mesenchymal–stromal cells despite similar differentiation potentials.* Experimental Cell Research, 2008. **314**(7): p. 1575-1584.
76. Sacchetti, B., et al., *No Identical “Mesenchymal Stem Cells” at Different Times and Sites: Human Committed Progenitors of Distinct Origin and Differentiation Potential Are Incorporated as Adventitial Cells in Microvessels.* Stem Cell Reports, 2016. **6**(6): p. 897-913.
77. Hochmann, S., et al., *The enhancer landscape predetermines the skeletal regeneration capacity of stromal cells.* Science Translational Medicine, 2023. **15**(688): p. eabm7477.
78. Bae, H.C., et al., *Hypoxic condition enhances chondrogenesis in synovium-derived mesenchymal stem cells.* Biomaterials Research, 2018. **22**(1): p. 28.
79. Zarychta-Wiśniewska, W., et al., *The Influence of Cell Source and Donor Age on the Tenogenic Potential and Chemokine Secretion of Human Mesenchymal Stromal Cells.* Stem Cells Int, 2019. **2019**: p. 1613701.
80. Herrmann, M., et al. *Phenotypic Characterization of Bone Marrow Mononuclear Cells and Derived Stromal Cell Populations from Human Iliac Crest, Vertebral Body and Femoral Head*. International Journal of Molecular Sciences, 2019. **20**, DOI: 10.3390/ijms20143454.
81. Li, X., et al., *Comprehensive characterization of four different populations of human mesenchymal stem cells as regards their immune properties, proliferation and differentiation.* Int J Mol Med, 2014. **34**(3): p. 695-704.
82. Kern, S., et al., *Comparative Analysis of Mesenchymal Stem Cells from Bone Marrow, Umbilical Cord Blood, or Adipose Tissue.* Stem Cells, 2006. **24**(5): p. 1294-1301.
83. Siegel, G., et al., *Phenotype, donor age and gender affect function of human bone marrow-derived mesenchymal stromal cells.* BMC Medicine, 2013. **11**(1): p. 146.
84. Akiyama, H., et al., *The transcription factor Sox9 has essential roles in successive steps of the chondrocyte differentiation pathway and is required for expression of Sox5 and Sox6.* Genes Dev, 2002. **16**(21): p. 2813-28.
85. Capdevila, J. and R.L. Johnson, *Endogenous and ectopic expression of noggin suggests a conserved mechanism for regulation of BMP function during limb and somite patterning.* Dev Biol, 1998. **197**(2): p. 205-17.
86. Zuk, P.A., et al., *Human adipose tissue is a source of multipotent stem cells.* Mol Biol Cell, 2002. **13**(12): p. 4279-95.
87. Grigoriadis, A.E., J.N. Heersche, and J.E. Aubin, *Differentiation of muscle, fat, cartilage, and bone from progenitor cells present in a bone-derived clonal cell population: effect of dexamethasone.* J Cell Biol, 1988. **106**(6): p. 2139-51.
88. Lehmann, J.M., et al., *Peroxisome proliferator-activated receptors alpha and gamma are activated by indomethacin and other non-steroidal anti-inflammatory drugs.* J Biol Chem, 1997. **272**(6): p. 3406-10.
89. Kim, S. and N. Moustaid-Moussa, *Secretory, endocrine and autocrine/paracrine function of the adipocyte.* J Nutr, 2000. **130**(12): p. 3110s-3115s.
90. Smith, P.J., et al., *Insulin-like growth factor-I is an essential regulator of the differentiation of 3T3-L1 adipocytes.* J Biol Chem, 1988. **263**(19): p. 9402-8.
91. Leinninger, G.M., et al., *Phosphatidylinositol 3-kinase and Akt effectors mediate insulin-like growth factor-I neuroprotection in dorsal root ganglia neurons.* Faseb j, 2004. **18**(13): p. 1544-6.
92. Rosen, E.D. and O.A. MacDougald, *Adipocyte differentiation from the inside out.* Nat Rev Mol Cell Biol, 2006. **7**(12): p. 885-96.

93. Menghini, R., et al., *Phosphorylation of GATA2 by Akt increases adipose tissue differentiation and reduces adipose tissue-related inflammation: a novel pathway linking obesity to atherosclerosis.* Circulation, 2005. **111**(15): p. 1946-53.
94. Rosen, E.D., et al., *Transcriptional regulation of adipogenesis.* Genes Dev, 2000. **14**(11): p. 1293-307.
95. Tamori, Y., et al., *Role of peroxisome proliferator-activated receptor-gamma in maintenance of the characteristics of mature 3T3-L1 adipocytes.* Diabetes, 2002. **51**(7): p. 2045-55.
96. Tong, Q., et al., *Function of GATA transcription factors in preadipocyte-adipocyte transition.* Science, 2000. **290**(5489): p. 134-8.
97. Gregoire, F.M., C.M. Smas, and H.S. Sul, *Understanding adipocyte differentiation.* Physiol Rev, 1998. **78**(3): p. 783-809.
98. Nakamura, T., et al., *Temporal gene expression changes during adipogenesis in human mesenchymal stem cells.* Biochemical and Biophysical Research Communications, 2003. **303**(1): p. 306-312.
99. Sekiya, I., et al., *Adipogenic Differentiation of Human Adult Stem Cells From Bone Marrow Stroma (MSCs)*.* Journal of Bone and Mineral Research, 2009. **19**(2): p. 256-264.
100. Zippel, N., et al., *Purinergic Receptors Influence the Differentiation of Human Mesenchymal Stem Cells.* Stem Cells and Development, 2011. **21**(6): p. 884-900.
101. Dominici, M., et al., *Minimal criteria for defining multipotent mesenchymal stromal cells. The International Society for Cellular Therapy position statement.* Cytotherapy, 2006. **8**(4): p. 315-7.
102. Kanawa, M., et al., *Age-dependent decrease in the chondrogenic potential of human bone marrow mesenchymal stromal cells expanded with fibroblast growth factor-2.* Cytotherapy, 2013. **15**(9): p. 1062-72.
103. Selle, M., et al., *Influence of age on stem cells depends on the sex of the bone marrow donor.* J Cell Mol Med, 2022. **26**(5): p. 1594-1605.
104. Sammour, I., et al., *The Effect of Gender on Mesenchymal Stem Cell (MSC) Efficacy in Neonatal Hyperoxia-Induced Lung Injury.* PLoS One, 2016. **11**(10): p. e0164269.
105. Rodríguez, J.P., et al., *Abnormal osteogenesis in osteoporotic patients is reflected by altered mesenchymal stem cells dynamics.* J Cell Biochem, 1999. **75**(3): p. 414-23.
106. de Oliveira, G.L., et al., *Bone marrow mesenchymal stromal cells isolated from multiple sclerosis patients have distinct gene expression profile and decreased suppressive function compared with healthy counterparts.* Cell Transplant, 2015. **24**(2): p. 151-65.
107. Pachón-Peña, G., et al., *Obesity Determines the Immunophenotypic Profile and Functional Characteristics of Human Mesenchymal Stem Cells From Adipose Tissue.* Stem Cells Transl Med, 2016. **5**(4): p. 464-75.
108. Kern, S., et al., *Comparative analysis of mesenchymal stem cells from bone marrow, umbilical cord blood, or adipose tissue.* Stem Cells, 2006. **24**(5): p. 1294-301.
109. Choi, J.R., K.W. Yong, and W.K.Z. Wan Safwani, *Effect of hypoxia on human adipose-derived mesenchymal stem cells and its potential clinical applications.* Cell Mol Life Sci, 2017. **74**(14): p. 2587-2600.
110. Hu, X., et al., *Transplantation of hypoxia-preconditioned mesenchymal stem cells improves infarcted heart function via enhanced survival of implanted cells and angiogenesis.* J Thorac Cardiovasc Surg, 2008. **135**(4): p. 799-808.
111. Hung, S.P., et al., *Hypoxia promotes proliferation and osteogenic differentiation potentials of human mesenchymal stem cells.* J Orthop Res, 2012. **30**(2): p. 260-6.

112. De Bari, C., et al., *Multipotent mesenchymal stem cells from adult human synovial membrane.* Arthritis Rheum, 2001. **44**(8): p. 1928-42.
113. Okita, K., et al., *An Efficient Nonviral Method to Generate Integration-Free Human-Induced Pluripotent Stem Cells from Cord Blood and Peripheral Blood Cells.* Stem Cells, 2013. **31**(3): p. 458-466.
114. Kögler, G., et al., *Cytokine production and hematopoiesis supporting activity of cord blood–derived unrestricted somatic stem cells.* Experimental Hematology, 2005. **33**(5): p. 573-583.
115. Terheyden-Keighley, D., et al., *GMP-compliant iPS cell lines show widespread plasticity in a new set of differentiation workflows for cell replacement and cancer immunotherapy.* Stem Cells Translational Medicine, 2024. **13**(9): p. 898-911.
116. Strober, W., *Trypan blue exclusion test of cell viability.* Curr Protoc Immunol, 2001. **Appendix 3**: p. Appendix 3B.
117. Jaatinen, T. and J. Laine, *Isolation of hematopoietic stem cells from human cord blood.* Curr Protoc Stem Cell Biol, 2007. **Chapter 2**: p. Unit 2A.2.
118. Noble, P.B. and J.H. Cutts, *Separation of blood leukocytes by Ficoll gradient.* Can Vet J, 1967. **8**(5): p. 110-1.
119. Riccardi, C. and I. Nicoletti, *Analysis of apoptosis by propidium iodide staining and flow cytometry.* Nat Protoc, 2006. **1**(3): p. 1458-61.
120. Beerman, I., et al., *Quiescent hematopoietic stem cells accumulate DNA damage during aging that is repaired upon entry into cell cycle.* Cell Stem Cell, 2014. **15**(1): p. 37-50.
121. Mohrin, M., et al., *Hematopoietic Stem Cell Quiescence Promotes Error-Prone DNA Repair and Mutagenesis.* Cell Stem Cell, 2010. **7**(2): p. 174-185.
122. Mboni-Johnston, I.M., et al., *Sensitivity of Human Induced Pluripotent Stem Cells and Thereof Differentiated Kidney Proximal Tubular Cells towards Selected Nephrotoxins.* International Journal of Molecular Sciences, 2024. **25**(1): p. 81.
123. Mohammadi, S., et al., *Toxic compounds from tobacco in placenta samples analyzed by UPLC-QTOF-MS.* Journal of Pharmaceutical and Biomedical Analysis, 2017. **145**: p. 331-338.
124. Zhang, M., et al., *Induced Pluripotent Stem Cells Are Sensitive to DNA Damage.* Genomics, Proteomics & Bioinformatics, 2013. **11**(5): p. 320-326.
125. Desmarais, J.A., et al., *Apoptosis and failure of checkpoint kinase 1 activation in human induced pluripotent stem cells under replication stress.* Stem Cell Res Ther, 2016. **7**: p. 17.
126. González, F., et al., *Homologous recombination DNA repair genes play a critical role in reprogramming to a pluripotent state.* Cell Rep, 2013. **3**(3): p. 651-60.
127. Ruiz, S., et al., *Limiting replication stress during somatic cell reprogramming reduces genomic instability in induced pluripotent stem cells.* Nat Commun, 2015. **6**: p. 8036.
128. Furda, A.M., et al., *Oxidants and not alkylating agents induce rapid mtDNA loss and mitochondrial dysfunction.* DNA Repair (Amst), 2012. **11**(8): p. 684-92.
129. Biechonski, S., M. Yassin, and M. Milyavsky, *DNA-damage response in hematopoietic stem cells: an evolutionary trade-off between blood regeneration and leukemia suppression.* Carcinogenesis, 2017. **38**(4): p. 367-377.
130. Sane, M.S., et al., *Characterization of an umbilical cord blood sourced product suitable for allogeneic applications.* Regen Med, 2019. **14**(8): p. 769-789.
131. Hordyjewska, A., Ł. Popiołek, and A. Horecka, *Characteristics of hematopoietic stem cells of umbilical cord blood.* Cytotechnology, 2015. **67**(3): p. 387-396.

132. Hao, Q.L., et al., *A functional comparison of CD34 + CD38- cells in cord blood and bone marrow.* Blood, 1995. **86**(10): p. 3745-53.
133. McKenzie, J.L., et al., *Reversible cell surface expression of CD38 on CD34-positive human hematopoietic repopulating cells.* Experimental Hematology, 2007. **35**(9): p. 1429-1436.
134. Casorelli, I., et al., *Methylation damage response in hematopoietic progenitor cells.* DNA Repair, 2007. **6**(8): p. 1170-1178.
135. Tao, W., et al., *Profiling of differentially expressed apoptosis-related genes by cDNA arrays in human cord blood CD34⁺ cells treated with etoposide.* Experimental Hematology, 2003. **31**(3): p. 251-260.
136. Tanaka, T., et al., *Induction of ATM Activation, Histone H2AX Phosphorylation and Apoptosis by Etoposide: Relation to Cell Cycle Phase.* Cell Cycle, 2007. **6**(3): p. 371-376.
137. Cheng, T., et al., *Hematopoietic Stem Cell Quiescence Maintained by p21^{cip1/waf1}.* Science, 2000. **287**(5459): p. 1804-1808.
138. de Feraudy, S., et al., *A minority of foci or pan-nuclear apoptotic staining of γH2AX in the S phase after UV damage contain DNA double-strand breaks.* Proceedings of the National Academy of Sciences, 2010. **107**(15): p. 6870-6875.
139. Lützkendorf, J., et al., *Resistance for Genotoxic Damage in Mesenchymal Stromal Cells Is Increased by Hypoxia but Not Generally Dependent on p53-Regulated Cell Cycle Arrest.* PLOS ONE, 2017. **12**(1): p. e0169921.
140. Cobb, A.M., et al., *Runx2 (Runt-Related Transcription Factor 2) Links the DNA Damage Response to Osteogenic Reprogramming and Apoptosis of Vascular Smooth Muscle Cells.* Arteriosclerosis, Thrombosis, and Vascular Biology, 2021. **41**(4): p. 1339-1357.

Acknowledgments

First, I would like to thank my supervisor Prof. Dr. Gesine Kögler for giving me the opportunity to pursue my PhD in her esteemed institute. Her guidance, expertise and unwavering support throughout this journey have been greatly valuable.

I thank my second supervisor Prof. Dr. Sebastian Wesselborg from the Institute of Molecular Medicine I for the support he has given me. Thank you for proofreading all the progress reports and the manuscripts and for your valuable feedback and the critical questions that were important for improving my project.

I would like to thank Prof. Dr. Gerhard Fritz from the Institute of Toxicology for giving me the opportunity to join the toxicology graduate program GRK2578. His insightful and critical questions have been instrumental in helping me expand my perspective beyond cell biology, allowing me to approach problems with the mindset of a toxicologist. I am especially grateful for his thought-provoking discussions during progress report days, which continually pushed me to think more critically and deeply. Additionally, I truly appreciate his openness and support, always providing a listening ear whenever challenges arose. His guidance has been invaluable throughout this journey.

Thanks to the GRK2578 coordinators Dr. Daniela Geist and Dr. Claudia von Montfort for always being there to help with any paperwork problems as well as answering all my questions. Your support in listening to any problems and your willingness to find solutions has meant a lot to me. I truly appreciate everything you've done to make my time here run smoothly.

Thanks to Prof. Dr. James Adjaye for giving me the opportunity to use machines in his institute and to PD Dr. Nina Graffmann and Vanessa Cristina Meira de Amorim for introducing me to the culture of iPSCs and for all the motivational chats we had every now and then.

I would like to sincerely thank all members of the GRK2578 for their valuable input, generous support and collegial collaboration throughout my PhD. Whether through insightful discussions, sharing missing reagents or offering help with experiments, your contributions have been an essential part of this project and I am truly grateful for your support.

Thank you Dr. Stefanie Liedtke for your valuable support especially during the early stages of my PhD. Your guidance and patience were so important and helped me learn new techniques and concepts. I deeply appreciate your willingness to always be there to answer my questions and provide clarity whenever I needed it.

I would also like to thank my amazing colleagues for always being there to cheer me up when things got too stressful. Thank you Fabienne Becker for always providing calm and balance when things felt overwhelming. Thank you Rigveda Nitin Bhave for your humor, encouragement and friendship that have made even the toughest days more manageable. Thank you Janine Korn for always being there when I needed any help in the lab. You were always ready to lend a hand. I really appreciate that. I am truly grateful to have shared this experience with wonderful people that have become real friends. I will miss the daily lunch breaks with you!

I would like to extend my deepest thanks to the entire team at the ITZ for creating such a collaborative and supportive working environment. Lutz Körschgen, Andrea Meyer, Almuth Düppers, Sabine Többen, Sadiye Yalcin, Isabella Schewtschuk and Holger Greßmann, Dr. Rüdiger Sorg, Dr. Angeliki Datsi, Lea Falkowski, Nico Vallieri, thank you for the incredible continuous support during the three years but also for the fun moments we have collected. Each of you has contributed to making my PhD journey not only enriching but also enjoyable.

I would like to thank my friends, Anna Rita, Farhad, Cassandra, Charlie, Christin, Paweł, Arshia, Julia, Julian, Esther and Noémi. The beautiful memories we have created together during this time have been a beacon of light giving me the energy and motivation to persevere through all challenges. Thank you for being there for me and making this journey so much brighter.

I would like to express my deepest gratitude to my parents, whose unwavering support, love and encouragement have been the foundation of my journey. It is because of your sacrifices that I had the opportunity to come to Germany and pursue my dreams. This accomplishment is as much yours as it is mine.

Special thanks goes to my sister Yasmina Ouzin for her unconditional support and for always being there for me. Our daily phone chats are what always put a smile on my face and what I looked forward the most. I am so grateful to have you in my life!

Huge thanks also to Susanne Busch, Oliver Max Busch and Maik Busch for their support, kindness, listening and readiness to help whenever challenges arose. Thank you for making me feel like a part of your family. Your care and understanding have been a great comfort and strength.

Max Busch, a huge thank you for your unconditional love and support throughout this whole journey. Without you, none of this would have been possible. I am so grateful to have you by my side. I love you!